Broadband Millimetre-Wave Radio over Fibre Systems

Leif A Johansson

A thesis submitted to the University of London for the Degree of Doctor of Philosophy
in Electronic and Electrical Engineering

Department of Electronic and Electrical Engineering
University College London
June 2002

Broadband Millimetre-Wave Radio over Fibre Systems

Abstract

This thesis concerns the generation and transmission of millimetre wave modulated optical signals for broadband radio over fibre applications. The millimetre wave modulated optical source used for this application should be able to produce single sideband modulation with high modulation depth and high power to overcome the fibre chromatic dispersion and attenuation for transmission distances longer than a few kilometres. In addition to these demands, the source should have long-term stability and the potential for low cost. Previous sources do not satisfy these demands.

In this work, a novel millimetre wave modulated optical source is demonstrated, the first millimetre wave modulated optical injection phase-lock loop. It is shown how stable and efficient generation of single sideband modulated optical signals can be accomplished using standard components and how this source can be used for transmission of broadband millimetre wave modulated optical signals over up to 65 km of unamplified standard singlemode fibre.

Experimental results are presented on the generation of a single sideband modulated optical signal with high spectral purity- -93 dBc/Hz at 10 kHz offset and -107 dBc/Hz at 2 MHz offset, wide locking range- more than 30 GHz and wide tuneability- potentially from 4 GHz to more than 60 GHz. This source has been used for optical transmission of a 140 Mbit/s amplitude shift keyed modulated 36 GHz carrier over 25 km of unamplified standard single mode fibre and over 65 km using optical amplification. The source has also been used to demonstrate optical transmission of a 68 Mbit/s DPSK modulated 36 GHz carrier over 65 km unamplified standard single mode fibre, using a modulated reference. This is the longest demonstrated unamplified transmission of broadband (>10 Mb/s) millimetre wave radio over fibre transmission and the widest bandwidth reference modulation applied to either an OPLL or an OIL based heterodyne system.

To Mira, my wife and companion, and to my family for always being there.

Acknowledgements

First of all, I would like to acknowledge my supervisor, Professor Alwyn J. Seeds, for providing guidance based on many years of expertise in the area. His support and help have been extraordinary.

I would also like to acknowledge the help and friendship of my colleagues in the Microwave Optoelectronics group: Claudio Silva, Ed Burr, Ju Bin Song, Marianna Pantouvaki, Dave Wake, Steve Bennett, Xuan Huang, and most important, Chin-Pang Liu for the help with the electronics design when time was short. Dave Wake should be additionaly acknowledged for providing the laser diodes used in this work, as a part of his work at BT Adastral Park.

Finally, I would like to thank Nortel Networks and Dr. Mark Naden for the supervision and the financial support that made this work possible.

Table of Contents

List of Figures

List of Tables

List of Acronyms

ACTS	Advanced Communications Technologies and Services
ADSL	Asymetric Digital Subscriber Line
ASE	Amplifier Spontaneous Emission
ASK	Amplitude Shift Keying
B-ISDN	Broadband Integrated Services Digital Network
BER	Bit Error Rate
BPSK	Binary Phase Shift Keying
BRAN	Broadband Radio Access Networks
BWA	Broadband Wireless Access
CDMA	Code Division Multiple Access
CDM	Code Division Multiplexing
CNR	Carrier to Noise Ratio
CPFSK	Continous Phase Frequency Shift Keying
CRABS	Cellular Radio Access for Broadband Services
DFB	Distributed Feed-Back
DPSK	Differential Phase Shift Keying
DSF	Dispersion Shifted Fibre
DVB-S	Digital Video Broadcasting - Satellite
EAM	Electro Absorption Modulator

ECL	Emitter Coupled Logic
EDFA	Erbium Doped Fibre Amplifier
EOM	External Optical Modulator
ERC	European Radiocommunications Committee
FDD	Frequency Division Duplexing
FDM	Frequency Division Multiplexing
FM	Frequency Modulation
FSR	Free Space Range
FTTA	Fibre To The Area
FTTB	Fibre To The Building
FTTC	Fibre To The Curb
FTTH	Fibre To The Home
FWHM	Full Width Half Maximum
GSM	Global System for Mobile communications
HFR	Hybrid Fibre Radio
HIPERACESS	HIgh PErformance Radio ACCESS
IF	Intermediate Frequency
IM	Intensity Modulation
ISI	Intersymbol Interference
ISP	Internet Service Provider
LAN	Local Area Network
LMDS	Local Multipoint Distribution Services
LO	Local Oscillator
MBS	Mobile Broadband Services
MEDIAN	Wireless Broadband CPN/LAN for Professional and Residential Multimedia

MLL	Mode-Locked Laser
MMDS	Multichannel Multipoint Distribution System
MQW	Multiple Quantum Well
MVDS	Multipoint Video Distribution system
MZM	Mach-Zehnder Modulator
NADC	North American Digital Cellular
NRZ	Non-Return to Zero
OIL	Optical Injection Locking
OILO	Optically Injection Locked Oscillator
OIPLL	Optical Injection Phase-Lock Loop
OOK	On-Off keying
OPA	Operational Amplifier
OPLL	Optical Phase-Lock Loop
OQPSK	Offset Quadrature Phase Shift Keying
PCN	Personal Communications Network
PDC	Pacific Digital Cellular
PDF	Probability Density Function
PLL	Phase-Lock Loop
PMD	Polarisation Mode Dispersion
PRBS	Pseudo-Random Bit Sequencer
PSK	Phase Shift Keying
QAM	Quadrature Amplitude Modulation
QCSE	Quantum Confined Stark Effect
QPSK	QPSK
RF	Radio Frequency

RIN	Relative Intensity Noise
RMS	Root Mean Square
RX	Receiver
RZ	Return to Zero
SAMBA	System for Advanced Mobile Broadband Application
SCM	Subcarrier multiplexing
SFDR	Spurious Free Dynamic Range
SNR	Signal to Noise Ratio
SOA	Semiconductor Optical Amplifier
SSM	Standard Single Mode
TDD	Time Division Duplexing
TDM	Time Division Multiplexing
TE	Transversal Electric
TM	Transversal Magnetic
TRX	Transceiver
TX	Transmitter
UMTS	Universal Mobile Telecommunications System
WDM	Wavelength Division Multiplexing

Chapter 1

Introduction

This chapter will provide an introduction to the general topics relevant for the work that has been undertaken and that provides the main topic for this thesis. The first section, 1.1 gives an overview of millimetre-wave radio. The free-space transmission properties are outlined and the main application areas, notably fixed broadband wireless access, are listed. The second section, 1.2, introduces the area of radio over fibre. The main applications where it can with advantage be used and the benefits of using it are treated. Some properties of radio over fibre transmission and some systems aspects are also investigated. The chapter concludes with a statement of the objectives for and an outline of this thesis.

1.1 Millimetre-wave Radio

The millimetre-wave frequency band is strictly defined as the band falling within 30 to 300 GHz, corresponding to wavelengths in the range of 1 to 10 mm. The band of frequencies higher than 300 GHz is commonly refered to as the sub millimetre-wave band, while lower frequencies are simply refered to as microwaves. In this chapter, applications mainly falling within 20 to 70 GHz will be discussed and the term millimetre-wave is here used to include 20 to 30 GHz.

1.1.1 Radio frequency bandwidth requirements

As the bandwidth requirements are currently increasing in wired communications, bandwidth demand in wireless communications is likely to increase in an analogous way, but at a delayed time scale. Table 1.1 shows the required data rate for various services, the required data rate spans four orders of magnitude. The required RF bandwidth for each service can be assumed to be propotional to the data rate. Currently, Global System for Mobile communications (GSM) operates with a channel bandwidth of 104 kb/s at 900 MHz [1]. The future third generation Universal Mobile Telecommunications System (UMTS) is projected to give up to 2 Mb/s at 2 GHz [2], while the now widely adopted IEEE 802.11 wireless Local Area Network (LAN) standard presently supports 2 Mb/s bandwidths at 2.4 GHz [3]. Furthermore, fixed link broadband access in the Multichannel Multipoint Distribution System (MMDS) band at 2.5 GHz can support data rates of tens of megabits per second. A common feature for these standards are that they are using carriers of a few gigahertz and that only text, audio, and possibly compressed video services can be supported. If services with higher data rates are to be provided, such as listed in Table 1.1, microwaves simply does not have sufficient bandwidth for these applications to be supported. In order to support these services, millimetre-wave radio has to be used. Furthermore, even though microwaves augmented with multilevel modulation formats are currently giving adequate bandwidth for most common applications, there is little margin to accomodate higher data rate systems. An investment in millimetre-wave radio will therefore result in a more future-proof system. An additional powerful argument for millimetre-wave radio is cost considerations. In year 2000, the third generation UMTS spectrum was auctioned in Britain. 22 billion pounds was paid for a total of 155 MHz bandwidth. As a contrast, the auction of spectrum for millimetre-wave broadband wireless in the 28 GHz band grossed 38.2 million pounds for a total of 672 MHz bandwidth [4]. Bandwidth is simply much less expensive at millimetre-wave frequencies.

Table 1.1: Bandwidth demand for various services [5]

Service	Raw data rate
Voice (8b/8 kHz/1):	64 kb/s
CD quality stereo audio (16b/44.1 kHz/2):	1.4 Mb/s
Compressed digital video (MPEG):	2-8 Mb/s
Professional quality multichannel audio (24b/96 kHz/7):	16 Mb/s
Studio quality digital video (ITU-R 601):	216 Mb/s
Medical imaging quality digital video (NTT):	650 Mb/s
Studio quality digital HDTV:	1.08 Gb/s

1.1.2 Radio propagation characteristics

The propagation characteristics of millimetre-waves differ significantly from characteristics of lower frequencies. The short wavelength gives millimetre-waves semi-optical properties as sensitivity to shading and high free space loss. As a consequence, millimetre-wave radio is mostly utilised in line-of-sight configurations. The small wavelength also enables the design of small, high gain narrow beamwidth antennas [32]. The radio range is affected by a range of parameters:

- Free-space propagation loss: The free space propagation loss is the most important parameter determining the range and applications of millimetre-wave radio. The free-space loss has an inverse square dependence on the carrier frequency. This implies that for 30 GHz, we require a transmission power roughly three orders higher than within the GSM band (900 MHz), to transmit the signal the same distance. The free-space loss will be examined further later in this section.

- Multipath fading: Due to the short wavelenth of millimetre-waves, any scattering surfaces will appear relatively more 'rough' and will produce incoherent reflections, less likely to produce serious multipath propagation interference [7]. Add to this the common use of high gain antennas in millimetre-wave radio, and it is apparent that multipath fading is less troublesome than for microwave communications [8].

- Diffraction: The small wavelength also affects the diffraction properties. The angle of diffraction appearing when the wave is limited laterally is proportional to the wavelength. At millimetre-waves, large obstacles, such as buildings tends to 'cast shadows'. Therefore, line of sight radio transmission is preferable for millimetre-wave radio.

- Foliage losses: Water absorbs the millimetre-wave band to a higher degree than microwave frequencies. Therefore, losses due to vegetation in the line of sight are considerable for vegetation depths only a few metres thick. Semi-empirical models have been developed to predict these losses [9, 10].

- Rain attenuation: Rain drops are roughly of the same size as the radio wavelengths and therefore millimetre-wave radio is scattered by rain. The rate of rain attenuation is well known, it is estimated that 10 dB margin will cover most European locations 99.7 % of the time for cell sizes of about 5 km [11]. Estimates have also been published for USA [10].

- Interference: Interference from close transmitters in the same frequency range cannot be ignored, as it is a factor limiting the spatial frequency reuse ratio. Interference from close transmitters can be assumed to be broadband and uncorrelated, and therefore be added to the received noise floor [9]. However, any system margin allocated for rain attenuation will also cover interference, as the rain atenuation affects the interfering signals to a higher degree than the wanted signal [9]. The use of high gain antennas also reduces interference rate and allows for a higher degree of frequency reuse [12].

- Atmosperic gaseous losses: In the millimetre-wave frequency band, significant gaseous absorption bands exists. H_2O has absoption peaks at 24 GHz with 0.18 dB/km attenuation at sea level and other bands at 170 GHz and 320 GHz. O_2 has absorption peaks at 60 GHz with 17 dB/km attenuation at sea level and another at 120 GHz [10]. For any reasonable transmission distance at the more commonly used frequencies below 100 GHz, only the

60 GHz band experiences any significant increase in attenuation due to gaseous absorption, and then only for transmission distances exeeding 9 km, where gaseous losses are dominant. However, the exponential rate of decrease has the advantage of allowing a high degree of frequency reuse at 60 GHz. This has allowed unlicenced bands to be defined around 60 GHz both in the USA and Europe [13, 15]. Products exploiting this have already been developed [16]. 60 GHz is also a sutable band for secure wireless communications, as the exponential rate of decrease makes intercept less probable.

1.1.3 Free-space loss

The free-space transmission loss between a transmitting and receiving antenna is given by the usual formula:

$$P_r = P_t G_r G_t \left(\frac{c}{4\pi d f}\right)^2 \tag{1.1}$$

P_r :	Downlink power from the receiving antenna (W)
P_t :	Downlink power into the transmitting antenna (W)
G_r :	Gain of the receiving antenna
G_t :	Gain of the transmitting antenna
f :	Radio frequency (Hz)
c :	Speed of light ($3 \cdot 10^8$ m/s)
d :	Propagation distance (m)

The radio receiver can be assumed to be is limited by thermal noise, given by:

$$N_{th} = k_B T_0 F B \tag{1.2}$$

k_B :	$1.38 \cdot 10^-23$ J/K	Boltzmann's constant
T_0 :	295 K	Antenna noise temperature
B :	Hz	Noise bandwidth
F :		Receiver noise figure

the required received power can be derived by:

$$P_r = N_{th} \Gamma_f \gamma \tag{1.3}$$

Γ_f :	Fading power margin
γ :	Required received SNR

we can use equations 1.1, 1.2 and 1.3 to calculate the available transmission distance as a function of the transmitter antenna gain:

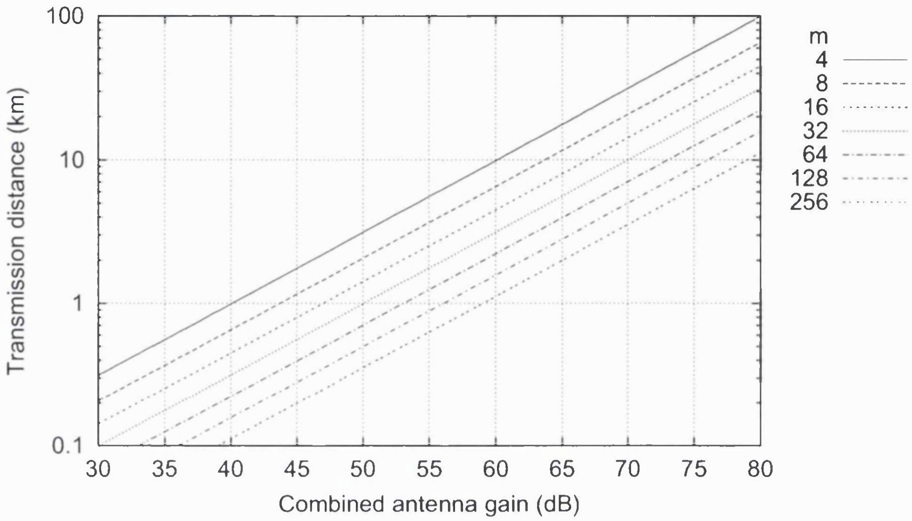

Figure 1.1: Available radio transmission distance as a function of transmitter and receiver combined antenna gain for different m-QAM modulation formats with a constant signal bandwidth. Parameters listed in Table 1.2.

Table 1.2: Parameters used in the power budget calculations for radio transmission.

Parameter:	Value:	m:	γ_r (dB):
P_t:	10 dBm	4:	12.60
BER:	10^{-5}	8:	16.21
f:	28 GHz	16:	19.46
Γ_f:	10 dB	32:	22.56
B:	50 MHz	64:	25.57
F:	3 dB	128:	28.56
		256:	31.53

$$d = \frac{c}{4\pi f}\sqrt{\frac{G_r G_t P_t}{P_r}} \tag{1.4}$$

Fig. 1.1 shows the available transmission distance as a function of transmitter and receiver combined antenna gain for different QAM (Quadrature Amplitude Modulation) modulation formats, with a constant signal bandwidth. The required SNR in the signal band, is given by the bit error rate for m-QAM modulation [17]:

$$P_e \simeq 4\frac{\sqrt{m}-1}{log_2(m)\sqrt{m}}Q\left(\sqrt{\frac{3\gamma}{m-1}}\right) \tag{1.5}$$

It is being assumed that the QAM is perfectly Gray coded, where each symbol error most likely causes one bit error [17]. The Q-function $Q(x)$ is given by:

$$Q(x) = \int_x^\infty \frac{1}{\sqrt{2\pi}} e^{-y^2/2} dy \tag{1.6}$$

The parameters used to obtain the graphs in Fig. 1.1 is shown in table 1.2. The transmitted power level is typical for most millimetre-wave radio applications. Increasing the transmitted power far beyond 15 dBm will steeply increase the cost of the power amplifiers [18]. The frequency, 28 GHz is a commonlly used band for wireless broadband access, with a typical allocated channel bandwidth of 50 MHz. The fading margin can be choosen quite low, giving margin for rain attenuation only, as fixed line of sight transmission is commonly used. All these parameters can vary slightly, but on the whole they give a typical power budget for a fixed millimetre-wave radio system. A number of conclusions can be drawn from Fig. 1.1. First, even for short transmission distances, hundreds of metres, a fair amount of antenna gain is needed even to transmit simple modulation formats, such as QPSK (Quadrature Phase Shift Keying = 4-QAM). Second, fixed links have been assumed. Assuming movable or mobile nodes requires significantly higher fading margin, further decreasing the range. This means that true mobile communications, using omnidirectional or low gain antennas such as being used in current cellular mobile telephony, will be very hard to achieve in practice. At least the transmitting or receiving antenna should have high gain, resulting in a restriction of millimetre-wave radio applications to point-to-point or point-to-multipoint transmission. A typical gain for a focused antenna is 30 to 35 dB, while a typical gain for an antenna covering a sector in a point-to-multipoint system is 10 to 15 dB for 90° to 30° sector angle [18]. A typical point-to-point link therefore has typically 60 to 70 dB total antenna gain, with a typical range of 10 to 30 km for QPSK modulation. A point-to-multipoint system with a total antenna gain of 40 to 50 dB has a range of 1 to 3 km. If more complex modulation schemes is used, the range is correspondingly reduced. An interesting possibility is the use of flexible modulation formats. In a point-to-multipoint system with 1 km total range, more complex modulation formats can with advantage be used for the more closer nodes. According to Fig. 1.1 a node 100 m away can receive 256-QAM, and nodes further away, can receive gradually less complex formats. In this manner, by using dynamic selection of modulation formats the overall bandwidth efficiency can be optimised without sacrificing transmission range.

1.1.4 Wireless Applications

Millimetre-wave radio is being used for a range of applications, mostly taking advantage of the inexpensive and abundant bandwidth available. Areas of applications for millimetre waves that has been proposed, or are in use include [19]:

- Satelite Communication: this is a well established area where millimetre waves have been used for some time for point-to-point links to and from orbiting satellites. The use of very high gain antennas allow satellite communications to take advantage of the bandwidth inherent in millimetre-waves.

- Video Distribution systems: The abundant bandwidth offered by the millimetre wave bands attracts attention for shortrange broadband high-definition video broadcasting, as a cost-efficient alternative to broadband cable distribution systems [20, 21]. Point-to-multipoint configuration is most commonly used. In Europe, the frequency band 40.5–42.5 GHz has been allocated for Multipoint Video Distribution system (MVDS)

- Wireless Local Area Networks: There has recently been an inreasing need for short-range high-speed wireless local area networks (LANs) for indoor applications. Millimetre wave systems are currently being developed to manage this demand [19]. In Europe, the 59.3 - 62.0 GHz band has been allocated for this purpose [13], as it takes advantage of the high degree of frequency reuse possible in this band [10]. The ACTS (Advanced Communications Technologies and Services) project AC006, MEDIAN (Wireless Broadband CPN/LAN for Professional and Residential Multimedia) had developed a demonstrator capable of transmitting 150 Mb/s data in this band [22]. In the USA the FCC has decided to assign the 59-64 GHz band for general purpose unlicensed devices for broadband wireless communication systems, however the development is at a very early stage, and it is expected that these systems will not come into use until around 2005, when necessary market demand has been built up [23].

- Microcellular Mobile Communication: Due to the increasing spectral congestion at microwave frequencies in the cellular phone market as the market expands, together with an emerging demand for broadband services, there is a need to move to higher frequency bands.

Millimetre wave frequencies are being investigated for this purpose [24, 25, 26]. In Europe, frequency bands around 40 and 60 GHz has been allocated by ERC (European Radiocommunications Committee) [13] to provide Mobile Broadband Services (MBS) compatible with B-ISDN (Broadband Integrated Services Digital Network). The ACTS project AC204, SAMBA (System for Advanced Mobile Broadband Application) has built a MBS trial platform in the 40 GHz band for 34 Mb/s data rate, 60m x 200m cell size and speeds up to 50 km/h [27].

- Fixed relay links: Longer distance point-to-point links using high gain antennas. One application is support infrastructure for mobile systems. In the UK, a 38 GHz band fixed link system has been developed for fixed links from 2 to 8 km, the PCN (Personal Communications Network) [26].

- Automotive sensing systems. Vehicle monitoring by radar, aims to improve driving safety in the next century. [19]. This application is now the only commercial use of higher frequencies in the 70 GHz band [28]. In the USA the 46.7-46.9 GHz and 76-77 GHz band is allocated

- Passive astronomical applications. Designated quiet bands have been allocated both in the USA and Europe for radio astronomy applications.

- Fixed Broadband Wireless Access (BWA). This is presently an emerging mass market utilising millimetre-wave frequencies. BWA is either using point-to-point or point-to-multipoint configurations. Common services are video distribution and broadband internet access. This is currently the highest volume market, and it is projected to grow quickly in the future. This is the most immediate application for the technologies described in this thesis.

1.1.5 Broadband wireless access

A number of options are presently available to increase the bandwidth between the Internet Service Provider (ISP) and the end users. The Asymetric Digital Subscriber Line (ADSL) uses existing twisted pairs of standard copper wire to simultaneously transmit voice and data. Upstream and downstream data rates up to 128 kb/s and 384 kb/s are available [29]. ADSL has the advantage that it uses existing infrastructure. The disadvantages are limited bandwidth and a requirement of proximity, within 6 km of the end user to a Central Office [29]. An alternative option that also takes advantage of existing infrastructure is access by cable modem. Data rates up to 1 Mb/s are available in the downstream path. However, the data rate decreases as the number of users increases and the links are highly asymmetrical with regard to uplink and downlink data rates. If no adequate wiring exists, or data rates exeeding what can be provided by existing wiring

Table 1.3: Frequency allocations in Europe and USA in the millimetre-wave frequency range.

Band (GHz)	Europe [13, 31]	USA [30, 34, 35]
24.0–24.25		Unlicenced ISM
24.25–25.25		Licenced ISM
24.0–30.0	Country specific BWA bands	
27.5–28.35		LMDS, block A
29.1–29.25		LMDS, block A
31.0–31.075		LMDS, block B
31.075–31.225		LMDS, block A
31.225–31.3		LMDS, block B
38.6–39.3		39 GHz BWA, block A
39.3–40.0		39 GHz BWA, block B
39.5–40.5	MBS (proposed)	
40.5–42.5	MVDS	
42.5–43.5	MBS (proposed)	
59.0–64		Unlicenced WLAN
59.3–62	Wireless LAN	
62.0–63.0	MBS (proposed)	
65.0–66.0	MBS (proposed)	

are demanded, alternative solutions are needed. Optical fibre connections can provide sufficient bandwith to cover demand for the foreseeable future. However, due to the cost of installing such connection, only large businesses can presently afford these.

Fixed broadband wireless access (BWA) provides an intermediate solution between existing electrical wiring and optical fibre, it can provide higher data rates than existing electrical wiring with lower intallation costs than optical fibre. Broadband wireless access is an emerging service that is predicted to reach a market value of $ 16 billion in 2005 [30] only in the 28 GHz band in the USA. This will provide the necessary mass market required to produce inexpensive millimetre-wave products, and will in turn enable other applications such as wireless LAN's to be more economically attractive. Fixed broadband wireless access provides a list of features [31, 29, 30]:

- High speed: Data rates exceeding 155 Mb/s are possible. These are greater than can be achieved using existing electrical wiring.
- Quick and inexpensive to install: No large investment in infrastructure, as no wires need to be installed, no right of way needs to be negotiated. Equipment costs are dominant. Quick installment allows fast marketing time and flexibility to increase capacity and investment with demand.
- High reliability: Wireless links are immune to cuts, floods and earthquakes. If need to repair arises, a wireless link can be repaired much more quickly than wired options.
- Low ownership costs: Low cost to repair and no need to lease cable infrastructure.

Altough lower frequency bands are utilised for BWA, such as the Multichannel Multipoint Distribution System (MMDS) band around 2.4 GHz in the USA, the millimetre-wave band is still attractive. The prime reason is the low cost of bandwidth and the abundance of bandwidth available, making future upgrading in response to increasing bandwidth demand possible. Despite these advantages the utilisation of these bands is presently relatively sparce. The major reason for this is the high price of millimetre-wave equipment and devices. Therefore, a very important research task will be to find inexpensive equipment for millimetre wave applications. Millimetre wave monolitic integrated circuits offer a potentially cheap solution, provided they are manufactured in large numbers [32]. This is only possible if mass market millimetre-wave systems are widely acceptable and attractive and one precondition of this is the allocation of spectum for these applications. Bands has been allocated for BWA and are listed in Table 1.3. In Europe, specrum allocations differ from country to country. Two main bands are used, 24-30 GHz and 39.5-43.5 [8, 13, 31]. In the UK, the bands 27.5 to 29.5 GHz and 40.5 to 43.5 GHz are currently in the process of being auctioned [14]. The 24.5 to 26.5 GHz band is also being considered for BWA. In the USA, the three main bands are 24 GHz to 25.5 GHz, 27.5 GHz to 31.3 GHz, refered to as the LMDS (Local Multipoint Distribution Services) band and 38.6 to 40 GHz refered to as the 39 GHz band [33, 15, 34]. Similar bands are allocated in Canada [35].

Standards are now being developed. In Europe BRAN (Broadband Radio Access Networks) is developing the HIPERACESS (HIgh PErformance Radio ACCESS) standard in the 40.5 to 43.5 GHz band [36]. In the USA IEEE has a working group, IEEE 802.16, defining standards for BWA systems [37]. These standards are currently under development, the issue of the standards will give further credibility for the development of BWA systems. At the moment BWA is marketed primarily to large and medium sized businesses that require higher data rates, and rural locations, where alternative access would be expensive to install. However, prices are decreasing, the cost of a radio link is halving every 7 years, while its data rate is doubling every three [30]. With these trends continuing in the future, Small Office/Home Office and Residential customers will be able to take advantage of this technology.

Fig. 1.2 shows a basic diagram of a typical BWA system architecture. A central control centre is connected to the core network, and/or any other source of the service to be provided, such as a satellite terminal. The central control centre is then connected to a local control station by either a direct fibre-optic connection, or via the core network. The local control station is used to control one or many antenna units, connected by a coax cable or a fibre-optic cable. Links between local control stations also exists. Finally, the antenna units are connected to the user stations by a wireless link, either direct or via a radio relay.

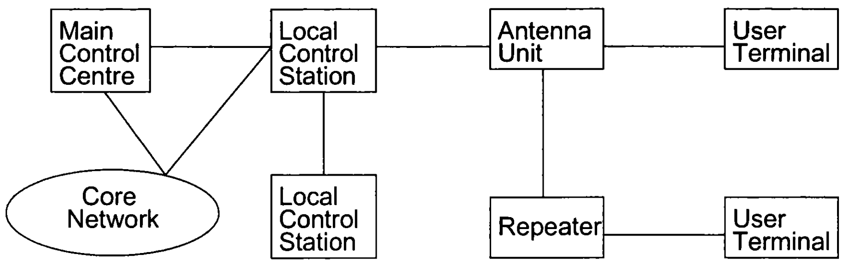

Figure 1.2: Diagram of typical BWA system architecture

The wireless access links can be divided roughly into two groups, point-to-point links and point-to-multipoint links. Point-to-point links have traditionally been used for radio infrastructure, radio trunk lines and radio access lines. Because of the high antenna gain and more relaxed power budget, point-to-point links can with advantage be used for longer transmission distances or for high data rates. Point-to-multipoint links uses a base station antenna with lower gain compared to point-to-point links. The option to be used in a BWA system is dependent on many factors. Point-to-multipoint links are with advantage used in higher density environments, when plenty of user stations are close by. Dynamic allocation of bandwidth is possible within each cell, allowing the data rate to be increased to individual base stations when overall demand is low. It can also be used when the locations for base station antennas are expensive, or sparse. Correspondingly, point-to-point links are with advantage used in more rural areas with plenty of space for antennas and long distances. Generally, point-to-multipoint type distribution is the most common for BWA. Fig. 1.3 shows an overview of a typical LMDS system architecture incorporating point-to-multipoint BWA, as described by the ACTS project, CRABS (Cellular Radio Access for Broadband Services) [38]. In the figure, there is a main coordination centre that is connected to the external network. Services are delivered from the main control centre, that can be located in the main coordination centre, to the LMDS cells via a feeder network. This network can consist of a combination of fibre/coax feeders and wireless point-to-point feeder links. The system architecture specified by

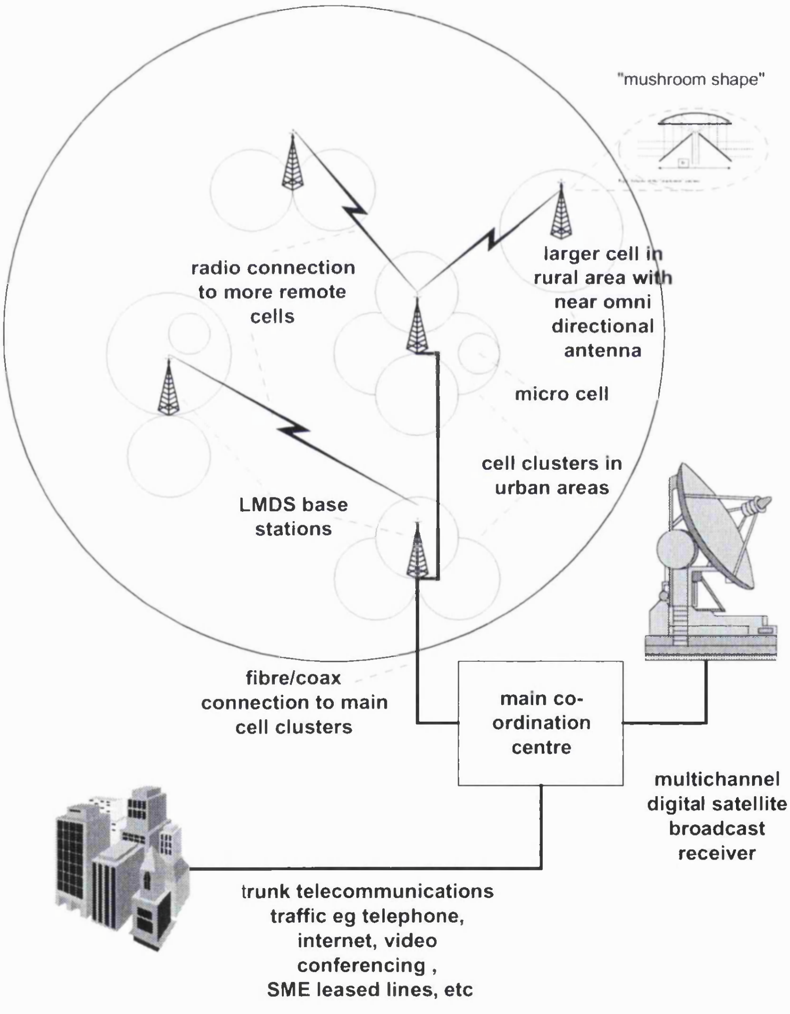

Figure 1.3: Overview of LMDS system architecture [38]

the CRABS project uses point-to-multipoint links with a 2-5 km cell radius, serving 70 % to 90 % of the population 99.99 % of the time. Each cell has a 2 GHz bandwidth, reaching 1.5 Gb/s gross capacity with QPSK modulation and up to 34 Mb/s channel data rate. An alternative architecture is outlined in [39]. This architecture uses point-to-point links in a mesh network, where each user node typically is a 1-4 way repeater. By using a total of up to between 6 and 10 successive hops, higher coverage densities, exceeding 90 %, can be achieved with better spectum efficiency than for a point-to-multipoint solution. In addition, unlike point-to-multipoint based systems, a mesh network can provide communication directly between the user nodes.

Multiplexing in the radio path has to be considered in a BWA system, multiplexing between users in the up and downlink and duplexing between up and downlink [18]. Frequency Division Multiplexing (FDM) uses a separate frequency channel for each user. When used for both up and downlink paths in a point-to-multipoint system, the system looks the same as a point-to-point system. Each user is provided with a fixed data rate and the user station compexity is relatively low. Generally, Time Division Multiplexing, (TDM) is more bandwidth efficient than FDM. It also allows for dynamic sharing of the composite bandwidth, allowing higher peak data rate to each user. TDM is especially useful for very bursty traffic. The disadvantage of TDM is increased required sensitivity of the user stations due to the higher received data rate and the increased complexity due to compression, expansion and time synchronisation needed for the signal in both user station and base station. TDM is suitable when a large number of users with low and irregular trafic, such as residential users, needs to be accomodated. One may also prefer to use FDM in the downstream path to assure a minimum access data rate, while using TDM in the upstream. Because of the need of both TDM and FDM in different situations, both modes of operation are now being incorporated in the developing IEEE 802.16 standard [40]. Code Division Multiplexing (CDM) is impractical for these data rates due to the complexity of the required chips. Duplexing is needed between uplink and downlink. By using Time Division Duplexing (TDD) only one signal band is needed in contrast to the separate up and downlink band needed for Frequency Division Duplexing (FDD). TDD has the advantage of allowing dynamic assymetry between up and downlink data rate capacity.

1.2 Radio over Fibre

Radio over fibre can be defined as the transmission of a radio signal over a path that is divided into a free space part and one part modulated onto a optical carrier and transmitted through a fibre optic link. For terrestial wireless applications, this was demonstrated by Cooper in 1990 [41], where he uses the optical fibre as a low loss extension to free space radio transmission. In a number of papers from Ogawa et al [42, 43, 44] this concept was developed. In [42] a number of different possible arrangements for radio over fibre were listed. The fibre radio concept for personal communications is further developed and put into a concept in [24] where the acronyms FTTA (Fibre To The Area), FTTC (Fibre To The Curb), FTTH (Fibre To The Home) and FTTB (Fibre To The Building) are defined. Other commonly used terms for radio over fibre include Hybrid Fibre Radio (HFR), or simply fibre radio and optical-wireless systems. The EURESCOM project P816, "Implementation framework for integrated wireless-optical access networks [45] attributes radio over fibre with the following characteristics:

1. The distribution segment between the service node and the remote antenna unit is implemented by optical fibre technology.
2. The drop segment is implemented by wireless (radio) technology.
3. In the distribution segment between the base station and the remote antenna unit, RF modulated lightwaves are used.
4. In the remote antenna units no baseband signal processing is involved.

1.2.1 Applications

Radio over fibre has found applications or potential applications over a range of areas. Antenna remoting to satellites is the area where radio over fibre techniques found their first practical applications. Bowers, et al [46] argues that due to the low loss in fibre, an antenna can be located remotely, free from terrestrial microwave interference and the received signal can be multiplexed and frequency translated at a convenient location far from the antenna. Two antennas separated by a large distance may also reduce the risk for outage due to rain. Such a remote antenna is most conveniently fed by an optical fibre from a central location. A transmission of 500 MHz bandwidth signals over 4 and 6 GHz subcarriers to and from a satellite antenna is demonstrated over 20 km fibre span [46]. A similar experiment, covering only the downlink can be found in [47].

Fibre radio has also been proposed for remote delivery of video services [20, 21, 48, 49]. Radio based distribution systems will offer relative savings as only a few distribution points need to be linked to the control station, compared to a directly wired broadband link to each home. The signals would be picked up by each user, using an inexpensive antenna capable of receiving millimetre-waves.

Wireless LANs is another application that radio over fibre is a natural candidate for. This could typically involve room sized radio paths and optical paths that can be measured in hundreds of metres. The relaxed power budget and low cost structure of such a system enables the use of passive antenna units, only powered by the received optical power [50, 51]. Millimetre wave radio over fibre has also been investigated for this purpose in the unlicensed 60 GHz band [52].

Possibly the main use for radio over fibre presently is within personal cellular mobile telecommunications. These systems are currently being manufactured for typical frequencies below 2 GHz. Typical areas where it is being used is to increase coverage of local hot spots, such as indoor shopping centres, airports and highways, and to extend coverage to places not otherwise covered, such as in underground rail tunnels. Radio over fibre is a strong candidate for use in millimetre-wave mobile communications, such as MBS. However, since MBS is currently in the research stage, there is not much activity relating to millimetre-wave radio over fibre at the moment.

The area where millimetre-wave over fibre perhaps has the greatest imediate potential is within the millimetre-wave radio market with the greatest potential, BWA systems. There are four locations within a BWA architecture, shown in Fig. 1.2, where radio over fibre can be used: between the main control centre and the local control station, between the local control station and the antenna unit, for distribution to the user antenna unit, and as a relay link between two antenna units. The second mentioned location is the first and obvious implementation point for radio over fibre. One local control unit can be used to receive data for and distribute modulated RF (Radio Frequency) signals to a multitude of antenna units. With this method, the local control station takes the functionality of a multicell radio base station. A range of advantages are then obtained [45]:

- Dynamic allocation of radio frequency resources. The aggregated bandwidth over many radio cells may be smaller than the sum of the peak bandwidths. Radio resources could be used where they are the most needed.

- Higher integration by resource sharing of functions such as power supply, clock distribution, micro controller processing capacity, memory, frequency stable reference, etc.

- Reduced operation and maintenance cost. Easier access to the bulk of the complexity in the system and simpler and more robust antenna units with lower risk of breakdown and longer lifetime. This is a considerable advantage if the antenna units are located in inaccessable places.

- Easier migration to new radio technologies, as a large part of the infrastructure is independent of frequency and modulation scheme. Easier to switch between service providers and protocols for the same reason.

Depending on the distance and frequency to be transmitted, Standard Single Mode (SSM) fibre, less expensive multimode fibre or cheap plastic fibre can be used in these links. One disadvantage of radio over fibre on this system level is that the migration from wireless to wired access points is not as natural as when one core network access point is used for each antenna unit.

Radio over fibre between the main control centre and the local control station would result in an even higher degree of centralisation of functionality, as the main control centre could control a large total number of antenna units that covers the entire local area. With this option, a very flexible system architecture is achieved. The frequency to be transmitted through each antenna can easily be changed, allowing central, adaptive and dynamic control of the frequency plan that is used. Other advantages listed above are also accentuated. New services can easily be added, only by modifying the main control centre. However, one major stumbling point is the cost of using the optical fibre. Transmission of analogue signals through optical fibre is less bandwidth efficient than transmission of baseband data signals. This can be used only if the installation or rental of dark optical fibre is inexpensive. Indoor distribution on the user side could with advantage be achieved between the outdoor antenna units and a local router, conected by inexpensive indoor plastic or multimode fibre. This has all the advantages that radio over fibre transmission between the main control centre and the local control station has, with the added benefit of less expensive installation of fibre. Relay links between two antenna units are useful when the radio signal needs to be routed around an obstacle when line of sight radio transmission is hard to achieve. instead of routing the baseband signal via the fibre with the corresponding modulation/demodulation, radio over fibre presents a much simpler and more attractive solution.

1.2.2 Fibre transmission properties

The fibre link part of radio over fibre is an analogue fibre optic link and as such it cannot be assumed to be transparent, that is delivering an output signal identical to the input signal. The signal will be modified by various effects that have to be considered.

Link gain, frequency response and range

The available transmission range of an analogue link is dependent on the total gain of the link, which is in turn dependent of the frequency to be transmitted. The link gain is defined as the output RF power divided by the input RF power. The total link gain is dependent on the cable loss and the loss of the interface to and from the cable. Three common sorts of cable will here be considered, electrical coaxial cable, multimode optical fibre and Standard Singlemode (SSM) optical fibre. In a conventional 50 Ω coaxial cable, the interface loss is negligible, as no special interface is needed in a 50 Ω system. However, the transmission loss is highly frequency dependent and generally high relative to transmission through optical fibre, especially at millimetre-wave frequencies. Coaxial cable is suitable for low frequencies and short distances only. Using low loss cables and 18 GHz carrier frequency, a maximum transmission distance is around 30-40 m before the transmission loss is higher than can be achived using a fibre optic link, including electro-optic and opti-electric conversion losses. The high price and loss of coaxial cables makes them unsuitable at millimetre-wave frequencies.

A fibre optic link is better used. The low cost of fibre optics and the low attenuation of the optical signal allows cheap and effective transport of the radio signal. Standard singlemode fibre offers the best performance, about 0.2 dB per kilometre attenuation, offering typically up to a few tens of kilometres of transmission range. If optical amplification is used the range can be greatly improved, however optical amplifiers are expensive components, and are not viable for use in a low cost system except for compensating for fibre splitting losses. The bandwidth of SSM fibre is very large indeed. The limitation lies in the electrooptical intefaces, i.e. the laser diode and photodetector in a directly modulated link. Laser diodes with 30 GHz modulation bandwidth has been reported [53], however commercially DFB (Distributed Feed-Back) lasers has usually a modulation bandwith up to about 10 GHz, too low for a directly modulated link, so generally high speed optical modulators, or more advanced signal generation methods has to be used. The frequency range of a SSM link for longer transmission distances will also be discussed further down under the subheading 'Fibre chromatic dispersion'.

Multimode fibre is often prefered to SSM fibre due to the lower cost of optical components. Because of the significantly larger fibre radius, fibre coupling of the optical components is much less complicated and less expensive. Multimode fibre has higher loss due to mode dispersion, limiting the typical transmission range to about 500 MHz·km at 1310 nm for baseband data communications [54]. However, due to the narrowband characteristics of the radio over fibre signal, transmission ranges exceeding 500 MHz·km at 1300 nm can be achieved at higher carrier frequencies [55]. It can be very hard to give any consistent value for the multimode fibre loss for these conditions due to the highly individual frequency response for different optical fibre [56]. In any case, the transmission loss is higher than for SSM fibre and multimode fibre is mostly used for transmission distances lower than 1 km.

Fig. 1.4 shows typical transmission gain versus fibre length for different sorts of cables. It is being assumed that multimode fibre components have somewhat higher coupling efficiency than SSM fibre and the average signal attenuation has been put to 7 dB/km according to [57] and Midwest Microwave CSY-80 cables with a microwave attenuation of 0.63 dB/m at 18 GHz have been used. These figures represents only a general picture which varies according to what components are being used. It is seen that coaxial cable is with advantage used for low transmission distances, both regarding cost and loss. Multimode fibre can be used for intermediate transmission distances, mainly because of the lower cost of the electro-optical components, and SSM fibre for higher transmission distances because of the lower loss.

Noise

In an analogue fibre optic link, extra noise will be added to the transmitted signal. In a properly designed link, noise originates from the following sources; optical receiver thermal noise including preamplifier noise, Relative Intensity Noise (RIN) of the optical source, photodetector shot noise and if optical amplification is used, Amplifier Spontaneous Emission (ASE) noise. The noise sources can be assumed to be uncorrelated as an effect of the random nature of the noise

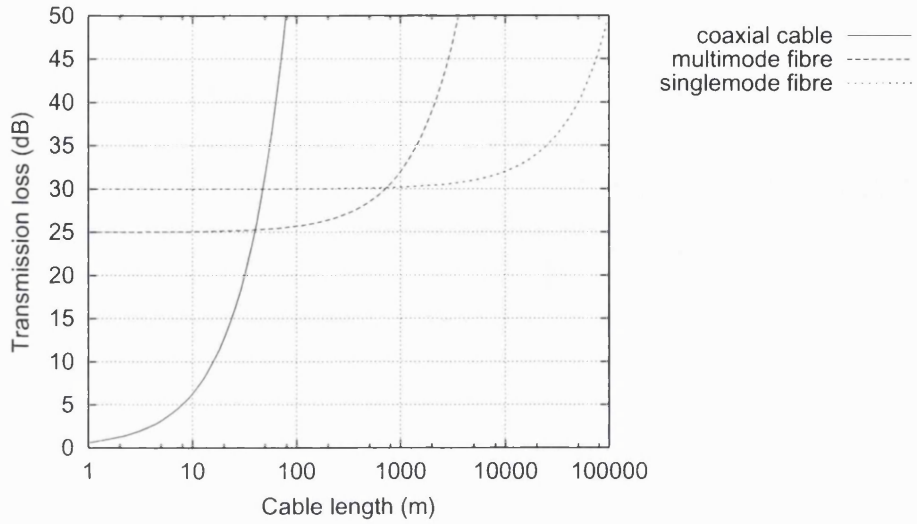

Figure 1.4: Electrical transmission loss for use of SSM fibre links, multimode fibre links and coaxial cable. 18 GHz carrier frequency and Midwest Microwave CSY-80 coaxial cable has been assumed

distribution, and therefore the total equivalent input noise power density to the preamplifier can therefore be expressed as:

$$N_t = N_{th} + N_{rin} + N_{shot} + N_{ase} \tag{1.7}$$

N_t :	Total equivalent input noise power density (W/Hz)
N_{th} :	Thermal and amplifier noise density (W/Hz)
N_{rin} :	Optical source relative intensity noise density (W/Hz)
N_{shot} :	Shot noise density of the photodetector (W/Hz)
N_{ase} :	Optical amplifier spontaneous emission noise density (W/Hz)

The thermal noise power spectral density of the receiver into the load to the photodetector is given by the following relation [58]:

$$N_{th} = 4k_B T_0 F \frac{Z_{pd} Z_l}{(Z_{pd} + Z_l)^2} \tag{1.8}$$

k :	$1.38 \cdot 10^{-23}$ J/K	Boltzmann's constant
T :	295 K	Photodetector equivalent noise temperature
F :		Pre-amplifier noise factor
Z_{pd} :		Photodetector impedance (Ω)
Z_l :		Load impedance (Ω)

The noise power density originating from the RIN of the optical source is given by:

$$N_{rin} = \varsigma (RI_{rx})^2 Z_l \tag{1.9}$$

ς : Optical source relative intensity noise (dBc/Hz)

R : Photodetector responsitivity (A/W)

I_{rx} : Received optical signal power (W)

The photodetector shot noise density is given by:

$$N_{shot} = 2q_e R I_{rx} Z_l F_{edfa} \tag{1.10}$$

q_e : $1.6022 \cdot 10^{-19}$ C Elementary electron charge

F_{edfa} : EDFA noise factor

The EDFA (Erbium Doped Fibre Amplifier) noise figure is only incuded in the formula if optical amplification is used. The noise figure is given by $F_{edfa} = 2n_{sp}$, where n_{sp} is the spontaneous emission factor of the EDFA [59]. The ASE noise is given by [60]:

$$N_{ase} = \frac{\lambda^2}{c\delta\lambda_f} 2R^2 I_{ase} I_{rx} Z_l + \frac{\lambda^2}{c\delta\lambda_f} (R I_{ase})^2 Z_l \tag{1.11}$$

λ : Optical wavelength

$\delta\lambda_f$: Optical filter bandwidth

I_{ase} : Received optical power due to ASE

The first term represents signal-ASE noise and the second term represents ASE-ASE noise.

The fibre optic link can be optimised in different manners, with different noise sources limiting the performance. In an unamplified optical link, thermal noise dominates at low received optical powers, laser RIN at high received optical power and laser shot noise can dominate at intermediate received optical power in a low-noise receiver. If optical amplification is used, care must be taken where the amplifier is located in the link. If the amplifier is located at the receiver end of the link, a low noise amplifier should be used together with an optical filter to reduce the received ASE noise power.

Dynamic range

The dynamic range is a measurement of the maximum signal power range that a link can support. The third order intermodulation product originates from the mixing of two strong carriers, which produces an unwanted carrier at an offset from one carrier, of the difference frequency. Generally, as in [61], the dynamic range is limited by the signal power and the point where the third order intermodulation product power is equal to the noise floor. This is called the Spurious Free Dynamic Range (SFDR). If only one carrier is modulated, the dynamic range can also be quantified by the ratio between the noise floor and the 1 dB compression point of the gain. The Dynamic range can be enhanced by minimising the noise and using very linear components that can support a very high modulation index, without producing significant third order intermodulation products. The following expression for the SFDR can be derived by dividing the third order intercept point, (IP_3), that is the extrapolated carrier power where the intermodulation products are of equal power to the fundamentals, with the noise floor level, and using the knowledge that the output signal power icreases linearly with the input signal power and the third order modulation products increases propotionally to the third power of the input signal power.

$$SFDR = \left(\frac{IP_3}{N_t}\right)^{\frac{2}{3}} \tag{1.12}$$

IP_3 is in turn given by:

$$IP_3 = P_{out}\sqrt{\frac{P_{out}}{P_{IM3}}} \tag{1.13}$$

P_{out} Output signal power (W)

P_{IM3} Third order intermodulation product power (W)

Generally, optical sources have lower linearity than optical detectors, therefore the challenge in linearising analogue optical links generally lies in producing highly linear optical sources.

The dynamic range can be a limiting factor in analogue fibre optic links. In wireless systems, the uplink path has the most stringent requirement of dynamic range, as many signals can be received by the base station with a wide range of power levels. The dynamic range requirements can be eased by using power control at the user terminals. For fixed BWA applications, dynamic range requirements are generally low enough not to be a limiting factor, as focused user antennas are used with fixed transmitted and received power level and line of sight transmission, limiting the range of received power levels.

Fibre transmission imparements

Transmitting an optical signal through long streches of fibre will distort the optical signals in different ways other than attenuating the signal, fibre chromatic dispersion and Polarisation Mode Dispersion (PMD) being the most important. Other effects due to fibre non-linear effects include self-phase modulation, cross-phase modulation, four wave mixing, stimulated Brillouin scattering and stimulated Raman scattering.

Chromatic dispersion is an important factor in analogue optical links, and has been examined both theoretically and experimentally [62, 63, 64]. Chromatic dispersion originates in the wavlength dependency of the refractive index of the optical fibre. At 1550 nm, a typical value of the chromatic dispersion is 17 ps/nm/km. At 1310 nm, the dispersion is negligible. When using double sideband modulation, chromatic dispersion induces a phase shift between upper and lower modulation sideband that results in a power penalty in the detected signal. The power penalty can be derived from equation A.7 in appendix A and can be experssed as:

$$\Gamma_D = cos^2\left(\pi D\frac{\lambda^2}{c}Lf_m^2\right) \tag{1.14}$$

D	17 ps/nm/km	Dispersion factor
λ	1550 nm	Optical wavelength
c	$3 \cdot 10^8$ m/s	Speed of light
L		Fibre length
f_m		Modulation frequency

Using this equation, the available transmission distances versus modulation frequency for different values of dispersion penalty. The result is plotted in Fig 1.5. We can observe that for millimetre-wave modulation frequencies, the available transmission distance is limited to a few or a fractions of kilometres. In order to overcome this problem, single-sideband modulation needs to be used, or alternatively some sort of dispersion compensation. Examples of dispersion compensation methods that have been used are dispersion shifted fibre [66] or chirped fibre gratings [65]. The use of single sideband modulation has the advantage over dispersion compensation that it is independent of the length of the optical fibre.

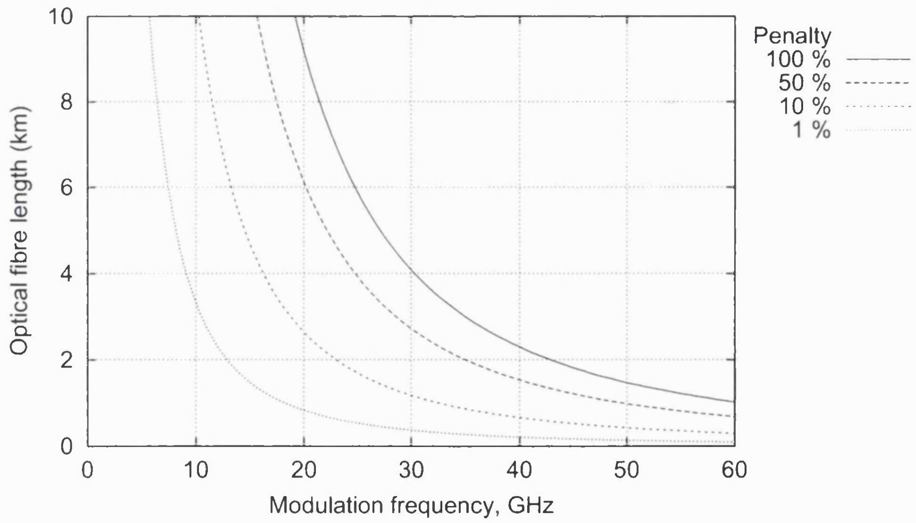

Figure 1.5: Available transmission distances versus modulation frequency for different values of dispersion penalty of optical fibre transmission for double sideband modulated signals. Singlemode fibre with 17 ps/km/nm dispersion has been assumed.

In the absense of fibre chromatic dispersion, other distorting factors, such as Polarisation Mode Dispersion (PMD) needs to be investigated. PMD arises due to birefringence of the optical fibre, where the refractive index varies according to the polarisation of the optical field. PMD is categorised into first order PMD and second order PMD. First order PMD induces a polarisation dependent differential delay. The birefringeance that causes the PMD can be assumed to be time variant, randomly distributed over the optical fibre, both in location and orientation of the birefringeance axes. The resulting PMD has therefore statistical properties [67]. Second order PMD is the wavelength dependence of the PMD. In baseband optical links, PMD has the effect of widening the optical pulses. In analogue links, PMD has two main effects, both dependent on second order PMD [69]. First, it gives rise to a nonlinear distortion, propotional to the modulation frequency. This distorts the signal when the wavelength dependence of the birefringeance interacts with the chirp of a modulated signal, creating an extra phase modulation of the optical signal [68]. The second effect is a wavelength dependent induced time delay, similar to the fibre chromatic dispersion, only with a randomly distributed magnitude. Because of the statistical nature of PMD, the average first order PMD induced time delay between different modes increases with the square root of the transmission distance, a typical value of the standard deviation of the polarisation dependent time delay being 0.01 to 0.8 $ps/\sqrt{km}$ for SSM fibre [45]. The standard deviation of second order PMD is proportional to both the modulation frequency and the transmission distance. This can be added to the value of the chromatic dispersion coefficient, as it has the same wavelength and transmission distance response. Generally in a system limited by the chromatic dispersion of the fibre, second order PMD can be ignored, as the standard deviation is much smaller than that due to the dispersion. However, unlike chromatic dispersion, PMD cannot be compensated for in a passive manner as the PMD is a random process, varying in time. PMD has been experimentally investigated for analogue links in [68, 69, 70].

1.2.3 System architectures

Millimetre-wave radio over fibre comes with some technical difficulties because of the high carrier frequency that is to be transmitted. The first is the difficulty of the generation of the millimetre-wave modulated optical carrier and the second is the dispersion penalty for double sideband modulation at these frequencies. Because of these difficulties, a range of architectures for delivering millimetre-wave radio over fibre can be considered, some being outlined in Fig. 1.6.

The first architecture outlined, is the most straight-forward one. The millimetre-wave radio signal is generated and modulated onto the optical carrier, both in the uplink and the downlink. The main advantage of this method is one of simplicity. The base station is taking the function of an optical to wireless repeater, including some gain, making the least complex base station in principle. However, presently optical sources with millimetre-wave modulation bandwidth are expensive and can also be complex, this is especially true for single sideband sources, if the use of dispersion compensation is to be avoided. This architecture has been demonstrated using an Elec-

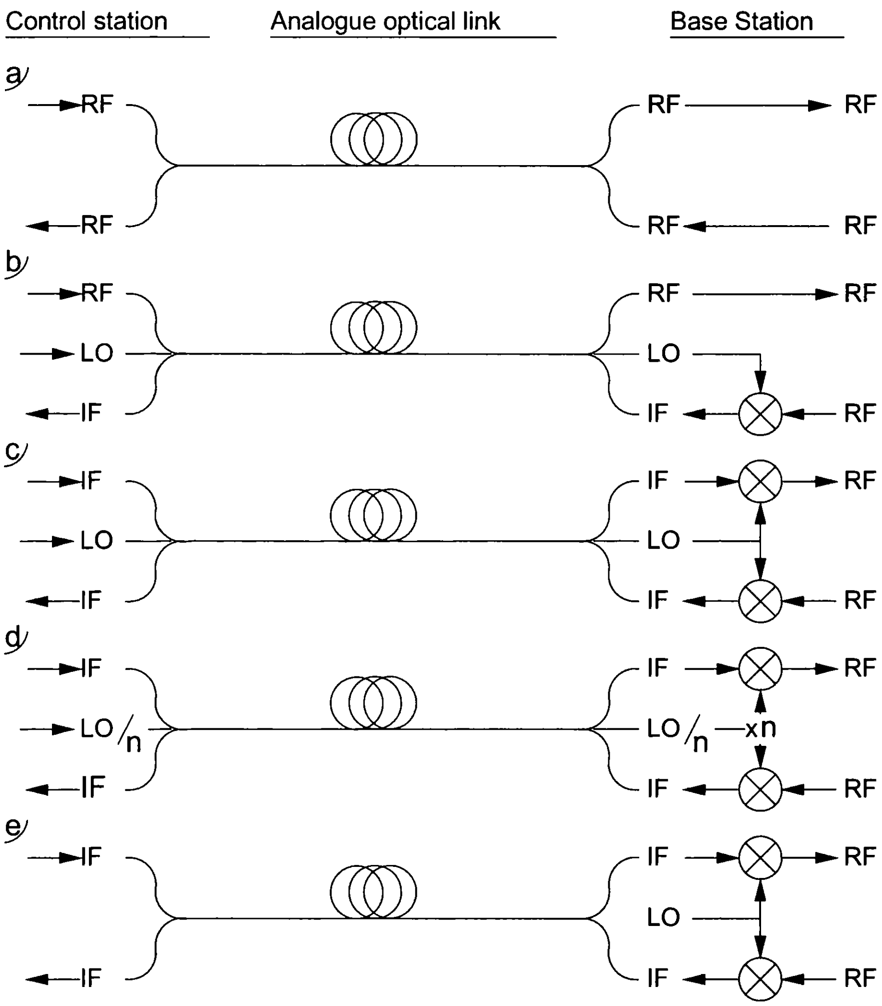

Figure 1.6: Diagrams for five different millimetre-wave radio over fibre architectures with signal frequencies annotated.

tro Absorption Modulator (EAM) in [71]. The architecture outlined in Fig. 1.6(b) and (c), uses optical delivery of a millimetre-wave carrier that is being used to downconvert the uplink signal, and in (c) also to upconvert the downlink signal. The advantage is that electrical to optical conversion in the base station can take place at a lower frequency, where component costs are lower and fibre cromatic dispersion no longer limits the use of double sideband modulation. In practice, the base station using this architecture can be less technically difficult and less expensive to design than the one outlined in (a), especially if system requirements, such as noise performance and linearity are high. These architectures are the ones most commonly used and have been demonstrated in [72, 73, 74]. If a reference signal that is a subharmonic of the millimetre-wave carrier is optically delivered to the base station, as in example (d), no millimetre-wave electro-optical components need to be used, allowing a less complicated and less expensive optical link to be used. The price is increased complexity of the base station. If the received reference signal is simply received, multiplied and used to frequency convert the uplink and downlink signal, the phase noise of the received reference signal is also multiplied and therefore the performance requirements of the optical link increases with the square of the multiplication factor. The solution to this problem is to use an oscillator that provides the required signal purity and phase-lock it to the received reference signal. This is demonstrated in [75]. However, phase-locking at high frequencies requires complicated circuitry. Using a free-running oscillator would combine a low frequency optical link with a relatively less complicated base staion. This is a good solution if the required frequency stability of the transmitted radio frequency is within the frequency drift range of the base station oscillator. If high frequency stability is required, no simplification of the base station is achieved, as a precision frequency reference is required in the base station to which to phase lock the oscillator.

So far, only simple architectures, connecting the control centre to one base station have been considered. If one control centre is being used with several base stations, network topologies have to be considered. The most simple option is the star topology, where each base station is connected to the control centre by an individual fibre. This topology does not require any multiplexing of the signals to be distributed to the base stations onto one fibre. The drawback is the inefficient use of the optical fibre. Often, when the cost of installing the fibre is significant, more efficient use of the fibre is desirable. Two common topologies that then can be considered are the tree topology, where the signal is transported on a single fibre first and split closer to the base stations, as demonstrated in [76]; and the ring topology, where one single strech of fibre is used to connect to all base stations and returns back to the control centre. The tree topology is well suited to the situation where all the base stations are gathered in a close area, well separated from the control centre. In both cases, multiplexing in the optical path is needed.

Two methods of multiplexing are usually considered, subcarrier multiplexing (SCM) and wavelength division multiplexing (WDM). Initially SCM was generally regarded as the preferred choice, partly because neighbouring microcells must have different carrier frequencies, to avoid interference, so the signals to the different base stations would intrinsically be sent over separate frequency bands. Blumenthal, et al [77], proposes SCM to simultaneously transmit base band data with control channels. Ohmoto, et al [78], investigate a dynamic transmission scheme where a spectrum delivery switch is used. The spectrum delivery switch directs the subcarrier channels to where they are needed the most, thus lowering the blocking probability. Other transmission systems using SCM have been proposed in [79, 80, 81, 82, 44]. A disadvantage of SCM is the high performance requirement on the components, especially in terms of low third order intermodulation distortion, due to nonlinearities in the laser diode. This problem increases with the number of subcarriers that are used [83]. Injection locking has been investigated to reduce third order intermodulation distortion in [84]. In [85] the effect of phase noise of the laser diode on a SCM system is also investigated. A second disadvantage is that the multiplexing is taking place in the electrical domain, requiring all base station optical receivers to receive the same composite optical signal that is being divided between them, providing poor efficiency, as each base station only would require a small part of the composite optical signal. SCM is suitable as a low cost alternative when the number of base stations is small.

WDM is achieved by separating the signals to the different base stations by using different optical wavelengths. The third order intermodulation distortion between channels is here a much smaller problem, even though crosstalk still is present [86], and higher efficiency is achieved, as only the relevant part of the composite optical signal is directed to each base station. A more flexible frequency allocation can also be applied, any RF frequency can be allocated to the different cannels, as they are applied to different optical carriers. Emerging technologies within WDM also promise future availability of inexpensive WDM devices, such as filters, wavelength sensitive couplers, etc. An example of WDM transmission has been proposed and demonstrated in [87]. A multi-frequency light source generates a number of different optical carriers, separated by a fixed frequency, each individually modulated by IF (Intermediate Frequency) signals. The signals are multiplexed, transported by fibre to an optical frequency DEMUX switch, which distributes the signals to the antenna units. The DEMUX selects two frequency components, which are mixed on the photodiode, to generate the mm-wave source. In this technique, only one optical source is needed to produce a large number of channels, however, this source is complicated by the multi-frequency requirement. The DEMUX switch can also actively direct the channels to different antenna units. Other WDM demonstrations can be found in [88, 89, 90, 91, 92].

1.3 Objectives and Outline of the Thesis

One of the major technical callenges in a millimetre-wave radio over fibre system is the generation of millimetre-wave modulated optical signals. This is because of the features that are desirable of this source, including:

- Single sideband modulation format, to avoid the use of dispersion compensation that is needed to transmit conventional double sideband modulated optical signals over longer spans of SSM fibre.
- High efficiency, in terms of efficient utilisation of the output power from the optical sources, i.e. low insertion loss and high optical to millimetre-wave conversion efficiency. This is needed to avoid the use of optical amplifiers.
- High spectral purity, to support complex multilevel modulation formats.
- High flexibility, both in terms of what modulation format that can be applied and the range of frequencies that can be generated.
- High stability and low potential cost, a requirement for any 'real-world' commercial application for the technology outside a protected laboratory environment and for production in larger numbers.

No single technology presently exists that satisfies these demands. The millimetre-wave modulated optical source is also important as it dictates what system architecture outlined in Fig. 1.6 can be used. A satisfactory solution of this technical challenge will provide a very important advance in the development of millimetre-wave radio over fibre systems. The two main objectives of this work are:

1. To realise a millimetre-wave modulated optical source that as far as possible satisfies the need for an efficient low-cost, high performance and highly flexible single sideband modulated optical source.
2. To use the developed optical source to demonstrate high performance millimetre-wave radio over fibre transmission.

The thesis describes the attempts to achieve these aims and the main achievements accomplished:

1. The development of the first millimetre-wave optical injection phase-lock loop.
2. The first millimetre-wave radio over fibre transmission experiment using optical phase-lock loop techniques.

3. The widest bandwidth modulation applied to the microwave reference in an optical phase-lock loop or an optical injection locking based heterodyne system.

4. The longest radio over fibre transmission demonstrated, supporting broadband data rates ($>$10 Mb/s) and not using optical amplification.

This thesis is divided into six chapters. This, the first chapter is the introduction. In this chapter a broad introduction of relevant topics is given together with a wide review of literature. The first section 1.1 gives a review of millimetre-wave wireless radio. The transmission properties are listed and the main applications, notably fixed wireless broadband access systems, are also reviewed. The second section, 1.2 gives a background to millimetre-wave radio over fibre. The main applications where it can with advantage be used and the benefits of using it are treated. Some properties of radio over fibre transmission and some systems aspects are also investigated. The chapter concludes with this statement of the objectives and outline of the thesis.

In the second chapter, 'Review of Millimetre Wave Radio over Fibre Transmission Experiments', different millimetre wave modulated optical sources are investigated. It is shown how these sources can be used to transmit data modulated millimetre wave radio signals over spans of optical fibre. In the introduction a number of desired features of the millimetre wave source were defined. Thereafter, the different sources of millimetre wave modulated optical signals that have been demonstrated were described. It was shown how data can be applied to these sources. Finally, some millimetre wave radio over fibre transmission experiments are summarised in Table 2.2. Based on these investigations, the strengths of the different sources can be defined in relation to the desirable features defined in the introduction of the chapter.

The third chapter, 'Carrier Generation and Transmission: Theory', describes the theoretical basis for the first demonstration of a millimetre wave OIPLL. The expected stabiity and spectral purity of the generated signal are predicted. The degradation of the generated carrier due to fibre transmission is also investigated, both with regard to the decorrelation of the two main optical lines and due to interference with the additional beats originating from the unwanted master laser FM sidebands.

In the fourth chapter, 'Carrier Generation and Transmission: Experiments', the first experimental demonstration of a millimetre wave OIPLL is described. Results showing the spectral purity, stability and frequency tuning range of the generated millimetre wave modulated output is accounted for. In addition, it is experimentally shown how the purity of an optically delivered millimetre wave signal can be improved by filtering in the optical receiver.

The following two chapters, 'Amplitude Shift Keying Transmission Experiments' and 'Differential Phase Shift Keying Transmission Experiments', treats the radio over fibre transmission demonstrations performed using two different modulation formats, amplitude shift keying in the fourth chapter and differential phase shift keying in the fifth chapter. The experimental setup is described. The theoretically expected performance is derived and compared to the experimentall results.

The last chapter, 'Conclusion', summarises the thesis and lists the main achievements and conclusions reached from this work. It also describes how this work could be extended in the future, and how and where it could be incorporated into a wider systems scenario.

References

[1] European Telecommunication Standard, document 'ETS 300 609-3', 1999.

[2] European Telecommunication Standards Institute, document UMTS 21.01 version 3.0.1, 1997.

[3] IEEE Std 802.11-1997 Information Technology- telecommunications And Information exchange Between Systems-Local And Metropolitan Area Networks-specific Requirements-part 11: Wireless Lan Medium Access Control (MAC) And Physical Layer (PHY) Specifications, 1997.

[4] www.spectrumauctions.gov.uk

[5] A. Seeds, "Photonic Technologies and Subsystems for Terabit Communications," *IEEE MTT-s Digest*, TU3E-2, pp. 615-618, 1999.

[6] T. Yoneyama and K. Honjo, "Recent advance of millimeter wave technology in Japan," *IEICE Transactions of Communications*, vol E79-B, pp 1729-1739, 1996.

[7] K.H. Craig and J.R. Norbury, "Interference mechanisms which affect frequency reuse on short line-of-sight millimetric links," *Eighth International Conference on Antennas and Propagation,* vol.2, pp. 999-1002, 1993.

[8] D.M. Bush, "MVDS:- an outline of standards and planning considerations," *IEE Colloquium on Radio Communications at Microwave and Millimetre Wave Frequencies,* Digest No. 1996/239 pp. 4/1-4/8, 1996.

[9] A. Seville and K.H. Craig, "Semi-empirical model for millimetre-wave vegetation attenuation rates," *Elec. Lett.*, vol. 31, pp. 1507-1508, 1995.

[10] Federal communications commission, bulletin number 70: "Millimeter wave propagation: spectrum management implications," 1997.

[11] K.H. Craig, M.P.M. Hall, L.R. Norbury, Y. Seville, M.J. Willis, J.A. Biddiscombe and T.G. Hayton, "Propagation research for millimetrewave cellular systems," *Tenth International Conference on Antennas and Propagation,* (Conf. Publ. No. 436), Vol. 2, pp. 383-386, 1997.

[12] J.R. Norbury, K.H. Craig and M.P.M. Hall, "Propagation research for millimetrewave cellular services," *IEE Colloquium on Radio Communications at Microwave and Millimetre Wave Frequencies,* (Digest No. 1996/239), pp. 12/1-12/4, 1996.

[13] ERC report 25, "Frequency range 29.7 MHz to 105 GHz and associated european table of frequency allocations and utilisations," Brussels, June 1994, revised in Brugge 1998.

[14] www.radio.gov

[15] http://www.fcc.gov/wtb/

[16] P. Mikkonen, "Modern 60 GHz Radio Link," *29'th European Microwave Conference - Munich,* pp. 83-86, 1999.

[17] F. Xiong, "Digital Modulation Techniques," Artech House INC, Norwood, Ma, 2000.

[18] K. Koga, Y. Fujimoto and S. Tejima, "Radio Link Configurations of Broad-band Wireless Access System," *IEEE International Conference on Personal Wireless Communication,* pp. 354-358, 1999.

[19] T. Ihara and K. Fulimura, "Research and development trends of millimetre-wave short-range application systems," *IEICE Transactions of Communications,* vol. E79-B, pp. 1741-1753, 1996.

[20] J. O'Reilly and P. Lane, "Remote delivery of video services using mm-waves and optics," *J. Lightwave Technol.,* vol. 12, pp. 369-375, 1994.

[21] J. Park and K.Y. Lau, "Millimetre-wave (39 GHz) fibre-wireless transmission of broadband multichannel compressed digital video," *Electron. Lett.* vol. 32, pp. 474-476, 1996.

[22] Wireless Broadband CPN/LAN for Proffessional and Residentioal Multimedia Applications (60 GHz), CEC Deliverable number: AC006/IMST/aaa/DS/P/001/c1.

[23] H.H. Meinel, "The market for short-haul line-of-sight millimeterwave transmission links," *IEEE MTT-s Digest,* pp. 487-488, 1996.

[24] S. Komaki and E. Ogawa, "Trends of fiber-optic microcellular radio communication networks," *IEICE Transactions of Electronics,* vol. E79-C, pp. 98-104, 1996.

[25] K. Morita and H. Ohtsuka, "The new generation of wireless communications based on fiber-radio technologies," *IEICE Transactions of Communications,* vol. E76-B, pp. 1061-1068, 1993.

[26] N. Imai, H. Kawamura, K. Inaki and Y. Karasawa, "Wide-band millimeter-wave/optical-network applications in Japan," *IEEE Trans. Microwave Theory Tech.,* vol. 45, pp. 2197-2207, 1997.

[27] M. Progler, "SAMBA: a mobile broadband enabler," *European Microwave Conference - Munich,* pp. 87-90, 1999.

[28] M.J. Marcus, "Spectrum Management Implications of Millimeter Wave Technology," *IEEE MTT-s Digest,* pp. 631-634, 1994.

[29] A.P.S. Khanna, "Broadband Wireless Access Trends and Challenges," *European Microwave Conference - Munich,* pp. 79-82, 1999.

[30] A. Dutta-Roy, "Fixed wireless routes for internet access," *IEEE Spectrum,* pp. 61-69, Sept. 1999.

[31] "Broadband Wireless Ready to Deliver," Microwave Engineering Europe, pp. 21–28 Sep.-Aug. 2000.

[32] T. Yoneyama and K. Honjo, "Recent advance of millimeter wave technology in Japan," *IE-ICE Transactions of Communications,* vol. E79-B, pp. 729-1739, 1996.

[33] Y.S. Rao and M.N. Roy, "An overview on harmonization of broadband wireless standards," *IEEE International Conference on Personal Wireless Communications,* pp. 178-183, 2000.

[34] A. Arunachalam, "Global standardization efforts of BWA systems based on cable modem," *IEEE Emerging Technologies Symposium: Broadband, Wireless Internet Access,* pp. 1-4, 2000.

[35] S. Marin, D. Weiner and J. McCoy, "Recommended LMDS band plan for systems in the united states," *1999 Emerging Technologies Symposium,* pp. 1-5, 1999.

[36] www.etsi.org/BRAN/

[37] www.grouper.ieee.org/802/16/

[38] Final Report ACTS project AC215 CRABS, document reference: AC215/TEL/RD/AR/P/D5P2B/b1

[39] P. Whitehead, "Mesh networks; a new architecture for broadband wireless access systems," *IEEE Radio and Wireless Conference, RAWCON 2000,* pp. 43-46, 2000.

[40] J. Foerster, G. Sater and A. Arunachalam, "LMDS standards architectural issues," *IEEE Wireless Communications and Networking Confernce, WCNC. 2000,* vol. 3, pp. 1590-1594, 2000.

[41] A.J. Cooper, "Fibre/radio for the provision of cordless/mobiletelephony services in the access network," *Electron. Lett.* vol. 26, pp. 2054-2056, 1990.

[42] H. Ogawa and Y. Kamiya, "Fiber-optic microwave transmission using harmonic laser mixing, optoelectronic mixing and optically pumped mixing," *IEEE Trans. Microwave Theory Tech.,* vol 40, pp. 2045-2051, 1991.

[43] H. Ogawa, D. Polifko and S. Banba, "Millimeter-wave fiber optics systems for personal radio communication," *IEEE Trans. Microwave Theory Tech.,* vol. 40, pp. 2285-2293, 1992.

[44] H. Ogawa and D. Polifko, "Fiber optic millimeter-wave subcarrier transmission links for personal radio communication systems," *IEEE MTT-S Digest,* pp. 555-558, 1992.

[45] "Enabling Technologies for Hybrid Fibre Radio Architectures (final results)," Project P816-PF, Implementation frameworks for integrated wireless-optical access networks, Deliverable 4, Feb. 2000.

[46] J.E. Bowers, A.C. Chipaloski, S. Boodaghians and J.W. Carlin, "Long distance fiber-optic transmission of C-band microwave signals to and from a satellite antenna," *J. Lightwave Technol.,* vol. LT-5, pp. 1733-1741, 1987.

[47] W.I. Way, R.S. Wolff and M. Krain, "A 1.3-μm 35-km fiber-optic microwave multicarrier transmission system for satellite earth stations," *J. Lightwave Technol.,* vol. LT-5, pp. 1325-1331, 1987.

[48] D. Wake, I.C. Smith, N.G. Walker, I.D. Henning and R.D. Carver, "Video transmission over a 40 GHz radio-fibre link," *Electron. Lett.* vol. 28, pp. 2024-2025, 1992.

[49] M.R. Phillips and T.E. Darcie, "Analog links for CATV applications," *LEOS 1993, Optical microwave interactions,* vol. M2.1, pp. 11-12, 1993.

[50] D. Wake, D. Johansson and D.G. Moodie, "Passive picocell: a new concept in wireless network infrastructure," *Electron. Lett.* vol. 33, pp. 404-406, 1997.

[51] T. Kagawa, Y. Doi, T. Ohno, T. Yoshimatsu, K. Tsuzuki and S. Mitachi, "Bi-directional Optical Microwave Transmission using a Base Station Without DC Electric Power Supply," *OSA Optical Fibre Conference, Technical Digest,* pp. WV2–1-WV2–3, 2001.

[52] K.-I. Kitayama, T. Kuri, R. Heinzelmann, A. Stohr, D. Jager, and Y. Takahashi, "A good prospect for broadband millimeter-wave fiber-radio access system-an approach to single optical component at antenna base station," *IEEE MTT-S, International Microwave Symposium Digest. 2000,* Vol. 3, pp. 1745-1748, 2000.

[53] E. Goutain, J.C. Renaud, M. Krakowski, D. Rondi, R. Blondeau and D. Decoster, "30 GHz bandwidth, 1.55 mu m MQW-DFB laser diode based on a new modulation scheme," *Electron. Lett.* vol. 32, pp. 896-7, 1996.

[54] ISO/IEC 11801:1995 (E), Information technology Generic cabling for consumer premises.

[55] L. Raddatz and I.H. White, "Overcoming the Modal Bandwidth Limitation of Multimode Fiber by Using Passband Modulation," *IEEE Photon. Tech. Lett.,* vol. 11, pp. 266-268, 1999.

[56] M. Webster, L. Raddatz, I.H. White, and D.G. Cunningham, "A Statistical Analysis of Conditioned Launch for Gigabit Ethernet Links Using Multimode Fiber," *J. Lightwave Technol.,* vol. 17, pp. 1532-1541, 1999.

[57] L. Raddatz, D. Hardacre, I.H. White, R.V. Penty, D.G. Cunningham, M.R.T. Tan and S.Y. Wang, "High bandwidth data transmission in multimode fibre links using subcarrier multiplexing with VCSELs," *Elec. Lett.,* Vol. 34, pp. 686-688, 1998.

[58] J.A. Betts, "Signal processing, modulation and noise", The English University Press Limited, London 1970.

[59] G.P. Agrawal, "Fiber-optic communication systems", 2nd edition, John Wiley & sons, Inc, New York, N.Y., 1997.

[60] S.L. Zhang, P.M. Lane, J. O'Reilly, "Effect of EDFA ASE noise on the performance of millimetre-wave fibre radio communication systems," *Microwave Photonics, MWP '96. Technical Digest,*, pp. 149-152, 1996.

[61] W.I. Way, "Optical fiber-based microcellular systems: an overview," em IEICE Transactions of Communications, vol. E76-B, pp. 1091-1102, 1993.

[62] H. Schmuck, "Comparison of optical millimetre-wave system concepts with regard to chromatic dispersion," *Elec. Lett.,* vol. 31, pp. 1848–1849, 1995.

[63] U. Gliese, S. Noeskov and T.N. Nielsen, "Chromatic dispersion in fiber-optic microwave and millimeter-wave links," *IEEE Trans. Microwave Theory Tech.,* vol. 45, pp. 1716-1724, 1997.

[64] P.M. Lane, K. Kitayama, "The interaction between fibre dispersion and laser phase noise in an ASK self-heterodyne millimetre-wave fibre-radio system," *IEE Proceedings-Optoelectronics,* Vol. 146, pp. 177-180, 1999.

[65] K. Kitayama, T. Kamisaka, K. Onohara and W. Chujo, "Dispersion effects of optical filter in DWDM millimeter-wave fiber-radio systems, *Microwave Photonics, MWP 2000. Technical Digest,*, pp. 133-136, 2000.

[66] Y. Doi, S. Fukushima, T. Ohno, Y. Matsuoka and H. Takeuchi, "Phase shift keying using optical delay modulation for millimeter-wave fiber-optic radio links," *J. Lightwave Tech.,* Vol. 18, pp. 301-307, 2000.

[67] G.J. Foschini and C.D. Poole, "Statistical theory of polarisation dispersion in single mode fibers", *J. Lightwave Tech.,* Vol. 9, pp. 1439-1456, 1991.

[68] P. Ciprut, B. Gisin, N. Gisin, R. Passy, J.P. Von der Weid, F. Prieto and C.W. Zimmer, "Second-Order Polarization Mode Dispersion: Impact on Analog and Digital Transmissions," *J. Lightwave Tech.,* Vol. 16, pp. 757-771, 1998.

[69] C.D. Poole and T.E. Darcie, "Distortion related to polarization-mode dispersion in analog lightwave systems," *J. Lightwave Tech.,* Vol. 11, pp. 1749-1759, 1993.

[70] B. Huttner, C. Geiser, and N. Gisin, "Polarization-Induced Distortions in Optical Fiber Networks with Polarization-Mode Dispersion and Polarization-Dependent Losses*J. Selec. Quantum Elec.,* Vol. 6, pp. 317-329, 2000.

[71] K.-I. Kitayama, A. Stohr, T. Kuri, R. Heinzelmann, D. Jager and Y. Takahashi,"An Approach to Single Optical Component Antenna Base Stations for Broad-Band Millimeter-Wave Fiber-Radio Access Systems," *IEEE Trans. Microwave Theory Tech.,* vol 48, pp. 2588-2595, 2000.

[72] L. Noel, D. Wake, D.G. Moodie, D.D. Marcenac, L.D. Westbrook and D. Nesset, "Novel techniques for high-capacity 60-GHz fiber-radio transmission systems," *IEEE Trans. Microwave Theory Tech.,* vol 45, pp. 1416-1423, 1997.

[73] G.H. Smith and D. Novak, "Broadband millimeter-wave fiber-radio network incorporating remote up/downconversion," *IEEE MTT-S, International Microwave Symposium Digest. 1998*, Vol. 3, pp. 1509-1512, 1998.

[74] AC083 FRANS Fibre Radio ATM Network and Services FINAL REPORT Document Ref. Nr.: AC083-SEL-CRC-AR-P-005-b1.

[75] T. Berceli, S. Kudszus, M. Schlechtweg, A. Zolomy, G. Jaro, T. Marozsak and E. Udvary: "Optical millimeter wave generation utilizing a subharmonic reference," *IEEE MTT-S, International Microwave Symposium Digest.*, Vol. 3, pp. 1749-1752, 2000.

[76] H. Schmuck, R. Heidelmann and R. Hofsetter, "Distribution of 60 GHz signals to more than 1000 base stations," *Electron. Lett.,* vol. 30, pp. 59-60, 1994.

[77] D.J. Blumenthal, J. Laskar, R. Gaudino, Sangwoo Han; M.D. Shell and M.D. Vaughn, "Fiber-optic links supporting baseband data and subcarrier-multiplexed control channels and the impact of MMIC photonic/microwave interfaces," *IEEE Trans. Microwave Theory Tech.,* vol. 45, pp. 1443-1450, 1997.

[78] R. Ohmoto, H. Ohtsuka and H. Ichikawa, "Fiber-optic microcell radio systems with a spectrum delivery scheme," *IEEE Journal of Selected Areas in Communnications,* vol. 11, pp. 1108-1117, 1993.

[79] J.C. Fan, C.L. Lu and L.G. Kazovsky, "Dynamic range requirements for microcellular personal communication systems using analog fiber-optic links," *IEEE Trans. Microwave Theory Tech.,* vol. 45, pp. 1390-1397, 1997.

[80] Y. Suda, K. Tsukamoto and S. Komaki, "Multichannel coherent SCM Optical Transmission system using radio-to-optic direct conversion scheme," *Int. Topical Meeting Microwave Photonics,* vol. TU3-3, pp. 41-44, 1996.

[81] Z. Ahmed, D. Novak, R.D. Waterhouse and H-F. Liu, "37 GHz fiber-wireless system for distribution of broad-band signals," *IEEE Trans. Microwave Theory Tech.,* vol. 45, pp. 1431-1435, 1997.

[82] O. Kagami, M. Ogasawara, F. Yamamoto, H. Ichikawa and K. Shimokawa, "Subcarrier optical transmission techniques for wireless local loop (WLL)," *Int. Topical Meeting Microwave Photonics,* vol. TU4-4, pp. 73-76, 1996.

[83] H. Mizuguti, T. Okuni, S. Komaki and N. Morinaga, "Performance analysis of optical fiber link for microcellular mobile communication systems," *IEICE Trans Electron,* vol. E76-C, pp. 271-277, 1993.

[84] X.J. Meng, T. Chau D.T.K. Tong,and M.C. Wu, "Suppression of second harmonic distortion in directly modulated distributed feedback lasers by external light injectionS," *Electron. Lett.,* Vol. 34, pp. 2040-2041, 1998

[85] T. Ohtsuki, I. Sasase and S. Mori, "The effects of laser phase noise on optical coherent coded subcarrier multiplexing system with distributing local oscillator in local loop," *IEICE Trans. Electron,* vol. E76-C, pp. 293-299, 1993.

[86] D. Castleford, A. Nirmalathas and D. Novak, "Impact of optical crosstalk in fibre-radio systems incorporating WDM," *Int. Topical Meeting Microwave Photonics,* pp. 51-54, 2000.

[87] K. Kitayama, T. Kuri, H. Yokoyama and M. Okuno, "60 GHz millimeter-wave generation and transport over OFDM fiber-optic networks," *Int. Topical Meeting Microwave Photonics,* vol. TU3-5, pp. 49-53. 1996.

[88] D.K. Davies and A.P. Goutzoulis, "Wavelength-multiplexed analog fiber optic link for wideband radio-frequency and local oscillator signal transmission," *Optical Engineering,* vol. 31, pp. 2323-2329, 1992.

[89] N.J.Frigo, P.P. Iannone, P.D. Magill, T.E. Darcie, M.M. Downs, B.N. Desai, U. Koren, T.L. Koch, C. Dragone, H.M. Presby and G.E. Bodeep, "A wavelength-division multiplexed passive optical network with cost-shared components," *IEEE Photon. Thechnol. Lett.* vol. 6, pp. 1365-1367, 1994.

[90] K. Kitayama, "Highly spectral efficient OFDM wireless networks by using optical SSB modulation," *Int. Topical Meeting Microwave Photonics,* vol. FR2-4, pp. 231-234, 1997.

[91] R.A. Griffin, P.M. Lane and J. O'Reilly, "Radio-over fiber distribution using an optical millimeter-wave/DWDM overlay," *Optical Fiber Communication Conference Technical Digest,* vol. 2, pp. 70-72, 1999.

[92] T. Tsuchiya, T. Shiraishi and J. Arata, "Major factors affecting fiber-optic transmission system design for radio base stations," *IEICE Trans. Commun,* vol. E76-B, pp. 1136-1144, 1993.

Chapter 2

Review of Millimetre Wave Radio Over Fibre Transmission Experiments

This chapter surveys the different methods that have been used to generate millimetre wave modulated optical signals for radio over fibre transmission and how these sources have been used in millimetre wave data transmission experiments. The introduction 2.1 identifies some desired features of the millimetre wave modulated optical source. Section 2.2 reviews the different methods by which millimetre wave modulated optical signals can be generated and the following section, 2.3, compares how these sources perform when they are used for radio over fibre transmission experiments. Methods by which the data can be applied to the generated optical signal are also investigated in this section. The conclusion, section 2.4 summarises how the different sources fare in terms of the desired features defined in the introduction.

2.1 Introduction

There has been comprehensive research on methods to impose millimetre wave modulated by data onto optical carriers. A variety of sources have been demonstrated including two laser optical heterodyne sources, mode locked lasers and external optical modulator based methods. Which source is the most suitable depends on a range of factors. The first and most important factor that needs to be considered is in what type of application scenario the source will be used. A short range, non multiplexed indoor radio over fibre link serving only short wireless radio paths is likely to require low cost, low power components and an architecture allowing for low cost, low complexity base station units to be used. In contrast, for radio over fibre transmitted over longer spans of fibre, 1-100 km, the dominating cost will be the installation or lease of fibre and more complex and higher performance components can with advantage be used. Furthermore, if a radio over fibre network using WDM is used, only components compatible with WDM should be used.

Optical amplification is more realistically used in a WDM network, as many channels can split the cost of the amplifier, but for low cost single links, the use of WDM should be avoided. Also important is the availability of the technology. If the technology is based on components that are currently in commercial production, there is a strong argument for using that technology for any application to be utilised in the near future. More experimental sources based on custom devices will either require that the device will be put in commercial production for other applications or that the millimetre wave radio over fibre market will grow to sufficient size to support the commercialisation of that source.

Another important factor is the performance of the source. Millimetre wave radio will be modulated at high data rates with complex modulation formats. For example, 16-QAM modulation requires a SNR of about 20 dB for a BER of 10^{-5}. In a typical 40 MHz band, this corresponds to an average double sideband noise level lower than -99 dBc/Hz around the generated optical carrier. More complex modulation formats require even purer signals. If multiple modulation schemes can be used, the source must not be limited by what sort of modulation can be applied. The source needs to be sufficiently stable to be used in real systems for very long periods of time without failure. Naturally, the source must also be able to generate the frequency range that is required.

The fibre chromatic dispersion has to be considered. As discussed in Section 1.2, double sideband millimetre wave modulated optical signals are severely limited in distance to roughly one kilometre if no form of dispersion compensation is used according to Fig. 1.5. For this reason single sideband modulated sources are preferred to double sideband sources. Double sideband modulation can however be used for longer transmission distances if some sort of dispersion compensation is used. Demonstrated methods includes optical filtering of the optical signal [1, 2], the use of dispersion shifted fibre [3, 4] and dispersion compensation using a chirped fibre grating [5]. The problem with these methods is that optical filtering requires wavelength stable optical sources and dispersion compensation only works for a certain predetermined transmission range.

To summarise, there are a number of factors that need to be considered, depending on the application scenario. Some desired features are:

- Single sideband modulation
- High generated millimetre wave power
- High spectral purity
- Wide frequency range
- Stable operation
- Flexible modulation format

2.2 Methods of Carrier Modulation

There is a multitude of methods of imposing millimetre-wave modulation onto an optical carrier. These sources of millimetre-wave modulated optical signals can be categorised in different manners. Possible categorisation includes single/double sideband modulated sources, direct/external modulation and one/two laser based sources.

2.2.1 External optical modulators

Externally modulated sources have generally suffered from high insertion loss or high drive voltage. One reason is that materials that require low driving voltage often have a high refractive index and are therefore difficult to achieve good coupling to fibre. A second limit to travelling wave type modulators is a mismatch in the optical and electrical group velocity, putting a limit to the possible length of the modulator.

Ti:LiNbO$_3$ travelling wave Mach-Zehnder modulators that can be modulated at 100GHz with a driving voltage of 5.1 V, and MQW modulators with a bandwidth of 40GHz and a drive voltage of 1.8 V [6] have been reported. Commercially available external optical modulators (EOM) exist with a bandwidth of 45 GHz [7]. Polymer Mach-Zehnder modulators have the potential for optical and electrical group velocity matching, and therefore high speed, low voltage operation. Polymer modulators have been demonstrated at 100 GHz modulation frequency and others with 1.2 V driving voltage [8].

One disadvantage of Mach-Zehnder modulators for analogue applications is the sinusoidal response of applied voltage, causing either high nonlinearities or poor extinction ratios. Electro-absorption modulators can achieve high linearity [9] and are therefore much more attractive for analogue applications. A second advantage is that the EAM can be modulated at high frequencies. 40 GHz operation has long been possible [10, 11] and been used for analogue links [12]. Recently, the frequency range has improved, and analogue links using an EAM at 60 GHz have been demonstrated [1, 13]. Furthermore, the EAM can be used to transmit and receive optical signals simultaneously by both detecting and modulating the incoming optical signal at different modulation frequencies [14]. With this configuration, passive operation without any other power supply than the incoming optical power is possible [15]. Other EAM transceivers have been demonstrated at 17 GHz [16] and at 60 GHz [17]. High speed integrated laser diode-EAM modules with modulation bandwidths up to 50 GHz have also been demonstrated [19, 18, 20].

Common application of external optical modulators produces double sideband modulated signals, sensitive to the chromatic dispersion of the fibre. Several methods have been demonstrated to create single sideband modulated signals using external optical modulators. The most straightforward method is to use an optical filter to simply filter away one of the generated modulation sidebands [21, 22]. More advanced methods include modulator configurations that generates either suppressed carrier single sideband modulated output or suppressed sideband single sideband modulated output. Suppressed carrier modulation can be generated by biasing a Mach-Zehnder modulator to V_{π}, where the transmission is minimised [23]. This method has been demonstrated for both 40 GHz [24] and 60 GHz [25] radio over fibre. An alternative method is to use a travelling wave Mach-Zehnder modulator in a Sagnac fibre-interferometer. The carrier will be extinguished in the interferometer, but since the travelling wave modulator only modulates the field travelling in one direction efficiently, the sidebands will be transmitted [26]. A modified version based on separate amplitude and phase modulation that is independent of the applied RF power level to the modulator has been proposed [27]. Suppressed carrier modulation can be realised by driving a two electrode Mach-Zehnder modulator biased at quadrature with a reference $\pi/2$ out of phase [28]. A variation of this method can be realised by using two modulators separately with the reference $\pi/2$ phase shifted [29].

2.2.2 Single source modulation

At microwave frequencies, direct modulation is the most common method to generate modulated optical signals. Direct modulation of laser diodes combines high efficiency, relatively high linearity and low cost. Therefore, direct modulation of laser diodes is the first choice for radio over fibre applications at microwave frequencies [30]. However the modulation bandwidth is limited and direct modulation produces double sideband modulated signals with limited fibre transmission range at millimetre wave modulation frequencies. Modulation bandwidths exceeding 40 GHz have been reported for unpackaged 1100 nm lasers [31] and 25 GHz for a packaged 1550 nm DFB laser [32], and then only at very high bias currents and for small signal modulation. The modulation bandwidth can be increased by including a designated modulation section in a multisection laser. This has been demonstrated producing a 1550 nm DFB laser with 30 GHz 3dB modulation bandwidth, possible to modulate at 40 GHz [33], by modulation of an integrated saturable absorber. A second way to increase the modulation frequency of semiconductor lasers is the use of a resonantly enhanced external cavity laser [34, 36, 35]. The high speed capability is achieved by tuning the external cavity length to resonance at the required frequency. This method gives an enhanced modulation response only in a narrow band around the resonance frequency.

An alternative method includes the generation of an optical comb and selecting the beat between two, or more optical lines, giving the required frequency. One simple manner this can be achieved by is to use the nonlinearities of a laser diode to generate harmonics of the modulation frequency [37, 38, 39]. The unused optical lines can then with advantage be filtered away, leaving only those that directly contribute to the required millimetre-wave beat [2]. A different kind of optical comb generator is offered by optical pulse sources, such as mode-locked lasers. Optical pulse generators have been developed as sources for high speed Return to Zero (RZ) data transmission. With pulse widths down to 180 fs [40], frequencies on the order of a terahertz could be generated and the requirement on low pulse jitter also ensures spectral purity of the beat between the optical lines. Both integrated [41, 42, 43, 44], external cavity [40, 45, 46], and fibre based sources [47, 48] have been used to synthesise millimetre-wave modulated optical signals. An optical comb has also been realised using an amplified fibre loop [49] with 1.8 THz frequency span.

Common to all optical comb generators is that a multitude of optical lines that are generated whilst only two, or a few lines contribute to the generated millimetre-wave signal. This is therefore not a very efficient method of generating millimetre-wave modulated optical signals. Dual mode lasers do not have this disadvantage. By using one semiconductor laser with two lasing modes, a millimetre-wave modulated optical signal can be generated. Phase stabilisation can then be achieved by mode locking with either electrical injection of a stable reference [41, 50, 51, 52], or optical injection [53, 54].

2.2.3 Two source optical heterodyning

By generating two optical frequencies and using the beat signal corresponding to the frequency difference, produced on the photodetector, a millimetre wave signal can be generated [55]. This is a very attractive method of generating millimetre-wave modulated optical carriers for several reasons. The efficiency of the optical to millimetre-wave transduction is high, ideally 100%, that is all optical power is contributing to the generated signal. The range of frequencies that can be generated is very large, with no intrinsic degradation of the optical to millimetre-wave efficiency at higher frequencies, the limiting factor is the bandwidth of the photodetector used. Single sideband modulated optical signals are also automatically generated, resistant to chromatic dispersion. The limitation of this method is that the purity of the generated millimetre-wave signal is determined by the linewidth of the lasers used. Therefore, narrow linewidth lasers need to be used to produce beats of acceptable purity, such as solid state lasers [55] or external cavity fibre grating lasers [56]. Increased frequency stability has also been achieved using a monolithically integrated free-running optical heterodyne source [57]. If generated signals of high spectral purity or absolute frequency stability are required, however, the relative phase between the lasers needs to be controlled.

One method of overcoming the phase noise of the free-running sources is feed-forward modulation [58, 59]. The optical output of two free-running heterodyned lasers are coupled together and part of the output signal is then detected and used to modulate the remaining output signal by an external modulator. This produces a beat between the fundamental laser lines and the modulation sidebands corresponding to the reference frequency. A similar experiment where the modulator only modulates the output of the slave laser has also been demonstrated [60], as shown in Fig. 2.1. This source has also been used to demonstrate radio over fibre experiments at 40 GHz [61].

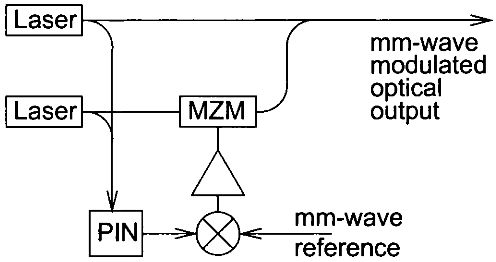

Figure 2.1: Basic schematic of a feed-forward signal generation arrangement.

The most common method of correlating the phase between two lasers is optical injection locking. It has been long known that the phase of two lasers can be correlated by optical injection locking [62]. The first heterodyne injection locked signal generation using injection of semiconductor laser modulation sideband was demonstrated in 1982, first using one slave laser [63], later two slave lasers [64] and generating millimetre-wave frequencies [65]. Injection locking has the advantage that standard singlemode lasers can be used to generate very high modulation frequencies with high spectral purity, by using an optical comb generator, for example an external cavity pulse generator, and injection locking slave lasers to the comb lines, as outlined in [66]. This type of widely tuneable source has later been demonstrated [67, 68]. A potentially more low-cost source has been developed using the nonlinearities of a semiconductor laser to produce an optical comb to that the slave lasers can be locked [69]. This source has then been used for 60 GHz radio over fibre experiments [57, 70]. An alternative scheme of sideband injection locking by strong injection locking and modulation of the slave laser has been also demonstrated [71]. This source has also been used to demonstrate 60 GHz radio over fibre transmission [72]. A common problem with optical injection locking methods is limited locking range. The locking range is typically limited to a few GHz and assuming standard DFB lasers are being used with a temperature stability of typically 10 GHz/K, a temperature shift on a milli-Kelvin order is sufficient to cause the system to fall out of lock.

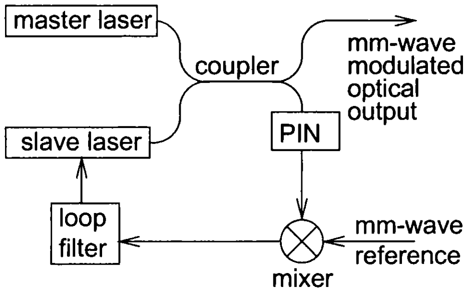

Figure 2.2: Basic schematic of a fibre based optical phase-lock loop.

A heterodyning technique that has the potential of producing high power, narrow linewidth signals with a wide tuning range is the Heterodyne Optical Phase Lock Loop (OPLL) . An illustration of the basic operation of an OPLL is shown in Fig. 2.2. A photodetector detects the beat between master and slave laser. The phase of the beat is then compared to the reference, and the error signal is filtered and fed back into the slave laser as negative current feedback. The slave laser is here taking the equivalent role of the current controlled oscillator in a conventional phase-lock loop. The main limitation of the OPLL is the amount of laser phase noise present and the loop delay. Generally, OPLL demonstrations can be divided into two groups. The first group, narrowband OPLLs uses line-narrowed lasers with a very low linewidth. By using lasers with linewidth in the kHz region, relaxed loop delay times of tens of nanoseconds can be used with good results. Microwave frequencies [73, 74] and millimetre-wave frequencies have been generated [75]. The second group, wideband OPLLs uses standard DFB lasers, with a linewidth in the MHz region. With these linewidths, the loop delay must be made very low for good results, in the picosecond region. This requires specialised electronics and excludes the use of fibre optics. Demonstrations generating microwave modulated optical signals haves been performed [76, 77, 78], with loop delay times as low as 400 ps [77]. No millimetre-wave radio over fibre demonstration has previously been performed using an OPLL based source.

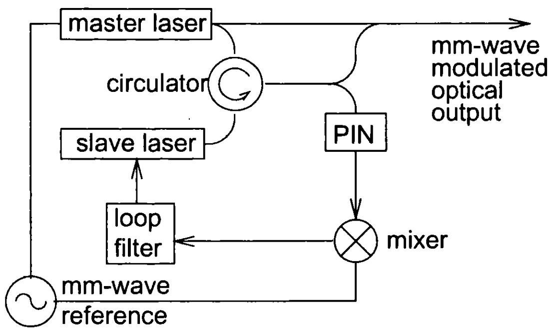

Figure 2.3: Basic schematic of a fibre based optical injection phase-lock loop.

One method of combining the advantages of optical injection locking and the OPLL, the possibility to use standard wide linewidth lasers with the long term stability offered by the OPLL, without the requirement for narrow laser linewidth or extremely short loop delay time, is the optical injection phase-lock loop (OIPLL) [79]. Fig. 2.3 shows a schematic of an heterodyne OIPLL. In addition to a phase-lock loop configuration, an injection locking path is also added for the slave laser to lock to a master laser modulation sideband. An homodyne OIPLL [80] and an heterodyne OIPLL at microwave frequencies have previously been demonstrated [81].

2.2.4 Summary

Table 2.1 summarises some of the available sources for millimetre-wave modulated optical signals. The table is divided into two parts covering laser mode locked sources and modulator based sources. Parameters included in the table are frequency tuning range, noise, phase error variance, modulation index and locking range. Most presented methods have the capability of generating widely tuneable signals. Laser mode locking is generally limited in frequency by the bandwidth of the photo detector used. In modulator based methods, the frequency tuning range is simply equal to the bandwidth of the modulator. For direct modulation of semiconductor lasers, the modulation bandwidth is normally too low for millimetre-wave applications, and the exceptions are usually only valid for small signal modulation. Resonantly enhanced lasers have a very narrow modulation bandwidth around a millimetre wave resonance frequency. External modulators exist with sufficient bandwidth for most applications. Noise and phase error variance have been primarily investigated for mode locked sources, where too low locking bandwidth can have a degenerating impact on the signal purity. For broadband modulator based sources, the noise performance can generally be assumed to be limited by the modulation source and the relative intensity noise of the optical source. Locking range is only relevant for mode locking based sources, where precision frequency stabilisation is needed in all cases except for the OIPLL configuration, to obtain stable operation. Two parameters not included in the table are RF drive power and optical power utilisation efficiency. External optical modulator based methods suffer from generally high required driving voltage and optical insertion loss. In contrast, the mode locking sources can have higher complexity, especially two source locking.

2.3 Methods for Imposition of Data

A second problem relating to the generation of millimetre wave modulated optical signals after the generation of millimetre-wave modulation is the imposition of the data onto the millimetre-wave subcarrier. Fig. 2.4 shows four basic principles for how the data can be imposed on a generated single sideband modulated millimetre wave subcarrier. Equivalent categorisation can be made for double sideband modulation.

2.3.1 Baseband modulation

This is the most commonly demonstrated principle. It has two advantages, it can be simple to implement and it is very efficient as no unwanted optical lines are generated that are not directly contributing to the generated data modulated millimetre-wave signal. In the most straight-forward, double sideband modulated case, the data is directly applied to the millimetre-wave reference, typically by switching the phase in a mixer with the binary data signal, producing PSK modulation [12, 17]. The modulated reference is then used to modulate a high speed external modulator. With this method, any modulation format can be generated. Single sideband modulation can thereafter be generated by filtering away one of the optical modulation sidebands [1], or using suppressed sideband external modulation [28]. Single sideband modulation can also be achieved by applying

Table 2.1: Summary of selected mode locking based and modulator based millimetre wave modulated optical sources: OPLL, OIL , OIPLL, Feed-forward modulation (FFM), dual mode mode locked laser ($2\times$MLL), Mach-Zehnder modulator (MZM), suppressed sideband MZM (SSB MZM), directly modulated semiconductor laser (DMSL) and resonantly enhanced semiconductor laser (RHSL).

Ref.	Source	Freq. range	noise @ 10 kHz 10 MHz	Phase error variance	Mod. index	Locking range
Gliese *et al* [77]	OPLL	3-18 GHz	−125 dBc/Hz −102 dBc/Hz	0.04 rad^2 1 GHz b/w	—	1.15 GHz
Logan [67]	OIL	1-94 GHz	−108 dBc/Hz —	—	—	<1 GHz
Walton *et al* [81]	OIPLL	8, 16 GHz	−94 dBc/Hz −95 dBc/Hz	0.003 rad^2 100 MHz b/w	—	24 GHz
Wake *et al* [50]	$2\times$MLL	6-60 GHz	−77 dBc/Hz —	—	10-20 %	500 MHz
Bordonalli *et al* [51]	$2\times$MLL	14.8 GHz	−94 dBc/Hz −102 dBc/Hz	—	50 %	400 MHz
Pajarola *et al* [53]	$2\times$MLL	0.1-60 GHz	−78 dBc/Hz −120 dBc/Hz	0.0007 rad^2 5 MHz b/w	—	—
Griffin *et al* [60]	FFM	4-40 GHz	−78 dBc/Hz −113 dBc/Hz	0.005 rad^2 500 MHz b/w	—	n/a
Noguchi *et al* [6]	MZM	0-105 GHz	—	—	—	n/a
Smith *et al* [82]	SSB MZM	0-40 GHz	—	—	—	n/a
Weisser *et al* [31]	DMSL	0-40 GHz	—	—	—	n/a
Georges *et al* [35]	RHSL	45 GHz ±300 MHz	—	—	low	n/a

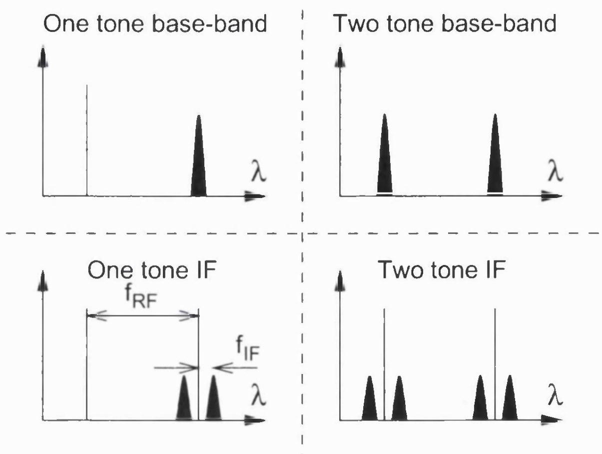

Figure 2.4: Basic principles for the imposition of modulation onto a single sideband millimetre wave modulated optical carrier.

a modulated reference to a mode-locked dual mode laser [83, 52], or to a phase correlated optical heterodyne, such as an OPLL [85]. The disadvantage is that amplitude modulation cannot be used because of the constant output power of the lasers/lasermodes. If modulation is applied to a subharmonic reference, the available modulation formats is further limited by the multiplication of the phase/frequency, such as in [86], where a 4 GHz reference with analogue FM was used for harmonic upconversion in a DFB laser. For two source heterodyne systems, a more attractive alternative is to modulate the output of one of the sources with an external modulator. 1 Gbit/s phase modulation [87] has been demonstrated in this manner. Furthermore, the phase correlation and modulation functions can be combined in the same modulating signal in a feed-forward configuration [59], allowing free-running lasers to be used. An alternative method to impose PSK modulation on a millimetre wave modulated optical signal is by optical delay switching [4, 84]. It involves switching the optical signal between two or more optical paths, each individually phase shifted corresponding to the PSK phase shift.

Two tone baseband modulation is more rarely demonstrated. It is generated when an external modulator is applied to a single sideband modulated optical signal. However, only ASK modulation can be applied in this manner, as demonstrated for the output of a dual mode laser [53], or combined RF and baseband modulation of a external modulator [12]. Phase and frequency modulation will only affect the optical phase/frequency of the input signal, not the phase/frequency of the relative beat signal of the two optical components.

2.3.2 IF modulation

Even though incorporating the modulation directly on the millimetre-wave subcarrier produces the most efficient use of the available optical power in generating the modulated millimetre wave signal, applying the modulation to a separate IF signal can on some occasions be preferred. One example is if the millimetre wave modulated optical signal is generated by some sort of injection locking process, where no form of amplitude modulation such as ASK, or more commonly used, some kind of QAM would be possible to generate. However, by imposing the modulation on an IF subcarrier, any modulation format can be generated by intensity modulation of the subcarrier. A second example is when a system architecture as illustrated by Fig. 1.6 in example b and c, where a pure millimetre-wave carrier needs to be delivered to downconvert the uplink signal and possibly the uplink signal. By applying the modulation to an IF subcarrier on one of the two optical lines, the optical carrier can be extracted at the base station and the data signal can be detected either on a IF subcarrier, or on an RF subcarrier using photonic upconversion.

In a two source optical heterodyne system, one tone IF modulation can conveniently be applied to only one of the optical sources. It can be achieved by direct modulation of one of the optical sources, such as frequency modulation [69, 57] or phase modulation by current modulation within the locking range of an injection locked laser [70]. An external modulator can also be used to modulate one of the optical lines [87]. If an external modulator or a mode-locked laser is used to generate single sideband millimetre wave modulation, the optical lines must be separated for one to be modulated externally. This has been achieved by using optical filters in different configurations [23, 22, 88]. Two tone IF modulation does not require filtering as both optical lines are modulated. The complexity is now lower at the price of lower tolerance to the chromatic dispersion [89], although it is better than double sideband millimetre wave modulation. This arrangement has been demonstrated using a mode locked laser [3]. A variation of the same principle is found if an IF modulated optical signal is millimetre wave modulated using a suppressed carrier external amplifier arrangement. The resulting optical signal will now be similar to the previous case with the added advantage that several IF modulated optical signals can be millimetre wave modulated in one single external modulator [90].

If a radio over fibre architecture shown in example c in Fig. 1.6 is used, the IF subcarrier is upconverted to RF in the electrical domain in the base station. Generation of millimetre wave modulation and IF subcarrier data modulation can now be seen as two separate processes. The IF signal can still be imposed on the same optical signal as the millimetre wave modulation, for example in an external optical modulator [28, 82]. The IF subcarrier can also be transported on a separate optical carrier on a different wavelength [71, 72]. By designating a separate wavelength to the millimetre wave modulated optical carrier, the same source can be shared between several base stations in a radio over fibre WDM network. The price is a slightly more complicated base station, but if a millimetre wave carrier still needs to be extracted for downconversion of the uplink signal in the base station, the penalty is not severe.

2.3.3 Summary

Table 2.2 summarises some selected radio over fibre transmission experiments. Parameters investigated are millimetre wave modulation source, how the data modulation has been applied, bit rate and modulation format, RF and IF (if any) frequency used, transmission length, if optical amplification is used at the transmitter or receiver, and finally, what method of dispersion management is used. It is seen that a wide range of sources have been used to demonstrate radio over fibre transmission: two source heterodyning, dual mode mode locked lasers and external optical modulators. BPSK modulation is used in the majority of experiments, due to simplicity of implementation at data rates typically around 100-200 Mbit/s, but a range of alternative formats and significantly higher modulation rates have been demonstrated. An interesting observation can be made from the fibre length whether optical amplification was used. It is seen that in the cases where no optical amplification was needed, millimetre wave external modulation was never used and unamplified transmission distances greater than 10 km have only been demonstrated using OIL and OPLL technologies. This illustrates the advantage of optical heterodyning against the best external modulator based sources. Typically for bit rates around 100 Mbit/s received optical power in the range of −10 dBm to −20 dBm is needed for error-free detection. Optical heterodyning based sources using typical lasers with a few milliwatt optical output power achieve sufficient output power to overcome the fibre attenuation for fibre lengths above 10 km. In contrast, the high insertion loss of millimetre wave optical modulators, particularly in suppressed sideband or suppressed carrier operation, makes optical amplification necessary to overcome the fibre attenuation. Most experiments used single sideband modulated sources to manage the fibre dispersion. Those that do not, either use filtering to remove one of the modulation sidebands, or use dispersion compensation in the form of dispersion compensating fibre. In a few cases, no dispersion management is used and transmission is over either very short fibre lengths, or fibre lengths not corresponding to a large penalty due to dispersion are demonstrated.

2.4 Conclusions

In this chapter different millimetre wave modulated optical sources have been reviewed. Also reviewed is how these sources can be used to transmit data modulated millimetre wave radio signals over spans of optical fibre. In the introduction a number of desired features of the millimetre wave source were defined. Thereafter, the different sources of millimetre wave modulated optical signals that have been demonstrated were described. It was shown how data can be applied to these sources. Finally, some millimetre wave radio over fibre transmission experiments are summarised in Table 2.2. Based on these investigations, the strengths of the different sources can be defined in relation to the desirable features defined in the introduction:

- Single sideband modulation: The requirement for single sideband modulation makes two mode locking methods, such as two laser heterodyne sources or two mode mode locked lasers attractive. Suppressed carrier or suppressed sideband external modulation is another option. High speed conventional optical modulators and direct modulation of laser diodes are not suitable for this purpose.

- High generated millimetre wave power: Based on the performance of the transmission experiments it is clear that heterodyning two lasers, for example in an OIL or an OPLL configuration is the most attractive option. High levels of optical power are generated with a high modulation index, enabling successful transmission over tens of kilometres without the use of optical amplification.

- Spectral purity: By its nature, modulator based methods are limited in purity by the spectral purity of the millimetre wave reference and the relative intensity noise of the optical source.

Table 2.2: Summary of selected millimetre wave radio over fibre transmission experiments: SSB (single sideband), FFM (feed-forward modulation), RHSL (resonantly enhanced semiconductor laser), MLL (mode locked laser), 2×MLL (dual mode mode locked laser), SC (suppressed carrier), SSB (suppressed sideband), OIMR (optoelectronic image reject mixer), DSF (dispersion shifted fibre).

Ref.	Source	modulation applied to	modulation format	RF / IF	Fibre length EDFA	disp. comp.
Braun *et al* [69]	2×DFB	to free-running laser	140 Mb/s CPFSK	63 GHz —	0 km no EDFA	SSB
Braun *et al* [57]	OIL	to locked laser	155 Mb/s OQPSK	64 GHz 140 MHz	12.8 km no EDFA	SSB
Noel *et al* [71]	OIL	separate DFB	120 Mb/s QPSK	60 GHz 1.35 GHz	100 km TRX EDFA	SSB
Nielsen *et al* [85]	OPLL	To reference	6 MHz PAL video	7.6 GHz —	25 km no EDFA	SSB
Gliese *et al* [87]	OPLL	SOA	1 Gb/s QPSK	9 GHz —	0 km no EDFA	SSB
Gliese *et al* [87]	OPLL	EOM	100 Mb/s BPSK	9 GHz 2 GHz	25 km no EDFA	SSB
Georges *et al* [59]	FFM	To reference	150 Mb/s BPSK	39 GHz —	2.2 km no EDFA	SSB
Nagarajan *et al* [34]	RHSL	To reference	40 Mb/s BPSK	35 GHz —	200 m no EDFA	—
Helmholt *et al* [3]	MLL	EOM	155 Mb/s DPSK	60 GHz 400 MHz	3 km TX EDFA	DSF
Pajarola *et al* [53]	2×MLL	EOM	200 Mb/s ASK	58 GHz —	25 km TX EDFA	SSB
Pajarola *et al* [53]	2×MLL	EOM	50 Mb/s ASK	43 GHz 150 MHz	25 km TX EDFA	SSB
Ohno *et al* [52]	2×MLL	To reference	500 Mb/s BPSK	39.6 GHz —	1-9 km no EDFA	Filter
Ahmed *et al* [91]	2×MLL	EOM	200 Mb/s BPSK	37 GHz 2.5 GHz	10 km RX EDFA	SSM
Doi *et al* [84]	EAM	delay switching	2 Gb/s BPSK	40 GHz —	5 km TX EDFA	DSF
Kuri *et al* [1]	EAM	To reference	2×156 Mb/s DPSK	60 GHz —	85 km TX EDFA	filter
Cadiou *et al* [12]	EAM	To reference	2.048 Mb/s BPSK	38 GHz —	20 km TX EDFA	—
Cadiou *et al* [12]	EAM	Data to EAM	800 Mb/s ASK	38 GHz —	20 km TX EDFA	—
Ozeki *et al* [88]	SC-MZM	OIRM	156 Mb/s ASK	60 GHz 2 GHz	20 km TX EDFA	SSB
Griffin *et al* [90]	SC-MZM	To laser	28 Mb/s 16-QAM	33 GHz 1.8 GHz	0 km TX EDFA	SSB
Smith *et al* [92]	SSB-MZM	To reference	155 Mb/s BPSK	38 GHz —	50 km TX EDFA	SSB
Smith *et al* [82]	SSB-MZM	IF to MZM	155 Mb/s BPSK	39 GHz 2.5 GHz	40 km TX EDFA	SSB

In a properly configured modulator based source, spectral purity should not be a problem. In locking based methods, the noise of the free-running heterodyne will need to be correlated. Depending on the noise reduction properties of the locking mechanism, spectral purity could be an issue. However, It has been demonstrated that sufficient spectral purity (<-99 dBc/Hz over a 40 MHz b/w) can be achieved.

- Wide frequency range: The frequency range of directly modulated semiconductor lasers make them not suitable for millimetre wave radio over fibre applications, as large signal modulation at millimetre-wave frequencies is not possible. The exception would be resonantly enhanced modulation, but then modulation is only possible in a narrow band around resonance.

- Stable operation: For modulator based methods, stable operation is generally not a problem if some temperature control is applied. If not, Mach-Zehnder modulators can experience some drift of the bias point that would need stabilisation. In the case of locking based methods, the stability can be a problem. Most published values are on the order of 1 GHz. The notable exception is the OIPLL with a locking range of 24 GHz, enough to be stable over a range of environmental conditions.

- Flexible modulation formats: This is a problem for locking based methods. Due to the constant output power of the two modes, modulation of the millimetre wave reference is restricted to frequency or phase modulation. If modulation formats including amplitude modulation, such as QAM modulation are to be applied, the modulation must be applied to an IF subcarrier that is used to modulate one or two of the lines, with a power loss of the generated millimetre wave signal. One way around this is to use remote upconversion in a slightly more complicated base station. Modulator based methods can generally accommodate most common modulation formats.

As mentioned in the introduction, which source is the most suitable depends on the application scenario. Presently, there are not many millimetre wave radio over fibre links in use and still less WDM radio over fibre networks. It is reasonable to believe that millimetre wave over fibre will initially be applied to inexpensive single span links, before more complex networks are deployed. Therefore, there will be a need for sources with high efficiency in generated millimetre wave power to overcome the fibre attenuation, single sideband modulation to overcome the chromatic dispersion and a possibility to construct with commercially available components for cost concerns. The requirement for efficiency and single sideband modulation makes external modulator based sources unsuitable. The requirement for stability makes most mode locked sources unsuitable. The conclusion is hence that the OIPLL shows an attractive combination of features that make it a strong candidate for the early development for millimetre wave radio over fibre applications. It is a stable and efficient single sideband modulated source that is possible to construct with commercially available components. If a wide range of modulation formats needs to be applied, the OIPLL can be combined with the remote upconversion technique in the base station. However, no millimetre wave OIPLL has yet been demonstrated.

References

[1] T. Kuri, K.-I. Kitayama, A. Stohr and Y. Ogawa, "Fiber-optic millimeter-wave downlink system using 60 GHz-band external modulation", *IEEE J. Lightwave Tech.*, vol. 17, pp. 799-806, 1999.

[2] P.A. Davies, A.P. Foord and K.E. Razavi, "Millimetre-wave signal generation by optical filtering of frequency modulated laser spectra", *Elec. Lett.*, vol. 31, pp. 1754-1756, 1995.

[3] C.H. Helmholt, U. Kruger and G. Grosskopf, "A mobile broad-band communicatio system based on mode-locked lasers" *IEEE Trans. Microwave Theory Tech.*, vol. 45, pp. 1424-1430, 1997.

[4] S. Fukushima, Y. Doi, T. Ohno, Y. Matsuoka and H. Takeuchi, "New phase-shift keying technique based on optical delay switching for microwave optical link", *IEEE Photon. Tech. Lett.*, vol. 11, pp. 1036-1038, 1999.

[5] K.-I. Kitayama, "Ultimate performance of optical DSB signal-base millimeter-wave fiber-radio system: effect of laser phase noise", *IEEE J. Lightwave Tech.*, vol. 17, pp. 1744-1781, 1999.

[6] K. Noguchi, O. Mitomi and H. Miyazawa, "Millimeter-wave Ti:$LiNbO_3$ optical modulators", *IEEE J. Lightwave Tech.*, vol. 16, pp. 615-619, 1998.

[7] N. Imai, H. Kawamura, K. Inaki and Y. Karasawa, "Wide-band millimeter-wave/optical-network applications in Japan", *IEEE Trans. Microwave Theory Tech.*, vol 45, pp. 2197-2207, 1997.

[8] W.H. Steier, M.-C. Oh, H. Zhang, A. Szep, L.R. Dalton, C. Zhang, H.R. Fetterman, D.H. Chang, H. Erlig and B. Tsap, "Recent advances in low voltage, high frequency polymer electro-optic modulators", *Optical Fibre Communications Conference Technical Digest*, pp. MJ1–1-MJ1–3, 2001.

[9] K.K. Loi, J.H. Hodiak, X.B. Mei, C.W. Tu, W.C.S. Chang, D.T. Nichols, L.J. Lembo and J.C. Brock, "Low-loss 1.3 μm MQW electroabsorption modulators for high-linearity analog optical links", *IEEE Photon. Tech. Lett.*, vol. 10, pp. 1572-1574, 1998.

[10] O. Mitomi, I. Kotaka, K. Wakita, s. Nojima, K. Kawano, Y. Kawamura and H. Asai, "40-GHz bandwidth InGaAs/InAlAs multiple quantun well optical intensity modulator", *Applied Optics,* vol. 31, pp. 2030-2035, 1992.

[11] F. Devaux, P. Bordes, A. Ougazzaden, M. Carre and F. Huet, "Experimental optimisation of MQW electroabsorption modulators with up to 40 GHz bandwidths", *Elec. Lett.*, vol. 30, pp. 1347-1348, 1994.

[12] J.F. Cadioul, F. Devaux, J.F. Veillard, B. Merdy, J. Guena, E. Penard and P. Legaud, "Electroabsorption modulator for radio over fibre at 38 GHz", *Elec. Lett.*, vol. 31, pp. 1273-1274, 1995.

[13] T. Kuri, K.-I. Kitayama and Y. Ogawa, "Fiber-optic millimeter-wave uplink system incorporating remotely fed 60-GHz-band optical pilot tone", *IEEE Trans. Microwave Theory Tech.*, vol. 47, pp. 1332-1337, 1999.

[14] L.D. Westbrook and D.G. Moodie, "Simultaneous bi-directional analogous fibre-optic transmission using an electroabsorption modulator", *Elec. Lett.*, vol. 32, pp. 1806-1807, 1996.

[15] D. Wake, D. Johansson and D.G. Moodie, "Passive picocell: a new concept in wireless network infrastructure", *Elec. Lett.*, vol. 33, pp. 404-406, 1997.

[16] A. Stohr, K.-I. Kitayama and D. Jager, "Full-duplex fiber-optic RF subcarrier transmission using a dual-function modulator/photodetector", *IEEE Trans. Microwave Theory Tech.*, vol. 47, pp. 1338-1341, 1999.

[17] T. Kuri, K.-I. Kitayama and Y. Takahashi, "60-GHz-band full-duplex radio-on-fiber system using two-RF-port electroabsorption transceiver", *IEEE Photon. Tech. Lett.*, vol. 12, pp. 419-421, 2000.

[18] Y. Akage, K. Kawano, S. Oku, R. Iga, H. Okamoto, Y. Miyamoto and H. Takeuchi, "Wide bandwidth of over 50 GHz travelling-wave electrode electroabsorptin modulator integrated DFB lasers", *Elec. Lett.*, vol. 37, pp. 299-300, 2001.

[19] H. Takeuchi, K. Tsuzuki, K. Sato, M. Yamamoto, Y. Itaya, A. Sano, M. Yoneama and T. Otsuji, "NRZ operation at 40 Gb/s of a compact module containing an MQW electroabsorption modulator integrated with a DFB laser", *IEEE Photon. Tech. Lett.*, vol. 9, pp. 572-574, 1997.

[20] H. Kawanishi, Y. Yamauchi, N. Mineo, Y. Shibuya, H. Murai, K. Yamada and H. Wada, "EAM-integrated DFB laser modules with more than 40 GHz bandwidth", *IEEE Photon. Tech. Lett.*, vol. 13, pp. 954-956, 2001.

[21] J. Park, W.V. Sorin and K.Y. Lau, "Elimination of the fibre chromatic dispersion penalty on 1550 nm millimetre-wave optical transmission", *Elec. Lett.*, vol. 33, pp. 512-513, 1997.

[22] AC083 FRANS Fibre Radio ATM Network and Services FINAL REPORT Document Ref. Nr.: AC083-SEL-CRC-AR-P-005-b1.

[23] J.J. O'Reilly, P.M. Lane, R. Heidemann and R. Hofstetter, "Optical generation of very narrow linewidth millimetre wave signals", *Elec. Lett.*, vol. 28, pp. 2309-2311, 1992.

[24] H.J. Thomas, N. Imai and E. Ogawa, "An optical bi-phase modulator for millimeter wave subcarrier systems", *IECIE Trans. Electron.*, vol. E79-C, pp. 32-38, 1996.

[25] H. Schmuck, R. Heidemann and R. Hofstetter, "Distribution of 60 GHz signals to more than 1000 base stations", *Elec. Lett.*, vol. 30, pp. 59-60, 1994.

[26] M.Y. Frankel and R.D. Esman, "Optical single-sideband supressed-carrier modulator for wide-band signal processing", *IEEE J. Lightwave Tech.*, vol. 16, pp. 859-863, 1998.

[27] L.T. Nichols and R.D. Esman, "Single sideband techniques and applications", *Optical Fibre Communications Conference Technical Digest*, pp. ThW1–1-ThW1–3, 1999.

[28] G.H. Smith, D. Novak and Z. Ahmed, "Overcoming chromatic-dispersion effects in fiber-wireless systems incorporating external modulators", *IEEE Trans. Microwave Theory Tech.*, vol. 45, pp. 1410-1415, 1997.

[29] E. Vergnol, F. Devaux, D. Tanguy and E. Penard, "Integrated lightwave millimetric single side-band source: design and issues", *IEEE J. Lightwave Tech.*, vol. 16, pp. 1276-1284, 1998.

[30] A.J. Cooper, "Fibre/radio for the provision of cordless/mobiletelephony services in the access network," *Electron. Lett.* vol. 26, pp. 2054-2056, 1990.

[31] S.Weisser, E.C. Larkins, K. Czotscher, W. Benz, J. Daleiden, I. Esquivias, J. Fleissner, J.D. Ralston, B. Romero, R.E. Sah, A. Shonfelder and J. Rosenzweig, "Damping-limited modulation bandwidths up to 40 GHz in undoped short-cavity $In_{0.35}Ga_{0.65}As$-GaAs multiple-quantum-well lasers", *IEEE Photon. Tech. Lett.*, vol. 8, pp. 608-610, 1996.

[32] P.A. Morton, T. Tanbaun-Ek, R.A. Logan, N. Chand, K.W. Wecht, A.M. Sergent and P.F. Sciortino, Jr., "Packaged 1.55 μm DFB laser with 25 GHz modulation bandwidth", *Electron. Lett.* vol. 30, pp. 2044-2046, 1994.

[33] E. Goutain, J.C. Renauld, M. Krakowski, D. Rondi, R. Blondeau and D. Decoster, "30 GHz bandwidth, 1.55 μm MQW-DFB laser diode based on a new modulation scheme", *Electron. Lett.* vol. 32, pp. 896-897, 1996.

[34] R. Nagarajan, S. Levy, A. Mar and J.E. Bowers, "Resonantly enhanced semiconductor lasers for efficient transmission of millimetre wave modulated light", *IEEE Photon. Tech. Lett.*, vol. 5, pp. 4-6, 1993.

[35] J.B. Georges, D.M. Cutrer, O. Solgaard and K.Y. Lau, "Optical transmission of narrowband millimeter-wave signals", *IEEE Trans. Microwave Theory Tech.*, vol. 43, pp. 2229-2241, 1995.

[36] S. Levy, R. Nagarajan, A. Mar, P. Humphrey and J.E. Bowers, "Fibre-optic PSK subcarrier transmission at 35 GHz using a resonantly enhanced semiconductor laser", *Electron. Lett.* vol. 28, pp. 2103-2104, 1992.

[37] N.G. Walker, D. Wake and I.C. Smith, "Efficient millimetre-wave signal generation through FM-IM conversion in dispersive optical fibre links", *Electron. Lett.* vol. 28, pp. 2027-2028, 1992.

[38] D. Mathoorasing and K. Kazmierski, "1.55 μm DFB VUG laser for millimetre wave applications", *Electron. Lett.* vol. 30, pp. 1957-1958, 1994.

[39] J.P. Gouy, M.F. Tarrega, S. Mezzour, P.A. Roland and D. Decoster, "Millimeter-wave optical links at 38 GHz based on laser diode nonlinearities", *Microwave and Optical Tech. Lett.*, vol. 16, pp.34-38, 1997.

[40] R. Ludwig and A. Ehrhardt, "Turn-key-ready wavelength-, repetition rate- and pulsewidth-tunable femtosecond hybrid modelocked semiconductor laser", *Electron. Lett.* vol. 31, pp. 1165-11167, 1995.

[41] L.Y. Kim, M. Pelusi, Z. Ahmed, H.-F. Liu and Y. Ogawa, "Ultrastable millimetre-wave signal generation using hybrid modelocking of a monolithic DBR laser", *Electron. Lett.* vol. 31, pp. 733-734, 1995.

[42] K. Sato, A. Hirano, M. Asobe and H. Ishii, "Chirp-compensated 40 GHz semiconductor modelocked lasers integrated with chirped gratings", *Electron. Lett.* vol. 34, pp. 1944-1946, 1998.

[43] T. Kuri and K.-I. Kitayama, "Long-term stabilized millimeter-wave generation using a high-power mode-locked laser diode module", *IEEE Trans. Microwave Theory Tech.*, vol. 47, pp. 570-574, 1999.

[44] K. Sato, A. Hirano, N. Shimizu and I. Kotaka, "High-frequency and low-jitter optical pulse generation using semiconductor mode-locked lasers", *IEEE Trans. Microwave Theory Tech.*, vol. 47, pp. 1251-1256, 1999.

[45] L. Zhai, A.J. Lowery, Z. Ahmed, N. Onodera and R.S. Tucker, "Locking bandwidth of mode-locked semiconductor lasers", *Electron. Lett.* vol. 28, pp. 545-546, 1992.

[46] D. Novak and R.S. Tucker, "Millimetre-wave signal generation using pulsed lasers", *Electron. Lett.* vol. 30, pp. 1430-1431, 1994.

[47] W.H. Loh, D. Atkinson, P.R. Morkel, M. Hopkinson, A. Rivers, A.J. Seeds and D.N. Payne, "Passively Mode-locked Er^{3+} fiber laser using a semiconductor nonlinear mirror", *IEEE Photon. Tech. Lett.*, vol. 5, pp. 35-37, 1993.

[48] M. Horowitz, C.R. Menyuk, T.F. Carruthers and I.N. Duling, III, "Theoretical and experimental study of harmonically modelocked fiber lasers for optical communication systems", *IEEE J. Lightwave Tech.*, vol. 18, pp. 1565-1574, 2000.

[49] S. Bennett, B. Cai, E. Burr, O. Gough and A.J. Seeds, "1.8-THz bandwidth, zero-frequency error, tunable optical comb generator for DWDM applications", *IEEE Photon. Tech. Lett.*, vol. 11, pp. 551-553, 1999.

[50] D. Wake, C.R. Lima, P.A. Davies, "Optical generation of millimeter-wave signals for fiber-radio systems using a dual-mode DFB semiconductor laser", *IEEE Trans. Microwave Theory Tech.*, vol. 43, pp. 2270-2276, 1995.

[51] A.C. Bordonalli, B. Cai, A.J. Seeds and P.J. Williams, "Generation of microwave signals by active mode locking in a gain bandwidth restricted laser structure", *IEEE Photon. Tech. Lett.* vol. 8, pp. 151-153, 1996.

[52] T. Ohno, K. Sato, S. Fukushima, Y. Doi and Y. Matsouka, "Application of DBR mode-locked lasers in millimeter-wave fiber-radio system", *IEEE J. Lightwave Tech.*, vol. 18, pp. 44-49, 2000.

[53] S. Pajarola, G. Guekos, P. Nizzola and H. Kawaguchi, "Dual-polarization external-cavity diode laser transmitter for fiber-optic antenna remote feeding", *IEEE Trans. Microwave Theory Tech.*, vol. 47, pp. 1234-1240, 1999.

[54] J. Hong and R. Hui, "Tunable millimeter-wave generation with subharmonic injection locking in two-section strongly gain-coupled DFB lasers", *IEEE Photon. Tech. Lett.* vol. 12, pp. 543-544, 2000.

[55] G.J. Simonis and K.G. Purchase, "Optical generation, distribution and control of microwaves using laser heterodyne", *IEEE Trans. Microwave Theory Tech.*, vol. 38, pp. 667-669, 1990.

[56] F.N. Timofeev, S. Bennett, R. Griffin, P. Bayvel, A.J. Seeds, R. Wyatt, R. Kashyap and M. Robertson, "High spectral purity millimetre-wave modulated optical signal generation using fibre grating lasers", *Elec. Lett.* vol. 34, pp. 668-669, 1998.

[57] R.-P. Braun, G. Grosskopf, H. Heidrich, C. Helmholt, R. Kaiser, K. Kruger, U. Kruger, D. Rohde, F. Schmidt, R. Stenzel and D. Trommer, 'Optical microwave generation and transmission experiments in the 12- and 60 GHz region for wireless communications", *IEEE Trans. Microwave Theory Tech.*, vol. 46, pp. 320-329, 1998.

[58] O. Solgaard, J. Park, J.B. Georges, P.K. Pepeljugoski and K.Y. Lau, "Millimeter wave, multigigahertz optical modulation by feedforward phase noise compensation of a beat note generated by photomixing of two laser diodes", *IEEE Photon. Tech. Lett.* vol. 5, pp. 574-577, 1993.

[59] J.B. Greorges, J. Park, O. Sorgaard, P.K. Pepeljugoski M. Sayed and K.Y. Lau, "Transmission of 300 Mbit/s BPSK at 39 GHz using feedforward optical modulation", *Elec. Lett.* vol. 30, pp. 160-161, 1994.

[60] R.A. Griffin and K. Kitayama, "Optical millimetre-wave generation with high spectral purity using feed-forward optical field modulation", *Elec. Lett.*, vol. 34, pp. 795-796, 1998.

[61] K.-I. Kitayama and R.A. Griffin, "Optical downconversion from millimeter-wave to IF-band over 50-km-long optical fiber link using an electroabsorption modulator", *IEEE Photon. Tech. Lett.* vol. 11, pp. 287-289, 1999.

[62] H.L. Stover and W.H. Steier, "Locking of laser oscillators by light injection", *Applied Phys. Lett.*, vol. 8, pp.91–93, 1966.

[63] L. Goldberg, H.F. Taylor and J.F. Weller, "FM sideband injection locking of diode lasers", *Elec. Lett.*, vol. 18, pp. 1019-1020, 1982.

[64] L. Goldberg, H.F. Taylor, J.F. Weller and D.M. Bloom, "Microwave signal generation with injection-locked laser diodes", *Elec. Lett.*, vol. 19, pp. 491-493, 1983.

[65] L. Goldberg, A.M. Yurek, H.F. Taylor and J.F. Weller, "36 GHz Microwave signal generation with an injection-locked laser diode", *Elec. Lett.*, vol. 21, pp. 814-815, 1985.

[66] K. Kikuchi, C.-E. Zah and T.-P. Lee, "Amplitude-modulation sideband injection locking characteristics of semiconductor lasers and their application", *IEEE J. Lightwave Tech.*, vol. 6, pp. 1821-1830, 1988.

[67] R.T. Logan, "All-optical heterodyne RF signal generation using a mode-locked-laser frequency comb: theory and experiments", *IEEE MTT-S Int. Microwave Symposium Digest*, pp. 1741-1744, 2000.

[68] S. Fukushima, C.F.C. Silva, Y. Muramoto and A.J. Seeds, "10 to 110 GHz tunable opto-electronic frequency synthesis using optical frequency comb generator and uni-travelling-carrier photodiode", *Elec. Lett.*, vol. 37, pp. 780-781, 2001.

[69] R,P. Braun, G. Grosskopf, D. Rohde and F. Schmidt, "Optical miilimetre-wave generation and transmission experiments for mobile 60 GHz band communications", *Elec. Lett.*, vol. 32, pp. 626-628, 1996.

[70] R,P. Braun, G. Grosskopf, D. Rohde and F. Schmidt, "Low-phase-noise millimeter-wave generation of 64 GHz and data transmissionusing optical sideband injection locking", *IEEE Photon. Tech. Lett.* vol. 10, pp. 728-730, 1998.

[71] L. Noel, D. Marcenac and D. Wake, "120 Mbit/s QPSK radio-fibre transmission over 100 km of standard fibre at 60 GHz using a master/slave injection-locked DFB laser source", *Elec. Lett.*, vol. 32, pp. 1895-1897, 1996.

[72] L. Noel, D. Wake, D.G. Moodie, D.D. Marcenac L.D. Westbrook and D.Nesset,"Novel techniques for high-capacity 60-GHz fiber-radio transmission systems", *IEEE Trans. Microwave Theory Tech.*, vol. 45, pp. 1416-1423, 1997.

[73] R.C. Steele, "Optical phase locked loop using semiconductor laser diodes", *Elec. Lett.*, vol. 19, pp. 1242-1243, 1983.

[74] Z.F. Fan, P.J.S. Heim and M. Dagenais, "Highly coherent RF signal generation by optical phase locking of external cavity semiconductor lasers", *IEEE Photon. Tech. Lett.* vol. 10, pp. 719–721, 1998.

[75] A.C. Davidson, F.W. Wise and R.C. Compton, "Low phase noise 33-40-GHz signal generation using multilaser phase-locked loops", *IEEE Photon. Tech. Lett.* vol. 10, pp. 1304-1306730, 1998.

[76] R .T. Ramos and A.J. Seeds, "Fast heterodyne optical phase-lock loop using double quantum well laser diodes", *Elec. Lett.*, vol. 28, pp. 82-83, 1992.

[77] U. Gliese, N.T. Nielsen, M. Bruun, E.L. Christensen, K.E. Stubkjaer, S. Lindgren and B. Broberg, "A wideband heterodyne optical phase-locked loop for generation of 3-18 GHz microwave carriers", *IEEE Photon. Technol. Lett.*, vol. 4, pp. 936–938, 1992.

[78] L.N. Langley, M.D. Elkin, C. Edge, M.J. Wale, U. Gliese, X. Huang and A.J. Seeds, "Packaged semiconductor laser optical phase-locked loop (OPLL) for photonic generation, processing and transmission of microwave signals", *IEEE Trans. Microwave Theory Tech.*, vol. 47, pp. 1257–1264, 1999.

[79] R.T. Ramos, P. Gallion, D. Erasme, A.J. Seeds and A.C. Bordonalli, "Optical injection locking and phase-lock loop combined systems", *Optics Lett.*, vol. 19, pp. 4–6, 1994.

[80] A.C. Bordonalli, C. Walton and A.J. Seeds, "High-performance homodyne optical injection phase-lock loop using wide-linewidth semiconductor lasers", *IEEE Photonics Technology Letters*, vol. 8, pp. 1217-1219, 1996.

[81] C. Walton, A.C. Bordonalli and A.J. Seeds, "High-performance heterodyne optical injection phase-lock loop using wide linewidth semiconductor lasers", *IEEE Photonics Technology Letters*, vol. 10, pp. 427–429, 1998.

[82] G.H. Smith, D. Novak, C. Lim and K. Wu, "Full-duplex broadband millimetre.wave optical transport system for fibre-wireless access", *Elec. Lett.*, vol. 33, pp. 1159-1160, 1997.

[83] R. Nagarajan, S. Levy and B.E. Bowers, "Millimeter wave narrowband optical fiber links using external cavity semiconductor lasers", *IEEE J. Lightwave Tech.*, vol. 12, pp. 127-136, 1994.

[84] Y. Doi, S. Fukushima, T. Ohno, Y. Matosouka and H. Takeuchi, "Phase shift keying using optical delay modulation for millimeter-wave fiber-optic rado links", *IEEE J. Lightwave Tech.*, vol. 18, pp. 301-307, 2000.

[85] T.N. Nielsen, U. Gliese, T. Christensen, H. Hoegh and K.E. Stubkjaer, "Highly linear and transparent 3-18 GHz optical microwave link", *IEEE MTT-S Int. Microwave Symposium Digest*, pp. 491-494, 1994.

[86] D. Wake, I.C. Smith, N.G. Walker, I.D. Henning and R.D. Carver, "Video transmission over a 40 GHz radio-fibre link", *Elec. Lett.*, vol. 28, pp. 2024-2025, 1992.

[87] U. Gliese, T. Norskov, S. Norskov and K.E. Stubkjaer, "Multifunctional fiber-optic microwave links based on remote heterodyne detection", *IEEE Trans. Microwave Theory Tech.*, vol. 46, pp. 458-468, 1998.

[88] Y. Ozeki, K. Nishikawa, M. Kishi and M. Tsuchiya, "60-GHz optoelectronic image rejection mixer and its application to a 156 Mb/s fiber-optic mm-wave link", *IEEE Photonics Technology Letters*, vol. 13, pp. 361-363, 2001.

[89] R.A. Griffin, P.M. Lane and J.J. O'Reilly, "Dispersion-tolerant subcarrier data modulation of optical millimetre-wave signals", *Elec. Lett.*, vol. 32, pp. 2258-2260, 1996.

[90] R.A. Griffin, P.M. Lane and J.J. O'Reilly, "Radio-over fiber distribution using an optical millimeter-wave/DWDM overlay", *Optical Fibre Communications Conference Technical Digest*, pp. WD6–1-WD6–3, 1999.

[91] Z. Ahmed, D. Novak, R.D. Waterhouse and H.-F. Liu, "37 GHz fiber-wireless system for distribution of broad-band signals", *IEEE Trans. Microwave Theory Tech.*, vol. 45, pp. 1431-1435, 1997.

[92] G.H. Smith and D. Novak, "Broad-band millimeter-wave (38 GHz) fiber-wireless transmission system using electrical and optical SSB modulation to overcome dispersion effects", *IEEE Photon. Tech. Lett.*, vol. 10, pp. 141-143, 1998.

Chapter 3

Carrier Generation and Transmission: Theory

This chapter treats the theory for the method chosen for the generation of single sideband millimetre wave modulated optical signals, the Optical Injection Phase-Lock Loop (OIPLL) and the expected fibre transmission properties of the generated millimetre wave modulated optical output. Results from theory and experimental demonstration are presented. The Introduction, 3.1, gives a general description of the OIPLL and the reasons for picking this generation method. Previous work that has been done relating to the OIPLL is also reviewed in the Introduction. The next section, 'Theory', 3.2 lays out a theoretical basis for the treatmet of the stability and noise performance. 'Fibre Transmission Effects' 3.3 investigates the expected effect of fibre transmission on the optical output of the OIPLL. The last section, 'Conclusion' 3.4 identifies the main conclusions that can be drawn from the chapter.

3.1 Introduction

Optical heterodyning is chosen for the generation of millimetre-wave modulated optical signals. There are three advantages. The first is that single sideband optical modulation is automatically generated, providing resistance to chromatic dispersion. The second is the wide frequency range that it is possible to generate. The limit is the bandwidth of the photodetector. Finally, the output power from the optical sources can be transduced into millimetre wave power with high efficiency. The optical injection phase-lock loop provides the best option amongst heterodyning technologies. It combines the advantages of OPLL and OIL technologies, without their limitations. The optical phase-lock loop can lock two semiconductor lasers with a potentially very wide locking range. However, the component requirements are very demanding. In order to achieve proper phase locking, either the loop delay time must be very short, or the linewidth of the optical sources must be very narrow. In contrast, the OIL can be designed around standard DFB lasers and still generate a low noise level. However, the locking range is narrow, and in order for OIL to work reliably, it needs to be contained in a carefully controlled environment. The OIPLL provides the best of the two technologies, allowing standard DFB lasers to be used in a system with low phase noise and wide locking range. The OIPLL is a particularly attractive option if only standard electrical and optical components can be used.

Systems incorporating both phase-lock loop and injection locking techniques were first demonstrated in the electrical domain. In 1971, a homodyne injection phase-lock loop system was demonstrated [1]. A second homodyne demonstration is found in [2]. Heterodyne versions have also been demonstrated, generating an 11 GHz output [3], and a 96 GHz output using a subharmonic reference [4]. The optical equivalent of the injection phase-lock loop, using semiconductor lasers was first proposed in 1994 [5, 6], where a theoretical analysis was presented. In this analysis [5], it was concluded that the main limitation of the OIPLL arose from competition between the two locking processes caused by mismatch in the optical paths in the OIPLL. A homodyne OIPLL was first experimentally demonstrated in 1996, using a free-space optical arrangement [7]. Later the work was extended to include an heterodyne OIPLL, generating an 8 GHz and a 16 GHz beat signal.

In this chapter the theoretical background describing the OIPLL with a millimetre wave modulated output will be presented. Furthermore, it is shown how what was described as the main limitation of the OIPLL can be overcome, giving the potential for extended locking range compared to previous demonstrations.

3.2 Theory

3.2.1 Fundamental stability

Figure 3.1 provides a schematic of the function of a heterodyne OIPLL. In the figure, two feedback loops can be identified, an optical phase-lock loop and optical injection locking, modelled in the form of an equivalent first order phase lock loop, with zero time delay. In the OPLL, the master and slave laser optical field, with the phase: $2\pi f_m t + \phi_m$ and $2\pi f_s t + \phi_s$, are mixed on a photodetector, producing an heterodyne difference frequency. The heterodyne frequency is then mixed with the reference source frequency, with phase: $2\pi f_r t + \phi_r$, producing the error signal: $\phi_e = \phi_m - \phi_s + \phi_r$. The error signal is fed through the loop filter, $F(s)$, and the FM-response of the slave laser, $H_s(s)$, to produce a frequency tuning of the slave laser. An explicit evaluation of the theory of an OPLL is found in Appendix C, where equation C.12 gives an expression for the frequency tuning of the slave laser induced by the OPLL.

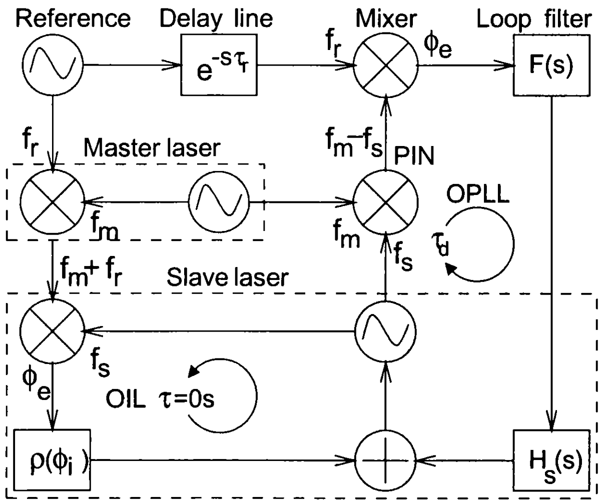

Figure 3.1: OIPLL schematic illustrating control feedback functions.

$$\frac{d\phi_{ms}}{dt} = 2\pi K_{opll}\phi_e * h_{lf} * h_s * \delta(t-\tau_d) \tag{3.1}$$

ϕ_{ms}	Master-slave laser phase difference
K_{opll}	OPLL gain
ϕ_e	Phase error
h_{lf}	Loop filter impulse response
h_s	Impulse response of slave laser frequency tuning
τ_d	Loop delay time

In the second feed-back loop, the injection locking, the master laser frequency is mixed with the reference by the means of direct modulation of the master laser. The resulting optical frequency, with a phase: $2\pi f_m t + \phi_m + 2\pi f_r t + \phi_r$, is used to lock the slave laser phase, $2\pi f_s t + \phi_s$, with a phase offset of ϕ_i. The resulting corresponding frequency tuning is: $\phi_e = \phi_m - \phi_s + \phi_r - \phi_i + \phi_\delta$, where ϕ_δ is the differential phase between the OPLL and the OIL feed-back. When modelled in the form of a first order feed-back loop, the injection locking process provides frequency control of the slave laser. In Appendix B, the expression for this is evaluated in equation B.28, here put in similar terms to those used for the OPLL:

$$\frac{d\phi_{ms}}{dt} = \frac{\sqrt{\rho(1+\alpha^2)}}{\tau_p}\cos(\phi_i + \arctan\alpha)\phi_e = K_{oil}\phi_e \tag{3.2}$$

ρ	Injection ratio
α	Slave laser phase-amplitude coupling factor
τ_p	Slave laser photonic lifetime
ϕ_i	Injection locking phase
K_{oil}	OIL injection gain

By combining the two feed-back processes, 3.1 and 3.2, the expression for the frequency tuning of the slave laser valid for the OIPLL is found:

$$\frac{d\phi_{ms}}{dt} = 2\pi K\phi_e * h_{lf} * h_s * \delta(t-\tau_d) + K_{oil}\phi_e \tag{3.3}$$

Both the expressions given above for ϕ_e must be valid in a combined OIL-OPLL system. This can only be true if $\phi_\delta = \phi_i$. Equation 3.3 can be translated into the frequency domain by the Laplace transform:

$$\mathscr{L}\left\{\frac{d\phi_{ms}}{dt}\right\} = K\phi_e H_s F_s e^{-s\tau_d} + K_{oil}\phi_e \tag{3.4}$$

$s = 2\pi jf$ The complex Laplace variable

H_{lf} Laplace transform of h_{lf}

H_s Laplace transform of h_s

The open loop gain, $G_s = \phi_{ms}/\phi_e$, closed loop gain, $H_s = \phi_{ms}/\phi_r$ and error function, $1 - H_s = \phi_e/\phi_r$ can now be defined:

$$G_s = \frac{KH_{lf}H_s e^{-s\tau_d} + K_{oil}}{s} \tag{3.5}$$

$$H_s = \frac{G_s}{1+G_s} \tag{3.6}$$

$$1 - H_s = \frac{1}{1+G_s} \tag{3.7}$$

Assuming that a second order, type II active phase-lock loop filter with loop parameters given from equations C.19 to C.21 in Appendix C is used, and that the slave laser FM response is uniform, the open-loop gain function can now be written:

$$G_s = \frac{-(f_n^2 + 2j\zeta f_n f)e^{-2\pi jf\tau_d} + fK_{oil}}{f^2} \tag{3.8}$$

f_n Loop natural frequency

ζ Zero delay loop damping factor

By studying the open-loop gain, the fundamental stability of the OIPLL can be quantified. The critical frequency is obtained by solving the equation $G = -1$ for both the phase and amplitude, when put into polar form [9]:

$$f_z = \sqrt{(2\zeta^2 f_n^2 - \frac{K_{oil}^2}{2}) + \sqrt{(2\zeta^2 f_n^2 - \frac{K_{oil}^2}{2})^2 + f_n^4}} \tag{3.9}$$

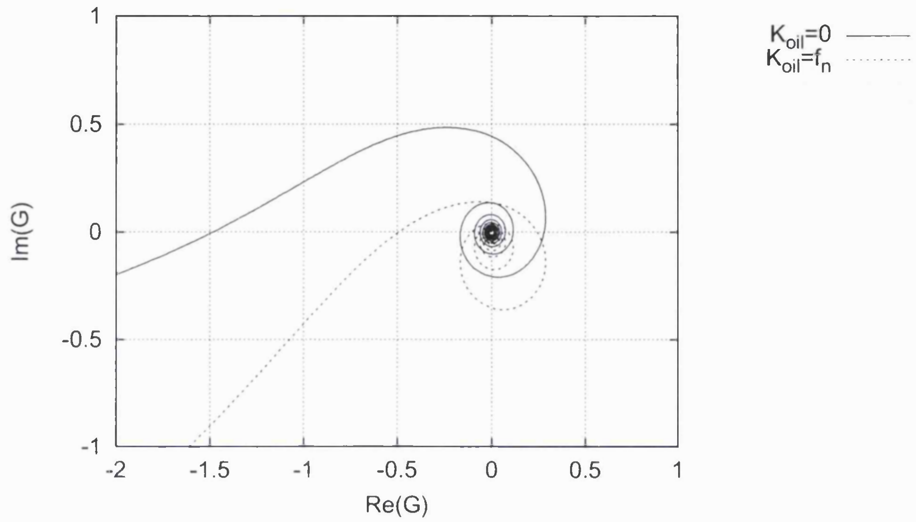

Figure 3.2: Nyquist plot for OIPLL using second order, type II filter with and without injection present, $1/7f_n$ loop delay and $1/\sqrt{2}$ OPLL loop damping.

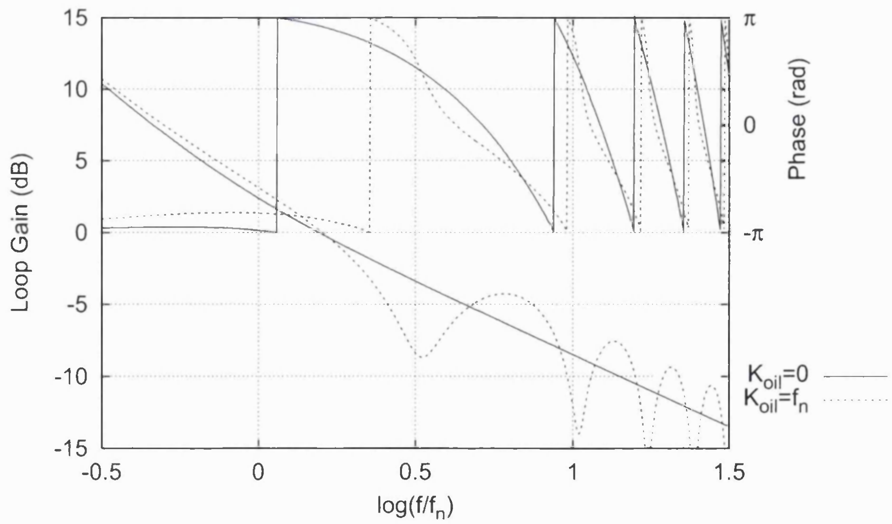

Figure 3.3: Bode plot for OIPLL using second order, type II filter with and without injection present, $1/7f_n$ loop delay and $1/\sqrt{2}$ OPLL loop damping.

Assuming that the loop time delay is one seventh of the inverse natural frequency, $\tau_d = 1/7f_n$ and the loop damping $\zeta = 1/\sqrt{2}$, the loop stability can be observed in a Nyquist plot, Fig. 3.2 and a Bode plot, Fig. 3.3 with and without injection present. When no injection is present, $K_{oil}/f_n = 0$, the locking is unstable. This can be concluded from the Nyquist plot by observing that the corresponding graph passes outside the $[0,-1]$ point. The locking is unstable because the loop delay is too large for the loop bandwidth used. To achieve stable locking with the OPLL only, either the loop delay or the loop natural frequency needs to be decreased. If the injection ratio is activated, the locking becomes stable, if the injection locking is large enough to prevent the instabilities caused by the time delay in the phase lock loop. In the Nyquist plot this is shown since the graph never passes outside the $[0,-1]$ point. In the Bode plot, the oscillations in the gain originates from the sum of the injection locking and the phase lock loop. The conclusion is that by using optical injection, higher natural frequency and therefore higher OPLL loop gain can be used without losing stability. Alternatively, a longer loop time delay can be used in an OIPLL than in the corresponding OPLL. In this case, the OIPLL loop bandwidth will be determined by the injection locking gain, K_{oil}. The loop bandwidth can be expressed as the 3 dB bandwidth of the closed loop gain, H. Fig. 3.4 shows the closed loop gain as a function of frequency for different values of injection locking gain and the 3 dB bandwidth corresponds to the injection locking gain. The significance of the loop bandwidth is as a measure of the bandwidth of the injected signal the OIPLL will be able to successfully phase track, paricularly important if the injected signal is phase or frequency modulated.

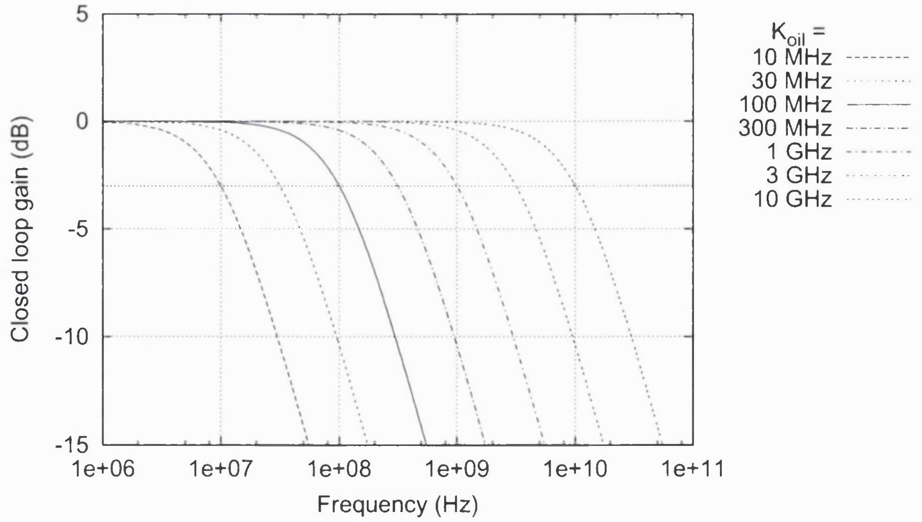

Figure 3.4: OIPLL open loop gain for different values of injection-locking gain. Low phase lock loop gain assumed.

3.2.2 Noise performance

In order to analyse the noise performance of the OIPLL, the noise sources that contribute must be identified. The noise sources can be divided into two categories, intensity noise added in the optical receiver, and the phase noise of the oscillators. The noise performance of the OIPLL can now be derived in the same manner as for the OPLL in appendix C.31:

$$S = |1-H|^2 S_n - |H|^2 S_{in} \tag{3.10}$$

Where S_n is the laser noise squared error density and S_{in} is the additive phase noise square error density. The additive noise sources are those usual for an optical receiver; laser RIN, shot noise and thermal noise of the receiver, in the absence of any optical amplifiers. The phase noise of the reference source is in these calculations assumed to be zero, however, in any real system, the reference noise will be a lower limit to the possible spectral purity of the generated signal. The phase noise spectral density of the two other oscillators, the laser sources, is given from the laser heterodyne linewidth:

$$S_n = \frac{\delta f_{ms}}{2\pi f^2} \tag{3.11}$$

Considering the upper and lower noise bands after downconversion and the conversion from intensity noise into phase and amplitude noise, as described in Appendix C, the phase noise spectral density originating from additive noise can be expressed as:

$$S_{in} = N_{in} \tag{3.12}$$

Equation 3.10 can now be used to calculate the total output phase error variance from the OIPLL where H is given by equation 3.6. Fig. 3.5 shows a typical phase noise density spectrum for an OIPLL. As a reference, the phase noise density spectrum is also shown for the corresponding OPLL, OIL and the free-running laser. At high frequencies, outside the bandwidth of both the injection locking and the phase-lock loop, the phase noise is limited by the free-running laser noise. At intermediate frequencies, the phase noise performance is limited by the injection locking, which usually has a wider locking bandwidth than the phase-lock loop. The OPLL provides phase noise reduction greater than the OIL close to the carrier frequency, down to levels corresponding to the additive noise originating in the receiver. The greater phase noise reduction at low frequencies is due to the higher order of the phase-lock loop using an integrating loop-filter and active current feed-back. This results in an OIPLL with greater phase-noise reducing capabilities than either OIL or OPLL used alone.

Integrating the single sideband phase error density function, S over the noise bandwidth, B, the total phase error variance can be calculated:

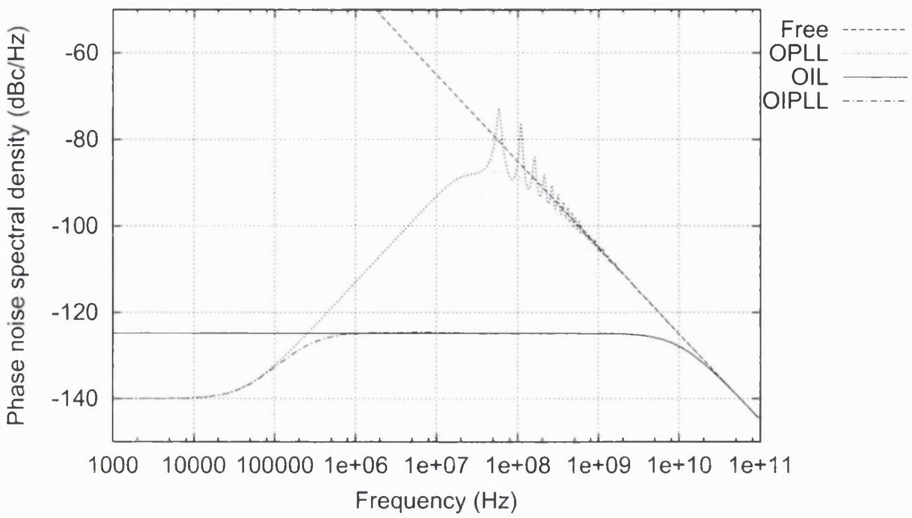

Figure 3.5: Phase error density as a function of offset frequency from generated carrier for a free-running laser, OPLL only, OIL only and the OIPLL. Parameters used: -140 dBc/Hz laser RIN, 200 MHz heterodyne linewidth, 50 MHz OPLL natural frequency, $1/\sqrt{2}$ loop damping, 10 GHz injection rate.

$$\sigma^2 = 2\int_0^B S df \tag{3.13}$$

The total phase error variance needs to be small, ($\sigma^2 < 0.25$ rad^2 [10]) for the linear OPLL analysis in Appendix C to be valid. Fig. 3.6 shows the loop time delay versus summed laser linewidth that would be required to achieve a phase error variance of 0.01 rad^2 in an OPLL. Fundamental stability is ensured by having zero delay damping $\zeta = 1/\sqrt{2}$, and a 10 dB loop gain margin, that is a natural frequency, f_n ten times lower than the critical frequency, f_z. If fibre-pigtailed components are to be used, the loop delay time will typically be about 10 ns. This would require a summed laser linewidth of only 60 kHz if 0.01 rad^2 phase error variance is to be achieved. That would require specialised laser structures, such as external cavity lasers to be used. On the other hand, if conventional DFB lasers, with a typical summed linewidth of 10 MHz are used, the loop time delay has to be lower than 100 ps. This cannot be achieved using fibre optics, and it is very difficult to achieve using bulk optics. The lowest loop time delay reported in an OPLL so far is 400 ps [11, 12]. Adding an injection locking path to the OPLL, creating an OIPLL provides a method of using standard lasers in a fibre based system with large loop delay. This is because the injection locking provides phase reduction independent of the loop delay. Fig. 3.7 shows the expected phase error variance versus loop delay time for various injection ratios in the OIPLL. Standard wide linewidth lasers with 10 MHz summed linewidth has been assumed. When no optical injection is present, the performance is that of an OPLL. Zero delay damping and 10 dB gain margin have been assumed. The other curves show the decreasing phase error variance with increasing injection. The same loop parameters has been assumed. An injection locking equivalent loop gain of 1 GHz results

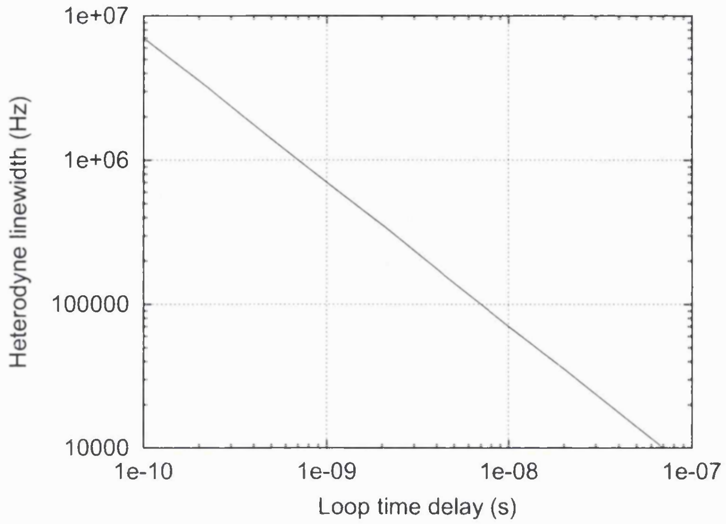

Figure 3.6: Loop time delay versus summed laser linewidth required to achieve 0.01 rad^2 phase error variance in an OPLL with 10 times gain margin and $1/\sqrt{2}$ loop damping.

in a phase error variance of 0.005 rad^2, even for loop time delays exceeding 10 ns. In general terms, with high injection ratio and long loop delay, the phase error variance is independent of the loop delay. This is because the bulk of the phase error reduction is provided by the injection locking. Therefore, very long time delay and a very narrowband OPLL can be used without much degradation of phase noise. When the phase noise reduction is dependent on the injection locking,

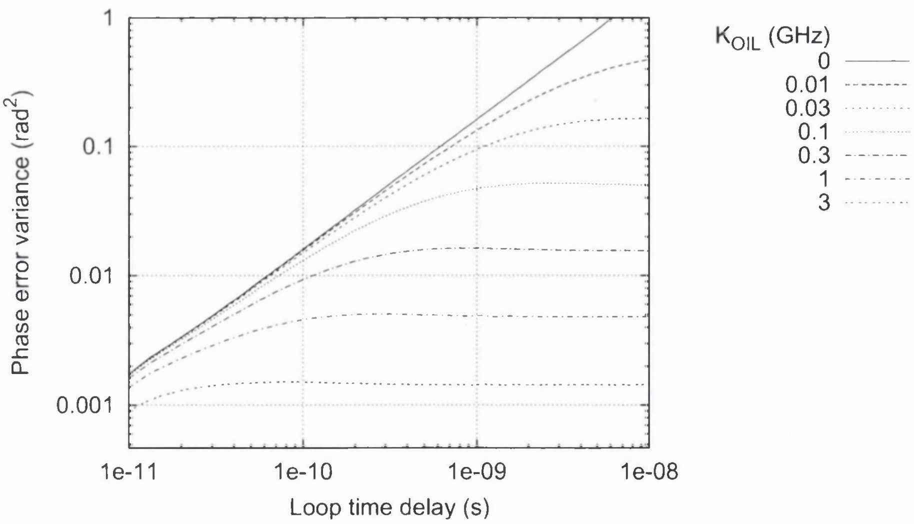

Figure 3.7: Expected phase error variance versus loop delay time for en OPLL and for OIPLL's with varying injection ratios, 10 times OPLL gain margin, $1/\sqrt{2}$ loop damping, 10 MHz heterodyne bandwidth and 10 ns loop delay.

there is a linear relation between the heterodyne laser linewidth and the noise power density, as illustrated by Fig. 3.8. Also, the relation between the laser heterodyne linewidth and the total phase error variance is linear if the noise bandwidth is much higher than the OPLL bandwidth. The more important role of the phase-lock loop part in an OIPLL than phase noise reduction is to

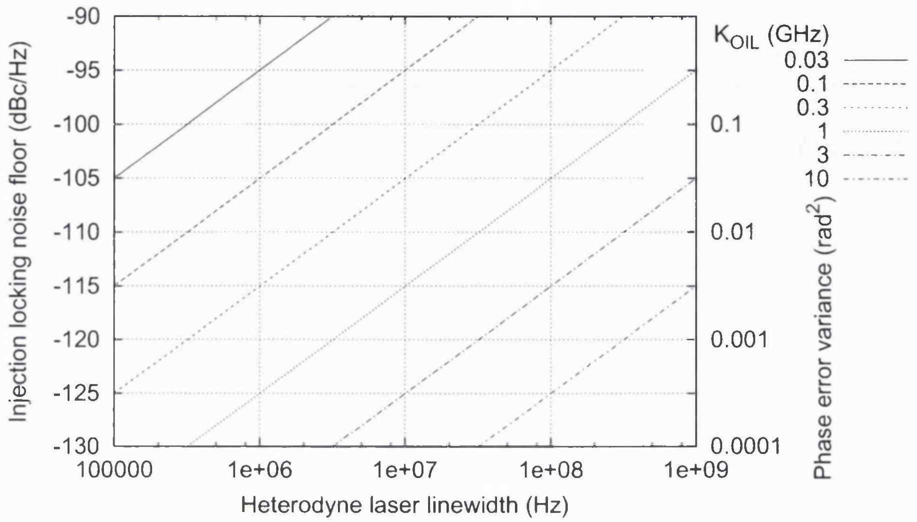

Figure 3.8: OIPLL phase noise floor and phase error variance versus heterodyne laser linewidth for various injection rates, a narrowband OPLL ($f_n = 100kHz$, $\zeta = 1/\sqrt{2}$) and 10 ns loop delay.

ensure long term stability. This can be illustrated by Fig. 3.9. It shows the phase error variance of OIL as a function of the injection phase. The curve is divided into one stable part and one unstable part, because of the asymetry induced by the phase-amplitude coupling factor, α and the limitation of the injection phase, $|\phi_i| < \pi/2$, as discussed in Appendix B. Also shown in Fig. 3.9 is the linear relation between the injection phase and the detuning of free-running slave laser frequency relative to the point of optimum phase noise reduction. In a system using injection locking only, the phase error suppression will degrade as the frequency of the free-running master or slave laser changes. A typical DFB laser has a temperature tuning coefficient of about 10 GHz/K. It is clear that only a small change in temperature will degrade the performance or even throw the OIL out of lock. By using an active integrating filter with very high DC gain, the locking range of an OIPLL can be made much greater than for OIL only, as a narrowband OPLL can be viewed as active current feedback that is used to compensate for the measured drift of the injection phase. The fundamental limitation to the locking range of the OIPLL is the continous frequency tuning range of the slave laser.

3.2.3 Differential Phase Effects

As two locking processes are involved in the OIPLL, the phase error is measured at two separate points, in the mixer and in the slave laser, as seen in Fig. 3.1. The difference between these two measurements is denoted ϕ_δ. As reasoned above, in a locked OIPLL, ϕ_δ is equal to the injection locking phase, ϕ_i. If this were not the case, the OPLL would try to tune the free-running frequency

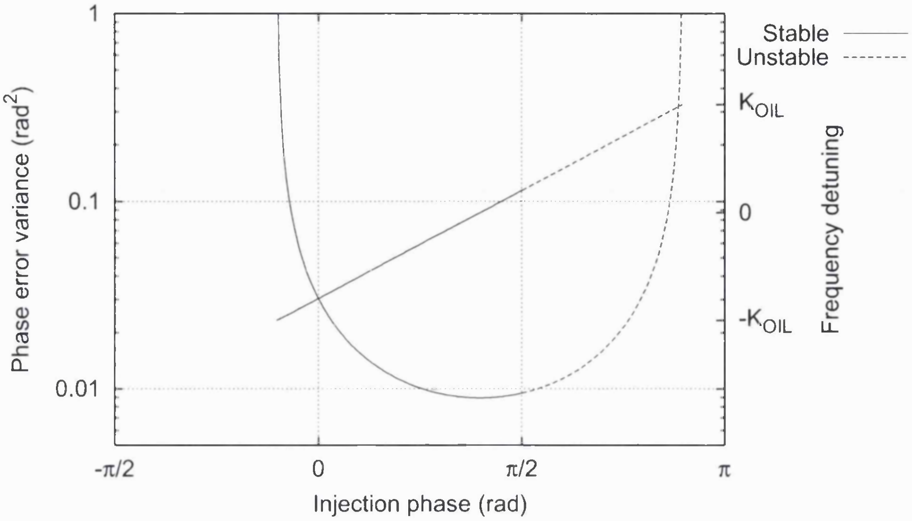

Figure 3.9: Phase error variance and corresponding free-running slave laser frequency shift as a function of the injection phase of OIL. Parameters used are: $\alpha = 3$, 10 times OPLL gain margin, $1/\sqrt{2}$ loop damping, 30 MHz heterodyne bandwidth and 10 ns loop delay.

of the slave laser to change the injection phase according to Fig. 3.9, until either $\phi_\delta = \phi_i$ or the OIPLL fell out of lock. As a consequence, the injection phase can be exactly selected for optimum phase noise suppression by controlling the differential phase, typically by using an adjustable delay line in the path of the reference signal, as in Fig. 3.1. The phase measured in the mixer can be calculated by using the time delays defined in Fig. 3.10. The phase measured in the mixer including path delays is:

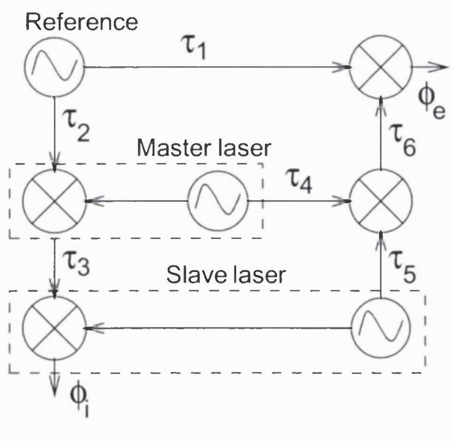

Figure 3.10: Path delays used to calculate the differential locking phase.

$$\phi_e = 2\pi f_m(t - \tau_4 - \tau_6) + \phi_m - 2\pi f_s(t - \tau_5 - \tau_6) - \phi_s + 2\pi f_r(t - \tau_1) + \phi_r \tag{3.14}$$

The phase at the slave laser including path delays is:

$$\phi_e - \phi_\delta = 2\pi f_m(t - \tau_3) + \phi_m - 2\pi f_s(t) - \phi_s + 2\pi f_r(t - \tau_2 - \tau_3) + \phi_r \tag{3.15}$$

By using $\phi_i = \phi_\delta$, the following relation is found:

$$\phi_i = 2\pi f_m(\tau_3 - \tau_4 - \tau_6) - 2\pi f_s(-\tau_5 - \tau_6) + 2\pi f_r(\tau_2 + \tau_3 - \tau_1) \tag{3.16}$$

In the locked state, $\phi_s = \phi_m + \phi_r$, and:

$$\phi_i = 2\pi f_m(\tau_3 - \tau_4 + \tau_5) + 2\pi f_r(\tau_2 + \tau_3 - \tau_1 + \tau_5 + \tau_6) \tag{3.17}$$

There are two sets of paths that need to be matched, one with regard to the reference frequency, and one with regard to the optical frequency of the master laser. Because of the different frequencies, the path length sensitivity is very different for the two cases, in the first case one period corresponds to the reference wavelength, on a millimetre-scale, while the other corresponds to the optical wavelength, more than three orders lower, on a micrometre scale.

If a fibre-based system is used, the delay times will be dependent on the temperature of the fibre, according to [13]:

$$\frac{1}{t}\frac{dt}{dT} = \frac{1}{\eta}\frac{d\eta}{dT} + \frac{1}{L}\frac{dL}{dT} + \frac{1}{\eta}\frac{d\eta}{dL}\frac{dL}{dT} \tag{3.18}$$

T : Temperature
η : Refractive index
L : Fibre length

The first term is the temperature dependent change of the refractive index of the fibre, the second term is the thermal expansion of the fibre and the last term is the index change due to the photoelastic effect. Normally, the first term is the dominant. The combined effect has been experimentally investigated, and a typical value for the relative thermal change in the optical path of SSM fibre is $7.3 \cdot 10^{-6}$ /K [14]. For an optical wavelength of 1550 nm, and a fibre length path of 10 m, a temperature change of only 5.3 mK will cause a phase shift of $\pi/2$, enough to shift ϕ_i to the unstable region, as illustrated in Fig. 3.9, and cause the OIPLL to fall out of lock. It is clear that when using fibre-optics, either very short lengths of fibre have to be used, or the fibre must be placed in a carefully controlled environment. However, there is a special case when none of this is necessary. This is when the master laser field reflected from the slave laser is used for mixing on the photodetector and $\tau_4 \equiv \tau_3 + \tau_5$. Any change in optical path will then affect both paths equally, and cancel each other out, not affecting the locking phase. The injection phase, ϕ_i, is now only affected by differential paths on a millimetre scale, large enough not to be affected by any environmental factors. Furthermore, since the reference signal has a very long coherence length, an integer number of reference wavelengths could be added to the injection phase, without any degradation of the OIPLL performance: $\phi_i = \phi_\delta + 2\pi n$.

3.3 Fibre Transmission Effects

In the next chapter 4, the magnitude of the master laser FM sidebands are predicted and compared to experimentally established measurements. Using these relative amplitudes of the master laser modulation sidebands from $-3 \cdot f_m$ to $+3 \cdot f_m$: -33.9 dBm, -19.6 dBm, -7.6 dBm, -2.2 dBm, -7.8 dBm, -20.2 dBm and -34.2 dBm, and ignoring modulation sidebands of higher order than 3, the modulated master laser spectra can be represented as a sum of frequency components:

$$E_{ml}(t) = \sum_{m=-3}^{3} E_{ml,m} e^{i2\pi(\nu_{ml}+mf_m)t} \tag{3.19}$$

The reflected master laser field from the slave laser can be estimated from Fig. 4.12 and be expressed in the form:

$$E_r(t) = \sum_{m=-3}^{3} E_{r,m} e^{i2\pi(\nu_{ml}+mf_m)t} \tag{3.20}$$

At the output of the OIPLL the following signal is obtained:

$$E_{out}(t) = \Gamma_1 E_{ml}(t+\tau_d) + \Gamma_2 E_r(t) + \Gamma_2 E_{sl} e^{\{j(2\pi(\nu_{ml}+3f_m)+\phi_{ms})t\}} \tag{3.21}$$

$\Gamma_{1,2}$: Optical loss from couplers and splices
τ_d : Differential time delay between master laser main path and reflected path (s)
Γ_r : Master laser reflection loss at the slave laser
ϕ_{ms} : Phase between master sideband and slave laser

The first component represents the master laser field, the second component represents the reflected master laser field from the slave laser, and the third component represents the slave laser field locked to the master laser third harmonic modulation sideband. Assuming the relative amplitudes of the master laser components above, a slave laser reflection loss of 20 dB and no excess losses in splices and couplers, the penalty due to master-slave laser injection phase, differential time delay, τ_d and fibre dispersion can be calculated if we use the fibre transfer function, defined in Appendix A, equation A.4:

$$H(f) = e^{-j\pi D\frac{\lambda^2}{c}Lf_m^2} \tag{3.22}$$

D : Fibre dispersion (ps/km/nm)
λ : Optical wavelength (nm)
L : Fibre length (m)

With all these factors included, the worst case scenario for the variation in detected millimetre wave power related to master-slave laser injection phase is 7.7 dB. However, the variation is dependent on the differential time delay, and delays other than zero will result in a lower sensitivity to the injection phase. In a similar manner, the variation due to differential time delay is periodical with a maximum of 14 dB between maxima and minima at zero injection phase. Using the fibre transfer function, a periodical dependence to the fibre transmission length is found, as seen in Fig. 3.11, with 5.5 dB difference between highest maxima and lowest minima. The master-slave laser injection phase is stabilised by the optical phase-lock loop part to the point of optimum noise suppression which is close to $\pi/2$ and the differential time is stabilised by the path length stabilisation that can be tuned to give optimum detected power. For longer fibre lengths, some of the fibre dispersion dependent penalty can be offset by compensation of the differential time delay. Also shown in Fig. 3.11 is an additional penalty in detected millimetre wave power due to the

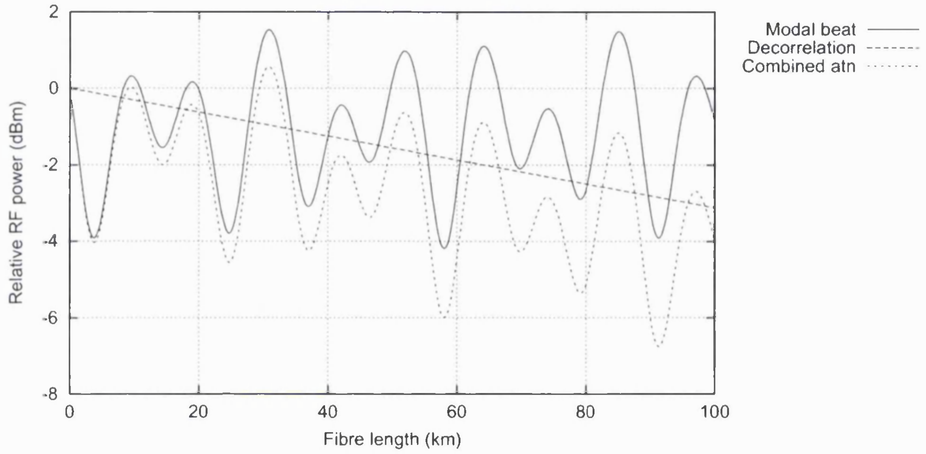

Figure 3.11: Power penalty versus fibre length of detected millimetre wave power due to dispersion effects, fibre attenuation disregarded.

gradual decorrelation of the optical frequency components, given by equation A.16 in appendix A:

$$\Gamma_d = e^{2\pi\delta f_{ms} D \frac{\lambda^2}{c} L f_m \cdot 10} \tag{3.23}$$

δf_{ms} : Master-slave laser heterodyne linewidth (Hz)

D : Fibre chromatic dispersion (ps/nm/km)

For a 36 GHz modulation at 1540 nm with fibre dispersion of 20 ps/nm/km and combined laser linewidth of 240 MHz, this gives an equivalent optical attenuation of 0.016 dB/km. This figure is small, compared to the fibre attenuation; 0.2 dB/km. However, this degradation of detected millimetre wave power affects the carrier to noise ratio, as this degradation is relative to the noise floor. The evolution of the carrier to noise ratio over fibre transmission from 0 km to 200 km of fibre, described by equation A.15 in appendix A, is shown in Fig. 3.12. In Fig. 3.13, the relative noise floor originating from decorrelation is illustrated together with the noise floor originating

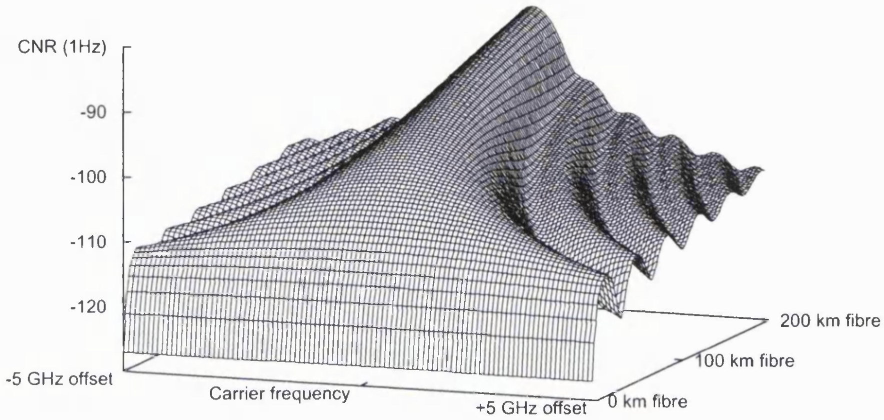

Figure 3.12: CNR for transmission up to 200 km of fibre as a function of frequency offset from carrier frequency, 36 GHz, ignoring other noise terms than due to carrier decorrelation. Fixed input optical power has been assumed.

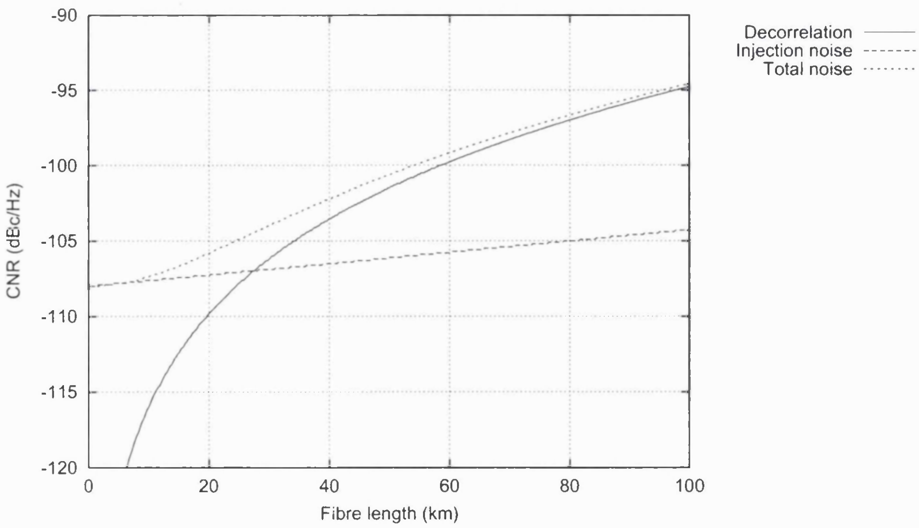

Figure 3.13: Degradation of carrier to noise ratio at 10 kHz offset from a 36 GHz carrier due to fibre chromatic dispersion for fixed input optical power. 240 MHz combined laser linewidth and 17 ps/nm/kn dispersion have been assumed.

from the imperfect injection locking, all at 10 kHz offset frequency from the generated carrier. A fixed received optical power is assumed.

3.4 Conclusions

In this chapter, the theoretical basis for the first demonstration of a millimetre wave OIPLL is described, including fundamental stability, noise performance and differential path effects. The expected behaviour of the generated millimetre wave modulated output for transmitted through fibre is also investigated. It is found that the use of a combined OPLL and OIL system overcomes many of the limitations of using either an OPLL or OIL alone, such as the requirement for narrow linewidth lasers or short loop delay of the OPLL, or the limited locking range of the OIL. The combination will allow the use of a wider bandwidth OPLL because of the stabilising effect or the injection locking. Furthermore, it is shown how the stability problems relating to differential path effects, as reported from earlier work with the OIPLL, can be overcome by using the reflection of the master laser field from the slave laser. The degradation of the generated carrier due to fibre transmission is investigated, both with regard to the decorrelation of the two main optical lines and due to interferrence with the additional beats originating from the unwanted master laser FM sidebands.

References

[1] G. Sato, “Stabilized oscillators by using injection locking and phase-locked loop”, *Electron. & Comm. in Japan*, vol. 54-B, pp. 59–65, 1971.

[2] P.K. Runge, “Phase-locked loops with signal injection for increased pull-in range and reduced output phase jitter”, *IEEE Trans. Comm.*, vol. COM-24, no. 6, pp. 636–644, 1976.

[3] J. Berenguer, J. Bara, E. Artal, I. Corbella and A. Cameron, “Improvement of the pull-in range and acquisition time of a microwave P.L.L. system by injection locking the V.C.O.”, *IEEE 41st Annual Frequency Control Symposium*, pp. 524–526, 1987.

[4] T. Berceli, S. Kudszus, M. Schlechtweg, A. Zolomy, G. Jaro, T. Marozsak and E. Udvary: “Optical millimeter wave generation utilizing a subharmonic reference,” *IEEE MTT-S, International Microwave Symposium Digest.*, Vol. 3, pp. 1749–1752, 2000.

[5] A.C. Bordonalli, A.J. Seeds and R.T. Ramos, “Low phase noise opticalphase-lock loops using combined injection locking and phase locking”, *IEE Colloquium on Microwave Opto-Electronics, London*, digest no. 1994/022, pp. 6/1–6/5, 1994.

[6] R.T. Ramos, P. Gallion, D. Erasme, A.J. Seeds and A.C. Bordonalli, “Optical injection locking and phase-lock loop combined systems”, *Optics Lett.*, vol. 19, pp. 4–6, 1994.

[7] A.C. Bordonalli, C. Walton and A.J. Seeds, “High-performance homodyne optical injection phase-lock loop using wide-linewidth semiconductor lasers”, *IEEE Photonics Technology Letters*, vol. 8, pp. 1217–1219, 1996.

[8] C. Walton, A.C. Bordonalli and A.J. Seeds, “High-performance heterodyne optical injection phase-lock loop using wide linewidth semiconductor lasers”, *IEEE Photonics Technology Letters*, vol. 10, pp. 427–429, 1998.

[9] A.C. Bordonalli, “Optical injection phase-lock loops”, PhD thesis submitted to University of London, Department of Electronic and Electrical Engineering, University College London, 1996.

[10] U. Gliese, "Optical Generation of Microwave Signals”, PhD. thesis, Electromagnetics Institute, Technical University of Denmark, Lyngby, Denmark, 1992.

[11] U. Gliese, N.T. Nielsen, M. Bruun, E.L. Christensen, K.E. Stubkjaer, S. Lindgren and B. Broberg, “A wideband heterodyne optical phase-locked loop for generation of 3-18 GHz microwave carriers”, *IEEE Photon. Technol. Lett.*, vol. 4, pp. 936–938, 1992.

[12] L.N. Langley, M.D. Elkin, C. Edge, M.J. Wale, U. Gliese, X. Huang and A.J. Seeds, "Packaged semiconductor laser optical phase-locked loop (OPLL) for photonic generation, processing and transmission of microwave signals", *IEEE Trans. Microwave Theory Tech.*, vol. 47, pp. 1257–1264, 1999.

[13] S. Nissila, J. Kostamovaara and R. Myllyla, "Thermal characteristics of optical delay in fibers used in pulsed laser rangefinding", *IEEE J. Lightwave Tech.*, vol. 9, pp. 1464–1466, 1991.

[14] C.E. Lee and H.P. Taylor, "Fiber-optic Fabry-Perot temperature sensor using a low-coherence light source", *IEEE J. Lightwave Tech.*, vol 9, pp. 129–134, 1991.

Chapter 4

Carrier Generation and Transmission: Experiments

This chapter treats the experimental work that has been carried out to demonstrate the first millimetre wave Optical Injection Phase-Lock Loop (OIPLL). The Introduction, 4.1, contrasts the experimental arrangement of the here demonstrated OIPLL with previous work. The next section, 'Optical Sources' 4.2 investigates the properties of the two DFB lasers the system is based upon. 'Experimental Arrangement' 4.3 gives the remaining details of the arrangement used to demonstrate the OIPLL. The obtained experimental data is presented in 'Experimental Performance', 4.4. The last section, 'Conclusion' 4.5 identifies the main achievements and gives some suggestions for future improvements of the system demonstrated in this chapter.

4.1 Introduction

Previously, the OIPLL has only been demonstrated for generation of lower than millimetre wave frequences, 8 GHz and 16 GHz [1]. It successfully demonstrated that the OIPLL concept can be realised, producing the spectral purity and stability of the opticaly generated microwave signal predicted by theory [2]. However, the experimental arrangement was based on free space bulk optics, as only free space optics can provide the optical path stability required for the general case of path stabilisation described in the last chapter, section 3.2. The use of bulk optics comes with a price, very sensitive optical alignment. The optical path is being split in a manner similar to a Michelson interferometer with a optical frequency conversion present in one of the arms in form of the slave laser. When recombining the two optical paths, great care must be taken to minimise wavefront overlap in order to preserve the efficiency of the optical heterodyne detection [3].

In this chapter the experimental results of the first heterodyne OIPLL with a millimetre wave modulated output will be presented. This has been achieved in a fibre-integrated arrangement, using only fibre-pigtailed optical components. Singlemode fibre does not have the limitation of wavefront misalignment, Because of the single mode operation. The efficiency of the heterodyne detection between two optical lines is determined by the polarisation matching only. Furthermore, using pigtailed optical components, the coupling losses can be made lower than what was achieved using bulk optics. The increased coupling efficiency here allows injection locking with good results to higher order master laser FM sideband, here the third, as compared to a maximum second order in [1]. Millimetre wave modulated optical signals can now be generated using 10 GHz master laser modulation frequency or higher. The main disadvantage of the use of fibre optics, instabilities in the optical path length, is in this experiment overcome by using the special path configuration described in the last chapter, section 3.2. A second effect is the interference of the master laser reflection from the slave laser. This chapted will describe one method to compensate for the effects of this interference.

4.2 Optical sources

The optical sources used in the OIPLL are two 16 quantum well InGaAs/InGaAsP DFB lasers [4] with a $\lambda/4$-shifted second order grating. The device length is 370 μm and the area of the active region is 0.18 μm^2. Other characteristics include a refractive index of 3.14, group refractive index in the range 3.67 to 3.85, internal loss around 29 cm^{-1}, differential gain in the region $5.5 \cdot 10^{-20} m^2$ to $6.5 \cdot 10^{-20} m^2$ and nonlinear gain suppression factor between $2 \cdot 10^{-23} m^3$ and $3 \cdot 10^{-23} m^2$ [5]. The combined linewidth of the two lasers was determined by observation of the heterodyne spectra. Fig. 4.1 shows the detected spectra together with a Lorentzian curve fit. The heterodyne beat linewidth was estimated to be about 240 MHz. The large value of the linewidth indicates a low Q-factor of the laser cavity. In order to design and model an OIPLL, a number of additional parameters need to be determined. These includes static and dynamic response to current injection, the phase-amplitude coupling factor (α-factor), modulated output spectra of the master laser and injection locking properties of the slave laser.

4.2.1 Static response

Fig. 4.2 shows the static tuning characteristics of the master and slave laser, both at 20°C. The choice of master laser is based on the frequency shift. The locking range of the OIPLL is dependent on the tuning range of the slave laser. In the 30 mA to 70 mA current injection range, the two lasers have 7.1 GHz and 29.0 GHz tuning range respectively. In order to achieve a large locking range, the laser with the wider tunability needs to be the slave laser. Also shown in Fig. 4.2 is the L-I curve of the two lasers. The master laser has the higher fibre-coupled output power at 70 mA bias. The threshold current is 22.2 mA for the master laser and 21.5 mA for the slave laser.

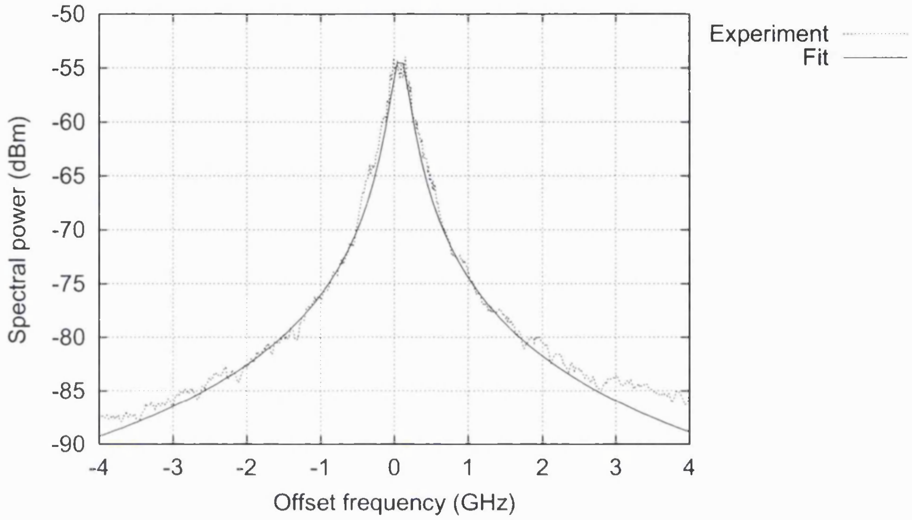

Figure 4.1: Free-running laser heterodyne spectra with the corresponding Lorentzian curve fit.

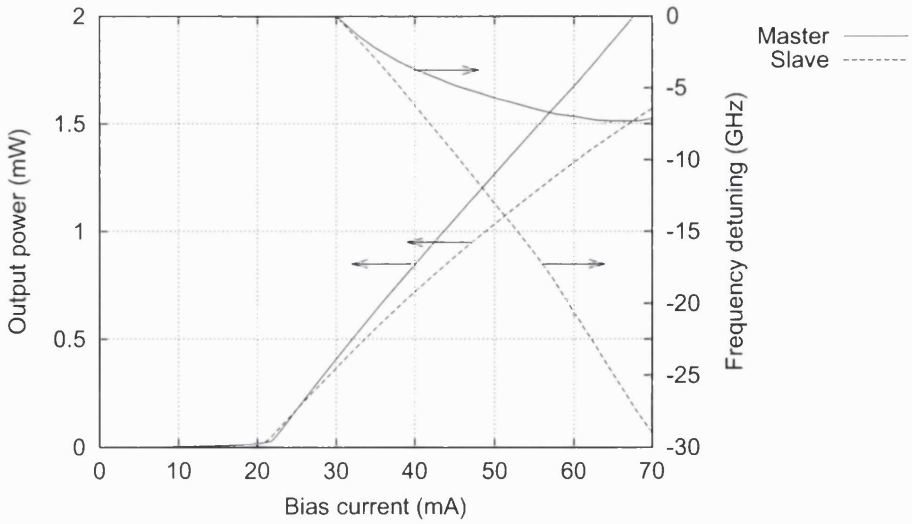

Figure 4.2: Static tuning characteristics of the master and slave laser.

4.2.2 Dynamic response

The dynamic response is important in two ways. First, the modulation bandwidth of the master laser determines what order modulation sideband the slave laser needs to be locked to in order to generate a given frequency. Second, the frequency modulation (FM) response of the slave laser can be a limiting factor for the phase-lock loop bandwidth. The modulation bandwidth was determined by using an HP8703A lightwave component analyser. The measured frequency response is shown in Fig. 4.3. The 3 dB modulation bandwidth of the master laser is larger than of the slave laser, 12 GHz and 10 GHz respectively at 60 mA bias and a temperature of 20°C.

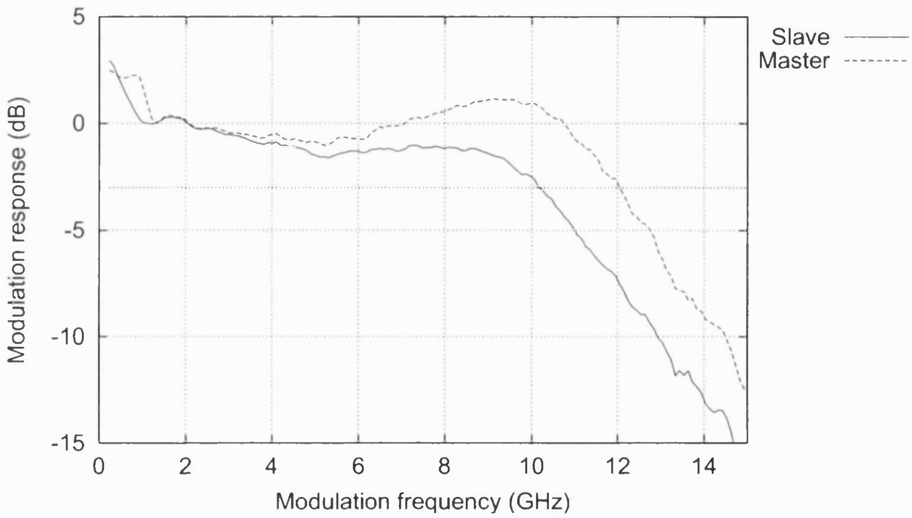

Figure 4.3: Intensity modulation response of master and slave laser.

Determining the FM response is not as straight forward as the intensity modulation response. Generally, the FM response is determined by some method of frequency to intensity conversion, usually using interferometric methods as Mach-Zender, Michelson or Fabry-Perot [8, 7, 6] interferometers. Common to all these methods is that they give a sinusoidal output amplitude response to the input optical frequency. The sinusoidal response can be derived by adding the incoming optical field with a time delayed version of itself:

$$E_{out} = |E_1|e^{2\pi jft+\phi} + |E_2|e^{2\pi jf(t+\tau_d)+\phi} \tag{4.1}$$

The power at the output is proportional to $|E_{out}|^2$, and can be written:

$$I_{out} = \Gamma_1 I_0 + \Gamma_2 I_0 + 2\iota I_0\sqrt{\Gamma_1\Gamma_2}cos(2\pi f\tau_d) \tag{4.2}$$

Γ_1 Optical loss path 1

Γ_2 Optical loss path 2

ι Coherence eficciency

From here, the extinction ratio is found:

$$\Gamma = \frac{2\iota\sqrt{\Gamma_1\Gamma_2}}{\Gamma_1 + \Gamma_2} \tag{4.3}$$

Assuming an FM response of df/di, the slope dependency of the injection current is:

$$\left.\frac{dI_{out}}{di}\right|_{FM} = \frac{df}{di} 4\iota\pi\tau_d I_0 \sqrt{\Gamma_1\Gamma_2} sin(2\pi f\tau_d) \tag{4.4}$$

If the frequency of the laser is changed by the injection current, a shift in the input amplitude results:

$$\left.\frac{dI_{out}}{di}\right|_{IM} = \frac{dI_0}{di}[\Gamma_1 + \Gamma_2 + 2\sqrt{\Gamma_1\Gamma_2} cos(2\pi f\tau_d)] \tag{4.5}$$

Ignoring cross products, the total slope will be:

$$\frac{dI_{out}}{di} = \left.\frac{dI_{out}}{di}\right|_{IM} + \left.\frac{dI_{out}}{di}\right|_{FM} \tag{4.6}$$

Even though the FM response has been converted into intensity , the FM response still needs to be separated from the IM response. This is achieved by tuning either the optical frequency, or τ_d to a point where the frequency sensitivity has equal and maximum opposite value, $sin(2\pi f\tau_d) = \pm 1$. By subtracting the results from these two points, the IM response is cancelled:

$$\left.\frac{dI_{out}}{di}\right|_{+} - \left.\frac{dI_{out}}{di}\right|_{-} = 2\frac{df}{di} 4\iota\pi\tau_d I_0 \sqrt{\Gamma_1\Gamma_2} \tag{4.7}$$

The FM response of the optical source can be easily be extracted from this relationship. The accuracy of the determination of the FM response is dependent on how accurately the optical frequency, or τ_d can be tuned to achieve $sin(2\pi f\tau_d) = \pm 1$. To investigate what impact a small tuning error has, One of the measurement points needs to differentiated:

$$\delta\left\{\left.\frac{dI_{out}}{di}\right|_{+}\right\} = \frac{df}{di} 4\iota\pi\delta\tau_d I_0 \sqrt{\Gamma_1\Gamma_2} + 4\pi\frac{dI_0}{di}\iota\sqrt{\Gamma_1\Gamma_2}(f\delta\tau_d + \delta f\tau_d) \tag{4.8}$$

The relative measurement error is then found by dividing equation 4.8 with half 4.7:

$$\Lambda = \frac{\delta\tau_d}{\tau_d} + \frac{(dI_0/di)(f\delta\tau_d + \delta f\tau_d)}{(df/di)\tau_d I_0} \tag{4.9}$$

Assuming that the change in path length is much smaller than the total path length, the equation can now be related to phase error:

$$\Lambda = \frac{(dI_0/di)\delta\varphi}{2\pi(df/di)\tau_d I_0} \tag{4.10}$$

This relation is very useful when determining the required differential path delay needed in the setup. From Fig. 4.2, a power slope of 0.025 mW/mA is found and a frequency slope of 0.85 GHz/mA at 65 mA bias of the slave laser. These values can be used as indicators for the required

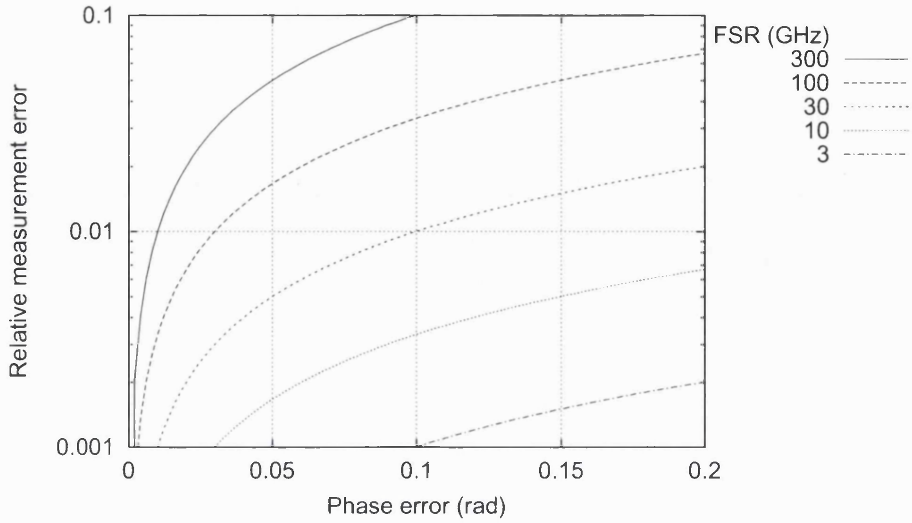

Figure 4.4: Relative measurement error as a function of phase tuning error in an FM measurement setup for different values of FSR.

path delay. The relative measurement error as a function of set phase error for different values of free space range (FSR) can now be plotted, corresponding to a time delay as: $FSR = 1/\tau_d$. The result is shown in Fig. 4.4. If a phase accuracy of 0.1 rad is possible and 1% relative error in the measurement is allowed, 30 GHz FSR would be required, corresponding to 1 cm differential path delay. This assumes that the FM response at the frequency measured is the same as at DC. If not, the FSR needs to be changed correspondingly. If a margin of a factor of ten is added to the FSR to cover for the frequency dependence of the slave laser FM response, an experimental setup with a differential path delay of 10 cm should be designed. Here, a free space, long cavity Fabry-Perot interferometer was used for this purpose. The Fabry-Perot reflectivity was optimised for operation at 1310 nm wavelength. At 1542 nm slave laser wavelength, the output of the Fabry-Perot mainly consisted of the zeroth and first order reflections, thereby producing a sinusoidal response to the optical frequency. The efficiency, Γ was about 0.25.

The measured FM response of the slave laser is shown in Fig. 4.5. The continous lines were obtained by using the output port of a network analyser to modulate the slave laser and connecting the input port to the output of the photo detector. The discrete points at frequencies lower than the network analyser bandwidth were obtained by directly observing the output signal on an oscilloscope. In Fig. 4.5 a dip in the magnitude of the FM response at about 8 kHz with a magnitude of 70 MHz/mA can be observed. With 10 cm FSR, this corresponds to 1.2% measurement error to a 0.1 rad error in the set phase. This dip is associated with a translation of the phase of the FM response from π at lower frequencies, to zero at higher frequencies. The physical reason for this is well known [9, 10, 11], at low frequencies, the FM response is determined by the red-shift from the heating of the laser chip with increasing injected current. At higher frequencies, the thermal

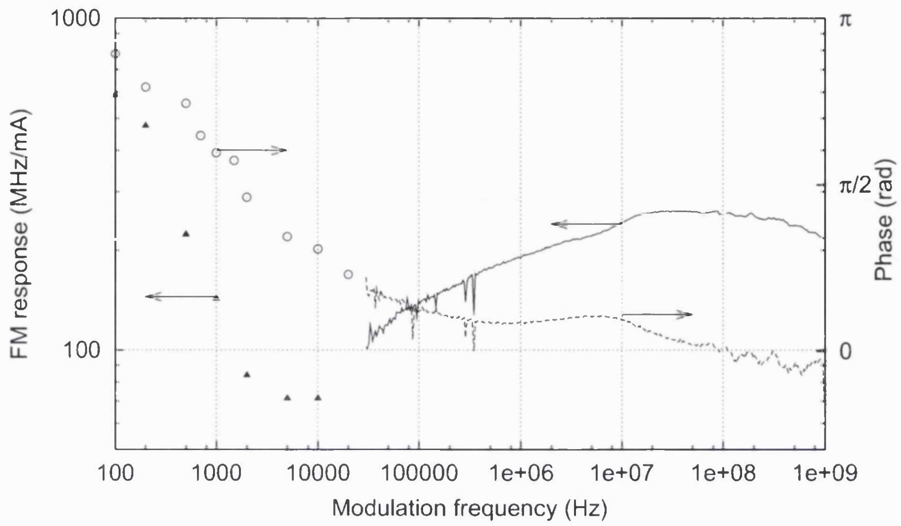

Figure 4.5: FM response for slave DFB laser. The continuos lines are obtained using a network analyser, while the discrete points represents discrete measurements.

effects decreases, and carrier effects with blueshift take over. In the transition between the two effects, a dip in the FM response is common for semiconductor lasers. The frequency of the dip is dependent on the relative magnitude of carrier and thermal effects and the roll-off rate of the thermal effects that is related to the heatsink configuration and packaging of the laser.

4.2.3 Phase-amplitude coupling factor

The phase-amplitude coupling factor, also referred to the α–factor plays an important role in determining the injection rate. Unfortunately, α cannot be measured directly. One indirect method of determining α, outlined in [12], is based on studying the injection locking properties of the DFB laser. In appendix B, the equations for the net gain and the frequency detuning of the injection locking is found B.13 and B.15:

$$\Delta G = -\frac{2}{\tau_o} Re\left\{\frac{E_{io}}{E_i}\right\} \tag{4.11}$$

$$-\frac{1}{\tau_p}\sqrt{\rho(1+\alpha^2)} < \omega_f - \omega_i < \frac{1}{\tau_p}\sqrt{\rho} \tag{4.12}$$

ΔG Differential gain

τ_o Photonic lifetime

ρ Injection ratio

ω_f Slave laser free running frequency

ω_i Slave laser locked frequency

Equation 4.11 tells us that zero relative change in output power from the injection locking occurs for $\phi = \pi/2$, corresponding to a detuning of ρ. 4.12 gives us the locking range: $\rho\sqrt{1+\alpha^2}$. α can now be determined from:

$$\alpha = \sqrt{\frac{\Delta\omega_m^2}{\Delta\omega_0^2} - 1} \tag{4.13}$$

In order to determine the half locking range, $\Delta\omega_m$ and the zero gain frequency shift, $\Delta\omega_0$, the shift in bias voltage over the slave laser locking range was measured as a function of the frequency shift from the free-running frequency, shown in Fig. 4.6. Zero volt shift in the voltage on the laser diode corresponds to zero gain injection. A total locking range of 7.1 GHz can be observed and a

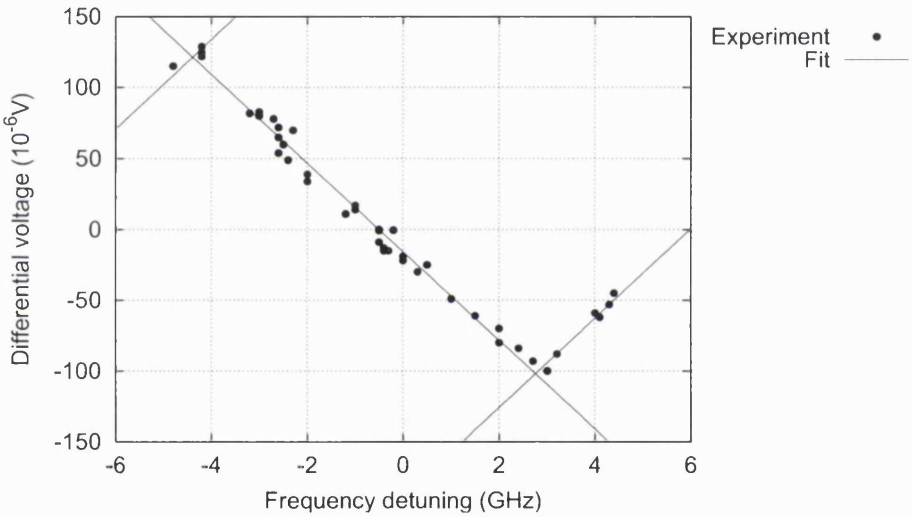

Figure 4.6: Bias voltage over the slave laser as a function of frequency detuning.

zero gain frequency detuning of 0.505 GHz. The standard deviation of these measurements was 8.1%. Based on these figures, the estimated value of α is 7.

4.2.4 Master laser modulated spectra

The field at the modulated output from the master laser takes the form [13]:

$$E_{ml}(t) = |E_{ml}|\left[1 + \frac{\iota}{2}\sin(2\pi f_\iota t + \phi_\alpha)\right]\exp\left\{j2\pi\nu_{ml}t - j\frac{\iota}{2}\alpha\sin 2\pi f_\iota t\right\} \tag{4.14}$$

E_{ml} : Master laser field (V/m)

ι : Modulation index

ν_{ml} : Master laser optical frequency (Hz)

f_ι : Modulation frequency (Hz)

α : Phase-amplitude coupling factor

ϕ_α : Phase offset between phase and intensity modulation

Using the Bessel function identity:

$$e^{-j\frac{\iota\alpha}{2}\sin x} = \sum_{m=-\infty}^{\infty} J_m(-\frac{\iota\alpha}{2})e^{jmx} \tag{4.15}$$

4.14 can be rewritten as:

$$\begin{aligned}\frac{E_{ml}}{|E_{ml}|} &= \sum_{m=-\infty}^{\infty} J_m(-\frac{\iota\alpha}{2})\exp\{j2\pi(\nu_{ml}+mf_\iota)t\} \\ &\quad -j\frac{\iota}{4}\sum_{m=-\infty}^{\infty} J_m(-\frac{\iota\alpha}{2})\exp\{j2\pi(\nu_{ml}+(m+1)f_\iota)t+j\phi_\alpha\} \\ &\quad +j\frac{\iota}{4}\sum_{m=-\infty}^{\infty} J_m(-\frac{\iota\alpha}{2})\exp\{j2\pi(\nu_{ml}+(m-1)f_\iota)t+j\phi_\alpha\}\end{aligned} \tag{4.16}$$

For high modulation frequencies, the phase between frequency and intensity modulation, ϕ_m is approximately zero. Fig. 4.7 shows the expected power of the modulation sidebands, together with experimental data obtained for a modulation power of -6.64 dBm. The data fits the expected values well at a modulation index of 0.28.

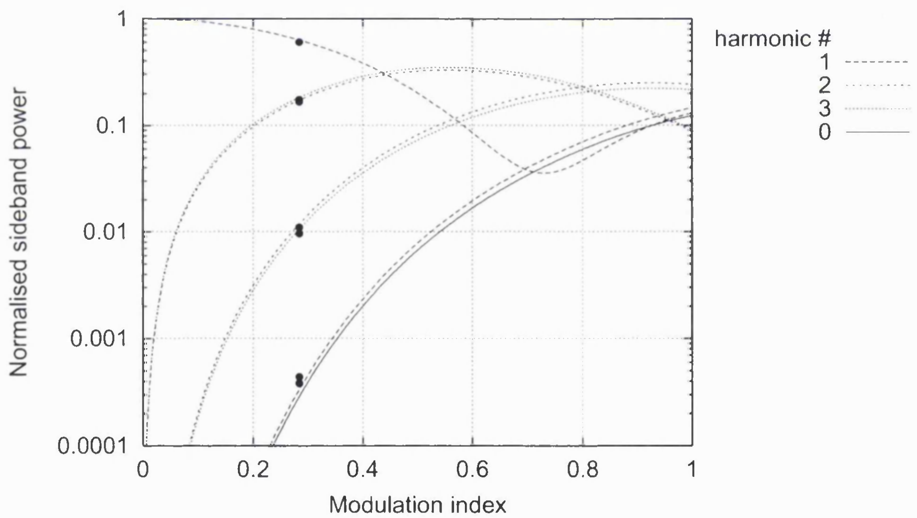

Figure 4.7: The expected relative power of the master laser modulation sidebands together with experimental data at -6.64 dBm modulation power.

4.2.5 Slave laser injection locking properties

As shown in the theoretical evaluation of the performance of the optical injection phase-lock loop, the injection locking characteristics of the slave laser plays a central role in determining the noise performance of the OIPLL. As derived in Appendix B, the locking bandwidth, K_{oil}, needs to be large in order to achieve high phase noise suppression. At the same time, the stability of the injection locking must be preserved, putting an upper limit to the allowed injection ratio. Fig. 4.8 shows the locking range of the slave laser as a function of injection ratio. The experimental data points are obtained by thermally tuning the master laser and observing the locking behaviour of the slave laser. The injection ratio was adjusted by a variable optical attenuator. The injection ratio plotted in the figure includes the fibre coupling loss. The lines were obtained with transmission line modelling, where the DFB laser is modelled as an active mirror, with gain and wavelength selectivity, as outlined in appendix B. The locking range was found by maximising the reflection, $|E/E_{in}|$, for a given free-running frequency offset of the slave laser. The unstable region was found by solving the eigenvalues in the characteristic matrix defined in equation B.21 in appendix B, and identifying the region where any of those has a real part greater than zero. The parameters used in this and the modelling to follow are found in Table 4.1. It is seen that for weak injection, stability is found within the whole locking range. This is also true for very strong injection, where the slave laser operates in a manner similar to a Semiconductor Optical Amplifier (SOA). For intermediate values of injection, stability is found only in a narrow band close to the boundary of the locking range. This is due to the phase-amplitude coupling factor, α. Setting α to zero in the modelling results in stable locking within the locking range for any injection ratio.

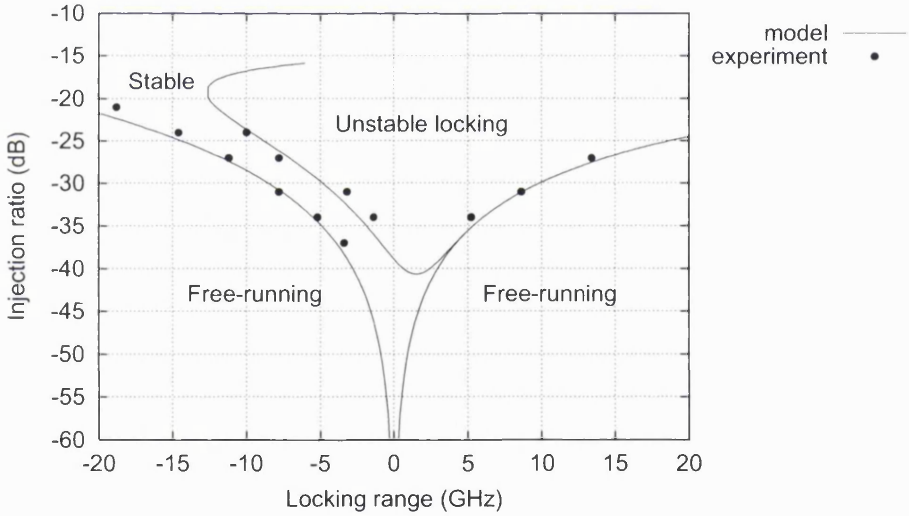

Figure 4.8: Slave laser stable and unstable injection locking range as a function of injection ratio.

Central to the function of the OIPLL is the reflection of the master laser field from the slave laser. As discussed in the theoretical section, the PLL part has to utilise the reflected master laser field in order to successfully phase-lock the slave laser. The rate of reflection will therefore determine the loop gain of the PLL. The reflection can be estimated by small signal analysis. Recalling the derived small signal solution, equation B.23, from appendix B:

$$e(\omega) = \frac{e_i(\omega) + Z(\omega)\left[e_i(\omega) + e_i^*(\omega)\right]}{j\omega + E_{io}} \tag{4.17}$$

If an additional injected line at a frequency offset f_i from the main injected line is assumed, the injected field can be written:

Table 4.1: Parameters used in laser modelling, estimated from results published in [5, 4, 14].

Output power:	4.3 mW
Fibre coupling loss:	5 dB
Wavelength:	1542 nm
Refractive index:	3.22
Group refractive index:	3.8
Cavity length:	370 μm
Active area:	0.18 μm^2
Differential gain:	$6 \cdot 10^{-20}$ m^2
Gain supression factor:	$2.5 \cdot 10^{-23}$ m^3
Internal absorption:	29/cm
Phase-amplitude coupling factor:	7

$$E_i = E_{io} + e_i e^{2\pi j f_i t} \tag{4.18}$$

The reflected amplitude at frequency offset f_i, the main peak, and $-f_i$, the image peak, can now be derived:

$$e_+ = \frac{e_i + e_i Z(f_i)/2}{2\pi j f_i + E_{io}} \tag{4.19}$$

$$e_- = \frac{e_i Z(-f_i)/2}{2\pi j f_i - E_{io}} \tag{4.20}$$

Reflected power relative to slave laser output power can now be plotted against the injection ratio. The result is shown in Fig. 4.9 for various offset frequencies. Assuming the slave laser is locked to the third harmonic FM sideband to the master laser modulated at 12 GHz, the reflected power of the various master laser lines can now be estimated as a function of master laser modulation index, using the relative power of the master laser FM sidebands plotted in Fig. 4.7. The reflected power increases linearly with the injected power for both main and image line. Also, when the offset frequency decreases, the power of both lines increases and the power of the mirror line approach the power of the main line.

The small signal approximation that has been used to obtain Fig. 4.9 requires the power of the additional injected line to be small relative to the main injected line or that the frequency offset to be much larger than the slave laser locking range. As a consequence, small signal modelling cannot be used to determine what frequency the master laser can be modulated at or what modulation index of the master laser should be used to obtain stable locking, when the slave laser is locked to a higher order master laser FM sideband. Large signal modelling has to be used. By

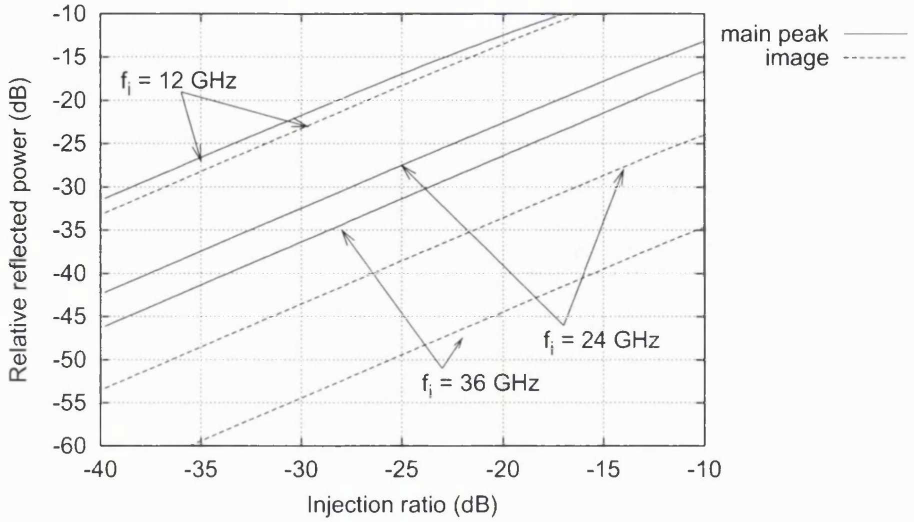

Figure 4.9: Relative reflected power as a function of injected power of additional injection line for 12 GHz, 24 GHz and 36 GHz frequency offset, and -30 dB injection ratio.

using the relations B.37 to B.41 in appendix B, the DFB laser can be modelled as an equivalent Fabry-Perot laser. The basic rate equations valid for a Fabry-Perot laser, B.1 and B.2, linked by the gain relation, B.4 in appendix B can then be solved numerically with the Runge-Kutta-Fehlberg method. Fig. 4.10 shows the optical spectra obtained from the large signal solution of the rate equations. The slave laser is being injection locked to the master laser third harmonic FM side-band, derived by equation 4.16. The modulation index is 0.28. At 12 GHz modulation, the slave laser is cleanly locked to the third harmonic with little distortion. When reducing the modulation frequency to 10 GHz, the locking is still stable, but an increase of noise can be observed. Further reducing the modulation frequency to 8 GHz, the locking shows clear signs of instability, as the additional master laser lines moves closer to the slave laser frequency and at 6 GHz modulation frequency, the locking shows entirely chaotic behaviour. Fig. 4.11 shows the optical spectra obtained from the large signal solution of the rate equations with varying modulation index of the master laser. When no modulation is applied to the master laser, the slave laser is free-running and has a Lorentzian lineform. The main and image line is still being reflected. If weak modulation is applied to the master laser, sidebands appear. No noise suppression can however be observed as the power of the third harmonic is too low to result in a locking range that has any impact within the resolution of the modelling. A modulation index of 0.3 results in relatively clean injection locking performance. Increasing the modulation index to 0.6 further improves the performance at the cost of attenuated master laser fundamental line that would result in a weak heterodyne beat between master laser fundamental and slave laser. The modelled results can be compared to the experimentally obtained spectra from master and slave laser, shown in Fig. 4.12, and show good agreement. The master laser modulation frequency is 12 GHz, and the modulation index is 0.28,

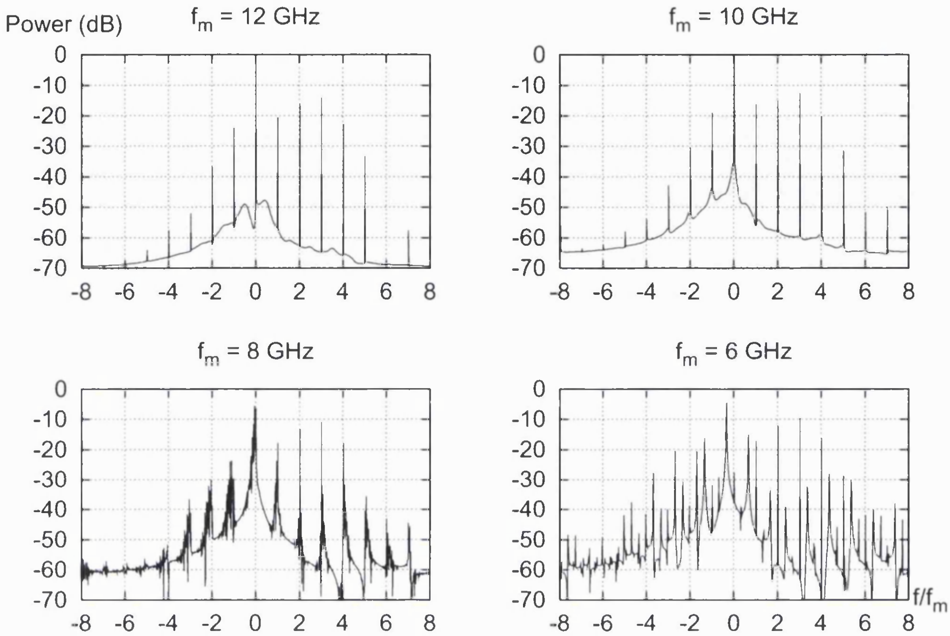

Figure 4.10: Large signal modelled slave laser spectra for 12 GHz, 10 GHz, 8 GHz and 6 GHz master laser modulation frequency and 0.28 modulation index.

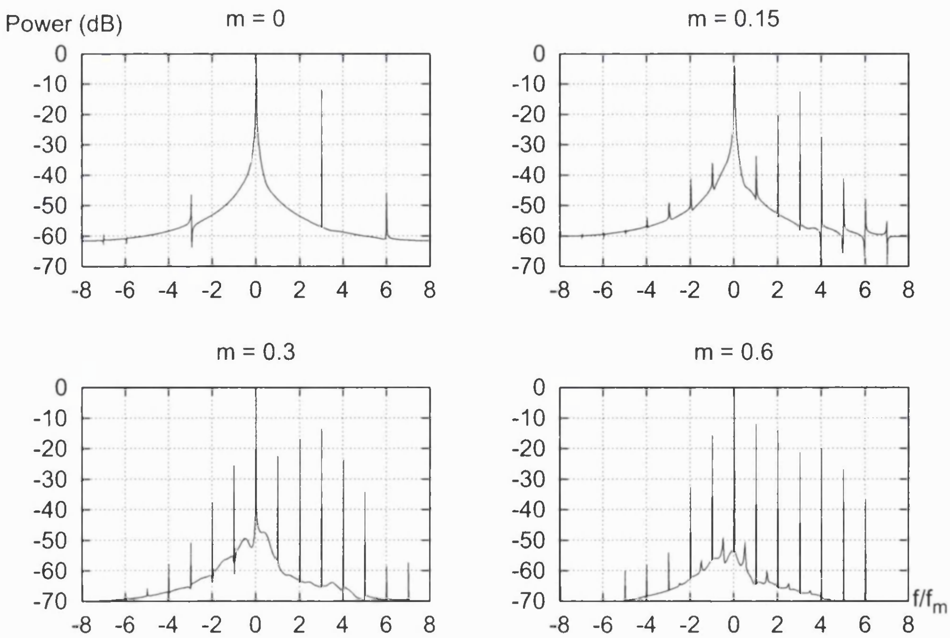

Figure 4.11: Large signal modelled slave laser spectra for an injected laser modulation index of 0, 0.15, 0.3 and 0.6 and 12 GHz master laser modulation frequency.

corresponding to the parameters used to obtain the first plot in Fig. 4.10.

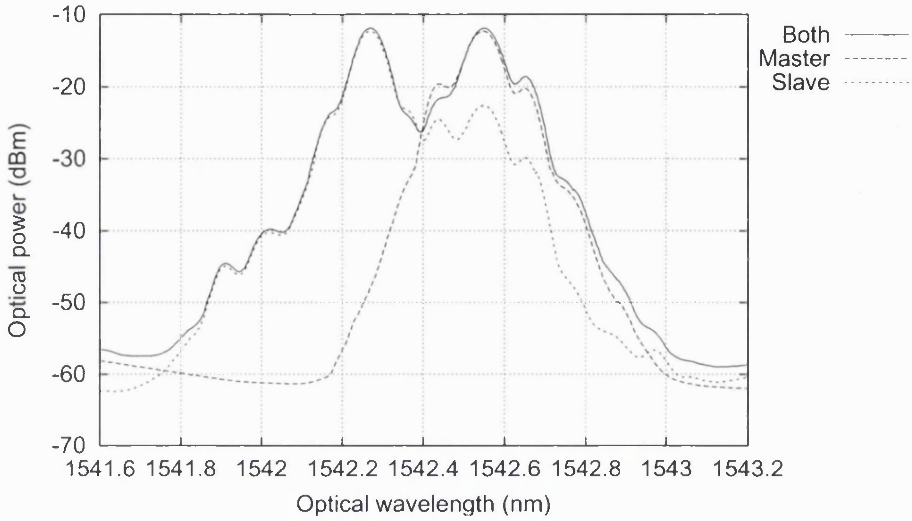

Figure 4.12: Detected spectra of modulated master laser, locked slave laser and the combined output from both lasers. (Resolution b/w: 0.07 nm)

4.3 Experimental Arrangement

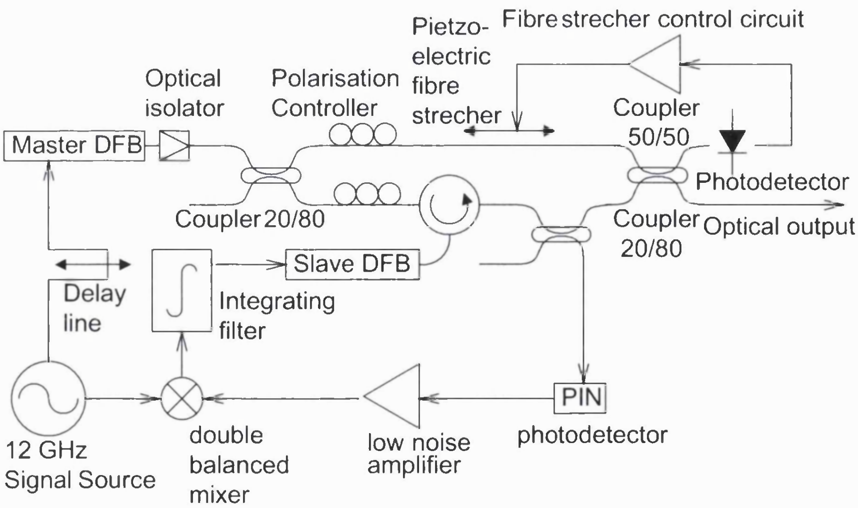

Figure 4.13: Schematic illustrating OIPLL experimental arrangement.

Fig. 4.13 shows a schematic illustrating the OIPLL experimental arrangement. The OIPLL is built in a fibre-based system using pig-tailed optical components, eliminating the requirement of optical alignment. The output power from a Rohde-Schwarz 10 MHz to 40 GHz signal synthesiser is equally divided in two. One part modulates the master laser, typically with between 5 dBm to 10 dBm modulation power at about 12 GHz frequency. The master laser is biased at 68 mA. Also, an adjustable delay line provides phase matching between the two locking processes, as discussed in the previous section. The output of the master laser is split in two paths, 80% later combines with the output of the slave laser in a 50/50 coupler, to provide the optical output of the OIPLL, and 20% is injected into the front facet of the slave laser. An optical circulator separates the injected master laser fields from the emitted field from the slave laser. Two optical polarisers are used. The first matches the polarisation of the master and slave laser fields, when combined at the output of the OIPLL. The second controls the polarisation of the master laser field injected into the slave laser. This provides a convenient way of regulating the injection locking ratio, defined as the ratio of the power of the injected field parallel with the slave laser field to the slave laser power. A second method of regulating the injection locking ratio is to change the master laser modulation power. The slave laser is tuned to lock to one of the third harmonic FM sideband of the injected field. 80% of the output of the slave laser power is combined with the master laser to form the optical output. A New Focus 1014 45 GHz PIN photodetector detects the remaining 20% of the slave laser power. A Miteq JS4-26004000-30-5A 26 GHz to 40 GHz low noise amplifier amplifies the 36 GHz beat that originates primarily between the slave laser field and the master laser fundamental line, reflected from the slave laser. The phase of the amplified 36 GHz signal is then detected in a Miteq DB0440LW1 double balanced mixer that is pumped in the third harmonic mode by the 12 GHz reference signal. An active filter finally provides the feedback signal into the slave laser.

The characteristics of the generated millimetre wave modulated optical signal were determined by detecting the heterodyne beat on a Discovery PIN photodetector, with 39 GHz bandwidth and about 0.4 A/W responsitivity at 1550 nm wavelength and 36 GHz modulation frequency. The photodetected signal is amplified in a Spacec Labs SLKa-35-4 26.5 GHZ–40 GHz low noise amplifier with 36.2 dB gain and 3.5 dB noise figure at 36 GHz. A modular HP70000-series spectrum analyser with an external preselected harmonic mixer then detected the modulated optical signal.

4.3.1 Path matching

Even though the differential phase between the injection locking and the phase locked loop is controlled by using the reflection of the master laser on the slave laser for feedback purposes, phase fluctuation effects will remain at the combined master-slave laser output. The reflected master laser field will interfere with the main part of the master laser field when the output from the two lasers are combined. If 6 dB relatively higher coupling loss is assumed and 12 dB reflection loss from the slave laser, the ratio of the two combined master laser fields is 1:8. This corresponds to 2.2 dB difference in master laser output power between constructive and destructive interference. As discussed in the first section of this chapter, very small differential changes in temperature can cause these power fluctuations. In a well designed OIPLL system, this is not acceptable and has to be controlled. The feedback method used in these experiments was stretching of the optical fibre with a piezo-electric translation stage. One of the optical outputs of the 50/50 fibre coupler was connected to the head of an optical power meter. The generated photocurrent was amplified by a simple high gain amplifier circuit, based around one Operational Amplifier (OPA) and one instrumental amplifier, generating an output in the range between 1.5 V to 28.5 V. Fig. 4.14 shows a circuit schematic of the piezo-electric translation stage driving circuit. The output signal controlled a piezo-driven translation stage, stretching the fibre and causing a differential phase shift between the two paths of the master laser field. The translation stage allowed 0V to 75V input with a total travel of 50 μm. The available feedback range was then 20 μm, corresponding to 12.9 wavelengths or 0.27°C shift in differential temperature between the two fibre paths. Under stable operating conditions, this compensation range was sufficient to control the intensity fluctuations.

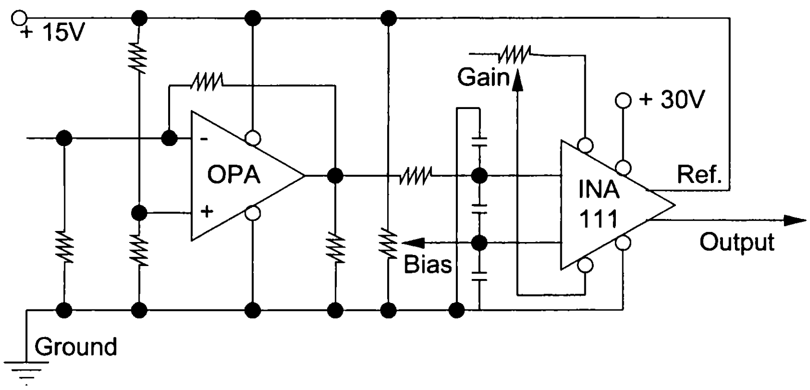

Figure 4.14: Circuit schematic of the Piezo-electric translation stage.

In addition to controlling the differential delay, the absolute magnitude of the differential delay needs to be minimised. The reason is that the differential delay will affect the coherence in the beat between the locked slave laser and the master laser in a similar manner to the differential delay caused by fibre chromatic dispersion, investigated in the previous section. In Fig. 3.13, the noise floor due to decorrelation exceeds the noise floor due to the finite locking range after about 27 km, corresponding to a dispersion induced delay of 0.13 ns. Therefore, the differential delay in the OIPLL should be lower than 0.13 ns, not to have any limiting effect of the overall performance. This corresponds to 26 mm fibre. The total length of the fibre exceeded 15 m so path matching by physically measuring the length of the fibre to a resolution lower than 26 mm is very awkward, considering the number of optical components and fibre splices in the optical path. An alternative method needs to be used. The method used here involves modulating the master laser with a network analyser. First, the main path of the master laser field, the path with the fibre stretcher in Fig. 4.13 is cut. The network analyser sweeps the modulation from low frequencies up to 6 GHz. The slave laser is then biased just below threshold, when it operates in a similar manner to a Semiconductor Optical Amplifier (SOA). Bias above the threshold will cause the slave laser to be injection locked, inducing a phase shift to the transmitted modulation signal and would therefore not be suitable for path matching purposes. The transmitted signal is then received and used to calibrate the network analyser. Next, contact is made between the two ends of the cut fibre, so some of the optical signal is transmitted through it, and the slave laser is biased to zero. Most of the master laser field transmitted through the OIPLL is now going through the broken fibre. By observing the received phase of the modulation phase over the whole span, up to 6 GHz, on the calibrated network analyser, the differential path delay can be calculated, and optical fibre can be added or removed. By following this procedure iteratively, a differential delay of a fraction of a millimetre can be achieved. The accuracy of the network analyser measurement is in practice better than 10° at 6 GHz, corresponding to 4.6 ps, or 0.92 mm fibre path. nb

4.3.2 Loop electronics

Two factors determined the design of the loop filter. The first factor is the linewidth of the heterodyne beat of the two free-running lasers, 240 MHz. A fibre based OIPLL will have a loop delay time exceeding 10 ns, and referring to Fig. 3.6 an OPLL with this time delay would require lasers with a heterodyne linewidth lower than 100 kHz in order to get a reasonable amount of phase noise suppression. With 240 MHz heterodyne laser linewidth, the OPLL would not be able to deliver any significant phase noise suppression, even if an ideal phase detector with a linear response was to be used in the loop, the phase error variance would then amount to 30 rad^2. Therefore, for the purposes of phase noise suppression, the designed OIPLL would have to be dependent on the injection locking. The role of the OPLL is then reduced to compensating for long term frequency drift falling outside the locking range of the injection locking and reducing close to carrier phase noise.

The second factor is the FM response of the slave laser, as plotted in Fig. 4.5. As can be seen in the figure, the FM response has a phase translation from π to 0 rad around a few kilohertz modulation frequency. If the OPLL feedback is done by current tuning of the slave laser, this leaves us with two options, either a very low pass filter is designed that uses only frequencies where the FM response of the slave laser has a redshift, or a filter that compensates for the FM response is designed. However, a filter that compensates for such a translation of phase cannot easily be designed with simple electronic components. Furthermore, even if such filter would be designed, there would be no significant contribution to the phase noise suppression of the OIPLL, as concluded above. On these grounds it was decided to use a low pass filter with only sufficient bandwidth to compensate for slow frequency drift.

The design of the filter is outlined in Fig. 4.15. It consists of two parts, the first part is a high gain Operational Amplifier (OPA) with a correction part for any bias offset originating from imperfections in the double balanced mixer. The gain of the OPA part is about 55 dB. A

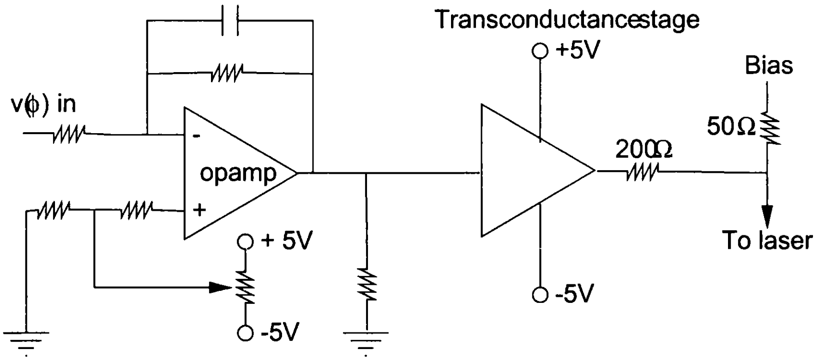

Figure 4.15: Design of active low-pass loop filter.

capacitor provides low pass filtering with a 3-dB cutoff frequency of 200 Hz. The second part is a transconductance amplifier, generating an output current proportional to the input voltage, about 0.14 A/V. The transconductance amplifier has ± 5V power supply and is therefore limited to about ± 4V at the output. By placing a 200Ω resistor at the output, the output current from the transconductance amplifier can be limited. Considering the bias voltage over the laser diode is –0.78 V at 60 mA bias and that the differential resistance of the slave laser is low above threshold, about 4Ω, the feedback current is limited to to –23 mA to +17 mA. This current clamp will prevent the slave laser from damage by excessive or negative bias. However, it will also limit the locking range of the OIPLL to a frequency tuning range of about 30 GHz for the slave laser.

4.4 Experimental Performance

4.4.1 Spectral Characteristics

Fig. 4.16 shows the detected 36 GHz heterodyne beat signal at 1 GHz span. The power scale is calibrated to show the millimetre wave power received from the photodetector. We can see that the beat between master and slave laser that used to have a Lorentzian line shape with as much as 240 MHz linewidth, as seen in Fig. 4.1, has now collapsed into a sharp delta-peak centred at three times the modulation frequency of the master laser, 36 GHz. The surrounding spectrum is clean, with a noise floor about 45 dB down from the peak power of -31.25 dBm. The resolution bandwidth was here 3 MHz. Fig. 4.17 shows the same beat signal with narrow span, 100 kHz with 1 kHz resolution bandwidth. The spectrum is still clean at this resolution with a noise floor about 65 dB down from the peak power.

In order to calculate the noise level correctly, some corrections for the spectrum analyser must be made. The relative noise power in 1 Hz bandwidth can be calculated by [15]:

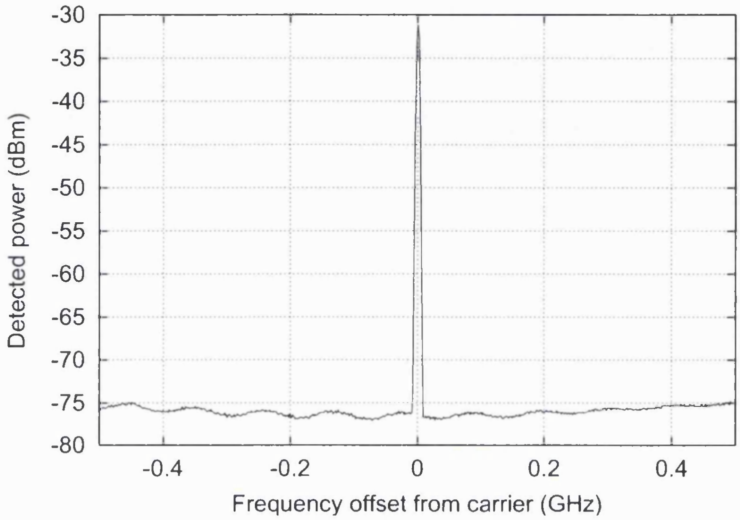

Figure 4.16: Detected OIPLL output spectra at 1 GHz span around 36 GHz. Resolution bandwidth: 3 MHz

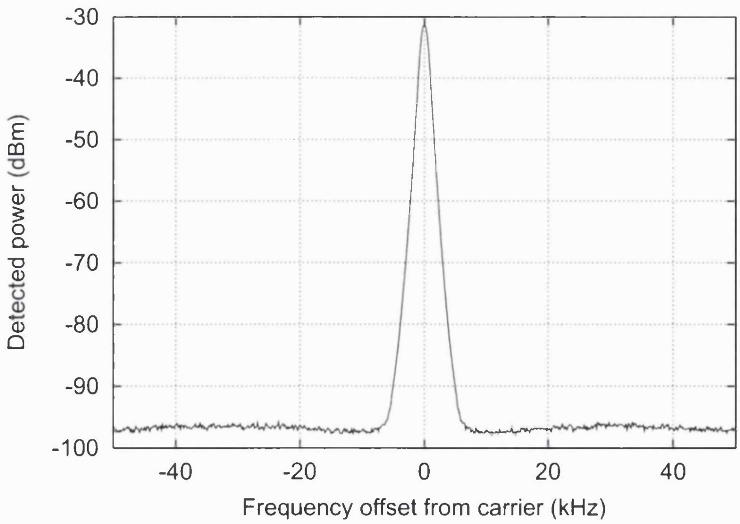

Figure 4.17: Detected OIPLL output spectra at 100 kHz span around 36 GHz. Resolution bandwidth: 1 kHz

$$S^{log}(df) = P_N(df) - P_S(f_0) - 10log(RBW/1Hz) - 2.5 + 0.5 \quad (4.21)$$

$P_N(df)$: Measured noise floor level at $df = f - f_0$ (dBm)

$P_S(f_0)$: Peak power (dBm)

RBW : Resolution bandwidth (Hz)

The -2.5 dB correction term is due to the filter shape of the spectrum analyser and the 0.5 dB correction term is due to the logarithmic amplifier. These values can vary from filter to filter and from spectrum analyser to spectrum analyser. However, they should give a good estimation for the effect of the filter and the amplifier in the spectrum analyser. The single sideband noise level can be measured at several frequency spans and incorporated into one graph with a logarithmic frequency scale. This is shown in Fig. 4.18 Also shown in the figure is the phase noise level

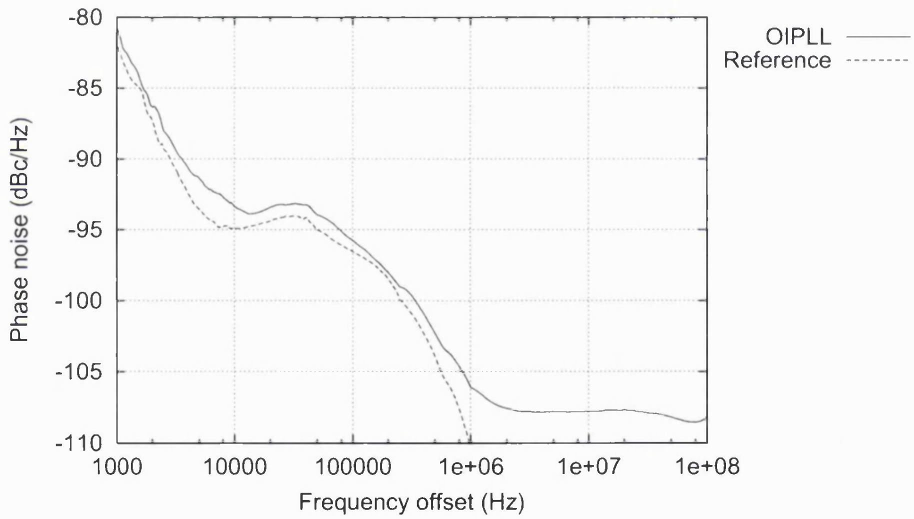

Figure 4.18: Detected single sideband noise level of optically generated 36 GHz signal and the reference on a logarithmic frequency scale.

of the multiplied reference signal. An additional correction term of $10 \cdot log(n^2)$, where n is the multiplication factor, here 3, has to be added to the reference noise level due to the frequency multiplication. The noise of the generated carrier is limited by the reference noise up to about 1 MHz offset frequency, where the noise curve flattens out to a noise floor at a level of about -107 dBc/Hz. The noise level at 10 kHz offset is about -93 dBc/Hz. The noise floor above 1 MHz frequency offset is explained by the limited locking range of the injection locking. Noise at a frequency that falls outside the locking range will not be suppressed by the injection locking. The injection locking range in given by equation B.15 in Appendix B:

$$-\frac{1}{\tau_p}\sqrt{\rho(1+\alpha^2)} < \omega_f - \omega_i < \frac{1}{\tau_p}\sqrt{\rho} \quad (4.22)$$

The injection gain is given by: $K_{oil} = \frac{\sqrt{\rho(1+\alpha^2)}}{\tau_p}\cos(\phi_i - \phi + \delta)$. According to the first order phase-lock loop model for the noise suppression of the injection locking, described by equations 3.10 and 3.11, an injection locking noise floor of -107 dBc/Hz would then correspond to an injection gain of 1.4 GHz, or a total locking range of 1.6 GHz. As discussed in the last chapter, this corresponds to a OIPLL loop bandwidth of about 1.4 GHz. In Fig. 4.19, the locking range for the injection locking is measured to be about 3 GHz. The divergence from the derived 1.4 GHz locking range can be attributed to the more complex case of multiline injection given by the modulated master laser field.

4.4.2 Locking Range

The locking range is a measurement of the stability of the generated signal. A wide locking range will allow the system to maintain the lock for longer with larger fluctuations in the environment, such as temperature changes of the laser packages. Any practical signal generation system must have large enough locking range to operate reliably for long periods of time outside a controlled laboratory environment. In the following, the locking range is defined as the total allowed range of detuning of the difference frequency between the master laser and the free-running slave laser while not loosing the phase correlation between master and locked slave laser. The tuning method chosen to investigate the locking range was shifting the free-running frequency of the slave laser by changing the injection current. Current tuning of the master laser was not practical because of the poor frequency tunability at higher bias currents, as seen in Fig. 4.2. Frequency tuning by changing the temperature of the lasers was not practical because of too low precision of the temperature controllers, that made the locking range measurement inexact, particularly when injection locking only was used. Fig. 4.19 shows the measured locking range for the OIPLL contrasted to the locking range using injection locking only. The phase error variance was obtained by integrating the normalised measured single sideband spectral density, such as shown in Fig. 4.18 from 100 Hz to 100 MHz and multiplying it by two. 100 MHz was choosen as a typical noise bandwidth for broadband wireless applications. It was assumed that the output power from the lasers was constant, so the noise measured in the spectra was due to phase noise.

In the figure, we can observe that using optical injection locking only, the locking range is only 3 GHz, with good phase noise suppression (lower than 0.01 rad^2 phase error variance) in a 1 GHz range. The temperature tuning of the lasers was about 9 GHz/K. From optimal locking conditions, a differential temperature shift of the lasers of only 100 mK will degrade the noise performance on the locking and above 300 mK temperature shift will cause the system to fall out of lock. In contrast, when the phase-lock loop circuit was added, the locking range increase tenfold to about 30 GHz, corresponding to about 3.3 K temperature shift, and the region with low phase noise

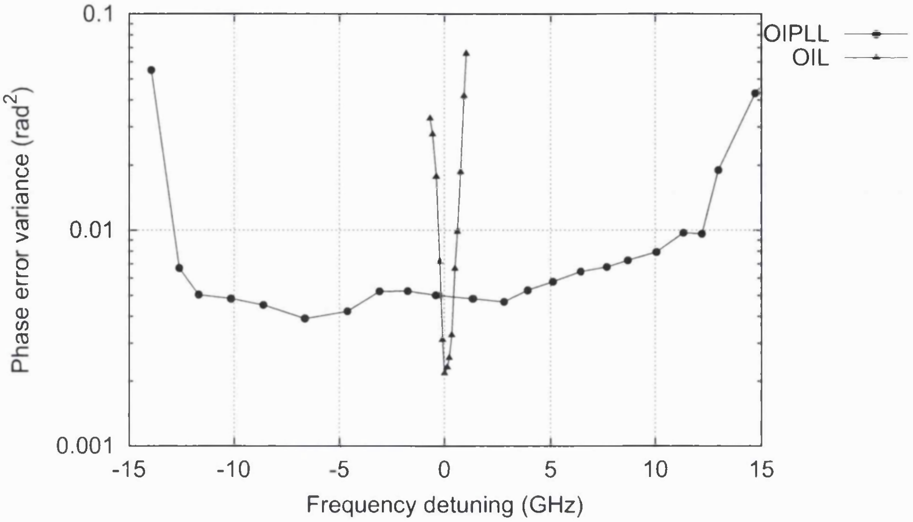

Figure 4.19: Measured locking range of OIPLL contrasted to the locking range of injection locking only. The x-axis shows the detuning of the free-running master-slave laser beat frequency and the y-axis shows the phase error variance, integrated over 100 MHz.

(less than 0.01 rad^2) is increased with a factor of 25 to 25 GHz, corresponding to 2.8 K allowed temperature shift. It should be pointed out that the locking range is here limited by the current clamps put on the filter. If some more efficient tuning method of the slave laser could be used such as temperature tuning, or a special laser with a designated tuning section, the locking range could be increased many times.

4.4.3 Frequency Range

When using the third harmonic FM sideband of the master laser to lock the slave laser, the maximum generated frequency is limited by the modulation bandwidth of the master laser, usable up to 13 GHz. The lower limit, around 24 GHz generated millimetre wave frequency, is determined by the stability of the injection locked system, as confirmed by the simulations shown in Fig. 4.10. If higher or lower order FM sidebands are used, the range of possible generated frequencies is much wider. Fig. 4.20 shows spectra of generated carrier frequencies from 4 GHz up to 60 GHz, spanning first to fifth order injected FM sideband. The span of each individual sweep was 1 GHz. All spans are placed in order to form a continous plot. At the frequency offset choosen for noise measurements, 10 MHz, the noise level is limited by the injection locking properties of the slave laser and not the reference, and can therefore be seen as a measurement of the quality of the generated signal. A general trend is that higher master laser modulation frequency generates a lower noise level beat because of less interference from lower order injected harmonic FM sidebands. For the same reason higher generated millimetre wave frequencies generally had better noise performance than lower frequencies. The upper limit to the generated frequency range was here determined by the equipment used to detect the signal. Due to the limitations of the devices used in the OIPLL, for generated frequencies outside the 26 GHz to 40 GHz range or not using the third harmonic for injection locking, only injection locking could be used. However, using a harmonic mixer in the PLL electronics and a very wideband amplifier, an OIPLL covering the entire frequency range can be constructed.

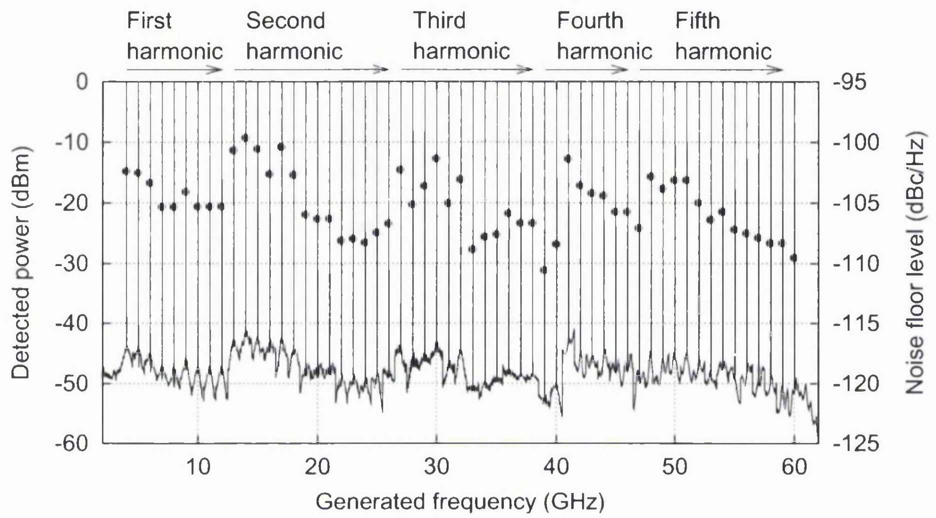

Figure 4.20: Spectra of OIPLL-generated carrier frequencies from 4 GHz up to 60 GHz with the slave laser FM sideband used for injection locking indicated. The left scale shows the relative power of the obtained spectra, normalised by the peak power. The right scale shows the noise level at 10 MHz offset frequency from the carrier, corresponding to the solid dots in the graph.

4.4.4 Fibre Transmission Response

In order to investigate the impact of the impact of fibre transmission, the spectral characteristics of the detected carrier have to be measured as a function of fibre transmission length. Fig. 4.21 shows the single sideband spectral characteristics for 0 km, 25 km, 40 km and 65 km fibre span. The noise floor at 0 km demonstrates the capabilities of the injection locking noise suppression. The increase in the level of the noise floor at 10 MHz offset matches reasonably well with the predictions in Fig. 3.13 (-108.0 dBc/Hz at 0 km fibre, -104.4 dBc/Hz at 25 km, -102.3 dBc/Hz at 40 km and -98.4 dBc/Hz at 65 km).

4.4.5 Receiver Filtering

As seen in Fig. 4.18, the spectral noise level of the OIPLL is determined by the reference up to about 1 MHz offset, where the performance is limited by the injection locking properties. This wideband noise, outside 1 MHz offset can be a limiting factor for high data rates or multilevel

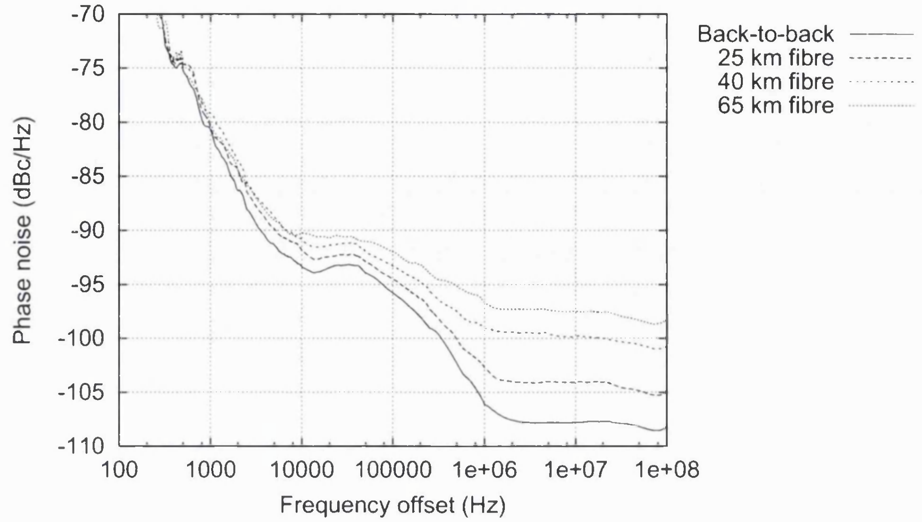

Figure 4.21: Fibre transmission effects on the noise characteristics of the generated carrier.

modulation formats. For instance, 256-QAM requires 31.5 dB SNR according to Equation 1.5 in chapter 1. In a 100 MHz noise bandwidth, this translates to a maximum noise level of -111.5 dBc/Hz. This noise performance is not provided by the OIPLL in the demonstrated configuration. One method of improving the spectral purity of the optically generated carrier is by carrier filtering in the optical receiver. However, designing a passive filter with 1 MHz half bandwidth at 36 GHz is difficult. An alternative is to use an active filter, such as a phase-lock loop or an injection locked oscillator. Systems using a phase-lock loop [16, 17] and combined phase-lock loop and injection locked oscillator [18] have been demonstrated. Here, an indirect Optically Injection Locked Oscillator (OILO) [19] is used. The circuit schematic of the OILO is shown in Fig. 4.22, a BT photodiode is employed as the photodetector [20] and the injection signal is applied to the end of the microstrip resonator, resulting in a free running oscillator frequency of 31.95 GHz. When the OILO was coupled to the 31.95 GHz modulated output of the OIPLL with 3.0 dBm output optical power, the locking range was 300 kHz. After 25 km fibre transmission, the locking range decreased to 120 kHz, due to a lower optical power, -3.8 dBm. The detected photocurrents in the BT photodiode were 0.26 mA and 0.035 mA respectively.

Fig. 4.23 provides an illustration of the improvements in noise performance using the OILO in the optical receiver compared with the photodetector plus low noise amplifier configuration used to obtain the previous results. Also shown in the figure is the detected free-running beat between master and slave laser. The wide linewidth of the lasers results in the wideband noise from the OIPLL, detected by the photodetector configuration. The wideband noise falls outside the locking range of the OILO, and does not therefore appear at the output of the OILO, where the noise floor is due to the harmonic mixer.

Fig. 4.24 shows a more detailed picture of the spectral characteristics using the OILO and

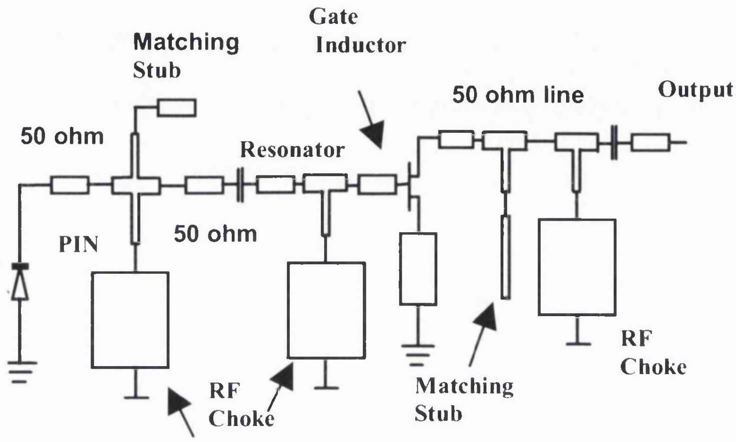

Figure 4.22: Circuit schematic of the OILO.

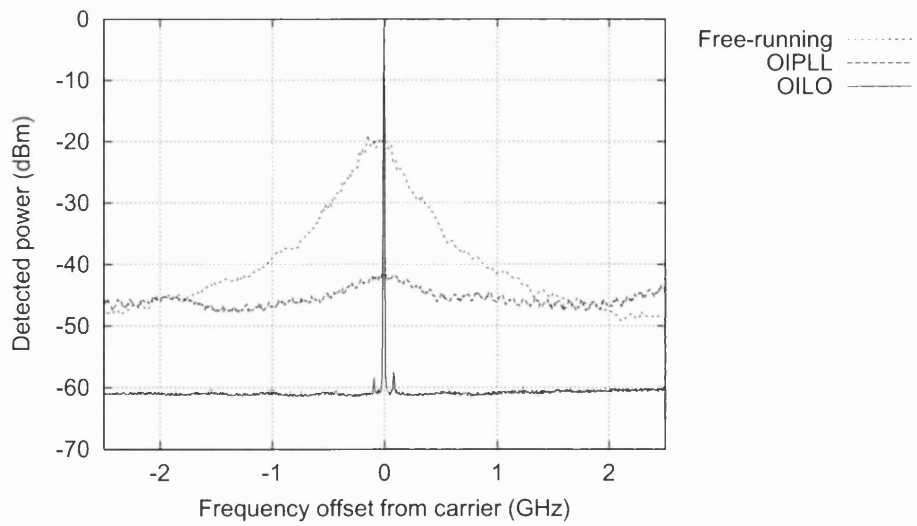

Figure 4.23: Detected 31.95 GHz signal using the OILO and photodetector configuration. Also shown is the free-running master and slave laser beat using the photodetector configuration.

the photodetector configuration. The unlocked characteristics of the OILO is also included for reference. For offset frequencies lower than the locking range of the OILO, the phase follows the phase of the reference, while at higher frequencies the spectral characteristics follows those of the free-running OILO. This results in a lower noise level from the OILO than from using the photodetector configuration for offset frequencies higher than 2 MHz offset. At high offset frequencies, the detected millimetre wave signal is limited by the noise floor of the harmonic mixer used. The spectral performance can be further improved by increasing the locking range of the OILO. In [19], a locking range of 2.6 GHz was reported. This locking range would be close to optimal, providing phase correlation for the region where the phase is determined by the phase of the reference and rejection of the wideband noise.

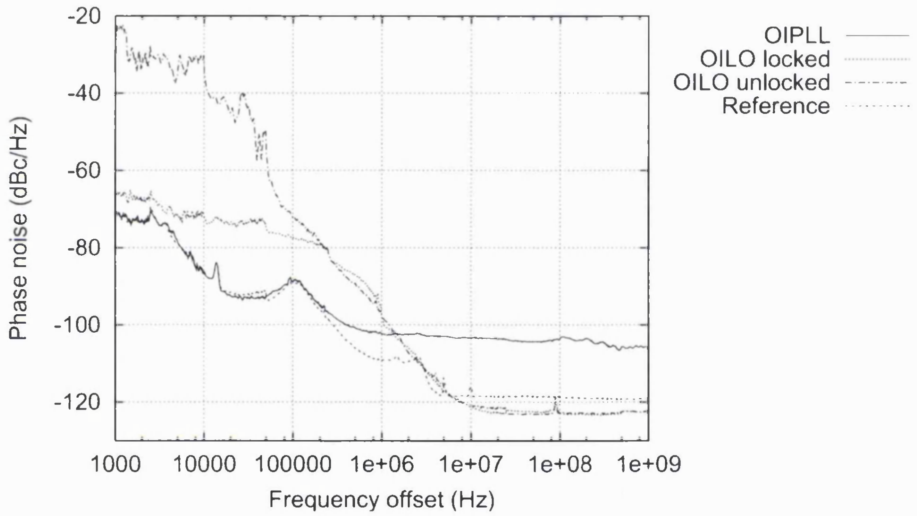

Figure 4.24: Noise spectrum for reference, free-running OILO, locked OILO and signal detected by photodetector configuration.

In addition to the improvement in noise performance that is obtained by using the OILO, a second advantage in generated millimetre wave power is obtained, this is illustrated in Fig. 4.25. At the output of the OIPLL, the generated power from the OILO and the photodetector plus amplifier is almost equal, about -2 dBm. After 25 km fibre transmission, the output power from the photodetector plus amplifier has decreased by 7 dB, due to fibre optical attenuation. In contrast, the output power from the OILO stays constant. This has the system advantage that any component incorporating the OILO can easily be designed to allow varying input optical power, while still producing a constant output power. The impact of the attenuated optical power from the fibre transmission can however be found in an increased close to carrier noise level due to the reduced injection power, also illustrated by Fig. 4.25

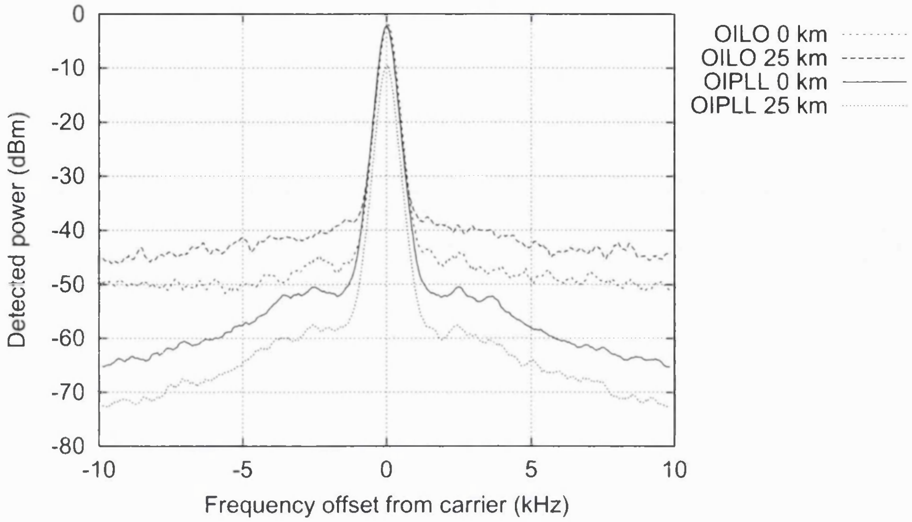

Figure 4.25: 31.95 GHz signal detected by OILO and photodetector after 0 km and 25 km fibre transmission. Resolution bandwidth: 300 Hz.

4.5 Conclusions

In this chapter, the first experimental demonstration of a millimetre wave OIPLL is described. It is experimentally shown how the stability problems relating to differential path effects can overcome by using the reflection of the master laser field from the slave laser. Modelling predicting the magnitude of the reflection and the stability of the injection locking was found to be in good agreement with experimentally established data. Experimental results of the spectral characteristics of the generated carrier and of the locking range were presented. The degradation of the generated carrier due to fibre transmission matched what would be expected. It is shown that the locking range was limited by the loop electronics design, and that the locking range could be greatly improved using alternative frequency tuning mechanisms of the slave laser. The potentially wide frequency range of the OIPLL was proved by demonstrating the generation of spectrally pure carriers in the range of 4 GHz to 60 GHz, limited by the frequency range of the test equipment. Due to limitations of the frequency range of the components, the PLL part could only operate between 26 GHz and 40 GHz. Outside this frequency range, only OIL was used. However, using suitabe components, the OIPLL could be designed to operate across the entire frequency range. Finally, it is shown how the spectral purity of the generated millimetre wave carrier could be improved further by carrier filtering in the optical receiver, improving the noise performance at offset frequencies beyond 2 MHz from the carrier.

There are two undesirable features of the demonstrated OIPLL. The first is the intensity fluctuations of the generated carrier. These fluctuations come from interference between the master laser field and the reflections of the master laser field from the slave laser, related to minute changes

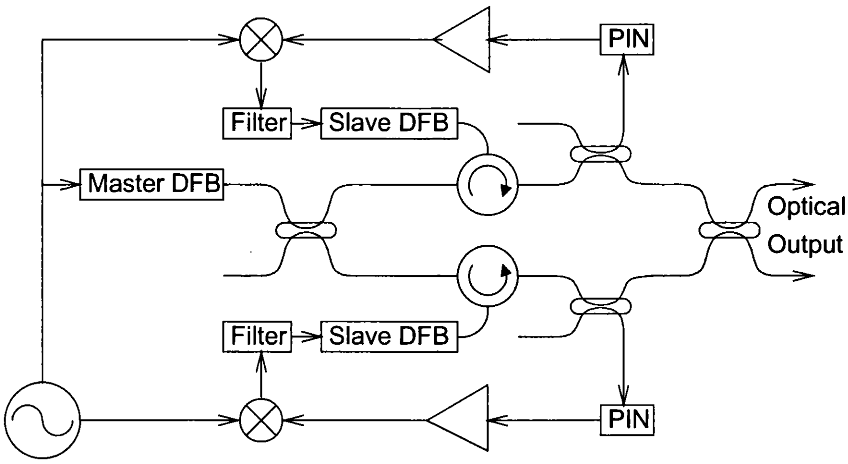

Figure 4.26: Schematic of improved OIPLL design.

in the length and refractive index of the optical fibre. Here, this was solved by detection of the optical intensity and using it as a feedback signal for a piezo-electric fibre stretcher. Although this control mechanism was successful, it would be desirable not to have to use it at all. The second undesirable feature is that the output of the OIPLL is not perfectly single sideband modulated. There are several unwanted FM sidebands from the master laser present in the optical output of the OIPLL, illustrated by the modulated master laser optical spectra, Fig. 4.12. These lines interferes constructively or destructively as a periodical function of transmission length due to the chromatic dispersion of the fibre. These two undesirable features can however be helped. If an OIPLL arrangement incorporating a second slave laser, locked to the image FM sideband of the master laser, as illustrated by Fig. 4.26, was constructed, the output signal of the OIPLL would mainly consist of the output from the two slave lasers. If the reflection of the master laser was reasonably low, the intensity fluctuations would now be reduced to a level not requiring any feedback control. Furthermore, the output would now be almost perfect single sideband modulated, having very high resistance to the effects of chromatic dispersion. The master laser can now be modulated at a higher depth, increasing the power of the selected FM sideband relative to lower sidebands. This would increase the stability of the injection locking and therefore provide better overall performance. Finally, the generated frequency of the carrier would automatically double, using the same components, or allowing the use of lower speed components in the OPLL part for a fixed generated frequency. Even lower speed components can be used if heterodyne detection between the slave laser line and reflected master laser line other than the fundamental is used in the OPLL.

References

[1] C. Walton, A.C. Bordonalli and A.J. Seeds, "High-performance heterodyne optical injection phase-lock loop using wide linewidth semiconductor lasers", *IEEE Photonics Technology Letters*, vol. 10, pp. 427–429, 1998.

[2] R.T. Ramos, P. Gallion, D. Erasme, A.J. Seeds and A.C. Bordonalli, "Optical injection locking and phase-lock loop combined systems", *Optics Lett.*, vol. 19, pp. 4–6, 1994.

[3] A.C. Bordonalli, "Optical injection phase-lock loops", PhD thesis submitted to University of London, Department of Electronic and Electrical Engineering, University College London, 1996.

[4] I.F. Lealman, M.J. Harlow, and S.D. Perrin, "Effects of Zn doping on modulation bandwidth of 1.55 μm InGaAs/InGaAsP multiquantum well DFB lasers", *Electron. Lett.*, vol. 29, pp. 1197–1198, 1993.

[5] I.F. Lealman, D.M. Cooper, S.D. Perrin, and M.J. Harlow,"Effect of Zn doping on differential gain and damping of 1.55 μm InGaAs/InGaAsP MWQ lasers", *Electron. Lett.*, vol. 28, pp. 1032–1034, 1992.

[6] G. Jacobsen, H. Olesen, F. Birkedahl and B. Tromborg, "Current/frequency-modulation characteristics for directly optical frequency-modulated injection lasers at 830nm and 1.3μm", *Electron. Lett.*, vol. 18, pp. 874–876, 1982.

[7] D. Welford and S.B. Alexander, "Magnitude and phase characteristics of frequency modulation in direct modulated GaAlAs semiconductor diode lasers", *IEEE J. Lightwave Tech.*, vol. LT-3, pp. 1092–1099, 1985.

[8] H. Olesen and G. Jacobsen, "Phase delay between intensity and frequency modulation of a semiconductor laser", *Proceedings of the 8th European Conference in Optical Communications*, paper B IV-4, pp. 291–295, 1982.

[9] W.B. Joyce nad R.W. Dixon, "Thermal resistance of heterostructure lasers", *J. Appl. Physics*, vol. 46, pp. 855–862, 1975.

[10] G.S. Pandian and S. Dilwali, "On the thermal FM response of a semiconductor laser diode", *IEEE Photonics Technology Letters*, vol. 14, pp. 130–133, 1992.

[11] J.E.A. Whiteaway, B. Garret, G.H.B. Thompson, C.J. Armistead and M.J. Fice, "The static and dynamic characteristics of single and multiple phase-shifted DFB structures", *IEEE J. Quantum Electron.*, vol. 28, pp. 1277–1293, 1992.

[12] R. Hui, A.D. Ottavi, A. Mecozzi and P. Spanno, "Novel measurement technique of α factor in DFB semiconductor lasers by injection locking", *Electron. Lett.*, vol. 26, pp. 997–998, 1990.

[13] A. Yariv, "Optical Electronics in Modern Communications," Fifth ed. *Oxford University Press, Inc.* New York, New York, 1997.

[14] M.C. Tatham, I.F. Lealman, C.P. Seltzer, L.D. Westbrook and D.M. Cooper, "Resonance frequency, damping, and differential gain in 1.5 μm multiple quantum-well lasers", *IEEE J. Quantum Electron.*, vol. 28, pp. 408–414, 1992.

[15] Spectrum analyzer measurements and noise", *Hewlett Packhard Application note 1303*, 1998.

[16] A. Hilto, A. Zolomy, T. Berceli, G. Jaro and E. Udvary, "Millimeter Wave Synthesizer Locked To An Optically Transmitted Reference Using Harmonic Mixing", *Int. Top. Meeting on Microwave Photonics '97 Digest*, pp. 91–94, 1997.

[17] R.A. Griffin, H.M. Salgado, P.M. Lane and J.J. O'Reilly, "System capacity for millimeter-wave radio-over-fiber distribution employing an optically supported PLL", *IEEE J. Lightwave Technology*, vol. 17, pp. 2480–2487, 1999.

[18] T. Berceli, S. Kudszus, M. Schlechtweg, A. Zolomy, G. Jaro, T. Marozsak and E. Udvary: "Optical millimeter wave generation utilizing a subharmonic reference," *IEEE MTT-S, International Microwave Symposium Digest.*, Vol. 3, pp. 1749–1752, 2000.

[19] X. Wang. N.J. Gomes, L. Gomez-Rojas, P.A. Davies and D. Wake, "Indirect optically injection-locked oscillator for millimeter-wave communication system", *IEEE Trans. Microwave Theory Tech.*, vol. 48, pp. 2596–2603, 2000.

[20] D. Wake, T.P. Spooner, S.D. Perrin and L.D. Henning, "50GHz InGaAs Edge-Coupled Pin Photodector", *Electron. Lett.*, vol. 27, pp 1073–1075, 1991.

Chapter 5

Amplitude Shift Keying Transmission Experiments

In this chapter, an OIPLL transmission experiment using the Amplitude Shift Keying (ASK) modulation format is described. Introduction, 5.1, outlines some previous work done with ASK modulated fibre optic transmission links and states the objectives of the demonstration described in this chapter. The next section, 'Experimental Arrangement' 5.2, describes the equipment, devices and layout of the experimental arrangement used, specifically how to apply data modulation to the millimetre-wave modulated output of the OIPLL and the receiver configuration, including the demodulation circuit. Section 5.3, 'Predicted Link Performance' predicts what noise sources should be limiting the performance of the link and the magnitude of those. An expression for bit errror rate versus received signal to noise ratio, for the receiver configuration used is derived. 'Experimental Results', 5.4 presents the experimental data obtained and relate these to what would be expected from the theory treated both by this chapter and previous chapters. Finally, the Conclusion summarises the most important findings of this chapter.

5.1 Introduction

Binary Amplitude Shift Keying (ASK), also called On-Off keying (OOK), is the most basic modulation format. It encompasses switching a sinusoidal carrier on and off by a binary signal. It is the first modulation format to be used, predating analogue signal modulation in the form of Morse coded radio. Presently ASK is the modulation format of choice in digital optical links due to simplicity of implementation of modulation and demodulation. ASK modulation has also been considered for coherent fibre optic links [1, 2]. In coherent fibre optic links, the ASK modulation format has the advantage that non-coherent receivers can be used, that are insensitive to laser phase noise [4, 5]. For analogue applications, transmission of an ASK modulated subcarrier [6] is less common due to poor bandwidth efficiency and the comparatively high required bit signal to noise ratio required for error-free transmission, especially using non synchronous demodulation. The situation where ASK modulation can with advantage be used, is when a simple and efficient way is needed to apply data modulation to the optical output of a dual frequency optical source by an external optical modulator [7, 8].

In this experiment, the OIPLL is used for a basic millimetre-wave over fibre transmission demonstration. This chapter describes 36 GHz, 140 Mbit/s Non-Return to Zero (NRZ) amplitude shift keyed (ASK) transmission experiments using an external optical modulator. The aim of this demonstration is to verify the suitability of the OIPLL as a millimetre-wave modulated optical source in such a system, foremost with regard to efficiency in the generation of the millimetre-wave modulated signals, and the fibre dispersion tolerance of the generated signals. Since the ASK modulation format is not severely affected by the phase noise of the generated carrier, this demostration does not provide any verification of the spectral purity of the generated carrier. The ASK modulation format is choosen for its relative ease of implementation and short setup time of modulation and demodulation techinques for the OIPLL, whilst still being able to demonstrate the above mentioned points.

5.2 Experimental Arrangement

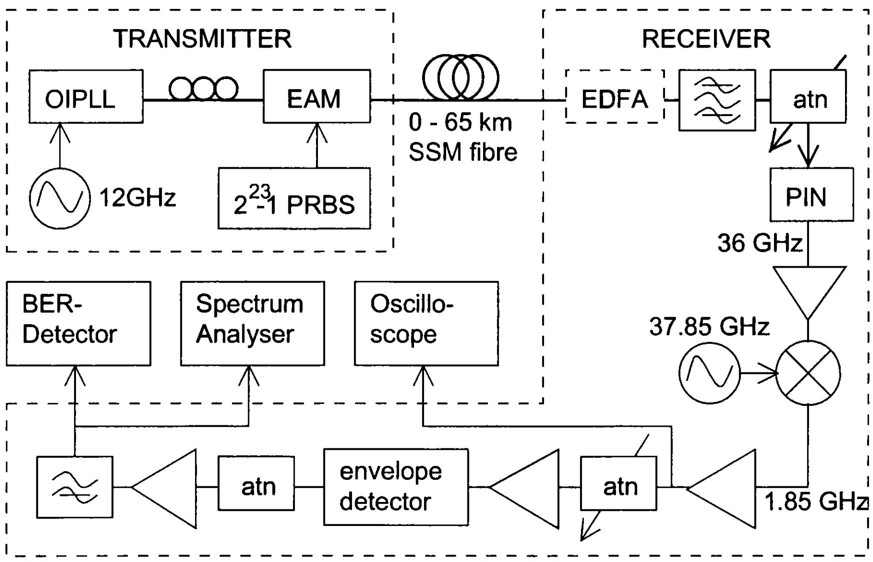

Figure 5.1: Schematic of 140 Mbit/s ASK radio over fibre transmission experiment. Thick line indicates optical path.

Figure 5.1 shows the experimental layout. An external optical modulator is connected to the millimetre-wave modulated optical output of the OIPLL. The output from a $2^{23} - 1$ word pattern 140 Mbit/s Pseudo-Random Bit Sequencer (PRBS) is used to switch the modulator on and

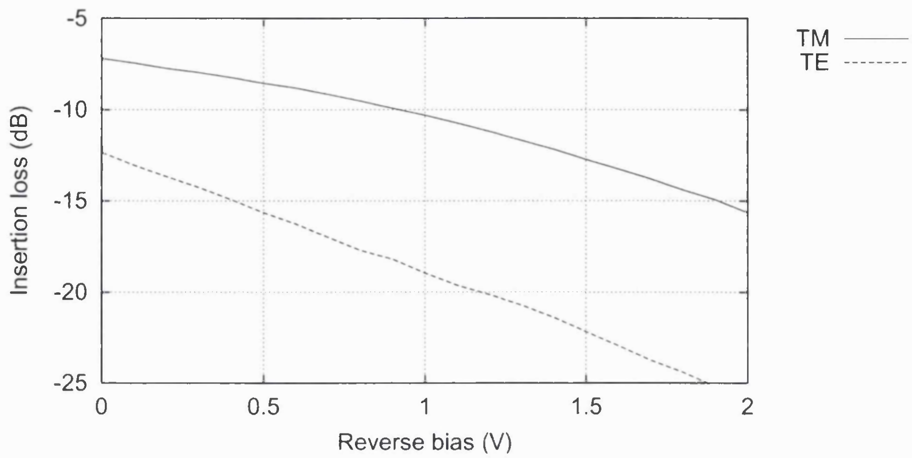

Figure 5.2: Static EAM insertion loss

off. The modulated optical signal is then transmitted through 0 km, 25 km, 40 km or 65 km of Standard Single-Mode optical fibre. For fibre lengths exceeding 25 km, an Erbium Doped Fibre Amplifier (EDFA) is needed to achieve error-free detection. A 1 nm bandwidth ASE filter reduces the Amplifier Spontaneous Emission (ASE) noise power and an optical attenuator regulates the received optical power. In the receiver, the modulated millimetre-wave signal is generated by the heterodyne beat of the two main lines from the OIPLL on the photodetector. The detected signal is downconverted to 1.85 GHz where a spectrum analyser detects the modulated spectra. An envelope detector recovers the bit stream. The Bit Error Rate (BER) is then detected in a bit error rate detector, and the eye diagram is observed on an oscilloscope.

5.2.1 Transmitter

ASK modulation was generated by using an optical Electro-Absorption Modulator (EAM) to switch the millimetre-wave modulated output from the OIPLL on and off. The modulators used here were developed for 10 Gbit/s data communications applications, so the 3-dB bandwidth of the modulator, about 10 GHz, is more than sufficient for the 140 MHz switching speed used here. Further details about the structure and performance of the modulator can be found in [9]. The EAM modulates the intensity of the optical signal by using the Quantum Confined Stark Effect (QCSE). By applying an electric field to the modulator quantum wells, the centre frequency of an exitonic absorption peak of the quantum well material is red-shifted with the increasing applied field. By using this phenomenon, a field-dependent change in the optical absorption is obtained at the operating wavelength. This is then used to modulate the transmitted optical field [10]. Fig. 5.2 shows the static insertion loss of the modulator as a function of applied voltage at an optical wavelength of 1540 nm. Clearly, the highest extinction ratio is found for input field with Transverse Electric (TE) polarisation, therefore TE polarisation of the input field should be used if the modulation depth is to be maximised. However if signal power is to be maximised, Transverse Magnetic (TM) polarisation is most suitable because of the much lower insertion loss. Fig. 5.3

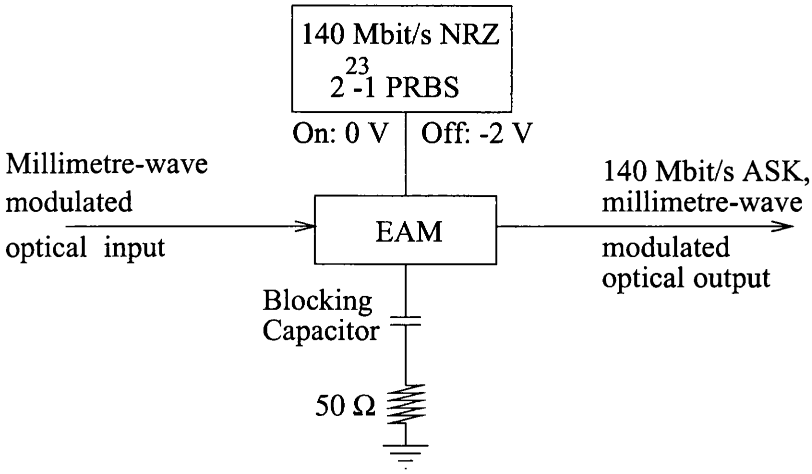

Figure 5.3: Setup for the generation of 140 Mbit/s ASK millimetre-wave modulated optical signal

shows the arrangement used to switch the modulator on and off. The output of the 140 Mbit/s baseband data signal of the PRBS was connected directly to the modulator. The 'on' state was generated by applying 0 V to the modulator and the 'off' state by applying -2 V. TM polarisation of the input optical signal was used because of the much lower insertion loss at the 'on' state, -7.3 dB instead of -12.5 dB for TE polarisation, resulting in a total higher output signal power. The arrangement was optimised for maximum transmitted optical signal power, therefore the smaller modulation depth at TM, 87% instead of 96% for TE, could be tolerated, as it had a much smaller impact on signal power than from the difference of overall absorption. With 1.8 dBm optical output power from the OIPLL, the average launched optical power after the modulator is -8.0 dBm. At the output of the modulator, a blocking capacitor prevented DC current from flowing through the modulator and a 50 Ω load was connected after the capacitor for impedance matching.

5.2.2 Receiver

Fig. 5.4 shows the layout of the design of the receiver. An EDFA was needed in order to boost signal power to achieve error-free detection for transmission distances over 25 km. After the amplifier, a 1 nm bandwidth optical filter was used to reduce the amplifier spontaneous emission noise. An optical attenuator was then used to regulate the received optical power. A 39 GHz bandwidth PIN photodiode was used to detect the 36 GHz 140 Mbit/s ASK modulated millimetre-wave signal. The detected signal was then amplified in a preamplifier with 3.5 dB noise figure and downconverted to 1.85 GHz in a double balanced mixer, using a 37.85 GHz Local Oscillator (LO) signal. Three microwave amplifiers and two attenuators, one stepwise variable, were then used to boost the signal power to pump the envelope detector without degrading the Signal to Noise

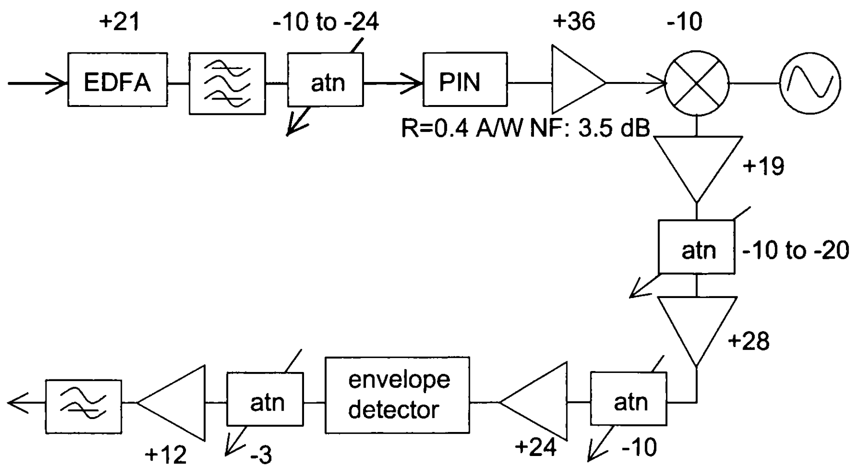

Figure 5.4: Layout of the receiver with component gain in dB included. Thick line indicates optical path.

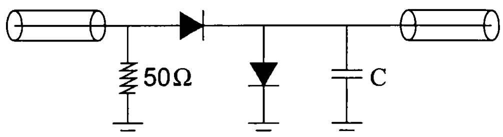

Figure 5.5: Layout of the design of the envelope detector

Ratio (SNR) by adding noise or saturating the amplifiers. The design of the envelope detector is shown in Fig 5.5. It is a simple linear envelope detector, based on two Schottky diodes with a threshold around 0.32 V. At the output of the detector, a capacitor of 10 pF is connected, to filter away the carrier frequency, when connected to a 50 Ω termination. The static response of the envelope detector is shown in Fig. 5.6. Between 0.5 V and 1.5 V input Root Mean Square (RMS) voltage, the slope of the detector response is about 0.3 V/V. The frequency response of the envelope detector is shown in Fig. 5.7. The bandwidth of the envelope detector is approximately 3 GHz. After the envelope detector, a 3 dB attenuator provides a 50Ω termination for the envelope detector and impedance matching for the baseband amplifier. The baseband amplifier has a 260 MHz bandwidth, providing low pass filtering before the BER is detected with large enough bandwidth to avoid intersymbol interference.

5.3 Predicted Link Performance

5.3.1 Receiver Noise Sources

The predicted performance of the receiver can be estimated. The first step is the estimation of the input noise sources. In a properly designed receiver, such as shown in Fig. 5.4, noise originates from the following sources; optical receiver thermal noise including preamplifier noise figure, Relative Intensity Noise (RIN) of the optical source, photodetector shot noise, ASE noise and

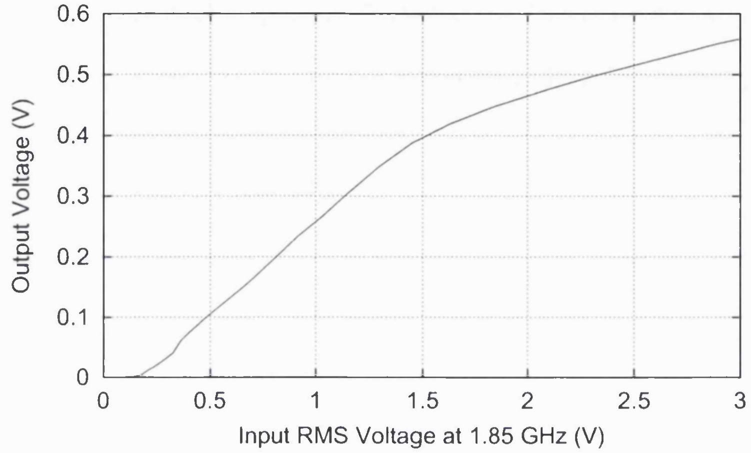

Figure 5.6: Static response of the envelope detector

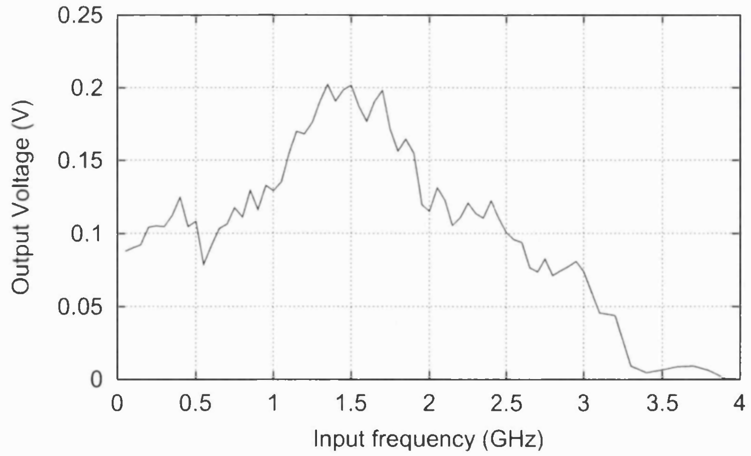

Figure 5.7: Frequency response of the envelope detector

amplitude noise of the generated carrier, each can be assumed mutually independent. The total equivalent input noise power density to the preamplifier can therefore be expressed as:

$$N_t = N_{th} + N_{rin} + N_{shot} + N_{ase} + N_{carr} \tag{5.1}$$

N_t :	Total equivalent input noise power spectral density
N_{th} :	Thermal and amplifier noise power spectral density
N_{rin} :	Optical source relative intensity noise power spectral density
N_{shot} :	Shot noise power spectral density from the photodetector
N_{carr} :	Amplitude noise of the generated carrier photodetector
N_{ase} :	Optical amplifier spontaneous emission noise power spectral density

The phase noise resulting from the optical generation of the millimetre-wave carrier can be neglected. Because of the constant amplitude of the field from the optical source, the carrier noise is dominated by phase-noise originating from the summed linewidth from the optical sources, δf_{ms}. ASK noncoherent demodulation is insensitive to phase noise, and if $\delta f_{ms} \ll 1/\tau_b$, where τ_b is the bit period, the contribution of the carrier phase noise can be neglected entirely from the calculations. Because of the phase correlation of the OIPLL, from where $\delta f_{ms} < 1$ Hz, this is clearly the case. However, due to the chromatic dispersion of the optical fibre, the correlation between the two laser lines will be partially decorrelated, resulting in additional amplitude noise of the carrier [3].

The thermal noise power spectral density of the receiver is given by equation 1.8 in the intoduction:

$$N_{th} = 4k_B T_0 F \frac{Z_{pd} Z_l}{(Z_{pd} + Z_l)^2} \tag{5.2}$$

F :	3.5 dB	Pre-amplifier noise figure
Z_{pd} :	50Ω	Photodetector impedance
Z_l :	50Ω	Load impedance

For the components used with values as above, the thermal noise power density is -170.4 dBm/Hz. The noise power density originating from the RIN of the optical source is given equation 1.9:

$$N_{rin} = \gamma (R I_{rx})^2 Z_l \tag{5.3}$$

γ :	-150 dBc/Hz	Optical source relative intensity noise
R :	0.4 A/W	Photodetector equivalent responsitivity
I_{rx} :		Received optical signal power

For the components used with values as above, the noise power density originating from the RIN of the optical source is lower than the thermal noise power density for input optical powers lower than 0.3 dBm. In other words, for input optical powers much lower than 0.3 dBm, the RIN of the optical source may be assumed to be zero with good approximation. The photodetector shot noise density is given by equation 1.10:

$$N_{shot} = 2q_e R I_{rx} Z_{pd} F_{edfa} \tag{5.4}$$

F_{edfa}	6 dB	EDFA noise figure

With a similar reasoning as above, the photodetector shot noise density equals the thermal noise density at 1.6 dBm received optical power if no optical amplification is used. If optical amplification is used, the photodetector shot noise density equals the thermal noise density at -4.4 dBm received optical power. Finally, the ASE noise is given by 1.11:

$$N_{ase} = \frac{\lambda^2}{c\delta\lambda_f} 2R^2 I_{ase} I_{rx} Z_{pd} + \frac{\lambda^2}{c\delta\lambda_f} (R I_{ase})^2 Z_{pd} \tag{5.5}$$

λ :	1542 nm	Optical wavelength
$\delta\lambda_f$:	1 nm	Optical filter bandwidth
I_{ase} :	-16.8 dBm	Received ASE optical power

The first term represents signal-ASE noise and the second term represents ASE-ASE noise. The ASE optical noise was determined by measuring the optical power after the optical filter with no optical input power to the EDFA. If no optical attenuation is used after the optical filter, the ASE-ASE noise power density is -165.6 dBm/Hz, higher than the thermal noise power density, and the Signal-ASE noise is the dominating noise term for received optical power higher than -24.6 dBm. Clearly, this receiver configuration is limited by the amplifier noise. The noise performance can however be improved if optical attenuation is used after the optical filter. If for instance 10 dB or more optical attenuation after the optical filter is assumed, the ASE-ASE noise power density is -185.6 dBm/Hz, significantly lower than the thermal noise power density, and the Signal-ASE noise is dominant for received optical power higher than -14.6 dBm.

Finally, the additive noise of the carrier due to the chromatic dispersion is given by equation A.15 in appendix A. The increase in the carrier to noise ratio due to this effect is plotted in Fig. 3.13 in chapter 3. This source of noise is dependent on the received power and also the fibre transmission length and can for longer lengths of fibre become a limiting noise factor.

To summarise the noise sources: If no optical amplification is used, the receiver is thermal noise limited for received optical power well below 0.3 dBm. If optical amplification is used and unless attenuation is applied to the output of the EDFA, the link performance will be limited by the EDFA noise. For long fibre transmission lengths, the decorrelation between the two laser lines due to chromatic dispersion can become a limiting factor.

5.3.2 Predicted Bit Error Rate

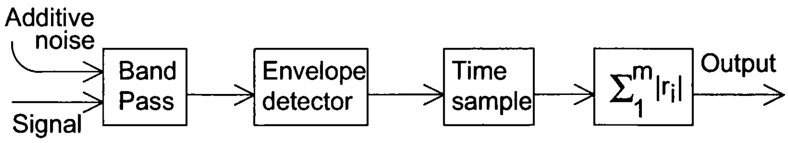

Figure 5.8: Reprenentation of envelope detection for the purpose of calculation of bit error rate.

In order to estimate the expected bit error rate, the amplitude demodulation can be represented according to Fig. 5.8. The input to the filter can be expressed as the signal, $\vec{e}(t)$, together with inphase and out of phase noise, $n_x(t)$ and $n_y(t)$, centered around the signal frequency, f_c. It is assumed that the unfiltered noise is white and Gaussian distributed. Seen in one bit time interval, the amplitude of the signal can be assumed to be constant. The signal phase, $\phi_c(t)$, can also be assumed to be constant because of the phase correlation from the OIPLL. The output of the filter can then be expressed as:

$$E(t) = [ecos\phi_e + n_x(t)]cos(f_ct + \phi_c) + [esin\phi_e + n_y(t)]sin(f_ct + \phi_c) \tag{5.6}$$

E : Signal field
e : Signal amplitude
f_c : Signal Centre frequency
ϕ_c : Signal phase
ϕ_e : Signal field argument
n_x : In-phase noise
n_y : Out-of-phase noise

The envelope detector detects the amplitude of the signal. In order to analyse the impact of any postdetection filter after the envelope detector, the same assumption as in [4] has to be made. Assuming the post detection bandwidth is determined by the bit rate, the postdetection filter ban be treated as as if summing m samples, m given by the ratio between the postdetection filter bandwidth and half the input noise bandwidth. Each sample is then given by:

$$\left|E_i(t)\right|^2 = [e_icos\phi_e + n_{xi}(t)]^2 + [e_isin\phi_e n_{yi}(t)]^2 \tag{5.7}$$

The output power from the filter can then be expressed as:

$$E^2 = \sum_{i=1}^{m} \left|E_i(t)\right|^2 \tag{5.8}$$

It is clear that E^2 is a sum of independent samples of the form $(e_i + n_i)^2$, where e_i are constant and n_i have a Gaussian distribution with a common variance. Therefore, by normalising the variable

E^2, the Probability Density Function (PDF) is given by the non-central χ^2 distribution with 2m degrees [11]:

$$p_q(q) = \frac{1}{2}\left(\frac{q}{\bar{q}}\right)^{(m-1)/2} e^{-(q+\bar{q})/2} I_{m-1}\left(\sqrt{q\bar{q}}\right) \tag{5.9}$$

σ_n^2 :		Variance of n_x and n_y
q :	E^2/σ_n^2	Normalised variable
$\bar{q}$:	$\sum_{i=1}^{m} e_i^2/\sigma_n^2$	Noncentrality parameter
I_{m-1} :		Modified Bessel function of order $m-1$

We can introduce the relative output amplitude, υ, and the equivalent input signal to noise power ratio, $\gamma_e = \bar{q}/4$, the division by 4 depends on the definition of σ_n^2 and the use of average input signal power. The equation 5.9 is then put in the form:

$$p_\upsilon(\upsilon) = p_q(q)\frac{dq}{d\upsilon} = 4\gamma_e \rho^m e^{-2\gamma_e(\upsilon^2+1)} I_{m-1}(4\upsilon\gamma_e) \tag{5.10}$$

υ :	$\sqrt{q/\bar{q}}$	Relative output amplitude
γ_e :	$\bar{q}/4$	Equivalent input signal to noise power ratio

In a similar manner, a situation where the input consists of noise only, the PDF of the normalised variable, q_0 is given by the central χ^2 distribution with 2m degrees [11]:

$$p_{q_0}(q_0) = \frac{1}{2^m\Gamma(m)} q_0^{m-1} e^{-q_0/2} \tag{5.11}$$

q_0 :	n/σ_n^2	Normalised variable
n^2 :	$\sum_{i=1}^{m} n_i^2/\sigma_n^2$	Noise output power from filter
$\Gamma(m)$:		Gamma function

where Γ is the gamma function. Again using the relative amplitude and the equivalent signal to noise ratio, the equation transforms to:

$$p_{\upsilon_0}(\upsilon_0) = p_{q_0}(q_0)\frac{dq_0}{d\upsilon_0} = \frac{4\upsilon_0\gamma_e}{\Gamma(m)}(2\upsilon_0^2\gamma_e)^{m-1} e^{-2\rho_0^2\gamma_e} \tag{5.12}$$

υ_0 :	$\sqrt{q_0/\bar{q}}$	Relative amplitude

The sum of the two derived PDF's is plotted in fig 5.9. A degradation of signal purity and an increase of the optimum threshold value can be observed for increasing values of m. However, the overall receiver performance is not sensitive to the shifting optimum threshold value, as the post detection baseband amplifier is not DC coupled.

With the knowledge of these two PDF's, the BER for the detected ASK modulated signal can be estimated. A binary one is represented by a received signal with noise, with a PDF given by

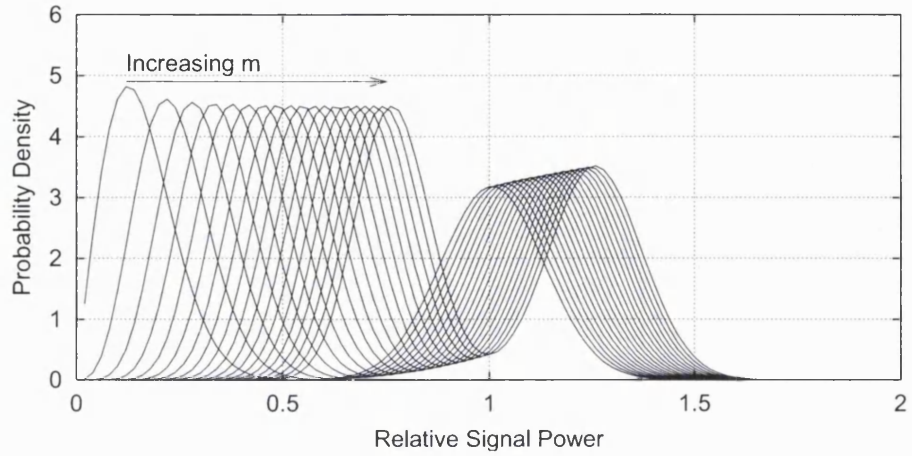

Figure 5.9: Probability density evolution with increasing input noise bandwidth for constant SNR: 12 dB $(1 \leq m \leq 20)$.

equation 5.10. A binary zero is represented by received noise only, with a PDF given by equation 5.12. The BER is then given by:

$$p_e = \frac{1}{2}\int_{-\infty}^{V_T} p_\upsilon(\upsilon)d\upsilon + \frac{1}{2}\int_{V_T}^{\infty} p_{\upsilon_0}(\upsilon_0)d\upsilon_0 \tag{5.13}$$

V_T : Relative decision threshold value

These two integrals are not easily solved analytically, they are better solved with numerical methods. The resulting bit error rate is plotted in 5.10 as a function of equivalent output signal to noise ratio, after the post detection filter, for different values of m. The case where $m = 1$, is equivalent to a rectangular IF filter with a half bandwidth corresponding to the bit rate. As the IF bandwidth increases in relation to the bitrate, higher SNR is required to achieve the same BER. A half IF bandwidth five times higher than the bitrate has an equivalent 0.9 dB SNR penalty.

5.4 Experimental Results

After transmission, detection and downconversion of the millimetre-wave modulated signal, the modulated spectra is detected in a spectrum analyser at 1.85 GHz. Fig. 5.11 shows the detected spectras for transmission over 0, 25, 40 and 65 km of fibre. Due to the optical amplification used for 40 and 65 km fibre span, the relative power difference between the four measurements does not correspond to a real relation, it is simply being set to a fixed interval, 5 dB, for clarity in the figure.

Fig. 5.12 shows the detected eye diagrams after transmission through 0, 25, 40 and 65 km span of fibre and demodulation for constant input optical power, -5 dBm. At this detected optical power, error free transmission is possible for all fibre spans, which is confirmed by the open eye

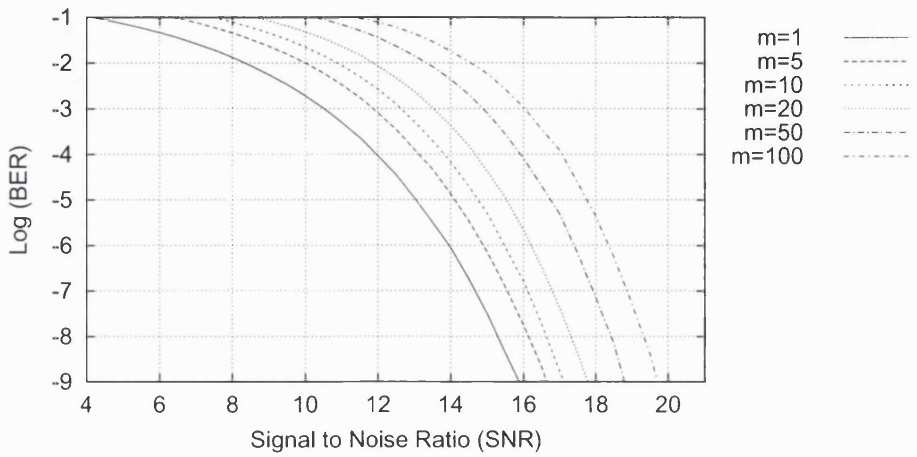

Figure 5.10: Theoretically predicted Bit error rate as a function of received SNR for different values of m.

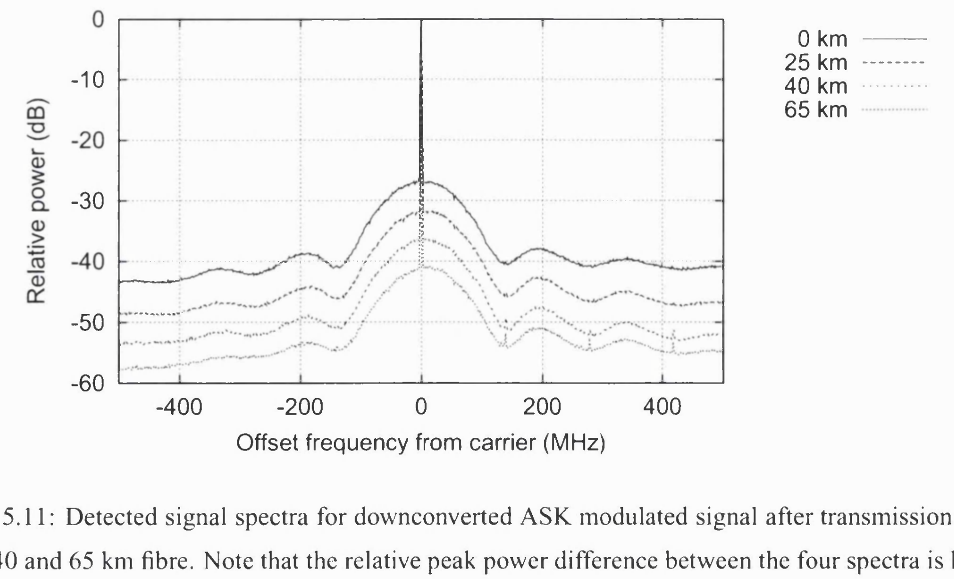

Figure 5.11: Detected signal spectra for downconverted ASK modulated signal after transmission through 0, 25, 40 and 65 km fibre. Note that the relative peak power difference between the four spectra is has been set to 5 dB to distinguish the graphs.

diagrams. As the detected optical power is decreased, the received SNR decreases and error free transmission becomes not possible. This is illustrated by Fig. 5.13, where the BER is plotted as a function of detected optical power for the various spans of fibre. For 0 km and 25 km of fibre, no optical amplification was needed, and for 40 km and 65 km of fibre, an EDFA was used to amplify the signal to the levels shown in the plots. The additional EDFA noise explains the flatter BER curves at low BER, after 40 km and 65 km fibre. For 40 km, the noise penalty in optical terms is 0.6 dB for -18 dBm received optical power, 0.4 dB for -17 dBm received optical power and 0.3 dB for -16 dBm received optical power. For 65 km, the noise penalty compared to thermal noise only is 1.5 dB for -18 dBm received optical power, 1.0 dB for -17 dBm received optical power and 0.7 dB for -16 dBm received optical power.

Table 5.1: Signal and noise power levels giving a BER of 10^{-9}

Fibre Span:	0 km	25 km	40 km	65 km
Optical Power:	-15.8 dBm	-17 dBm	-16 dBm	-13.3 dBm
Modulation Efficiency:	42%	56%	53%	46%
Electrical Power:	-63 dBm	-63 dBm	-61.4 dBm	-57.2 dBm
Optical Attenuation:	—	—	14 dB	12 dB
EDFA noise penalty:	—	—	0.6 dB	4.0 dB
Noise Power:	-81.4 dBm	- 81.4 dBm	-80.8 dBm	-77.4
Difference to theory:	1.8 dB	1.8 dB	2.8 dB	3.8 dB

The differences in required optical power for fixed BER for the different spans of fibre is explained by variations in the optical to millimetre-wave transduction efficiency, discussed earlier in chapter 3. At 25 km fibre span, -63 dBm received millimetre-wave power is measured for -17 dBm received optical power. With a photodetector responsitivity of 0.4 A/W, this corresponds to 56% optical to millimetre-wave conversion efficiency, defined as the ratio of received optical power that contributes to the generation of millimetre-wave power.

Using the same equation, B.45, as earlier, the theoretically predicted variations in optical to millimetre-wave transduction efficiency can be plotted in the same manner as done in the first curve in Fig. 3.11. Incorporating the experimentally derived penalties from Fig. 5.13, assuming a fibre dispersion of 20 ps/nm/km and adding 28 fs to the differential time delay of the two paths of the master laser, the experimental values derived from the displacements of BER curves in Fig. 5.13 can be plotted together with the theory in Fig. 5.14. We observe a good fit of experimental values to theory, verifying that the variations in required optical power can be explained by the effects from the fibre dispersion.

In order to compare the experimental BER with theory, the data in Fig. 5.13 needs tobe

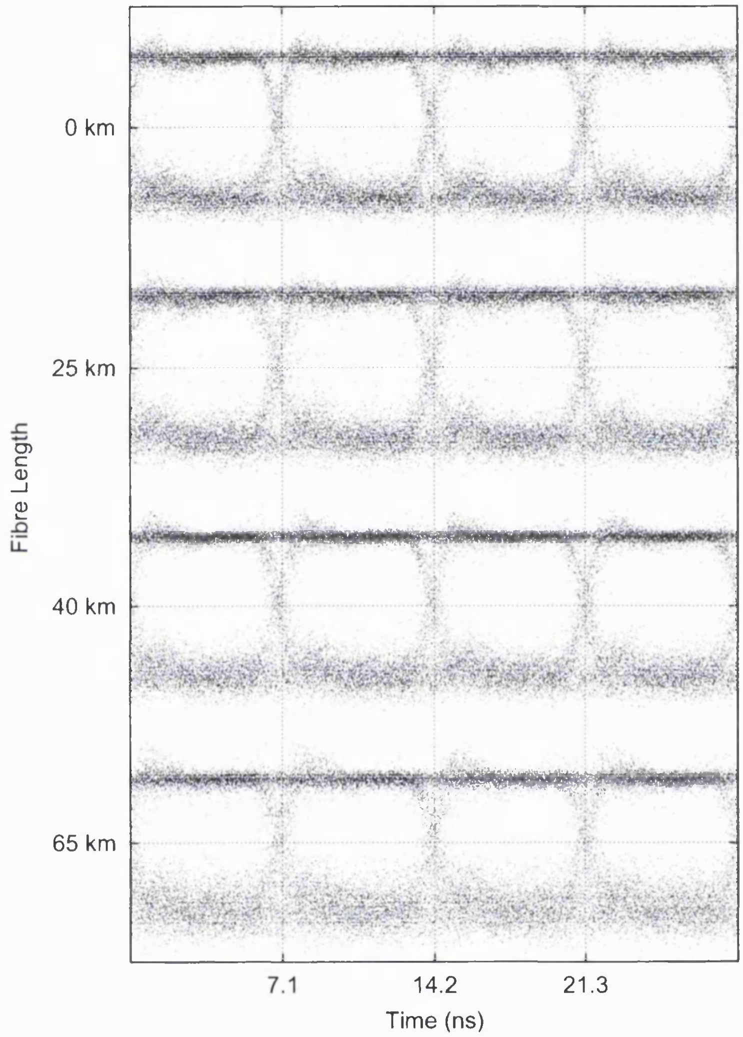

Figure 5.12: Detected eye diagrams for transmission through 0, 25, 40 and 65 km fibre.

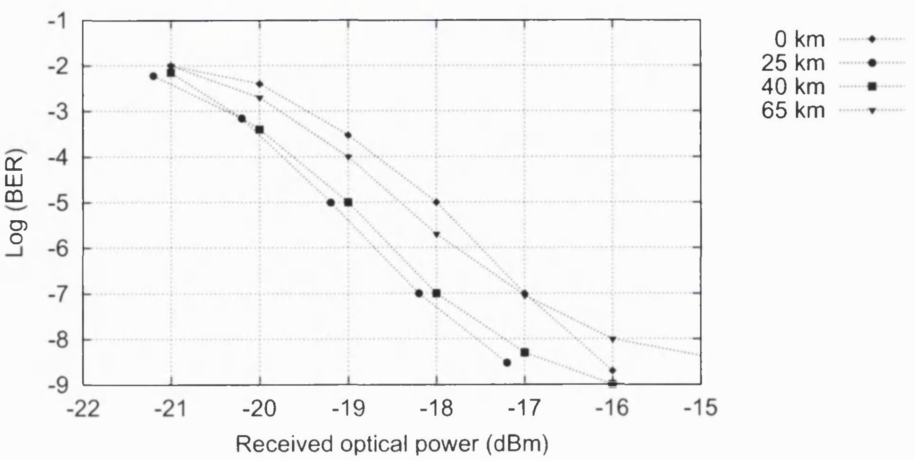

Figure 5.13: Bit error rate as a function of received optical power with corresponding curve fits.

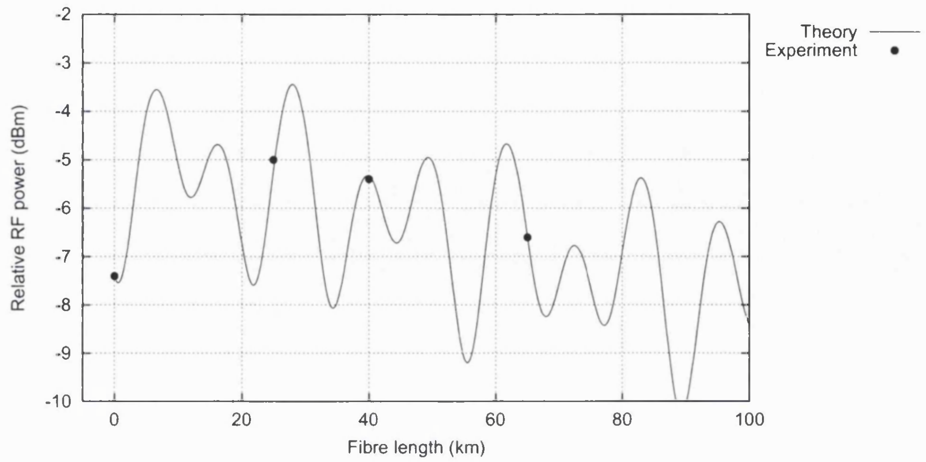

Figure 5.14: Comparison of experimental values to theoretically predicted optical to millimetre-wave conversion efficiency

converted into terms of received SNR. The detected signal power after 25 km fibre needed to achieve a bit error rate of 10^{-9} is -63 dBm. The receiver noise can with good approximation be assumed to be limited by the thermal noise, as no EDFA was used. From the previous section, the input thermal noise density is -170.4 dBm/Hz. The equivalent noise bandwidth is determined by the bandwith of the postdetection amplifier: 260 MHz. The input equivalent IF noise bandwidth is then 520 MHz. Given the 5 dB lower gain of the millimetre-wave mixer and preamplifier at the RF image frequency, 39.7 GHz, the equivalent RF noise bandwidth can be assumed to be $(520 + 520/10^{0.5})$ MHz = 680 MHz. The image frequency increases the inband noise power by 1.2 dB. Using these figures, the SNR is 19 dB. We can now convert the data for the BER in Fig. 5.13 into terms of SNR and compare it with the theoretical result showed in Fig. 5.10. The value of m is given by a division of half the IF noise bandwidth, given by the bandwidth of the envelopedetector (3/2 GHz), by the postdetection noise bandwidth, given by the bandwidth of the postdetection amplifier (260 MHz). This gives us $m = 5$ with a 0.9 dB SNR penalty, compared to when $m = 1$. Fig. 5.15 shows the measured BER together the corresponding curve fits and the BER that would expected from theory. For higher values of BER, there is a high degree of correlation between experiment and theory, but for lower BER, there is a slight degradation of required SNR in the experimental values. However, including a fixed 17.5 dB CNR in 680 MHz noise bandwidth to the theoretical prediction, the curve fit for 0 km and 25 km fibre span is obtained. The source for this fixed CNR can be accounted for by amplitude noise originating from the OIPLL carrier generation.

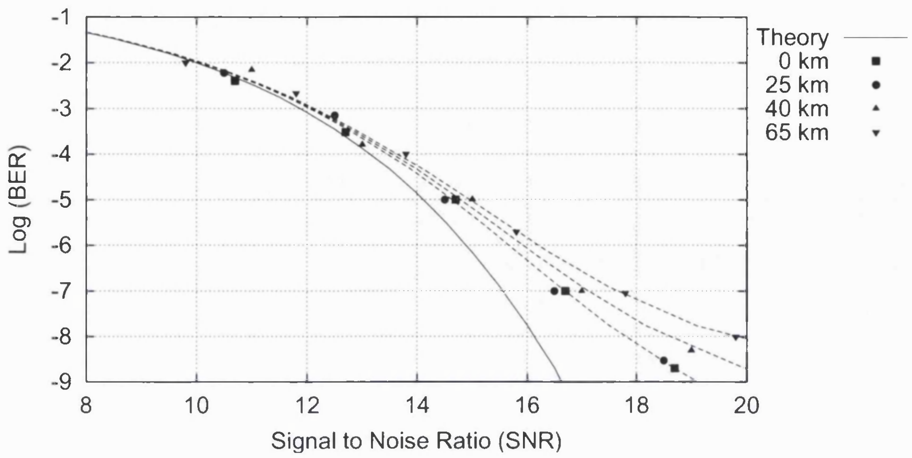

Figure 5.15: BER comparison between theoretical and experimental results.

5.5 Conclusion

In this chapter, transmission results of a 36 GHz millimetre-wave modulated optical carrier with 140 Mbit/s NRZ ASK data applied to it, have been presented. These results have been compared to theoretical predictions with good agreement obtained. Error-free transmission was achieved for 0, 25, 40 and 65 km of fibre. Evidence of the efficiency of the method of generation of millimetre-wave modulated optical signals was provided not only by the measured optical to millimetre-wave conversion efficiency, 56 % after 25 km fibre transmission, but also confirmed by the fact that error-free transmission was available for transmission for distances up to 25 km fibre span, even though the launched power was small, -8 dBm. An increase of launched power would give sufficient margin to overcome splitting losses, to serve a number of optical receivers. Tolerance to fibre dispersion was proved by the narrow range of required optical power needed to achieve a fixed BER for different lengths of fibre. The variations of required optical power fits very well with what theory predicts from the OIPLL, except for very low values of BER, where there is a small penalty in the experimental results obtained.

The receiver was found to be limited in performance by thermal noise and at low BER, the CNR of the generated millimetre wave modulated optical signal. If optical amplification was used, the receiver was also affected by signal-ASE noise. It was also found that the receiver design was suboptimal due to inadequate predetection filtering. A reduction of IF bandwidth by a factor of five, would in theory improve the receiver sensitivity by 0.9 dB electrical power. A second limitation of the receiver design used was lack of filtering at the image RF frequency at 39.7 GHz, before RF to IF downconversion. This adds a further 1.2 dB degradation of the receiver sensitivity.

This chapter has successfully verified the feasibility of the OIPLL as a heterodyne optical source for distribution of broadband data modulated millimetre-wave signals. However, due to the modulation format chosen, no evidence is provided to verify the phase stability of the source and therefore no conclusive evidence is provided that the OIPLL is suitable for more commonly used modulation formats like phase or phase/amplitude modulation. This topic will be addressed in the following chapter.

References

[1] T. Okoshi, "Heterodyne and Coherent Optical Fiber Communications: Recent Progress," *IEEE Trans. Microwave Theory Tech.*, vol. 30, pp. 1138–1148, 1982.

[2] L.G. Kazovsky and O.K.Tonguz, "ASK and FSK Coherent Lightwave Systems: A Simplified Analysis," *Journal of Lightwave Tech.*, vol. 8, pp. 338–352, 1990.

[3] U. Gliese, S. Noeskov and T.N. Nielsen, "Chromatic dispersion in fiber-optic microwave and millimeter-wave links," *IEEE Trans. Microwave Theory Tech.,* vol. 45, pp. 1716–1724, 1997.

[4] G.J. Foschini, L.J. Greenstein and G.V. Vannucci, "Noncoherent Detection of Coherent Lightwave Signals Corrupted by Phase Noise," *IEEE Trans. Comm.*, vol. 36, pp. 306–314, 1988.

[5] O.K.Tonguz,O.M. Tanrikulu and L.G. Kazovsky, "Performance of Coherent ASK Lightwave Systems with Finite Intermediate Frequency," *IEEE Trans. Comm.*, vol. 45, pp. 344–351, 1997.

[6] S. Watanabe, I. Yokota, T. Naito, T. Chikama, H. Kuwahara and T. Togue, "Polarisation-Insensitive Optical Coherent SCM System using Mixed Lightwave Transmission of Signal and Local Laser Light," *Elec. Lett.*, vol. 27, pp. 361-362, 1991.

[7] S. Pajarola, G. Guekos, P. Nizzola and H. Kawaguchi, "Dual-Polarisation External Cavity Diode Laser Transmitter for Fiber-Optic Antenna Remote Feeding," *IEEE Trans. Microwave Theory Tech.*, vol. 47, pp. 1234–1240, 1999.

[8] Y. Ozeki, K. Nishikawa, M. Kishi and M. Tsuchiya, "60-GHz Optoelectronic Image Rejection Mixer and its Application to a 156-Mb/s Fiber-Optic mm-Wave ink," *IEEE Photon. Tech. Lett.*, vol. 13, pp. 361–363, 2001.

[9] D.G. Moodie, M.J. Harlow, M.J. Guy, S.D. Perrin, C.W. Ford and M.J. Robertson, "Discrete Electroabsorption Modulators with Enhanced Modulation Depth," *Journal of Lightwave Tech.*, vol. 14, pp. 2035–2043, 1996.

[10] D.A.B. Miller, D.S. Chemla, T.C. Damen, A.C. Gossard, W. Wiegmann, T.H. Wood and C.A. Burrus, "Bandedge electroabsorption in quantum well structures: The quantum-confined Stark effect," *Phys. Rev. Lett.*, vol. 53, pp. 2173-2177, 1984.

[11] R.N. McDonough and A.D. Whalen, "Detection of Signals in Noise," Second edition. Academic Press, San Diego, California, pp. 140-141, 1995.

Chapter 6

Differential Phase Shift Keying Transmission Experiments

This chapter describes transmission experiments using the Differential Phase Shift Keying (DPSK) modulation format. The introduction, 6.1 outlines previous relevant work using phase modulation. The objectives of the demonstration are also stated. The following section, 'Experimental Arrangement' 6.2 describes the equipment, devices and layout of the experimental arrangement used to apply the modulation to the OIPLL and to demodulate successfully the received signal. In 'Predicted Performance' 6.3, the ability of the injection locked slave laser to track a phase modulated reference is derived and compared to numerical calculations. The noise sources in the receiver are investigated, and an expression for the expected BER is given. Section 6.4, 'Experimental Results' presents the experimental data obtained in the form of detected electrical spectra of the received signal, detected eye diagrams and BER curves. A comparison with what would be expected by the theory of section 6.3 is also provided for the BER curves. The conclusion, 6.5 summarises the most important findings in the chapter.

6.1 Introduction

PSK modulation offers the highest receiver sensitivity of the basic binary modulation formats, ASK, FSK and PSK. For this reason, PSK has been a prime candidate for coherent optical systems and has been investigated both theoretically [1] and experimentally [2]. Unlike the modulation format treated in the last chapter, ASK, phase modulation is also commonly used in wireless applications. Particularly common is some form of QPSK (quadrature phase shift keying) modulation, as it combines bandwidth efficiency with low required SNR. Examples of current systems using QPSK are CDMA (code division multiple access) cellular services, Iridium and DVB-S (Digital Video Broadcasting - Satellite) [3]. Furthermore, cellular systems like NADC

(North American Digital Cellular) and PDC (Pacific Digital Cellular) use differential QPSK [3]. At millimetre-wave frequencies, QPSK was the modulation format of choice in the ACTS wireless access project CRABS [4]. Basic phase modulation can also form part of adaptive modulation schemes, moving up in complexity from BPSK via QPSK to higher order QAM modulation [5], depending on what wireless link performance is available. The emerging IEEE 802.16 standard will include QPSK in the supported modulation formats [6]. For these reasons, QPSK modulation is very attractive to use in a millimetre wave over fibre demonstration. Notably, two high profile demonstrators have used this modulation format: QPSK by Noel, *et al* [7] and offset QPSK (OPQSK) by Braun, *et al* [8, 9]. However, due to the relative complexity of QPSK, the more simple BPSK [10, 11, 14, 12, 13] and DPSK [15, 16] modulation formats have more frequently been used, as modulation and demodulation is easy to achieve using simple components and a single data generator.

In the present experiments DPSK modulation has been chosen because of its simplicity of implementation. A further advantage of DPSK over BPSK is that simple demodulation can be achieved without carrier recovery or the use of synchronised frequency reference sources. The method chosen to implement the binary data on the millimetre wave subcarrier is one rarely used in optical heterodyne experiment, the use of a modulated reference signal. This has previously only been demonstrated using a 6 MHz PAL analogue video signal in an OPLL based system [11]. This demonstration serves many objects. It shows that the direct modulation bandwidth of a heterodyne system can be greatly increased compared to previous results, using the combination of OPLL and OIL technologies. It also demonstrates that the phase stability of the OIPLL is high enough for more realistic modulation formats to be used, that require a low phase noise level. Finally, by applying the modulation directly to the OIPLL it is shown how a complete millimetre wave modulated optical transmitter with data applied can be designed where the only opto-electronic components are two standard DFB lasers and photodetectors.

6.2 Experimental Arrangement

6.2.1 Transmitter

Fig. 6.1 shows a schematic of the experimental arrangement used to perform the PSK transmission experiments. A $2^{23}-1$ word pattern 68 Mbit/s Pseudo-Random Bit Sequencer (PRBS) produces a baseband data stream. The data is encoded into differential format, where a transmission of the signal level from high to low or from low to high, marks a binary zero, while no transition marks a binary one. A digital circuit had to be designed, based on Emitter Coupled Logic (ECL) to perform this encoding. The schematic of the design of the encoder is shown in Fig. 6.2. A MC10EL07 XOR-gate compares the input bit with the inverse of the previous differentially encoded output

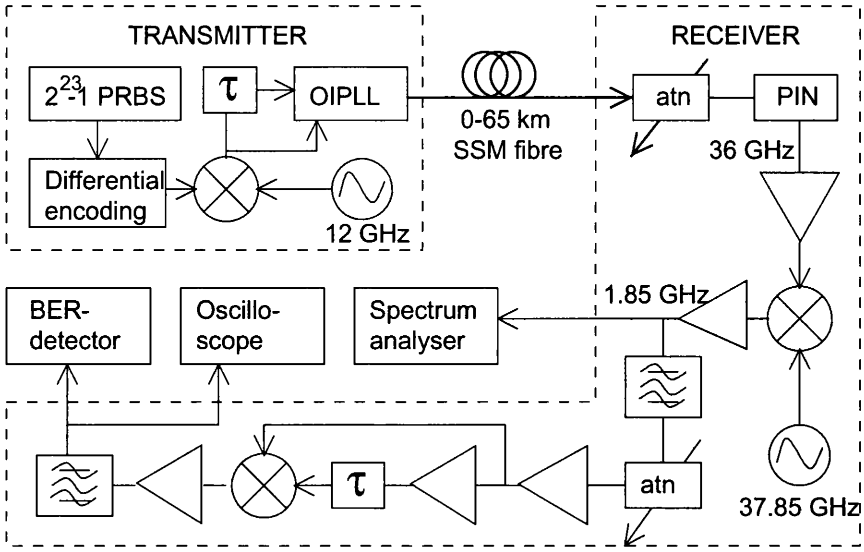

Figure 6.1: Schematic of 68 Mbit/s DPSK radio over fibre transmission experiment

bit. If there is no change in the binary value, the differentially encoded output bit value is one, and if there is a change, the output bit value is zero. In order to synchronise the two input signals into the XOR-gate, two MC10EL31 D-type flip-flops were used, triggered by the clock signal from the PRBS. The differentially coded baseband signal is then used to switch the phase of a 12 GHz

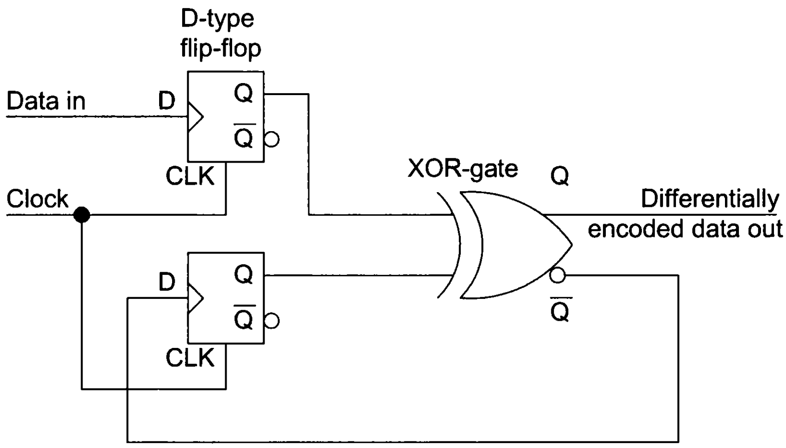

Figure 6.2: Schematic of Differential encoder.

reference with a Miteq DB0440LW1 double balanced mixer. At the output of the mixer, a 68 Mbit/s π-shifted DPSK modulated 12 GHz carrier is now generated. This is used as a reference for the OIPLL. Unlike the case where a pure sinusoidal carrier is used as reference for the OIPLL, absolute path matching between the injection locking path and the phase-lock loop path is here needed in order to achieve bit sychronisation. Therefore, the path of the reference that is used for the PLL phase detector is delayed to compensate for the extra relative optical path after the modulated master laser in the OIPLL. At the output of the OIPLL, an optical carrier, modulated at 36 GHz with π-shifted 68 Mbit/s DPSK data is formed. As not only the frequency, but also the phase of the reference signal is multiplied in the OIPLL, the DPSK modulation is now shifted by 3π, the generated 36 GHz modulated signal should have been 3π shifted. However, due to the limited phase tracking capabilities of the injection locking, the actual modulation at the output is π-shifted DPSK. Using pre-compensation for the multiplication of the phase, this method is applicable for multilevel phase modulation. Frequency modulation is also an alternative. However, the use of amplitude modulation is restricted by the constant output power of the slave laser.

The generated optical signal is transmitted through up to 65 km of SSM fibre. No optical amplification was needed in these transmission experiments.

6.2.2 Receiver

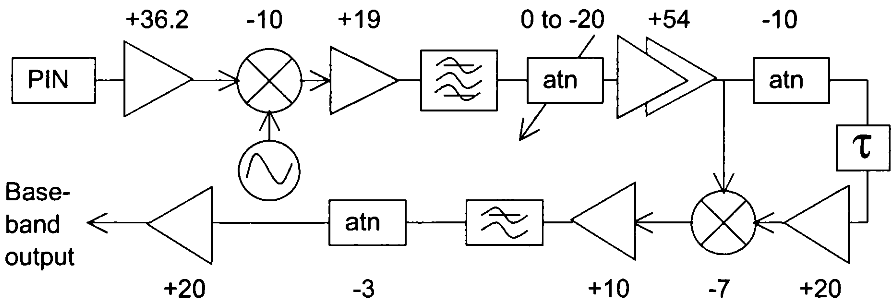

Figure 6.3: Schematic of 68 Mbit/s DPSK receiver configuration with component gain included.

Fig. 6.3 shows a detailed schematic of the receiver configuration with component gain included. At the receiver side, the signal is detected in a Discovery PIN photodetector, with 39 GHz bandwidth and about 0.4 A/W responsitivity at 1550 nm and 36 GHz modulation frequency. The photodetected signal is amplified in a Spacec Labs SLKa-35-4 26.5 GHz to 40 GHz low noise amplifier with 36.2 dB gain and 3.5 dB noise figure at 36 GHz. The signal is then downconverted to 1.85 GHz in a Miteq TB0440LW1 triple balanced mixer. The signal is further amplified and one tenth by power is detected in a spectrum analyser. The remainder of the signal is then bandpass filtered in a coupled line microstrip bandpass filter with 220 MHz bandwidth, to limit the noise bandwidth of the signal. The filter frequency response is plotted in Fig. 6.4. The power level of the bandpass filtered signal is regulated by a variable attenuator. A limiting amplifier further amplifies the 1.85 GHz signal. The reason that a limiting amplifier is used is to produce a suitable constant power level to pump the mixer later used for demodulation, and to protect the mixer used from too high pump power. The saturated power of the limiting amplifier was about -0.6 dBm. The gain response at 1.85 GHz is shown in Fig. 6.5. A DPSK modulated signal has the advantage that demodulation of the signal can be arranged in a relatively simple manner. Here, the DPSK modulated signal is split in two equal paths. One path is connected to the RF input of a Mini-Circuits

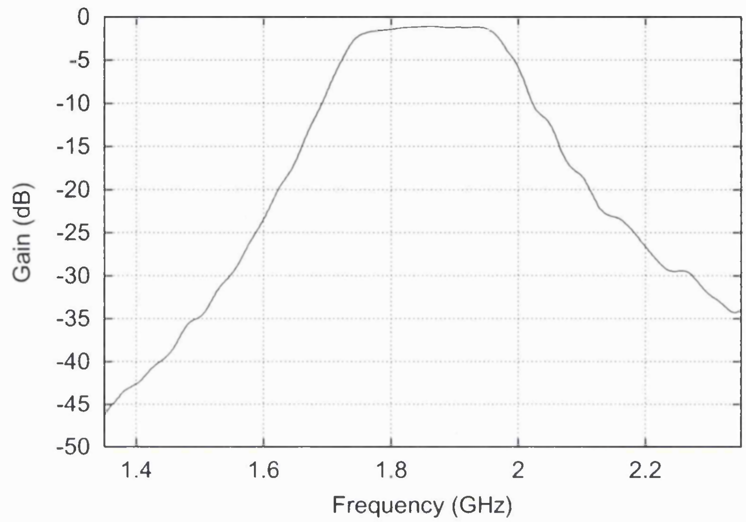

Figure 6.4: Frequency response of IF filter centered around 1.85 GHz.

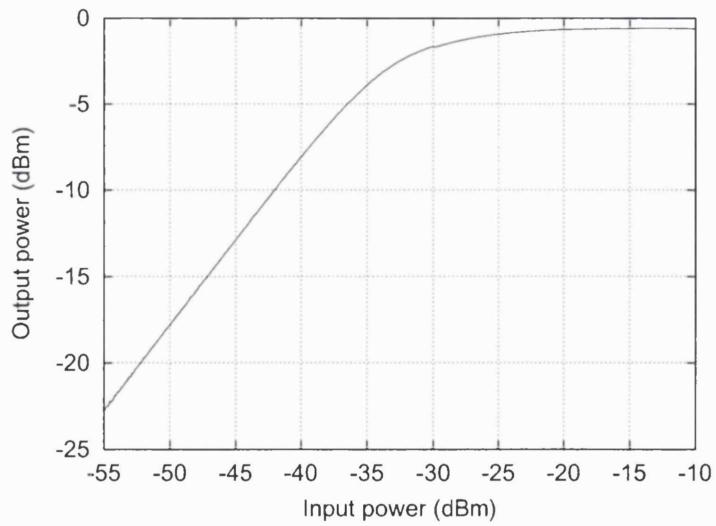

Figure 6.5: Output power from limiting amplifier as a function of input power.

ZFM-2000 double balanced mixer. The second path is amplified to a suitable level to pump the mixer. This path is delayed exactly one bit period, (68 MHz)$^{-1}$ = 14.7 ns. In the mixer, the phase of the signal is now compared with the phase of the signal one bit period ago. If there is a change in phase of the DPSK modulated signal, corresponding to a binary zero, the output from the mixer is negative. Correspondingly, for no change in phase, a binary one, produces a positive output from the mixer. The original bitstream is now recovered. After amplification, the signal is lowpass filtered. The bandwidth of this filter is limited by the condition for avoiding interference between neighbouring bits; $\tau_{bb} + \tau_{if} < \tau_b$, where τ_b is the bit period, τ_{if} corresponds to the reciprocal half bandwidth of the IF filter and τ_{bb} corresponds to the reciprocal bandwidth of the baseband filter. The baseband filter bandwidth used here was about 300 MHz. In addition to providing further noise filtering, the low pass filter was required to remove the impulses found in the demodulated baseband signal. These impulses appears because the output voltage of the mixer instantaneously dips to zero at a phase inversion of the input signal. The result is that between two output bits with negative output voltage, an impulse is found that needs to be limited for successful detection of the binary data. The signal is then further amplified, before the eye diagram is finally detected on an oscilloscope and the bit error rate is detected on a bit error rate detector.

6.3 Predicted Performance

6.3.1 OIPLL phase tracking performance

With DPSK modulation applied to the reference, the injection phase will make a step of π. Separating the real from imaginary part of equation B.1 in appendix B and eliminating the component containing the differential gain, the following relation is found:

$$\dot{\phi} = \frac{\sqrt{\rho}}{\tau_0}\left[\alpha\cos(\phi_i - \phi) + \sin(\phi_i - \phi)\right] + \left[\omega_f - \omega_i\right] - \alpha\frac{|\dot{E}|}{|E|} \tag{6.1}$$

ϕ	Slave laser phase
ρ	Injection ratio
τ_0	Laser cavity round-trip delay
ϕ_i	Injection phase
α	Phase-amplitude coupling factor
ω_f	Slave laser free running frequency
ω_i	Slave laser locked frequency
E	Slave laser field

Using the notation $\delta\phi = \phi_i - \phi + \arctan(\alpha)$, $\omega_0 = \sqrt{\rho(1+\alpha^2)}/\tau_0$ and $K = (\omega_f - \omega_i)/\omega_0$, the equation can now be simplified to:

$$\delta\dot{\phi} = \omega_0(\sin(\delta\phi) - K) \tag{6.2}$$

Integration gives [17]:

$$\tan\frac{\delta\phi}{2} = \frac{1}{K} - \frac{\sqrt{1-K^2}}{K} tanh\frac{\omega_0(t-t_0)}{2}\sqrt{1-K^2} \tag{6.3}$$

If $sin(\delta\phi) < K$, then $tanh$ in the expression should be substituted for $coth$. The phase can now be plotted as a function of the time. Setting the time constant t_0 to $t - t_0 = 0$ at the time of a phase inversion of the reference, the resulting plot is shown in Fig. 6.6 for different values relative detuning, K, and an injection locking gain of 1.4 GHz. In the figure, the 90% recovery time is just

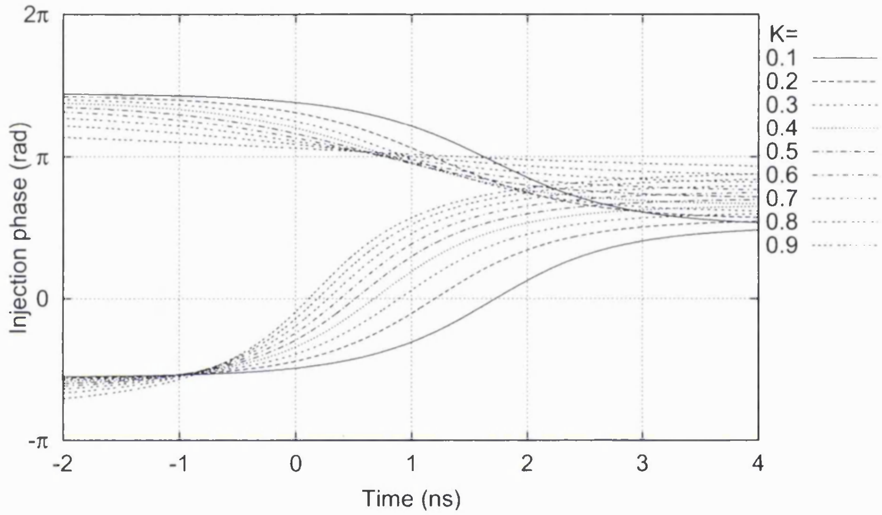

Figure 6.6: Injection phase ($\phi - \phi_i$) response to a step in reference phase. Time constant t_0 normalised to a phase step of π at $t = 0$. Other values of phase step will require different time calibration.

above twice the inverse injection locking gain, $1/K_{oil}$, varying a little with the steady state locking phase. It be observed that when the steady state locking phase approaches 0 rad, a phase shift of π represents an unstable equilibrium point with increased phase recovery time, Therefore, a small phase offset is desirable for optimum performance, not too much, as the phase noise suppression suffers close to the limits of the locking range, according to equation B.29. This also corresponds well to the expression for the loop bandwidth derived in chapter 3, equaling injection locking gain, sufficient to phase track a 140 Mbit/s frequency or phase modulated reference with an adequate frequency margin of a factor of ten. To validate the model developed for the phase tracking of the injection locking, the analytically obtained results should be compared to the results when the slave laser rate equations are solved numerically with the Runge-Kutta-Fehlberg method. Figure 6.7 shows the comparison for $K_{oil} = 1.4$ GHz with a very good agreement. The numerical solution also shows that the amplitude fluctuations are limited to an added negative pulse with a 0.9 ns pulsewidth and and relative peak power of -21.5 dB, at the time of the phase inversion. This confirms the assumption made that these fluctuations are small.

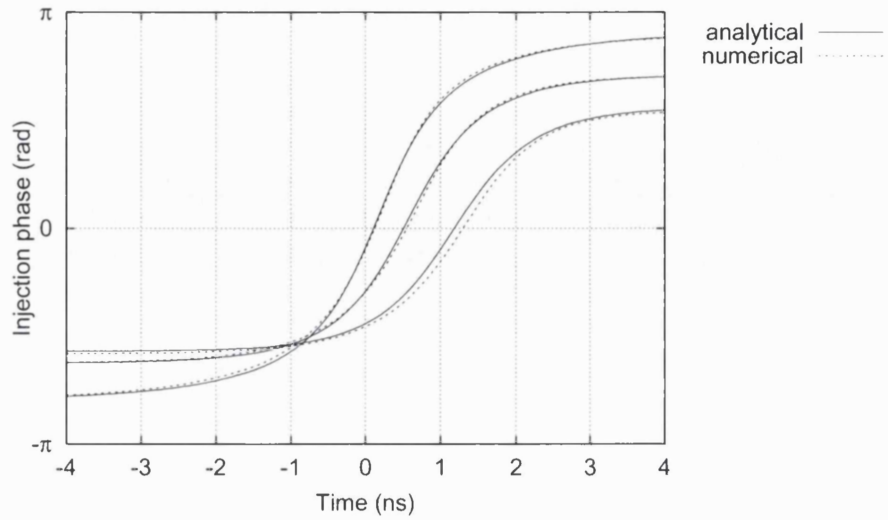

Figure 6.7: Comparison between numerical and analytical solution for the response of a phase step in the injected phase ($\phi - \phi_i$) for K=0.2, 0.5 and 0.9. Time scale calibrated to a phasechange of π at time zero.

The tracking delay can however have an impact of the performance of the OPLL. At the phase detector in the OPLL, the distorted output from the injection locking will be compared to the undistorted reference. For π-DPSK, where $\delta\phi(t_i) = 0$, the phase error will be:

$$\phi_e = \sum_i a_i \theta(t - t_i) \delta\phi(t - t_i) \tag{6.4}$$

where a_i is a random variable, either one or zero. The resulting OPLL feedback current will be modified by a convolution of the impulse response of the loop filter. If the filter is a second order type 2 filter, the feedback current will be:

$$i_e(t) = \phi_e(t) * K_f(1 - e^{-t/\tau_1})e^{-t/\tau_2} \tag{6.5}$$

According to Fig. 6.6, the phase will always recover with the same rotation, letting the mean value, $< \phi_e > \neq 0$. If the bit period is larger than both the time constants, τ_1 and τ_2, the feedback current will now be time independent and $i_e = K_f < \phi_e >$. The loop filter can easily be designed to compensate for this DC offset. However, if the bit period is higher or on the order of the time constants, nonlinear treatment of the OPLL is necessary, as the linearised equations for the OPLL are not valid. In this experiment, the bandwidth of the OPLL was limited by the FM response of the slave laser, with cutoff frequencies in the kHz region. At a data rate of 68 Mbit/s, the error will clearly be manifested as a DC component after the loop filter that can be compensated for.

6.3.2 Receiver noise

The noise sources in the DPSK optical receiver are the usual ones in the absence of any optical amplifiers:

$$N_t = N_{th} + N_{rin} + N_{shot} + N_{carr} \tag{6.6}$$

N_t :	Total equivalent input noise power spectral density
N_{th} :	Thermal and amplifier noise power spectral density
N_{rin} :	Optical source relative intensity noise power spectral density
N_{shot} :	Shot noise power spectral density from the photodetector
N_{carr} :	Carrier amplitude noise power spectral density

The thermal noise power spectral density of the receiver is given by equation 1.8 in the intoduction:

$$N_{th} = 4k_B T_0 F \frac{Z_{pd} Z_l}{(Z_{pd} + Z_l)^2} \tag{6.7}$$

F :	3.5 dB	Pre-amplifier noise figure
Z_{pd} :	50Ω	Photodetector impedance
Z_l :	50Ω	Load impedance

The noise power density originating from the RIN of the optical source is given by equation 1.9:

$$N_{rin} = \gamma (RI_{rx})^2 Z_l \tag{6.8}$$

γ:	-150 dBc/Hz	Optical source relative intensity noise
R :	0.4 A/W	Photodetector equivalent responsitivity
I_{rx} :		Received optical signal power

The photodetector shot noise density is given by equation 1.10:

$$N_{shot} = 2q_e RI_{rx} Z_{pd} \tag{6.9}$$

The additive noise of the carrier due to the chromatic dispersion is given by equation A.15 in appendix A. The increase in the carrier to noise ratio due to this effect is plotted in Fig. 3.13 in chapter 3. This source of noise is dependent on the received power and also the fibre transmission length and can for longer lengths of fibre become a limiting noise factor.

Unlike the ASK modulation format, DPSK modulated signals are sensitive to the phase error of the carrier. There are several sources of phase error including the phase error variance of the unmodulated carrier and the phase error originating from the reference modulation. The phase error of the unmodulated carrier is given by equation 3.10 from Chapter 3:

$$S = |1 - H|^2 S_n - |H|^2 S_{in} \tag{6.10}$$

The differential phase between two bits, $\phi_\delta = \phi(t) - \phi(t+T)$ can be related to the phase fluctuation spectra of the carrier as [18]:

$$S_{\phi\delta} = 4S_{\phi}sin^2(\pi Tf) \qquad (6.11)$$

The second source of differential phase error is due to the injection locking recovery time of the phase step in the DPSK modulated reference and can be derived from Fig. 6.7 for $K_{oil} = 5$ GHz. Assuming each bit sample of the demodulated signal is taken at $t = T/2$. Also assuming that the phase error is small enough for intersymbol interference (ISI) to be ignored, the phase error can be directly read from the figure as the difference between the phase when $t = T/2$ and the steady state value of the phase.

6.3.3 Predicted Bit Error Rate

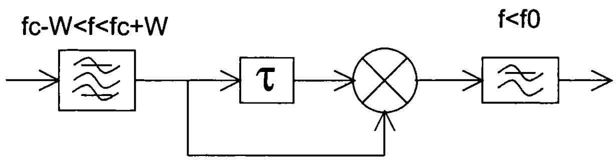

Figure 6.8: Schematic for DPSK demodulation arrangement.

Fig. 6.8 shows a schematic for the demodulation arrangement. The bit error rate probability of this detection method has been investigated in [19], which is here summarised. Using narrowband assumption, after the first filter the detected and downconverted signal can be written in the following form:

$$r(t) = [a(t) + n_c(t)]cos(2\pi fct) + n_s(t)sin(2\pi fct) \qquad (6.12)$$

Assuming an ideal rectangular frequency response bandpass filter with a sinc-shaped impulse response, $a(t)$ can now be written:

$$a(t) = 2Wa_0 \sum_i a_i \int_{t-(i+1)T}^{t-iT} sinc(2\pi WT)dT \qquad (6.13)$$

where a_i are independent binary random variables. Assuming the low pass filter after multiplication removes all components containing $2 \cdot fc$, the output sample, l, taken at the centre at the bit time is given by:

$$l = \frac{1}{2}[a(-T/2) + n_c(-T/2)][a(T/2) + n_c(T/2)] + \frac{1}{2}n_s(-T/2)n_s(T/2) \qquad (6.14)$$

where

$$a(-T/2) = a(T/2) = 4WP_a \int_0^{T/2} sinc(2\pi WT)dT \qquad (6.15)$$

P_a is the signal power density. The probability of error is now the probability that $l < 0$. n_c and n_s are Gaussian zero mean random variables with variances η/T. Because of the narrowband approximation, $n_c(-T/2)$ and $n_c(T/2)$ are not independent. However, $n_c(-T/2)+n_c(T/2)$ and $n_c(-T/2)-n_c(T/2)$ are independent. It can now be shown that the probability of error is [20, 19]:

$$P_e = Prob(l < 0) = \frac{1}{2}exp\left\{ -\frac{E_b}{\eta}\frac{2}{\pi^2 W}\left[\int_0^{\pi WT} sinc(x)dx\right]^2\right\} \tag{6.16}$$

Where $\frac{E_b}{\eta}$ is the bit signal to noise ratio. If the bandwidth of the post detection filter is smaller than W, the final probability is given by a sum of independent χ^2–distributed random processes, as described in chapter 5. For a postdetection filter with a bandwidth larger than W, the BER can be similarly derived according to equation 6.16 as a function of input signal to noise ratio for a range of values of WT. The result is shown in Fig. 6.9, where the noise power has been measured in the bandwidth $1/2T$. A restriction not included in this model is the impact of InterSymbol Interference (ISI). . Unless the filter is reset at the end of each bit period, ISI will be a limiting factor of the minimum filter bandwidth. The value $WT = 0.57$ in the plot is a local minimum of ISI, where the ISI can be ignored, and a 0.8 dB penalty to ideal DPSK demodulation is found. For $W = 110$ MHz and 68 Mbit/s, $WT = 1.6$ and the penalty is around 5 dB compared to ideal demodulation, excluding ISI.

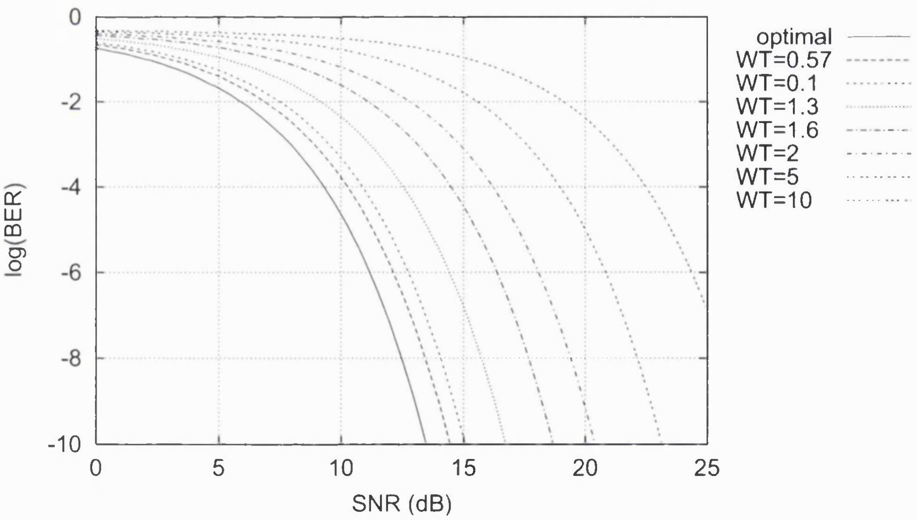

Figure 6.9: DPSK BER as a function of the SNR for different values of receiver IF bandwidths in a noise bandwidth of 1/2T.

So far, the effect on the differential phase error between consecutive bits has not been included in the calculations. The bit phase difference must be multiplied with $cos(\phi_\delta)$ when the BER is calculated. Assuming the differential phase error variance of the carrier is a Gaussian distribution with a variance, σ^2, the bit error rate, including the phase jitter can be written as:

$$P_e = \int_{\infty}^{\infty} \frac{1}{\sigma\sqrt{2\pi}} exp\left\{ -\frac{\phi_\delta}{2\sigma_\phi^2 \delta}\right\}\frac{1}{2}exp\left\{ -\frac{E_b}{\eta}\frac{2}{\pi^2 W}cos^2(\phi_\delta)\left[\int_0^{\pi WT} sinc(x)dx\right]^2\right\}d\phi_\delta \tag{6.17}$$

The bit error rate for an IF filter bandwidth of $WT = 1.6$ for different values of phase error variance is plotted in Fig. 6.10. In a similar manner, the impact of the modulation of the reference can also

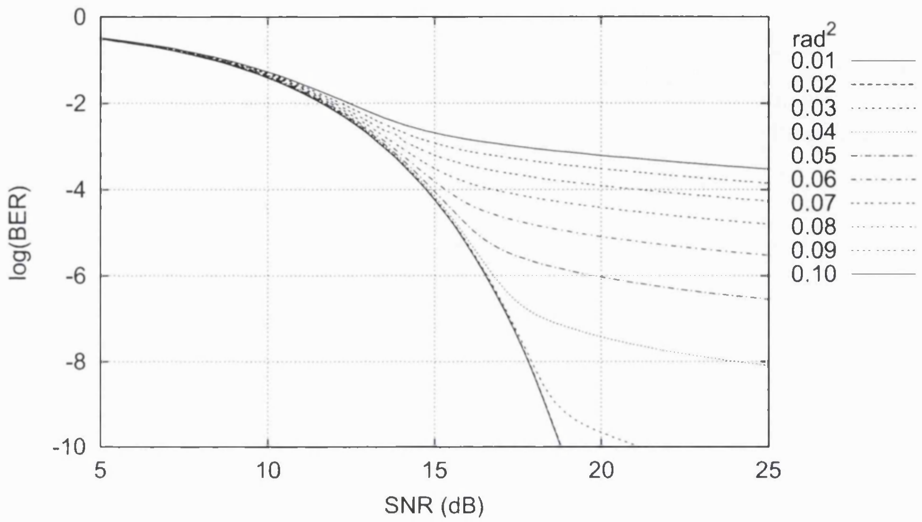

Figure 6.10: DPSK BER as a function of the SNR for different values of carrier phase error variance.

be correlated to the BER. There is a probability of 0.5 for a phase inversion between two bits with the corresponding phase error:

$$P_e = \frac{1}{4}exp\left\{-\frac{E_b}{\eta}\frac{2}{\pi^2 W}cos^2(\phi_\delta)\left[\int_0^{\pi WT} sinc(x)dx\right]^2\right\} + \frac{1}{4}exp\left\{-\frac{E_b}{\eta}\frac{2}{\pi^2 W}\left[\int_0^{\pi WT} sinc(x)dx\right]^2\right\} \tag{6.18}$$

Using the values of phase error in Fig. 6.7, for $K = 0.5$ and $K_{oil} = 5$ GHz. It is found that under these assumptions, the BER penalty is equivalent to a process limiting the signal power leaving the noise power constant for half of the samples. From Fig. 6.7 and equation 6.18, it can be derived that a bitrate of 1.3 Gbit/s requires an equivalent 3 dB higher signal to noise ratio to achieve the same BER as the ideal case, with the assumption that each bit sample is taken at $t = T/2$.

6.4 Experimental Results

After transmission, detection and downconversion of the millimetre-wave modulated signal, the 68 Mb/s DPSK modulated spectra is detected by a spectrum analyser at 1.85 GHz. Fig. 6.11 shows the detected spectra for transmission over 0, 25, 40 and 65 km of fibre. The relative power of the detected signal corresponds to the attenuation of the signal from the transmission through the fibre. Worth noting is the decreasing carrier to noise ratio, resulting in a flatter spectra at higher transmission lengths. Fig. 6.12 shows the detected eye diagrams after transmission through 0, 25, 40 and 65 km span of fibre and demodulation. At this detected optical power, error free transmission is possible for all fibre spans, which is confirmed by the open eye diagrams. The asymetry

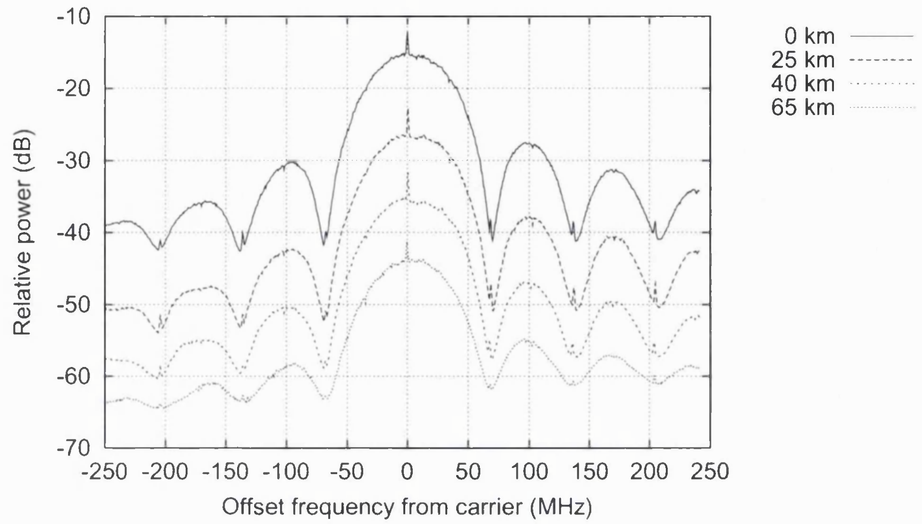

Figure 6.11: Detected signal spectra for downconverted DPSK modulated signal after transmission through 0, 25, 40 and 65 km fibre. The attenuated power corresponds to the signal attenuation of the fibre.

between two consecutive positive bits and two consecutive negative bits in the eye diagrams is due to incomplete filtering of the impulses appearing as a result of the demodulation, described in section 6.2. As the detected optical power is decreased, the received SNR decreases and error free transmission becomes not possible. This is illustrated by Fig. 6.13, where the BER is plotted as a function of detected optical power for the various spans of fibre. No optical amplification was needed for any of these transmission ranges. The differences in required optical power for fixed BER for the different spans of fibre is explained by variations in the optical to millimetre-wave transduction efficiency, discussed earlier in Chapter 3. At 0 km fibre span, -63.8 dBm received millimetre-wave power is measured for -17.5 dBm received optical power. With a photodetector responsitivity of 0.4 A/W, this corresponds to 62% optical to millimetre-wave conversion efficiency, defined as the proportion of received optical power that contributes to the generation of millimetre-wave power. The conversion efficiency for 25 km, 40 km and 65 km are 51%, 55% and 43 % respectively. Using the same equation, B.45, as earlier, the theoretically predicted variations in optical to millimetre-wave transduction efficiency can be plotted in the same manner as done in the first curve in Fig. 3.11. Incorporating the experimentally derived penalties from Fig. 6.13, assuming a fibre dispersion of 20 ps/nm/km, the experimental values derived from the displacements of BER curves is plotted in Fig. 6.13, together with the theory in Fig. 6.14. A good fit of experimental values to theory is observed, possibly with the exception of 65 km, where a slightly lower efficiency than expected is observed.

In order to compare the experimental BER with theory, the data in Fig. 6.13 is converted into terms of received SNR. The detected total signal power after 0 km fibre needed to achieve a bit error rate of 10^{-9} is -63.8 dBm. The receiver noise can with good approximation be assumed

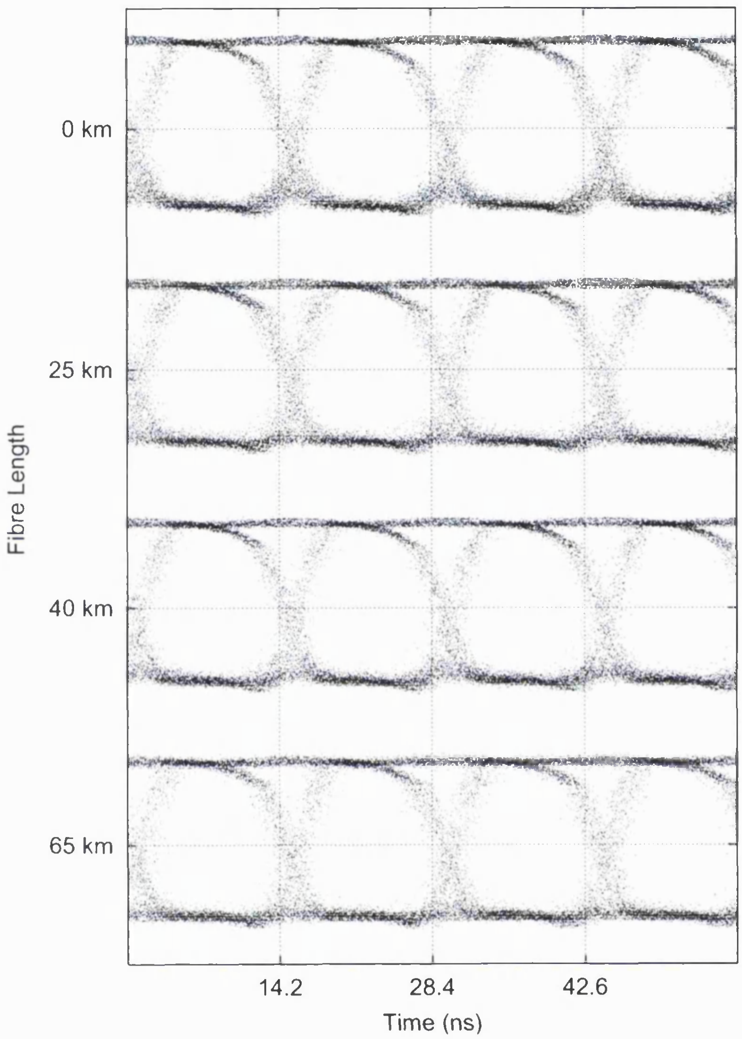

Figure 6.12: Detected eye diagrams for transmission through 0, 25, 40 and 65 km fibre.

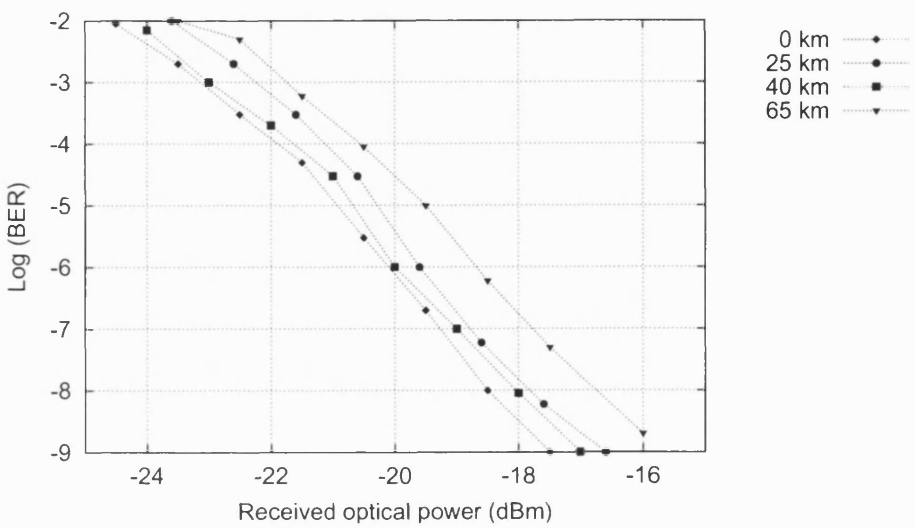

Figure 6.13: Measured bit error rate as a function of received optical power.

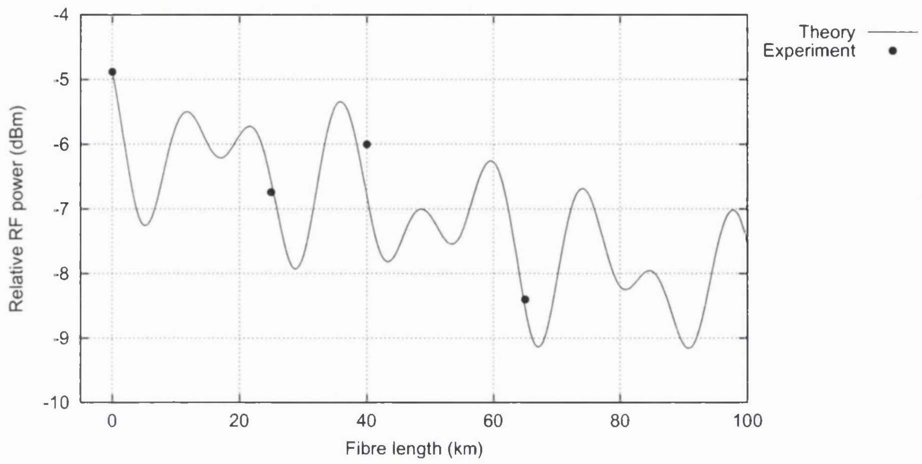

Figure 6.14: Comparison of experimental values to theoretically predicted optical to millimetre-wave conversion efficiency

to be limited by the thermal noise, as no EDFA was used. In the previous section, the receiver was limited by the thermal noise with a spectral density of -170.4 dBm/Hz. The equivalent noise bandwidth is normalised to the bitrate: 68 MHz, taking into account the image noise after down-conversion. The receiver noise power in this bandwidth is then -92.1 dBm, corresponding to a predicted SNR of 28.3 dB. The data for 0 km in Fig. 6.13 is converted into terms of SNR and compare it with the theoretical result showed in Fig. 6.9. The half bandwidth of the IF filter in the receiver is 110 MHz and $WT = 110$ MHz$/68$ MHz$= 1.6$. A significant degradation of the detected BER can be observed compared to the expected receiver noise limited performance. If the experimental BER performance of the receiver/demodulator is measured, however, the result matches theory well, as seen in the figure. The penalty must therefore be produced by the optical link. The degradation can be accounted for by a combination of an increased CNR produced by the injection locking process and a penalty in required SNR. If a 19 dB CNR in 68 MHz bandwidth, corresponding to -97.3 dBc/Hz, is included in the calculation, the slope of the experimental results match the theory. One possible explanation for the penalty in required SNR is distortion of the eyeform in the optical link. If a 2.7 dB penalty is added, the experiment matches theory in the figure. Also included is the impact of increased phase error variance. Increased phase error variance (here set to 0.04 rad^2) does not provide a good fit to the experimental data and is therefore not a likely candidate to explain the degradation of BER.

Increasing the bitrate to 140 Mbit/s, some degradation of performance is observed, illustrated by the Fig. 6.16 where the BER for different transmission lengths is plotted against received optical power. The curves in the plot can be fitted to the theoretically expected result for for $WT = 0.78$, with a fixed added CNR. The result is shown in Fig. 6.17. The equivalent CNR in a noise bandwidth equal to the bitrate is 17.3 dB, 16.8 dB, 15.6 dB and 15.1 dB for 0 km, 25

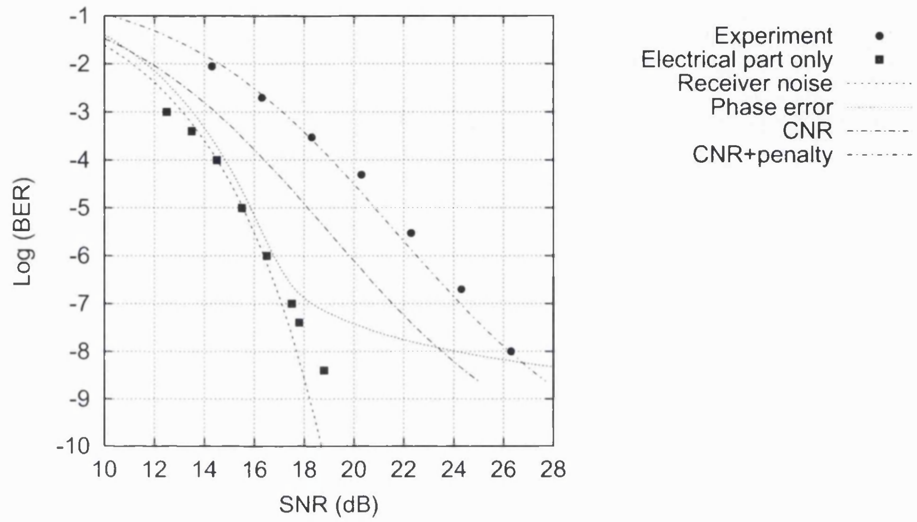

Figure 6.15: BER comparison between experimental and theoretical results, including 19 dB additive CNR and 0.04 rad^2 phase error variance.

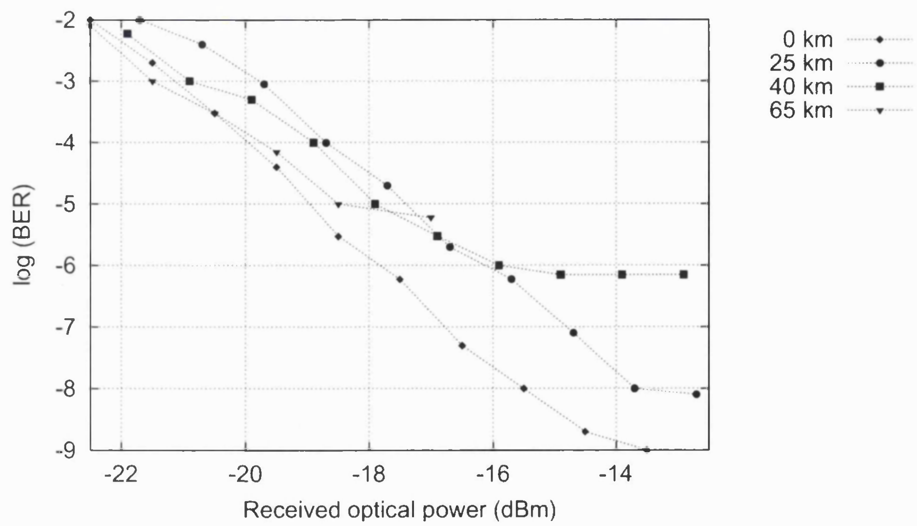

Figure 6.16: Measured bit error rate as a function of received optical power for 140 Mb/s bit rate.

km, 40 km and 65 km. Subtracting the fixed CNR found from the 68 Mbit/s data, 15.9 dB in 140 MHz noise bandwidth, this corresponds to a noise floor of -103.7 dBc/Hz, -102.7 dBc/Hz, 99.7 dBc/Hz and -98.8 dBc/Hz. A probable source for this noise is decorrelation of the carrier due to the chromatic dispersion. PSK modulation is expected to be more affected by the carrier decorrelation then ASK modulation, as it is a source for additional phase noise. These values approximate what would be expected from observing Fig. 4.21 in Chapter 3 well.

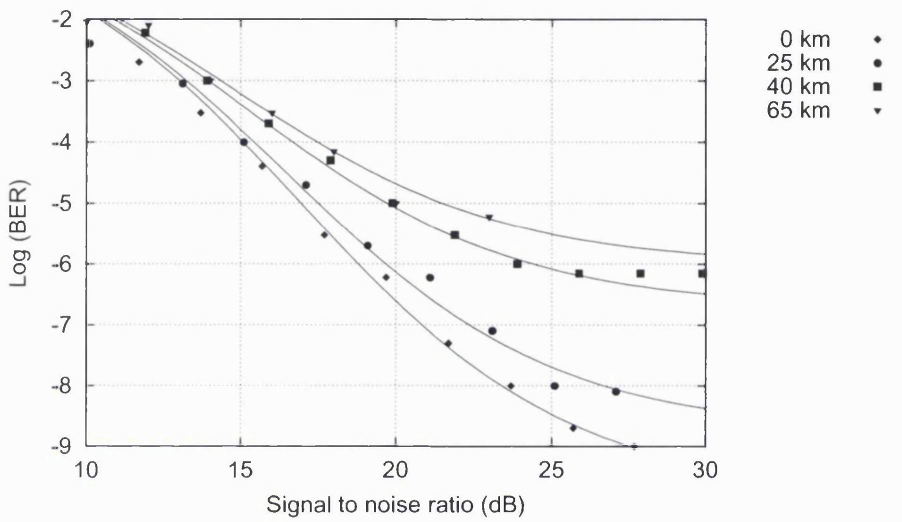

Figure 6.17: Bit error rate as a function of SNR for 140 Mb/s bit rate with theoretical curve fittings included.

6.5 Conclusion

In this Chapter transmission experiments using the OIPLL are derived. 68 Mbit/s DPSK modulation was applied to the reference source for the OIPLL, generating a 36 GHz DPSK modulated subcarrier. There are two advantages of applying the data modulation to the reference, the first being that no external optical modulator was needed, creating a millimetre wave modulated optical source capable of transmitting 68 Mbit/s DPSK modulation that is based around only two commercially available, potentially low cost DFB lasers. The second advantage is more efficient use of the optical power generated in the sources, as no insertion loss of a modulator needs to be accounted for. The efficiency of the signal generation technique is demonstrated by error free transmission (BER$< 10^{-9}$) for 0, 25, 40 and 65 km SSM optical fibre without any use of optical amplification. 62 % optical to millimetre wave efficiency was measured after 0 km fibre transmission. The BER was compared to the theoretical expectations and in addition to the receiver thermal noise, two limiting noise factors were found. The first factor was reduced sensitivity of the demodulation arrangement that could be explained by ISI caused by non-optimal bandwidth of the IF filter and a requirement for low pass filtering of the demodulated baseband signal. The second limiting factor was the CNR of the optically modulated subcarrier that could be explained by degraded performance of the injection locking due to the reference modulation. Increasing the bit rate further to 140 Mbit/s, error free transmission was no longer possible for fibre transmission lengths longer than 25 km. The cause of this was the additive noise generated by the decorrelation of the two heterodyne optical heterodyne lines due to fibre chromatic dispersion for longer transmission distances.

The important conclusions of this chapter are three. The first is the efficiency of the source. Even though the optical output power was moderate, less than 3 dBm, error free transmission was still possible over 65 km of unamplified SSM optical fibre. This is a benefit of the high proportion of the optical power (62%) that directly contributes to the generation of the millimetre wave signal. The second conclusion is that this is a potentially low cost solution, based on two standard lasers, capable of carrying millimetre wave signals with realistic modulation formats, such as PSK or FSK modulation. Finally, it was found that the limit to the data rate of PSK reference modulation of an OIPLL is not set by the phase tracking performance of the injection locking, rather by the noise performance of the OIPLL when using a modulated reference. Improving the performance of the OIPLL, by such methods as using lower linewidth lasers, higher data rates could be applied.

References

[1] L.G. Kazovsky, "Performance analysis and laser linewidth requirements for optical PSK heterodyne Communications systems", *IEEE J. Lightwave Tech.,* Vol. LT-4, pp. 415–425, 1986.

[2] D.A. Atlas and L.G. Kazovsky, "2 Gbit/s PSK heterodyne communication system using optical phase-locked loop," *Elec. Lett.,* vol. 26, pp. 1030–1032, 1990.

[3] Digital modulation in communications systems — an introduction", *Hewlett Packhard Application note 1298*, 1997.

[4] Final Report ACTS project AC215 CRABS, document reference: AC215/TEL/RD/AR/P/D5P2B/b1

[5] K. Koga, Y. Fujimoto and S. Tejima, "Radio Link Configurations of Broad-band Wireless Access System," *IEEE International Conference on Personal Wireless Communication,* pp. 354–358, 1999.

[6] A. Arunachalam, "Global standardization efforts of BWA systems based on cable modem," *IEEE Emerging Technologies Symposium: Broadband, Wireless Internet Access,* pp. 1–4, 2000.

[7] L. Noel, D. Wake, D.G. Moodie, D.D. Marcenac, L.D. Westbrook and D. Nesset, "Novel techniques for high-capacity 60-GHz fiber-radio transmission systems," *IEEE Trans. Microwave Theory Tech.,* vol. 45, pp. 1416–1423, 1997.

[8] R.-P. Braun, G. Grosskopf, H. Heidrich, C. von Helmolt, R. Kaiser, K. Kruger, U. Kruger, D. Rohde, F. Schmidt, R. Stenzel and D. Trommer, "Optical microwave generation and transmission experiments in the 12- and 60-GHz region for wireless communications," *IEEE Trans. Microwave Theory Tech.,* vol. 46, pp. 320–330, 1998.

[9] R.-P. Braun, G. Grosskopf, D. Rohde and F. Schmidt, "Low-phase-noise millimeter-wave generation at 64 GHz and data transmission using optical sideband injection locking, *IEEE Photon Tech. Lett.,* vol. 10, pp. 728–730, 1998.

[10] G.H. Smithand d. Novak, "Broad-band millimeter-wave (38 GHz) fiber-wireless transmission system using electrical and optical SSB modulation to overcome dispersion effects, *IEEE Photon Tech. Lett.,* vol. 10, pp. 141–143, 1998.

[11] U. Gliese, T.N. Nielsen, S. Norskov and K.E. Stubkjaer, "Multifunctional fiber-optic microwave links based on remote heterodyne detection," *IEEE Trans. Microwave Theory Tech.,* vol 46, pp. 458–468, 1998.

[12] S. Levy, R. Nagarajan, A. Mar, P. Humphrey and J.E. Bowers, "Fibre-optic PSK subcarrier transmission at 35 GHz using a resonantly enhanced semiconductor laser," *Electron. Lett.,* vol. 28, pp. 2103–2104, 1992.

[13] T. Ohno, K. Sato, S. Fukushima, Y. Doi and Y. Matsuoka, "Application of DBR mode-locked lasers in millimeter-wave fiber-radio system," *IEEE J. Lightwave Tech.,* Vol. 18, pp. 44–49, 2000.

[14] Y. Doi, S. Fukushima, T. Ohno, Y. Matsuoka and H. Takeuchi, "Phase shift keying using optical delay modulation for millimeter-wave fiber-optic radio links," *J. Lightwave Tech.,* Vol. 18, pp. 301–307, 2000.

[15] T. Kuri, K. Kitayama and Y. Ogawa, "Fiber-optic millimeter-wave uplink system incorporating remotely fed 60-GHz-band optical pilot tone," *IEEE Trans. Microwave Theory Tech.,* vol. 47, pp. 1332–1337, 1999.

[16] K.-I. Kitayana and R.A. Griffin, "Optical downconversion from millimeter-wave to IF-band over 50 km-long optical fiber link using an electroabsorption modulator," *IEEE Photon Tech. Lett.,* vol. 11, pp. 287–289, 1999.

[17] R. Adler, "A study of locking phenomena in oscillators," *Proc. IEE,* vol. 34, pp. 351–357, 1946.

[18] U. Gliese, "Optical Generation of Microwave Signals", PhD. thesis, Electromagnetics Institute, Technical University of Denmark, Lyngby, Denmark, 1992.

[19] J.H. Park, "On binary DPSK detection," *IEEE Trans. Commun.,* vol. 26, pp. 484–486, 1978.

[20] A.B. Carsson, "Communications systems" *2nd Ed.,* McGraw-Hill, pp. 396–404, 1975.

Chapter 7

Conclusion

7.1 Summary of the Thesis

Summary of chapter 1

The first chapter, 'Introduction', gives a broad introduction to relevant topics together with a review of relevant prior literature. The first section 1.1 gives a review of millimetre-wave wireless radio. The transmission properties are listed and the main applications, notably fixed wireless broadband access systems, are also reviewed. The second section, 1.2 gives a background to millimetre-wave radio over fibre. The main applications where it can with advantage be used and the benefits of using it are treated. Some properties of radio over fibre transmission and some systems aspects are also investigated. The chapter concludes with a statement of the objectives and outline of the thesis.

Summary of chapter 2

In the second chapter, 'Review of Millimetre Wave Radio Over Fibre Transmission Experiments', different millimetre wave modulated optical sources are investigated. It is shown how these sources can be used to transmit data modulated millimetre wave radio signals over spans of optical fibre. In the introduction a number of desired features of the millimetre wave source are defined. Thereafter, the different sources of millimetre wave modulated optical signals that have been demonstrated are described. It is shown how data can be applied to these sources. Finally, some millimetre wave radio over fibre transmission experiments are summarised in Table 2.2. Based on these investigations, the strengths of the different sources can be defined in relation to the desirable features defined in the introduction in the chapter.

The main conclusion of the chapter was that the single sideband millimetre wave modulated sources can be divided into two groups, modulator based sources and mode locking sources, the modes originating either from one source or from two sources. Modulator based sources have the limitation of inefficient utilisation of optical power, making the use of optical amplification in millimetre wave radio over fibre links necessary. Locking based sources had the limitation of generally poor stability in the form of narrow locking range. The one source that delivered sufficient power to avoid the use of optical amplification in the radio over fibre link together with a wide locking range was the optical injection phase-lock loop (OIPLL). However, no millimetre wave OIPLL has yet been demonstrated.

Summary of chapter 3

In this chapter, 'Carrier Generation and Transmission: Theory', the theoretical basis for the first demonstration of a millimetre wave OIPLL is described, including fundamental stability, noise performance and differential path effects. The expected behaviour of the generated millimetre wave modulated output for transmissoin through fibre is also investigated. It is found that the use of a combined OPLL and OIL system overcomes many of the limitations of using either an OPLL or OIL alone, such as the requirement for narrow linewidth lasers or short loop delay of the OPLL, or the limited locking range of the OIL. The combination will allow the use of a wider bandwidth OPLL because of the stabilising effect of the injection locking. Furthermore, it is shown how the stability problems relating to differential path effects, as reported from earlier work with the OIPLL, can be overcome by using the reflection of the master laser field from the slave laser. The degradation of the generated carrier due to fibre transmission is investigated, both with regard to the decorrelation of the two main optical lines and due to interference with the additional beats originating from the unwanted master laser FM sidebands.

Summary of chapter 4

In this chapter, 'Carrier Generation and Transmission: Experiments', the first experimental demonstration of a millimetre wave OIPLL is described. It is experimentally shown how the stability problems relating to differential path effects can be overcome by using the reflection of the master laser field from the slave laser. Modelling predicting the magnitude of the reflection and the stability of the injection locking was found to be in good agreement with experimentally established data. Experimental results of the spectral characteristics of the generated carrier and of the locking range were presented. The degradation of the generated carrier due to fibre transmission matched what would be expected. It is shown that the locking range was limited by the loop electronics design, and that the locking range could be greatly improved using alternative frequency tuning mechanisms of the slave laser. The potentially wide frequency range of the OIPLL was proved by demonstrating the generation of spectrally pure carriers in the range of 4 GHz to 60 GHz, limited by the frequency range of the test equipment. Due to limitations of the frequency range of the components, the PLL part could only operate between 26 GHz and 40 GHz. Outside this frequency range, only OIL was used. However, using suitable components, the OIPLL could be designed to operate across the entire frequency range. It is also shown how the spectral purity of the generated millimetre wave carrier could be improved further by carrier filtering in the optical receiver, improving the noise performance at offset frequencies beyond 2 MHz from the carrier.

Finally, a described is given of how two undesirable features of the demonstrated OIPLL can be avoided. By adding a second OIPLL slave laser, the intensity fluctuations of the generated carrier, due to differential path lengths and fibre chromatic dispersion, can be eliminated. By the efficient filtering of the master laser signal, the optical output is dominated by the slave laser modes, with a high suppression of unwanted sidemodes and low sensitivity to changes in the optical length.

Summary of chapter 5

In this chapter, 'Amplitude Shift Keying Transmission Experiments', transmission results of a 36 GHz millimetre-wave modulated optical carrier with 140 Mbit/s NRZ ASK data applied to it, are presented. These results have been compared to theoretical predictions with good agreement obtained. Error-free transmission was achieved for 0, 25, 40 and 65 km of fibre. Evidence of the efficiency of the method of generation of millimetre-wave modulated optical signals is provided not only by the measured optical to millimetre-wave conversion efficiency, 56 % after 25 km fibre transmission, but also confirmed by the fact that error-free transmission was available for transmission for distances up to 25 km fibre span, even though the launched power was small, -8 dBm. An increase of launched power would give sufficient margin to overcome splitting losses, to serve a number of optical receivers. Tolerance to fibre dispersion is proved by the narrow range of required optical power needed to achieve a fixed BER for different lengths of fibre. The variations of required optical power fits very well with what theory predicts from the OIPLL, except for very low values of BER, where there is a small penalty in the experimental results obtained.

The receiver is found to be limited in performance by thermal noise and at low BER, the CNR of the generated millimetre wave modulated optical signal. If optical amplification is used, the receiver is also affected by signal-ASE noise. It is also found that the receiver design was suboptimal due to inadequate predetection filtering. A second limitation of the receiver design used was lack of filtering at the image RF frequency at 39.7 GHz, before RF to IF downconversion. This adds a further 1.2 dB degradation of the receiver sensitivity. This chapter successfully verified the feasibility of the OIPLL as a heterodyne optical source for distribution of broadband data modulated millimetre-wave signals.

Summary of chapter 6

In this chapter, 'Differential Phase Shift Keying Transmission Experiments', transmission experiments using the OIPLL are derived. 68 Mbit/s DPSK modulation was applied to the reference source for the OIPLL, generating a 36 GHz DPSK modulated subcarrier. By applying the data modulation to the reference, no external optical modulator was needed, creating a millimetre wave modulated optical source capable of transmitting 68 Mbit/s DPSK modulation based around only two commercially available, potentially low cost DFB lasers. Moreover, the optical power generated in the sources is more efficiently used, as no insertion loss of a modulator needs to be accounted for. The efficiency of the signal generation technique is demonstrated by error free transmission (BER$< 10^{-9}$) for 0, 25, 40 and 65 km SSM optical fibre without any use of optical amplification. 62 % optical to millimetre wave conversion efficiency was measured after 0 km fibre transmission. The BER is compared to the theoretical expectations and in addition to the receiver thermal noise, two limiting noise factors are found. The first factor is reduced sensitivity of the demodulation arrangement that could be explained by ISI caused by non-optimal bandwidth of the IF filter and a requirement for low pass filtering of the demodulated baseband signal. The second limiting factor is the CNR of the optically modulated subcarrier that could be explained by degraded performance of the injection locking due to the reference modulation. Increasing the bit rate further to 140 Mbit/s, error free transmission was no longer possible for fibre transmission lengths longer than 25 km. The cause was the additive noise generated by the decorrelation of the two heterodyne optical heterodyne lines due to fibre chromatic dispersion for longer transmission distances.

The important conclusions are that even though the optical output power was moderate, less than 3 dBm, error free transmission was still possible over 65 km unamplified SSM optical fibre. This is a benefit of the high proportion of the optical power (62%) that directly contributes to the generation of the millimetre wave signal. It is a potentially low cost solution, based on two standard lasers, capable of carrying millimetre wave signals with realistic modulation formats, such as PSK or FSK modulation. Finally, it is found that the limit to the data rate of PSK reference modulation of an OIPLL is not set by the phase tracking performance of the injection locking, rather by the noise performance of the OIPLL when using a modulated reference. Improving the performance of the OIPLL, by such methods as using lower linewidth lasers, higher data rates could be applied.

7.2 Objectives Realised

In the introduction of the thesis, the two main objectives of this work were defined:

1. To realise a millimetre-wave modulated optical source that as far as possible satisfies the need for an efficient low-cost, high performance and highly flexible single sideband modulated optical source.

2. To use the developed optical source to demonstrate high performance millimetre-wave radio over fibre transmission.

The first objective has been demonstrated by the first millimetre wave optical injection phase-lock loop. It is based on two standard pigtailed DFB lasers and produces single sideband modulated optical signals with high purity, -93 dBc/Hz phase noise spectral density of the generated millimetre wave signal at 10 kHz offset. Stability is proven by the wide locking range, more than 30 GHz. Efficiency is proven by as high as 62% optical to millimetre-wave transduction efficiency and a potential frequency tuning range of 4 GHz to 60 GHz can be achieved using suitable components. The second objective has been demonstrated by two transmission experiments, 36 GHz 140 Mbit/s ASK modulated radio over fibre transmission over up to 65 km optical fibre, or 25 km unamplified fibre and 36 GHz 68 Mbit/s DPSK modulated radio over fibre transmission over up to 65 km unamplified optical fibre. No dispersion compensation was needed, indicating dispersion resistant generation of optical signals.

7.3 Novel Results

The principal novel results of this work are:

1. The development of the first millimetre-wave optical injection phase-lock loop. Previously an OIPLL based on free space optical components has been demonstrated at 8 and 16 GHz [1] with a locking range limited by the optical path matching in the experimental arrangement. In this work, significantly higher generated frequencies have been demonstrated. The main results are at 36 GHz, with a possibility of operation at 60 GHz and above, with the use of proper components. Furthermore, this has been demonstrated in a fibre-integrated experimental arrangement where the limitations of the locking range due to optical path matching is overcome. The locking range is here limited by the tuning range of the slave laser.

2. The first millimetre-wave radio over fibre transmission experiment using optical phase-lock loop techniques. Even though OPLL based generation of millimetre wave modulated optical signals has been demonstrated using external cavity lasers [2], these sources have not been used for radio over fibre transmission. The highest frequency where an OPLL has been used for broadband radio over fibre transmission is at 9 GHz [3].

3. The widest bandwidth modulation applied to the microwave reference in an optical phase-lock loop or an optical injection locking based heterodyne system. In OPLL based systems, the bandwidth limit for modulation is set by the loop delay. Even in a wideband OPLL with a loop delay as low as 400 ps, the demonstrated modulation bandwidth is 6 MHz [4]. In injection locking based systems, the limitations for locking to a modulated reference has not been experimentally investigated in the context of radio over fibre. Systems where data modulation has been applied to the injection current of the slave laser [5] and separate delivery of the data modulated on an IF subcarrier for remote upconversion at the base station [6] have been demonstrated. For coherent optical applications, injection locking has generally been applied as a method for carrier recovery from a modulated optical signal [7]. In the present work, successful locking to a non band-limited 68 Mbit/s DPSK modulated reference has been demonstrated. Furthermore, it is predicted that the bit rate can be increased to more than 1 Gbit/s in the locking range demonstrated, provided sufficient spectral purity can be achieved in the injection locking.

4. The longest millimetre wave radio over fibre transmission demonstrated, supporting broadband data rates (>10 Mb/s) and not using optical amplification. Notable previous broadband radio over fibre transmission experiments not using optical amplification include transmission of 6.8 GHz signals with a 36 MHz bandwidth over 35 km fibre using a directly modulated laser [8], transmission of 64 GHz, 155 Mb/s OQPSK modulated signals over 12.8 km fibre using optical injection locking [5] and transmission of 39.6 GHz, 500 Mb/s BPSK modulated signals over 9 km fibre using a dual mode, mode locked laser [9]. Here, radio over fibre transmission of a 36 GHz, 68 Mbit/s DPSK modulated carrier over 65 km optical fibre is demonstrated, using no optical amplification or dispersion compensation.

7.4 Further Work

This work can be further developed in a number of directions. In the concept of generation of millimetre wave modulated optical signals, the OIPLL will be greatly improved by the addition of a second injection locked laser. This will bring advantages in the form of increased stability of the generated millimetre wave power, increased resistance to fibre chromatic dispersion and it will allow the use of lower speed electronics, or generate higher frequencies. How this can be achieved is presented in more detail in the conclusion of chapter 4. One further improvement of the design of the OIPLL would be the application of uncooled laser diodes. If two uncooled laser diodes were to share the same heatsink, the large locking range would allow the OIPLL to retain lock over a range of external temperature conditions, as the differential temperature of the two lasers can vary in a range as large as 3.5°C without loss of lock. The use of uncooled lasers is attractive, as no Peltier cooler will be needed. As the expected lifetime of an uncooled DFB laser generally is longer than a Peltier cooler, the use of uncooled lasers in an OIPLL will not only result in a less complex arrangement, the expected lifetime of the OIPLL will also increase. This would be an important step towards a practical and potentially very low cost millimetre-wave modulated optical source.

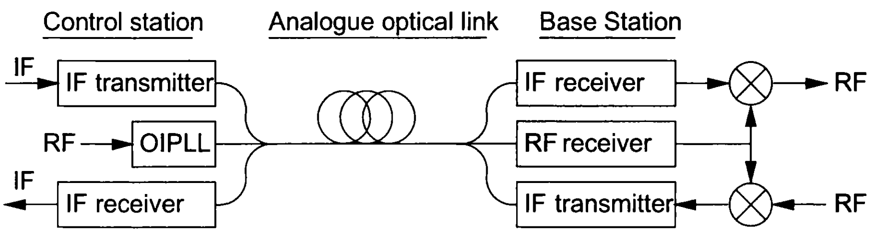

Figure 7.1: Proposed radio over fibre architecture including the OIPLL

In a systems situation, the OIPLL has been shown capable of transmission of phase/frequency modulated signals, or amplitude modulated signals, by two different methods of applying the data to the OIPLL. However, a convenient method of applying the more complex QAM modulation, commonly used in millimetre wave wireless applications, has not been demonstrated. Also, the modulation has been applied directly to the millimetre wave modulation. This has allowed very efficient transmission of the signals, enabling the long unamplified fibre transmission demonstrated here. In a scenario where radio over fibre link includes both an uplink and a downlink, and the base station needs to be of minimised complexity, a different approach has to be taken. In order to reduce complexity in the base station, the received uplink radio signal should be downconverted, to avoid using a millimetre-wave modulated optical signal source in the base station. Therefore, a pure unmodulated millimetre wave carrier needs to be delivered to the base station. One solution that satisfies both the need for QAM modulation and base station carrier delivery is outlined in Fig. 7.1. It is based on remote upconversion with optical delivery of the millimetre wave carrier on a separate optical wavelength. The data is applied to an IF subcarrier, at a frequency low enough to be directly modulated on to a low cost laser diode and transmitted through optical fibre with low dispersion penalty. Upconversion from and to millimetre wave frequencies then takes place in the base station. With this architecture, the technical difficulties of generating a millimetre wave modulated optical signal is then separated from the requirement of high performance, flexible transmission of a data modulated IF subcarrier. The OIPLL can then with advantage be used in combination with the OILO to deliver a very spectrally pure millimetre-wave carrier. Furthermore, a single OIPLL arrangement can be used to deliver a millimetre-wave carrier to a multitude of base stations, allowing cost sharing, with directly IF modulated WDM lasers delivering the data to the individual base stations.

References

[1] C. Walton, A.C. Bordonalli and A.J. Seeds, "High-performance heterodyne optical injection phase-lock loop using wide linewidth semiconductor lasers", *IEEE Photonics Technology Letters*, vol. 10, pp. 427–429, 1998.

[2] A.C. Davidson, F.W. Wise and R.C. Compton, "Low phase noise 33-40-GHz signal generation using multilaser phase-locked loops", *IEEE Photon. Tech. Lett.* vol. 10, pp. 1304-1306, 1998.

[3] U. Gliese, T. Norskov, S. Norskov and K.E. Stubkjaer, "Multifunctional fiber-optic microwave links based on remote heterodyne detection", *IEEE Trans. Microwave Theory Tech.*, vol. 46, pp. 458-468, 1998.

[4] T.N. Nielsen, U. Gliese, T. Christensen, H. Hoegh and K.E. Stubkjaer, "Highly linear and transparent 3-18 GHz optical microwave link", *IEEE MTT-S Int. Microwave Symposium Digest*, pp. 491-494, 1994.

[5] R,P. Braun, G. Grosskopf, D. Rohde and F. Schmidt, "Low-phase-noise millimeter-wave generation of 64 GHz and data transmissionusing optical sideband injection locking", *IEEE Photon. Tech. Lett.* vol. 10, pp. 728-730, 1998.

[6] L. Noel, D. Marcenac and D. Wake, "120 Mbit/s QPSK radio-fibre transmission over 100 km of standard fibre at 60 GHz using a master/slave injection-locked DFB laser source", *Elec. Lett.*, vol. 32, pp. 1895-1897, 1996.

[7] O. Lidoyne, P. Gallion and D. Erasme, "Analysis of a homodyne receiver using an injection-locked semiconductor laser", *IEEE J. Lightwave Tech:*, vol. 9, pp. 659-665, 1991.

[8] W.I. Way, R.S. Wolff and M. Krain, "A 1.3-μm 35-km fiber-optic microwave multicarrier transmission system for satellite earth stations," *J. Lightwave Technol.*, vol. LT-5, pp. 1325-1331, 1987.

[9] T. Ohno, K. Sato, S. Fukushima, Y. Doi and Y. Matsouka, "Application of DBR mode-locked lasers in millimeter-wave fiber-radio system", *IEEE J. Lightwave Tech.*, vol. 18, pp. 44-49, 2000.

Appendix A

Fibre Chromatic Dispersion

In standard singlemode fibre, the refractive index has a dependence on the optical frequency. For small frequency variations, relative to the absolute optical frequency, this result in a first order optical frequency dependent group delay according to:

$$\frac{d\tau}{d\nu} = \frac{d\tau}{d\lambda}\frac{d\lambda}{d\nu} = \left(-\frac{1}{L}\frac{d\tau}{d\lambda}\right)\left(\frac{\lambda^2}{c}\right)L = D(\lambda)\left(\frac{\lambda^2}{c}\right)L \tag{A.1}$$

τ : Time delay (s)
ν : Optical frequency (Hz)
λ : Optical wavelength (m)
L : Optical fibre length
D : Fibre chromatic dispersion

A typical value of the chromatic dispersion, D, is 17 ps/nm/km at 1550 nm in standard singlemode fibre. The group delay at an optical frequency ν, close to a central frequency, ν_c, is then given by:

$$\tau(\nu) \simeq \tau(\nu_c) + (\nu - \nu_c)\left.\frac{d\tau}{d\nu}\right|_{\nu=\nu_c} \tag{A.2}$$

And the phase of the optical signal is given by:

$$\phi(\nu) = 2\pi\int_0^{\nu} \tau(\nu')d\nu' = 2\pi\nu\tau(\nu_c) + 2\pi\left(\frac{(\nu-\nu_c)^2}{2} - \frac{\nu_c^2}{2}\right)\left.\frac{d\tau}{d\nu}\right|_{\nu=\nu_c} \tag{A.3}$$

The transfer function of the fibre is then given by:

$$H(f) = e^{-j\phi(f_m)} = e^{-j\pi D\frac{\lambda^2}{c}Lf_m^2} \tag{A.4}$$

where f_m is the offset frequency from ν_c; $f_m = \nu - \nu_c$. Consider an optical field consisting of three coherent optical components at ν_c and $\nu_c \pm f_m$:

$$E_{in} = E_0 e^{2\pi j\nu_c t+\phi_0(t)} + E_{us}e^{j(2\pi(\nu_c+f_m)t+\phi_0(t))} + E_{ls}e^{j(2\pi(\nu_c-f_m)t+\phi_0(t))} \tag{A.5}$$

E_0 Field of fundamental line

E_{ul} Field of upper modulation sideband

E_{ls} Field of lower modulation sideband

ϕ_0 Signal phase

After transmission over fibre, a frequency dependent relative phase shift multiplies the signal:

$$E_{out} = H(f)E_{in} = E_0 e^{j(2\pi\nu_c t+\phi_0(t))} + \\ + E_{us}e^{j(2\pi(\nu_c+f_m)t+\phi_0(t))}e^{-j\pi D\frac{\lambda^2}{c}Lf_m^2} + E_{ls}e^{j(2\pi(\nu_c-f_m)t+\phi_0(t))}e^{-j\pi D\frac{\lambda^2}{c}L(-f_m)^2} \quad (A.6)$$

Using square law detection in the receiver: $i_{pin} \sim |E_{out}|^2$, and separating the frequency terms at f_m we obtain:

$$i_{pin}\big|_{f=f_m} \sim E_0 E_{us} e^{2\pi jf_m t + j\pi D\frac{\lambda^2}{c}Lf_m^2} + E_0 E_{ls} e^{2\pi jf_m t - j\pi D\frac{\lambda^2}{c}Lf_m^2} \quad (A.7)$$

We observe that when the phase term $\pi D\frac{\lambda^2}{c}Lf_m^2 = \frac{\pi}{2} + n\pi$ where n is an integer, the detected signal has a minimum, and when $\pi D\frac{\lambda^2}{c}Lf_m^2 = n\pi$ there is a maximum. In double sideband modulation, when the upper sideband (E_{us}) is equal to the lower sideband magnitude (E_{ls}), total extinction of the signal occurs at regular intervals of fibre length, while for single sideband modulation, putting $E_{ls} = 0$, this effect is not present. As a numerical example, for D=17ps/nm/km, λ=1550 nm and 36 GHz modulation frequency, the first zero occurs at 2.8 km of fibre. For this reason, single sideband or close to single sideband modulation ($E_{us} >> E_{ls}$) is prefered if dispersion resistant modulation is required.

Single sideband modulation is not unaffected by fibre chromatic dispersion. Through fibre transmission, the coherence between the frequency components is gradually degraded due to the spectral width of the source(s). Since the spectral width of the source generally originates from phase fluctuations, this degradation is often termed phase-induced intensity noise. The single sideband modulated signal can be expressed as the sum of a laser field and a frequency (f_m) and time (τ_0) shifted image of itself, where the frequency shift corresponds to the modulation frequency and the time shift comes from the fibre chromatic dispersion:

$$\overline{E}(t) = \overline{E_0}(t) + \iota\overline{E_0}(t+\tau_0)e^{j2\pi f_m t} \quad (A.8)$$

ι corresponds to the amplitude ratio between the two fields. After square law photodetection, the autocorrelation function of the detected signal is related to the second order autocorrelation function as:

$$\mathscr{C}_I(\tau) = eR\mathscr{C}_E^{(2)}(0)\delta(\tau) + R^2\mathscr{C}_E^{(2)}(\tau) \quad (A.9)$$

where e is the electron charge, R is the detector responsivity and $\mathscr{C}_E^{(2)}(\tau)$ is the second order optical autocorrelation function:

$$\mathscr{C}_E^{(2)}(\tau) = <\overline{E}(t)\overline{E}^*(t)\overline{E}(t+\tau)\overline{E}^*(t+\tau)> \tag{A.10}$$

Inserting A.8 into A.10 and evaluating, 16 components are found of which the ten that include $e^{\pm j2\pi f_m t}$ can be ignored due to the time dependency. Putting $E_0(t) = \overline{E_0}e^{j(2\pi\nu_0 t+\phi(t))}$ the remaining terms are:

$$\frac{\mathscr{C}_E^{(2)}(\tau)}{E_0^4} = (1+\iota^2)^2 + \iota^2 e^{j2\pi f_m\tau} < e^{j(\Delta\phi(t+\tau_0,\tau)-\Delta\phi(t,\tau))} > + \iota^2 e^{-j2\pi f_m\tau} < e^{-j(\Delta\phi(t+\tau_0,\tau)-\Delta\phi(t,\tau))} > \tag{A.11}$$

where $\Delta\phi(t,\tau) = \phi(t+\tau) - \phi(t)$. Using the relation $< e^{\pm j\Delta\phi(t)} >= e^{-\frac{1}{2}<\Delta\phi(t)^2>}$ where $< \Delta\phi(t)^2 >$ is the phase error variance, the above expression can be rewritten:

$$\begin{aligned}\frac{\mathscr{C}_E^{(2)}(\tau)}{E_0^4} &= (1+\iota^2)^2 + 2\alpha^2\cos(2\pi f_m\tau)\cdot \\ &\cdot\exp\left\{-<\Delta\phi(\tau_0)^2> - <\Delta\phi(\tau)^2> + \frac{<\Delta\phi(\tau-\tau_0)^2>}{2} + \frac{<\Delta\phi(\tau-\tau_0)^2>}{2}\right\}\end{aligned} \tag{A.12}$$

For semiconductor lasers biased well above threshold, the phase error variance can be assumed to increase linearly with time:

$$<\Delta\phi(t)^2> = \Delta\nu_m|\tau| \tag{A.13}$$

where $\Delta\nu_m$ is the combined angular FWHM of the Lorentzian laser field spectrums. Using A.13 in A.12:

$$\frac{\mathscr{C}_E^{(2)}(\tau)}{E_0^4} = (1+\iota^2)^2 + \begin{cases} 2\iota^2\cos(2\pi f_m\Delta\nu_m\tau)e^{-2\gamma\tau} & ,\tau<\tau_0 \\ \\ 2\iota^2\cos(2\pi f_m\Delta\nu_m\tau)e^{-2\gamma\tau_0} & ,\tau_0<\tau \end{cases} \tag{A.14}$$

Inserting A.14 into A.9, disregarding the shot noise term $(eR\mathscr{C}_E^{(2)}(0)\delta(\tau))$ and using the Fourier transform gives us the heterodyne photocurrent spectra:

$$\begin{aligned}\frac{S_I(f)}{R^2E_0^4} &= (1+\iota^2)^2\delta(f) + \iota^2 e^{-2\pi\Delta\nu_m\tau}\delta(f-f_m) + \frac{\Delta\nu_m}{2\pi\Delta\nu_m^2 + (f-f_m)^2}\cdot \\ &\cdot\left[1 - e^{-2\pi\Delta\nu_m\tau}\left\{\cos(-2\pi(f-f_m)\tau) + \frac{\Delta\nu_m^2}{f-f_m}\sin(-2\pi(f-f_m)\tau)\right\}\right]\end{aligned} \tag{A.15}$$

The first term corresponds to the DC photocurrent term, the second term to the coherent beat between the two lines, and the third term represents the decorrelation. At small differential delay times ($\tau \sim 0$), the signal is dominated by the coherence term, for intermediate delay times the decoherent term takes the shape of a sinc spectrum and for very large delay times total decorrelation occurs and the total spectrum takes a Lorentzian shape.

For moderate fibre transmission lengths, two effects can be isolated. The first is the transfer of power from the coherent term to the incoherent term. A power penalty can be derived from A.15 and A.1:

$$\Gamma_d = e^{2\pi\Delta\nu_m D(\lambda)\frac{\lambda^2}{c}Lf_m} \tag{A.16}$$

The second effect is the increase in noise floor around the carrier, due to decorrelation originating from the second term.

Appendix B

Optical Injection Locking Theory

Fabry-Perot Lasers:

Consider a semiconductor laser with complex output electric field; E, a carrier number; N and an injected field; E_i. The following rate equation is then valid for the laser [1]:

$$\dot{E} = E\left\{ j\Delta\omega + \frac{1}{2}\left[G - \frac{1}{\tau_p} \right] \right\} + \frac{1}{\tau_o}E_i \tag{B.1}$$

$$\dot{N} = M - \frac{N}{\tau_e} - GP \tag{B.2}$$

G	Optical gain per second
τ_p	Photon lifetime
$\Delta\omega$	Slave laser frequency shift from resonant free running frequency, ω_f
τ_o	Laser cavity round trip time
M	Carrier injection rate
q	Electron charge
P	Photon number in laser cavity

In this appendix, all time derivates are represented by dots over the time dependent variable. Terms for the slave laser spontaneous emission and Langevin noise forces have here been excluded because of the much stronger injected field.

Equations B.2 and B.1 can be linearised if new variables are defined with steady state values and deviations from the steady state as:

$$E_i = E_{io} + \hat{e}_i$$
$$E = E_o + \hat{e}$$
$$P = P_o + \hat{p}$$
$$M = M_o + \hat{m}$$
$$N = N_o + \hat{n} \tag{B.3}$$

The deviation of the master laser field, $\hat{e}_i$ represents an injected field component that induces only a small perturbation on the laser cavity field. That means that $\hat{e}_i$ is either very small compared to the main field component, E_{mo}, or having a frequency shift from the central frequency, ω_m, far away from the locking range of the locked system. The gain can also be expressed in its first order Taylor expansion with photon number and carrier number as variable [2]:

$$G = \frac{1}{\tau_p} + G_N(N - N_f) + G_P(P - P_f) \tag{B.4}$$

G_N Differential gain relative to carrier number
G_P Differential gain relative to photon number
P_f Steady state free running photon number
N_f Steady state free running carrier number

Likewise, the frequency shift can be evaluated around the impact of chance in photon and carrier number:

$$\Delta\omega = \omega_f - \omega_i + \frac{\alpha}{2} G_N(N - N_f) + \frac{\beta}{2} G_P(P - P_f) \tag{B.5}$$

α Linewidth enhancement factor
β Factor relating to photon induced cange of refractive index
ω_f Free running laser centre frequency
ω_i Injected line centre frequency

The steady state equations can now be obtained by assuming no perturbations and making the time derivates zero:

$$0 = j(\omega_f - \omega_i) + \frac{1 + j\alpha}{2} G_N(N_o - N_f) + \frac{1 + j\beta}{2} G_P(P_o - P_f) + \frac{1}{\tau_o} \frac{E_{io}}{E_o} \tag{B.6}$$

$$0 = M_o - \frac{N_o}{\tau_e} - P_o \left(\frac{1}{\tau_p} + G_N(N_o - N_f) + G_P(P_o - P_f) \right) \tag{B.7}$$

Using the steady state gain, $G_o = \frac{1}{\tau_p} + G_N(N_o - N_f) + G_P(P_o - P_f)$, the two equations can be simplified as:

$$0 = j\Delta\omega_o + \frac{1}{2}\left(G_o - \frac{1}{\tau_p}\right) + \frac{1}{\tau_o}\frac{E_{io}}{E_o} \tag{B.8}$$

$$0 = M_o - \frac{N_o}{\tau_e} - P_o G_o \tag{B.9}$$

The linearised equations are now derived by inserting B.3 to B.7 into B.1 and B.2, and making all second order derivates zero:

$$\dot{\hat{e}} = E_o\left(\frac{1+j\alpha}{2}G_N\hat{n} + \frac{1+j\beta}{2}G_P\hat{p}\right) - \frac{\hat{e}E_{io}}{\tau_o E_o} + \frac{\hat{e}_i}{\tau_o} \tag{B.10}$$

$$\dot{\hat{n}} = \hat{m} - \frac{\hat{n}}{\tau_e} - P_o(G_N\hat{n} + G_P\hat{p}) - \frac{\hat{p}}{P_o}(M_o - \frac{N_o}{\tau_e}) \tag{B.11}$$

The stability around ω_o of the system is better studied if equation B.6 is simplified. If α is assumed to be equal to β and introducing the differential gain: $\Delta G = G_N(N_o - N_f) + G_P(P_o - P_f)$ and the steady state frequency deviation: $\Delta\omega = \omega_f - \omega_i + \frac{\alpha}{2}G_N(N - N_f) + \frac{\beta}{2}G_P(P - P_f)$:

$$0 = j(\omega_f - \omega_i) + \frac{1+j\alpha}{2}\Delta G + \frac{1}{\tau_o}\frac{E_{io}}{E_o} \tag{B.12}$$

By separating the real and imaginary parts, equation B.12 can be written as:

$$\Delta G = -\frac{2}{\tau_o}Re\left\{\frac{E_{io}}{E_i}\right\} \tag{B.13}$$

$$\omega_f - \omega_i = \frac{1}{\tau_o}\left\{Im\left\{\frac{E_{io}}{E_i}\right\} + \alpha Re\left\{\frac{E_{io}}{E_i}\right\}\right\} \tag{B.14}$$

Stability requires the differential gain, B.13 to be negative. By defining the injection ratio: $\rho = P_{io}/P_o = |E_{io}/E_i|^2$ and the injection phase, $\phi - \phi_i = \angle\{E_i/E_{io}\}$, the locking range is found from equation B.13 and B.14:

$$-\frac{1}{\tau_p}\sqrt{\rho(1+\alpha^2)} < \omega_f - \omega_i < \frac{1}{\tau_0}\sqrt{\rho} \tag{B.15}$$

Corresponding to a phase offset:

$$-\pi/2 + arctan(\alpha) < \phi - \phi_i < \pi/2 \tag{B.16}$$

If these requirements are not fulfilled, stable locking is not possilble. However, even if these conditions are fulfilled, dynamic stability may not exist within the locking range. In order to investigate dynamic stability, the linearised equations has to be investigated. The photon pertubation can be linked to the field by:

$$\hat{p} = \frac{|P_o|^2}{|E_o|^2}\left(|E|^2 - |E_o|^2\right) \approx P_o\left\{\frac{\hat{e}}{E_o} + \frac{\hat{e}^*}{E_o^*}\right\} \tag{B.17}$$

Equation B.10 and B.11 can then be normalised by E_o and τ_o and expressed as:

$$\dot{\hat{e}} = \zeta_n\hat{n} + \zeta_P P_o\left\{\hat{e} + \hat{e}^*\right\} - \hat{e}E_{io} + \hat{e}_i \tag{B.18}$$

$$\dot{\hat{n}} = \hat{m} - \hat{n}\Lambda_e - P_o\left\{\hat{e}^* + \hat{e}\right\}[G_o + G_P P_o] \tag{B.19}$$

where the recombination rate, $\Lambda_e = 1/\tau_e + P_o/G_N$, the complex differential gain, $\zeta_n = \frac{1+j\alpha}{2}G_N$ and the complex nonlinear gain, $\zeta_p = \frac{1+j\beta}{2}G_P$. this can be expressed in matrix format:

$$\begin{bmatrix} \frac{d}{dt} + E_{io} - \zeta_P P_o & -\zeta_P P_o & -\zeta_N \\ -\zeta_P^* P_o & \frac{d}{dt} + E_{io}^* - \zeta_P^* P_o & -\zeta_N^* \\ P_{so}(G_o + G_P P_o) & P_{so}(G_o + G_P P_o) & \frac{d}{dt} + \Lambda_e \end{bmatrix} \begin{bmatrix} \hat{e} \\ \hat{e}^* \\ \hat{n} \end{bmatrix} = \begin{bmatrix} \hat{e}_i \\ \hat{e}_i^* \\ \hat{m} \end{bmatrix} \tag{B.20}$$

Where the characteristic matrix is:

$$\mathbf{D} = \begin{bmatrix} \frac{d}{dt} + E_{io} - \zeta_P P_o & -\zeta_P P_o & -\zeta_N \\ -\zeta_P^* P_o & \frac{d}{dt} + E_{io}^* - \zeta_P^* P_o & -\zeta_N^* \\ P_{so}(G_o + G_P P_o) & P_{so}(G_o + G_P P_o) & \Lambda_e \end{bmatrix} \tag{B.21}$$

In order to have dynamic stability, the characteristic matrix needs to have eigenvalues with a positive real part, in addition to meeting the requirement of equation B.15. Taking the Fourier transform of B.20

$$\begin{bmatrix} j\omega + E_{io} - \zeta_P P_o & -\zeta_P P_o & -\zeta_N \\ -\zeta_P^* P_o & j\omega + E_{io}^* - \zeta_P^* P_o & -\zeta_N^* \\ P_{so}(G_o + G_P P_o) & P_{so}(G_o + G_P P_o) & j\omega + \Lambda_e \end{bmatrix} \begin{bmatrix} \hat{e}(\omega) \\ \hat{e}^*(-\omega) \\ \hat{n}(\omega) \end{bmatrix} = \begin{bmatrix} \hat{e}_i(\omega) \\ \hat{e}_i^*(-\omega) \\ \hat{m}(\omega) \end{bmatrix} \tag{B.22}$$

The solution to the above equation is the general solution for the small pertubation approximation. The solution can be greatly simplified by assuming zero carrier perturbation ($\hat{m} = 0$) and zero injection frequency detuning ($\Delta\omega_o = 0$), when the injected field is in phase with the laser field: $Im\{E_{io}\} = 0$. Eliminating $\hat{n}$ from the equation system and combining the expressions for $\hat{e}_i$ and $\hat{e}_i^*$, the equation can be solved as:

$$e(\omega) = \frac{e_i(\omega) + Z(\omega)\left[e_i(\omega) + e_i^*(\omega)\right]}{j\omega + E_{io}} \tag{B.23}$$

where

$$Z(\omega) = -\frac{\zeta_n P_o(G_o + G_P P_o)}{(j\omega + \Lambda)^2 + \Omega^2} - \frac{\zeta_P P_o(j\omega + \Lambda_e)}{(j\omega + \Lambda)^2 + \Omega^2} \tag{B.24}$$

and where $\Lambda = (E_{io} - G_P P_o + \Gamma_e)/2$ and $\Omega = \sqrt{P_o^2 G_N^2 [G_o + G_N P_o]^2 - [\Lambda - \Lambda_e]^2}$, are the decay rate and angular frequency of relaxation oscillations.

Noise performance

It is possible to estimate the noise reduction properties of injection locking by modelling the process as a first order optical phase lock loop with instant response, that is zero loop delay. Equation B.1 can now be broken up into real and imaginary parts:

$$Re\{\frac{\dot{E}}{E}\} = \frac{1}{2}\left(G_N\hat{n} + G_P\hat{p}\right) - \frac{1}{\tau_o}Re\{\frac{E_i}{E}\} \tag{B.25}$$

$$Im\{\frac{\dot{E}}{E}\} = \frac{\alpha}{2}\left(G_N\hat{n} + G_P\hat{p}\right) - \frac{1}{\tau_o}Im\{\frac{E_i}{E}\} - [\omega_f - \omega_i] \tag{B.26}$$

The pertubation of the injected field is assumed to be zero and again, α is assumed to be equal to β. Defining ϕ and ϕ_i as the steady state phase and injected steady state phase and $\hat{\phi}$ and $\hat{\phi}_i$ as the phase perturbations, and then assuming that the amplitudes of the laser and injected field is constant, the two equations above can be further linearised, combined and simplified to:

$$\dot{\hat{\phi}} = \frac{\sqrt{\rho}}{\tau_0}[\alpha\sin(\phi_i - \phi + \hat{\phi}_i - \hat{\phi}) + \cos(\phi_i - \phi + \hat{\phi}_i - \hat{\phi})] - [\omega_f - \omega_i] \tag{B.27}$$

Subtracting the steady state solution, equation B.27 can be further simplified to:

$$\dot{\hat{\phi}} = \frac{\sqrt{\rho(1+\alpha^2)}}{\tau_0}\cos(\phi_i - \phi + \tan^{-1}\{\alpha\})[\hat{\phi}_i - \hat{\phi}] \tag{B.28}$$

Following the treatment of the OPLL, the Laplace transform can here be applied, giving:

$$s\hat{\phi} = K_{oil}[\hat{\phi}_i - \hat{\phi}] \tag{B.29}$$

Where $K_{oil} = \frac{\sqrt{\rho(1+\alpha^2)}}{\tau_0}\cos(\phi_i - \phi + \delta)$. This can be rewritten as:

$$\hat{\phi} = H_{oil}\hat{\phi}_i \tag{B.30}$$

Where s is complex frequency and:

$$H_{oil} = \frac{K_{oil}}{s + K_{oil}} \tag{B.31}$$

By analogy with the phase lock loop model, the output phase error can be estimated using:

$$\hat{\phi}_{error} = [1 - H_{oil}]\hat{\phi}_n \tag{B.32}$$

Where $\hat{\phi}_n$ is the laser noise, similar to the OPLL case. Unlike the OPLL case, the modulation is here added to $\hat{\phi}_n$ when the injected signal is phase or frequency modulated. Note that no additive noise is present here, as a consequense of the injection locking mechanism. This expression can be used with good accuracy for the stable region with lower injection ratios.

DFB Lasers:

In order to investigate more complex laser structures, a similar method can be used to that of Tromborg et al [3]. The laser can be treated as an active mirror with a reflection function $r(\omega)$. Ignoring spontaneous emission, the reflected field can be expressed as:

$$E(\omega) = r(\omega)E_i(\omega) \tag{B.33}$$

Using the first order expansion around $1/r$:

$$\frac{1}{r} = \frac{1}{r_o}\left(1 - \frac{\delta[ln(r)]}{\delta\omega}\omega - \frac{\delta[ln(r)]}{\delta N}\hat{n} - \frac{\delta[ln(r)]}{\delta P}\hat{p}\right) \tag{B.34}$$

and the static solution for noise-free injection, $E_o(\omega_o) = r_o(\omega_o)E_{io}(\omega_o)$:

$$\left(1 - \frac{\delta[ln(r)]}{\delta\omega}\omega\right)\frac{\hat{e}}{E_o} = \frac{\delta[ln(r)]}{\delta N}\hat{n} + \frac{\delta[ln(r)]}{\delta P}\hat{p} + \frac{\hat{e}_i}{E_{io}} \tag{B.35}$$

For carrier number, the possible non-uniform distribution of photons and carriers needs to be considered, and equation B.2 is rewritten:

$$\dot{N} = M - \frac{N}{\tau_e} - \int_{cavity} G(\bar{x})\frac{\delta P}{\delta\bar{x}}(\bar{x})d\bar{x} \tag{B.36}$$

If the photon density perturbance is uniform through each cavity section, the following notation can be adopted:

$$\tau_o = j\frac{1}{r_o}\frac{\delta[ln(r)]}{\delta\omega} \tag{B.37}$$

$$\zeta_n = \frac{1}{\tau_o r_o}\frac{\delta[ln(r)]}{\delta N} \tag{B.38}$$

$$\zeta_p = \frac{1}{\tau_o r_o}\frac{\delta[ln(r)]}{\delta P} \tag{B.39}$$

$$P_o = \frac{2\pi\mu_0}{\hbar\nu c}\int_{cavity} |E(\bar{x})|^2\eta^2(\bar{x})d\bar{x} \tag{B.40}$$

$$G_o = \langle G(\bar{x})\rangle_{cavity} \tag{B.41}$$

μ_0 :	$4\pi \cdot 10^{-7}$ N/A^2	Permeability in vacuum
$\hbar$:	$1.045 \cdot 10^{-34}$ Js	Planck's constant
η		Refractive index

Time and field is normalised by τ_o and E_o, use equations B.37 to B.41 and again use the relation between field and photon number in equation B.17:

$$j\omega\hat{e}(\omega) = \zeta_n\hat{n}(\omega) + \zeta_p P_o\left\{\hat{e}(\omega) + \hat{e}^*(\omega)\right\} - \hat{e}(\omega)E_{i_o} + \hat{e}_i(\omega) \tag{B.42}$$

$$j\omega\hat{n}(\omega) = \hat{m}(\omega) - \hat{n}(\omega)\Gamma_e - P_o\left\{\hat{e}^*(\omega) + \hat{e}(\omega)\right\}[G_o + G_P P_o] \tag{B.43}$$

We see that equations B.42 and B.43 are identical to equations B.10 and B.11. This means that with the equivalent parameters B.37 to B.41 defined, the treatment for Fabry-Perot lasers can be used for more complex laser structures, such as DFB lasers. However, the τ_o parameter needs to be assumed to be real, that is no effective gain change with emission frequency, such as when the laser is operating near a longitudal resonance mode. The effective parameters τ_o, ζ_N and ζ_P

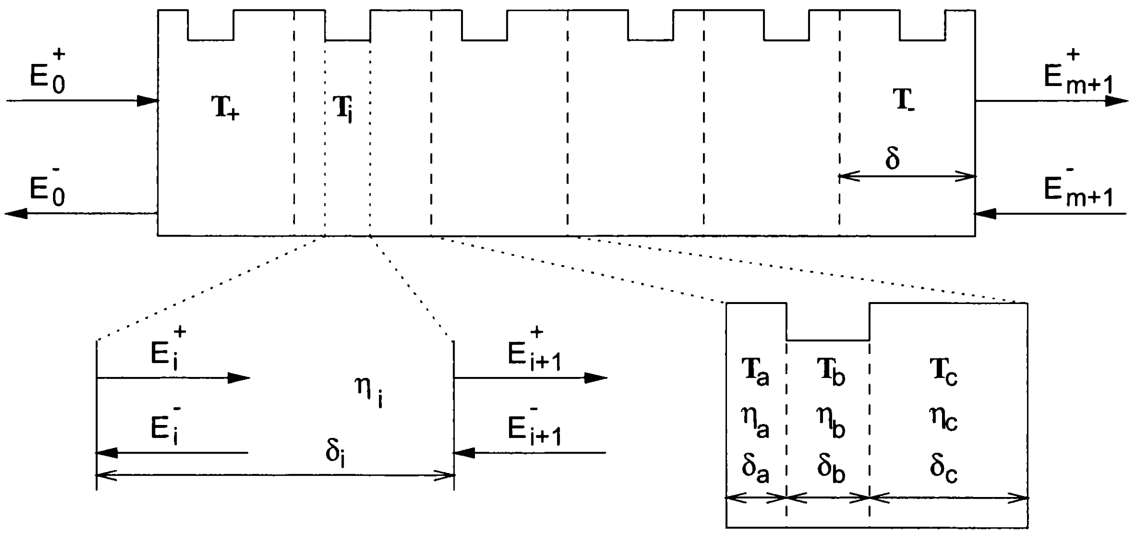

Figure B.1: Transmission line schematic of DFB laser.

can be obtained by the transmission line method. By dividing the laser structure into a number of thin transversal sections, each section can be assumed to have uniform refractive index, η_{gi}, gain, k_i, absorption, a_i, photon and carrier density and injection ratio. The length of the section is d_i. The electromagnetic field in each section can then be determined by transfering the boundary conditions, optical injection and emission at the laser output facets, to bordering sections. The transfer between two areas with different refractive index gives:

$$\begin{bmatrix} E_{i-1}^+ \\ E_{i-1}^- \end{bmatrix} = \begin{bmatrix} \frac{\eta_i+\eta_{i-1}}{2\eta_{i-1}}e^{j\delta_i} & \frac{\eta_i-\eta_{i-1}}{2\eta_{i-1}}e^{-j\delta_i} \\ \frac{\eta_i-\eta_{i-1}}{2\eta_{i-1}}e^{j\delta_i} & \frac{\eta_i+\eta_{i-1}}{2\eta_{i-1}}e^{-j\delta_i} \end{bmatrix} \begin{bmatrix} E_i^+ \\ E_i^- \end{bmatrix} \tag{B.44}$$

where $\delta_i = \omega\eta_i d_i/c$ and $\eta_i = \eta_{gi} - jc(a_i - k_i)/2\omega$. Rearranging the expression to locate all terms relating to section i-1 on the left side, the relation between section i and i-1 now reads:

$$\begin{bmatrix} E_{i-1}^+ + E_{i-1}^- \\ \eta_{i-1}(E_{i-1}^+ - E_{i-1}^-) \end{bmatrix} = \mathbf{T}_i \begin{bmatrix} E_i^+ + E_i^- \\ \eta_i(E_i^+ - E_i^-) \end{bmatrix} \tag{B.45}$$

where $\mathbf{T}_i$ is the transfer matrix for section i, given by:

$$\mathbf{T}_i = \begin{bmatrix} \cos\delta_i & \frac{j}{\eta_i}\sin\delta_i \\ j\eta_i\sin\delta_i & \cos\delta_i \end{bmatrix} \tag{B.46}$$

For a laser with m+1 sectors, such as the laser shown in Fig. B.1, the steady solution can be obtained by solving

$$\begin{bmatrix} E_0^+ + E_0^- \\ \eta_0(E_0^+ - E_0^-) \end{bmatrix} = \mathbf{T}_1\mathbf{T}_2\ldots\mathbf{T}_m\mathbf{T}_{m+1} \begin{bmatrix} E_{m+1}^+ + E_{m+1}^- \\ \eta_{m+1}(E_{m+1}^+ - E_{m+1}^-) \end{bmatrix} \tag{B.47}$$

and in each section

$$P_i = \frac{\mu_o n_{gi}^2}{\hbar\omega c}\int \varepsilon(\bar{x})d\bar{x}\int_0^{d_i}|E_i(z)|^2 dz \tag{B.48}$$

$$0 = M_i - \frac{N_i}{\tau_e} - \frac{c}{n_{gi}}\Gamma_i g_i(N_i)P_i \tag{B.49}$$

where P_i, N_i, M_i, Γ_i and ε_i are the photon, carrier population carrier injection rate, the waveguide confinement factor and the transverse field profile in section i. The electric field at a given point, z in section i is:

$$E_i = E_i^+ e^{j\delta_i\frac{z}{d_i}} + E_i^- e^{-j\delta_i\frac{z}{d_i}} \tag{B.50}$$

When carrier injection rate M_i and gain - carrier population relation $g_i(N_i)$ is known, the above equation can be solved. For a symmetric DFB laser shown in Fig. B.1, some simplification can be made by dividing the laser into n sections, representing each grating line.

$$\mathbf{T}_+ = \mathbf{T}_a\mathbf{T}_g\mathbf{T}_b \tag{B.51}$$

$$\mathbf{T}_- = \mathbf{T}_b\mathbf{T}_g\mathbf{T}_a \tag{B.52}$$

$\mathbf{T}_a\mathbf{T}_g\mathbf{T}_b$ is in turn given by:

$$\mathbf{T}_a\mathbf{T}_g\mathbf{T}_b = \frac{1}{1-\kappa^2}\begin{bmatrix} \cos\delta - \cos(\delta - 2\delta_c) - \cos\tilde{\delta} + \cos(\tilde{\delta} - 2\delta_c) & \frac{j}{\eta_1}[\sin\delta + \sin(\delta - 2\delta_c) - \sin\tilde{\delta} - \sin(\tilde{\delta} - 2\delta_c)] \\ j\eta_1[\sin\delta - \sin(\delta - 2\delta_c) - \sin\tilde{\delta} + \sin(\tilde{\delta} - 2\delta_c)] & \cos\delta + \cos(\delta - 2\delta_c) - \cos\tilde{\delta} - \cos(\tilde{\delta} - 2\delta_c) \end{bmatrix} \tag{B.53}$$

where $\kappa = \frac{\eta_1 - \eta_2}{\eta_1 + \eta_2}$, the grating period $\delta = \delta_a + \delta_b + \delta_c$, and $\tilde{\delta} = \delta - 2\delta_b$. δ_a, δ_b and δ_c is defined from Fig. B.1. $\mathbf{T}_-$ is obtained by exchanging the a-indices to c-indices and vice versa in equation B.53. Assuming that the carrier density variation along the cavity is small and can be considered as uniform, the laser structure can be represented by:

$$\mathbf{T} = \mathbf{T}_{ar}\mathbf{T}_{+}^{(m/2)}\mathbf{T}_{-}^{(m/2)}\mathbf{T}_{ar} \tag{B.54}$$

where $\mathbf{T}_{ar}$ is the antireflection section on the end of the facets and $\mathbf{T}_{o}$ is the middle section representing the phase-shift between the left and right grating. The eigenvalues of matix $\mathbf{T}_{+}$ and $\mathbf{T}_{-}$ are the same and can be expressed as $e^{\pm j\varphi}$ due to $|\mathbf{T}_{\pm}| = 1.$, the eigenvalues can now be solved as:

$$e^{\pm 2j\varphi} = \frac{\cos\delta - \kappa^2\cos\tilde{\delta}}{1-\kappa^2} \pm \sqrt{\left(\frac{\cos\delta - \kappa^2\cos\tilde{\delta}}{1-\kappa^2}\right)^2 - 1} \tag{B.55}$$

With this result, any power of $\mathbf{T}_{\pm}$ can be calculated using Cayley-Hamilton's theorem; any square matrix must satisfy its own characteristic equation, together with the relation $\mathbf{T}_{\pm}^{m} = t_1 X_1^m + t_2 X_2^m$ for any m.

$$\mathbf{T}_{\pm}^{m} = \frac{\sin m\varphi}{\sin\varphi}\mathbf{T}_{\pm} + \frac{\sin(m-1)\varphi}{\sin\varphi}\mathbf{I} \tag{B.56}$$

Where $\mathbf{I}$ is the identity matrix. The whole structure can be writen as

$$\mathbf{T} = \mathbf{T}_{ar}\left[\frac{\sin\frac{m}{2}\varphi}{\sin\varphi}\mathbf{T}_{+} + \frac{\sin(\frac{m}{2}-1)\varphi}{\sin\varphi}\mathbf{I}\right]\left[\frac{\sin\frac{m}{2}\varphi}{\sin\varphi}\mathbf{T}_{-} + \frac{\sin(\frac{m}{2}-1)\varphi}{\sin\varphi}\mathbf{I}\right]\mathbf{T}_{ar} \tag{B.57}$$

where $\mathbf{T}_{ar}\mathbf{T}_{+}\mathbf{T}_{-}\mathbf{T}_{ar}$ is given by:

$$\mathbf{T}_{ar}\mathbf{T}_{+}\mathbf{T}_{-}\mathbf{T}_{ar} = \frac{1}{(1-\kappa^2)^2}\begin{bmatrix} \psi_1 & j\chi_1 \\ j\chi_1 & \psi_1 \end{bmatrix} \tag{B.58}$$

where:

$\psi_1 = \cos 2\delta + \kappa^4 \cos 2\tilde{\delta} - \kappa^2[\cos 2(\delta - 2\delta_c) + \cos 2(\tilde{\delta} - 2\delta_c)]$

$\chi_1 = \sin 2\delta + \kappa^4 \sin 2\tilde{\delta} - \kappa^2[\sin 2(\delta - 2\delta_c) + \sin 2(\tilde{\delta} - 2\delta_c)]$

$\mathbf{T}_{ar}[\mathbf{T}_{+} + \mathbf{T}_{-}]\mathbf{T}_{ar}$ is given by:

$$\mathbf{T}_{ar}[\mathbf{T}_{+} + \mathbf{T}_{-}]\mathbf{T}_{ar} = \frac{2}{(1-\kappa^2)}\begin{bmatrix} \psi_2 & j\chi_2 + j\chi_3 \\ j\chi_2 - j\chi_3 & \psi_2 \end{bmatrix} \tag{B.59}$$

where:

$\psi_3 = \cos\delta - \kappa^2\cos\tilde{\delta}$

$\chi_2 = \sin\delta - \kappa^2\sin\tilde{\delta}$

$\chi_3 = \kappa[\sin(\delta - 2\delta_c) - \sin(\tilde{\delta} - 2\delta_c)]$

With injection to only one facet, $E_o^+ = E_{in}$, $E_o^- = E_{out}$, $E_{n+1}^+ = E_t$ and $E_{n+1}^- = 0$, and the transfer function can be written as:

$$\begin{bmatrix} E_{in} + E_{out} \\ E_{in} - E_{out} \end{bmatrix} = \mathbf{T}\begin{bmatrix} E_t \\ E_t \end{bmatrix} \tag{B.60}$$

The reflection is then given by

$$r = \frac{E_{out}}{E_{in}} = \frac{j\psi_3}{\frac{1}{2(1-\kappa^2)}\frac{\sin m\varphi}{\sin(m-1)\varphi}\left[\psi_1 + j\chi_1\right] + \left[\psi_2 + j\chi_2\right] + \frac{1-\kappa^2}{2}\frac{\sin(m-1)\varphi}{\sin m\varphi}} \tag{B.61}$$

From this equation the parameters needed for treating a symmetric DFB laser with the Fabry-Perot injection locking model are obtained, using equations B.37 to B.41.

References

[1] R. Lang, "Injection locking properties of a semiconductor laser," *IEEE J. Quantum Elec.* vol. QE-18, pp. 976–983, 1982.

[2] O. Lidoyne, P. Gallion and D. Erasme, "Analysis of a homodyne receiver using an injection-locked semiconductor laser," *J. Lightwave Tech.*, vol. 9, pp. 659–665, 1991.

[3] B. Tromborg, H.E. Lassen, and H. Olesen, "Traveling wave analysis of semiconductor lasers: modulation responses, mode stability and quantum mechanical treatment of noise spectra,"*IEEE J. Quantum Elec.* vol. 30, pp. 939–956, 1994.

Appendix C

Optical Phase Lock Loop Theory

A theoretical framework for optical phase locked loops can be adapted from control theory [1], and theory of conventional phase locked loops, [3, 2]. The following theory has been adapted from various sources [4, 6, 5]. A schematic of an OPLL, including the main parameters, is seen in Figure C.1.

Time domain equations

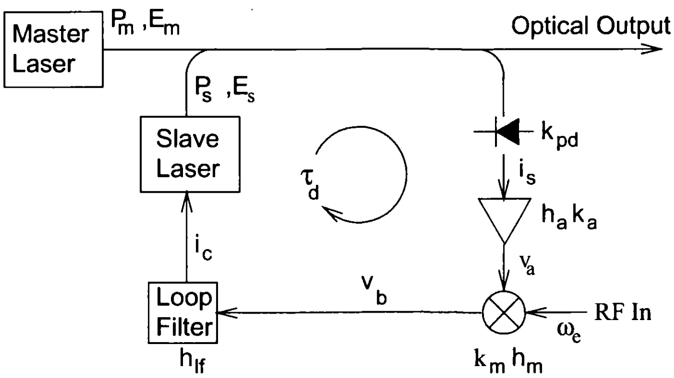

Figure C.1: Optical phase lock loop with expressions

The optical field emitted from the master and slave laser can be expressed as:

$$E_m = |E_m|e^{j(\omega_m t + \phi_m(t))} \tag{C.1}$$

$$E_s = |E_s|e^{j(\omega_s t + \phi_s(t))} \tag{C.2}$$

$E_{m,s}$ Optical field

$\omega_{m,s}$ Angular frequency

$\phi_{m,s}$ Absolute phase

After coupling, the total optical field will be:

$$E_{tot} = E_m + E_s \tag{C.3}$$

The average photocurrent from the photodetector can be expressed as:

$$I_s = RI_d \tag{C.4}$$

R Photodetector responsitivity

$I_d \propto E_{tot}^2$ Detected optical power

Combining Equation C.1, C.2, C.3 and C.4, the signal current can be expressed as:

$$i_{s0} = RI_m + RI_s + 2R\iota_{coh}\sqrt{I_m I_s}cos[(\omega_m - \omega_s)t + \phi_m - \phi_s] \tag{C.5}$$

$I_{m,s}$ Master and slave laser optical power (W)

ι_{coh} Coherence efficiency

Assuming that the optical fields have a matched polarisation in the fibre, the coherence efficiency will be equal to 1, and the AC term of the photocurrent is:

$$i_s = 2R\sqrt{I_m I_s}cos[(\omega_m - \omega_s)t + \phi_m - \phi_s] \tag{C.6}$$

After the amplifier, the following voltage is found:

$$v_a = k_a k_{pd} cos[(\omega_m - \omega_s)t + \phi_m - \phi_s] * h_a \tag{C.7}$$

k_a Amplifier gain

k_{pd} Photodetector gain ($2R\sqrt{I_m I_s}$)

k_a Amplifier impulse response

If a double balanced mixer is used with a sinusoidal phase response and assuming the mixer is pumped with enough power to be saturated, the output from the mixer is:

$$v_b = k_m k_a k_{pd} sin[(\omega_r - \omega_m + \omega_s)t + \phi_r - \phi_m + \phi_s] * h_a * h_m \tag{C.8}$$

k_m Mixer conversion efficiency

ω_r Reference signal angular frequency

ϕ_r Reference signal absolute phase

h_m Mixer equivalent impulse response

Including the effect of the loop filter and the round trip time delay of the loop, the current fed into the slave laser will be:

$$i_c = k_{lf} k_m k_a k_{pd} sin[(\omega_r - \omega_m + \omega_s)t + \phi_r - \phi_m + \phi_s] * h_a * h_m * h_{lf} * \delta(t - \tau_d) \quad \text{(C.9)}$$

k_{lf} Loop filter DC gain

h_{lf} Loop filter impulse response (A/V)

τ_d Loop round trip time delay

If the phase lock loop is in a locked state, $\omega_r - \omega_m + \omega_s = 0$ can be assumed, and the remaining phase difference, $\phi_e = \phi_r - \phi_m + \phi_s$ is small, so $sin(\phi_e) \approx \phi_e$. Also, to simplify calculations, linear components are assumed. Then the current fed into the slave laser will be:

$$i_c = k_{lf} k_m k_a k_{pd} \phi_e * h_{lf} * \delta(t - \tau_d) \quad \text{(C.10)}$$

The current injected into the slave laser will frequency modulate the slave laser as:

$$\frac{d\phi_s}{dt} = 2\pi k_s i_c * h_s \quad \text{(C.11)}$$

k_s Slave laser FM sensitivity

h_s Slave laser impulse response

Combining Equation C.10 and C.11, and assuming that the induced change in slave laser phase is equal to the induced change in the relative phase of the master and slave laser (ϕ_{ms}):

$$\frac{d\phi_{ms}}{dt} = 2\pi K \phi_e * h_{lf} * h_s * \delta(t - \tau_d) \quad \text{(C.12)}$$

$K = k_{lf} k_s k_m k_a k_{pd}$ Total loop gain

Frequency domain equations

Equation C.12 can be transformed to the frequency domain, by applying the Laplace transform:

$$\mathscr{L}\left\{\frac{d\phi_{ms}}{dt}\right\} = s\Phi_{ms} \quad \text{(C.13)}$$

$$\mathscr{L}\{2\pi K \phi_e * h_{lf} * h_s * \delta(t - \tau_d)\} = K\Phi_e(s)F(s)H_s e^{-s\tau_d} \quad \text{(C.14)}$$

$s = 2\pi jf$ The Laplace variable

$F(s)$ Laplace transform of $f(t)$

H_s Laplace transform of h_s

From control theory the following terms can be adapted [1]; the closed loop transfer function, ϕ_{ms}/ϕ_r:

$$H(s) = \frac{KF(s)H_s e^{-s\tau d}}{s + KF(s)H_s e^{-s\tau_d}} \quad \text{(C.15)}$$

the open loop transfer function, ϕ_{ms}/ϕ_e:

$$G(s) = \frac{H(s)}{1-H(s)} = \frac{KF(s)H_s e^{-s\tau_d}}{s} \tag{C.16}$$

and the error transfer function, ϕ_e/ϕ_r, is the relation between the reference signal and error of the generated signal:

$$1 - H(s) = \frac{s}{s + KF(s)H_s e^{-s\tau_d}} \tag{C.17}$$

Loop classification and stability

Optical phase locked loops are generally classified according to the kind of loop filter used. The order of the loop is determined by the order of the denominator of the open loop transfer function, and the order of the numerator can not exceed the order of the denominator if the filter is to be realisable. The type of loop is equal to the number of perfect integrators within the loop. Any loop is at least a type I loop, as the frequency tuning in the slave laser works as an integrator. By using a high gain amplifier with an integrating loop filter, a type II loop may be approximated.

A first order, type I loop has no loop filter. The filter transfer function, $F(s) = 1$. To retain stability, the loop gain is limited, implying limited phase noise reduction capabilities.

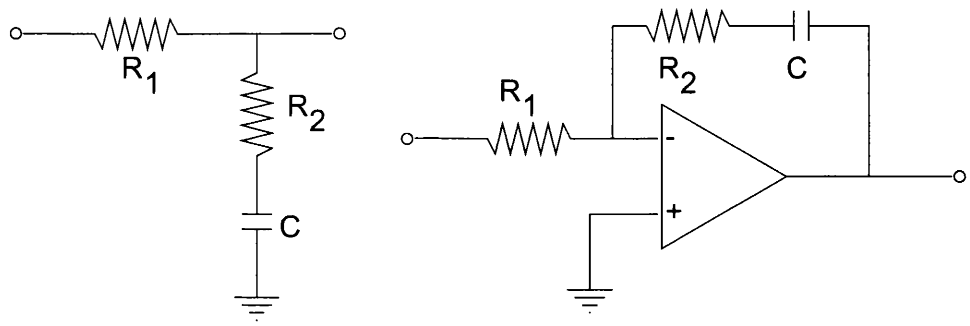

Figure C.2: Circuit diagram for second order passive and active filter

$$F(s) = \frac{1+s\tau_2}{1+s\tau_1} \tag{C.18}$$

$\tau_1 = Z_1 C \ \tau_2 = Z_2 C$ Filter time Constants

A second order filter generally delivers better performance. A type I, second order filter can be made as a low pass filter with a phase-lead correction to increase the loop gain to get higher locking bandwidth and a higher loop bandwidth, as in Figure C.2. An active second order, type II filter, Figure C.2, has even better characteristics. This has the following transfer function:

$$F(s) = \frac{1+s\tau_2}{s\tau_1} \tag{C.19}$$

An active second order, type II filter is the preferred choise for an OPLL, but if a very wideband loop is required, then a passive filter is preferred, as it offers a much lower group time delay.

The loop natural angular frequency, f_n and the loop damping, ζ, can be introduced according to:

$$\tau 1 = \frac{K}{2\pi f_n^2} \tag{C.20}$$

$$\tau 2 = \frac{2\zeta}{f_n} \tag{C.21}$$

Insertin C.20 and C.21 into C.19 and 3.8, the following steady state open loop transfer function is found:

$$G(f) = \frac{-(f_n^2 + 2j\zeta f_n f)e^{-2\pi j \tau_d}}{f^2} \tag{C.22}$$

where s has been exchanged for $2\pi jf$ where f is the frequency.

If the closed loop transfer function, H(s) in Equation 3.6 is studied, it is seen that the loop becomes unstable if the open loop transfer function has a phase of $-180°$ at the frequency of unity gain, f_z. This frequency may be deduced by putting $|G(f)| = 1$ and solving it for $f = f_z$:

$$f_z = f_n\sqrt{2\zeta^2 + \sqrt{4\zeta^4 + 1}} \tag{C.23}$$

To ensure stability in the loop, the frequency where the phase of the open loop gain, G(s), crosses $-180°$, $f_{2\pi}$ must be lower than the critical frequency,f_z. The difference between the angle $\angle G(f_z)$ and $-180°$ is denoted as the phase margin, while the ratio $1/G(f_{2\pi})$ is the gain margin. By applyinng these criteria, a restriction on the maximum allowed loop time delay can be deduced:

$$\tau_d < \frac{arctan\left(2\zeta\sqrt{2\zeta^2 + \sqrt{4\zeta^4 + 1}}\right)}{2\pi f_z} \tag{C.24}$$

Noise performance

In this section, the model for OPLL will be modified to take noise into account. With noise terms, the detected photocurrent can now be expressed as:

$$i_s = 2R\sqrt{I_m I_s}\{cos[(\omega_m - \omega s)t + \phi_m - \phi_s + \phi_n] + n\} \tag{C.25}$$

ϕ_n Laser phase noise

n Additive noise in the optical receiver

The amplitude noise term can be put in the following form, as are only a relatively narrow band around the beat frequency is interesting:

$$n = n_a cos(\omega_{ms}t + \phi_a) \tag{C.26}$$

ϕ_a Phase of additive noise

n_a Amplitude of additive noise

According to [7], when adding amplitude noise to a signal of larger amplitude, it can be divided into an amplitude component, n_a and a phase noise component, n_ϕ both with half of the power of the intensity noise. The amplitude component can here be disregarded, as it is much smaller than the signal amplitude.

If C.25 is used in place of C.6, the equivalent of equations C.13 and C.14 can be derived, with the noise terms included:

$$s\phi_{ms} = K(\phi_r + \phi_{in} - \phi_{ms} + \phi_n)F(s)e^{-s\tau_d} \tag{C.27}$$

The phase error at the optical output of the OIPLL is not directly affected by the additive intensity noise term that is being added at the photodetector, therefore, the phase error at the output of the OPLL with noise terms included can be expressed as:

$$\phi_e = \phi_{ms} - \phi_r + \phi_n \tag{C.28}$$

If this new expression for ϕ_e is used, the phase error due to the laser phase noise at the optical output of the OPLL is calculated by the error transfer function, ϕ_e/ϕ_r:

$$\phi_{e-n} = (1-H)\phi_n \tag{C.29}$$

In a similar manner, the phase error due to additive intensity noise is calculated by the open loop transfer function, $\phi_m s/\phi_r$:

$$\phi_{e-in} = H\phi_{in} \tag{C.30}$$

As the phase error terms calculated above are random and independent, the total square phase error density is given by the sum of the square densities of the two individual terms:

$$S = S_n|1-H|^2 + S_{in}|H|^2 \tag{C.31}$$

S Total square phase error density

S_n Square phase error density due to laser phase noise

S_{in} Square phase error density due to additive noise

References

[1] J.A. Betts, "Signal processing, modulation and noise," *The English University Press Limited*, London 1970.

[2] P.V. Brennan, "Phase locked loops: theory and practice," *MacMillan Press Ltd.*, Houndmills, Hampshire, 1996.

[3] F.M. Gardner, "Phaselock techniques," *2nd edition, John Wiley and sons,* 1979.

[4] M. Ohtsu, "Highly coherent semiconductor lasers," *Artech House Ltd,* Norwood, MA, 1992.

[5] A.C. Bordonalli, "Optical injection phase-lock loops," PhD thesis submitted to University of London, 1996, Department of Electronic and Electrical Engineering, University College London.

[6] R.T. Ramos, "Optical phase lock loops using semiconductor lasers," PhD thesis submitted to University of London, 1992, Department of Electronic and Electrical Engineering, University College London.

[7] W.P. Robins, "Phase noise in signal sources," *IEE Telecommunications Series 9, 2nd revised edition,* 1982: Peter Pereginus Ltd., London.